

Egg-white derived bioactive peptides improve insulin resistance and non-alcoholic fatty liver  
disease in mice: mechanisms of action

by

Stepheny Carneiro de Campos Zani

A thesis submitted in partial fulfillment of the requirements for the degree of

Doctor of Philosophy

Department of Physiology

University of Alberta

© Stepheny Carneiro de Campos Zani, 2023

## ABSTRACT

Metabolic syndrome is a condition characterized by the presence of multiple co-morbidities including hypertension, dyslipidemia, obesity and hyperglycemia. More recently, non-alcoholic fatty liver disease (NAFLD) has been included in this cluster as the hepatic manifestation of the metabolic syndrome. Lifestyle interventions are the first line of therapy for these co-morbidities and while pharmacological treatment is available for some of them, life-long adherence to treatment is challenging. Others, such as NAFLD remain without approved pharmacological therapy.

Food-derived bioactive peptides are short amino acid sequences derived from a parent protein from a food source. Bioactive peptides, beyond their nutritional value modulate physiological processes; therefore, they have a role in disease management. We are interested in egg-derived bioactive peptides and our group showed before that egg white hydrolysate and bioactive peptides have antihypertensive effects in vivo and anti-inflammatory and adipogenic activity in vitro. Moreover, in vitro these peptides prevent angiotensin II- and tumor necrosis factor alpha-induced insulin resistance.

Given the crosstalk between the conditions in the metabolic syndrome, I hypothesized that two bioactive peptides derived from the egg white, Peptide 2 (QAMPFRVTEQE) and IRW, would promote beneficial effects on diet-induced metabolic dysfunction. More specifically, I focused on insulin resistance and NAFLD.

To address this hypothesis C57BL/6 mice were fed high-fat diet (HFD) for 6 weeks to induce obesity and glucose intolerance. After that, their diet was supplemented with either of the peptides (Peptide 2 or IRW) for another 8 weeks. Another group received HFD and rosiglitazone, an insulin sensitizer and the third group continued receiving HFD only.

Throughout the 14-week period one group received a low-fat diet. Glucose tolerance, insulin sensitivity and body composition were assessed in vivo. After euthanasia, blood, skeletal muscle, adipose tissue, and liver tissues were collected. Plasma biochemical analysis was performed using ELISA and colorimetric commercial kits. Insulin signaling, lipolysis, adipogenesis markers, renin-angiotensin system components, mitochondria and lipid metabolism were assessed by western blot, qPCR or functional assays. NAFLD features were characterized by biochemical and histological analysis.

Overall, Peptide 2 improved systemic insulin resistance and restored adipose tissue insulin signaling, thereby normalizing the lipolytic response to insulin. The actions of Peptide 2 on adipose tissue may in part explain the observed decrease in hepatic lipid accumulation. IRW improved insulin resistance and insulin signaling in skeletal muscle but not in adipose tissue. IRW prevented NAFLD, concurrent with increasing fatty acid oxidation and mitochondria content in the liver. I propose that the peptides are exerting their effects via membrane bound receptors, such as via angiotensin II type 2 receptor (AT2R) or angiotensin 1-7 receptor (MasR); however, this requires further evaluation.

In conclusion, in this thesis I provide evidence that bioactive peptides promote beneficial effects in an obese, glucose intolerant mouse model. More specifically, these peptides both improve insulin signaling and reduce hepatic steatosis, thus providing a potential novel therapeutic option for NAFLD, which currently lacks approved pharmacological treatment.

## PREFACE

This thesis is an original work done by Stepheny Carneiro de Campos Zani. The research project, of which this thesis is a part, received research ethics approval from the University of Alberta Research Ethics Board, Project Name “Effect of bioactive peptides on metabolic syndrome”, No. 1472. This research project was funded by Alberta Livestock and Meat Agency (ALMA) and the Natural Sciences and Engineering Research Council of Canada (NSERC) discovery grant. I was funded by the Canadian Institutes of Health Research (CIHR), by the Faculty of Graduate Studies and Research (FGSR) of the University of Alberta, the Faculty of Medicine and Dentistry and Alberta Diabetes Institute (ADI) during the execution of this project.

Chapter 3 of this thesis is a publication entitled “An egg white-derived peptide enhances systemic insulin sensitivity and modulates markers of non-alcoholic fatty liver disease in obese, insulin resistant mice”. This article was published on the journal *Metabolites*. 2023 (January 24;13(2):174. doi: 10.3390/metabo13020174). It is a collaboration with the following authors: Ren Wang, Hellen Veida-Silva, Robin D. Clugston, Jessica T.Y. Yue, Marcelo A. Mori, Jianping Wu and Catherine B. Chan. I participated in the study design, performed the experiments, analyzed the data, and prepared the manuscript for submission under the supervision of Dr. Catherine Chan and co-supervision of Dr. Jianping Wu. Moreover, I supervised the undergraduate student who performed some of the experiments.

Chapter 4 is a publication entitled “IRW (isoleucine–arginine–tryptophan) improves glucose tolerance in high-fat diet fed C57BL/6 mice via activation of insulin signaling and AMPK pathways in skeletal muscle”. This article was published on the journal *Biomedicines*. 2022 (May 26;10(6):1235. doi: 10.3390/biomedicines10061235). It is a collaboration with the following authors: Myoungjin Son, Khushwant S. Bhullar, Catherine B. Chan, and Jianping Wu.

I performed the experiments in WAT, analyzed all the data, and wrote the manuscript's first and last draft.

Chapter 5 is a manuscript not submitted for publication yet. The article is entitled "IRW prevents high-fat diet induced non-alcoholic fatty liver disease by preserving mitochondrial content and enhancing hepatic fatty acid oxidation capacity". This chapter reflects a collaboration with the following authors: Emily Berg, Xu Jiang, Alexandra Knox, Evan Ackroyd, Aaron Getachew, Jianping Wu and Catherine B. Chan. I performed experiments, data analysis, visualization and wrote the first draft of the manuscript. In addition, I supervised the undergraduate students involved in this project, who performed some of the experiments. The in vivo study was performed in collaboration with Xu Jiang.

In all the articles I am first author and details about collaborators' participation is given in each specific chapter.

## **DEDICATION**

I would like to dedicate this thesis to my younger self and to all the young girls who are struggling to find a chance to pursue their dreams. Do not give up on your dreams and find strength on those who are there to support you. Amazing things are ahead of you.

## ACKNOWLEDGMENTS

The completion of this thesis would not have been possible without the support and encouragement of many people. Each of you have contributed to my personal and professional growth and I hope one day I am able to retribute all the kindness that I have received from you.

First, I want to give a special thank you to my husband, Henrique Zani, and to my children Carlos Henrique and Maria Luiza for believing in me, sometimes more than I did. Moving to another country was not easy on any of us, but despite that, you have always demonstrated your support and, without knowing, gave me the strength to pursue my dreams. My journey would not have been as rewarding as it was without you. I love you!

I cannot find enough words to thank my supervisor, Dr. Catherine Chan. Thank you for believing in my potential and for the encouragement over the past few years. Your words pushed me beyond my comfort zone and encouraged me to conquer what I thought was impossible. Thank you for shaping my growth while at the same time allowing me to be who I am.

Thank you to my co-supervisor, Dr. Jianping Wu and committee member Dr. Jessica Yue. Throughout the years you have been closely following my trajectory. Be certain that your actions and words have played a big role in my professional growth that I am forever thankful for. Thank you to my examiners Dr. Robin Clugston (candidacy), Dr. John Ussher, and Dr. Mary-Ellen Harper. I am grateful to benefit from your expertise and kindness.

Thank you to all the collaborators who participated in this project including, but not limited to: Dr. Jessica Yue, Dr. Robin Clugston, Dr. Marcelo Mori (Brazil), Sam Kinney, and Bryan Lum. Your expertise and technical skills were greatly appreciated. I hope the future brings fruitful collaborations between us. Thank you to Dr. Jamie Mitchell, Dr. Saswati Das and Kim

Sawada from the physiology department. Sometimes we find friendship and kindness where we least expect. Your support was essential in my journey.

A huge thank you to my lab mates from whom I had the pleasure to learn from, Dr. Hui Huang, Emily Berg, Emad Yuzbashian, Carla Sosa, Dr. Carolina Archundia Herrera, Dr. Zohre Hashemi, Salma Moftah and to the undergraduate students Ren Wang, Alexandra Knox, Aaron Getachew, Evan Ackroyd and Dineli Fernando. You were the ones who endured my everyday mood, stress, and questions, but were also responsible for good laughs throughout the years. Without your support I am certain that the days in the lab would have been incredibly long, quiet, and filled with boredom. You were part of a special chapter in my life, and you can count on me for anything that you need in the future.

Finally, thank you to Dr. Nayara Lopes for your friendship and conversations in Portuguese when English seemed to be overwhelming, and to Dr. Fabiana Almeida who has been more than a friend and supported me through good and bad moments in this immigrant life. Thank you to my family and friends in Brazil, who without having any clue about what I do, always found kind words to encourage me to persevere a little longer.

*“Imagine all the people you meet in your life. There are so many. They come in like waves, trickling in and out with the tide... Sometimes the waves bring with them things from deep in the bottom of the sea and they leave those things tossed onto the shore. Imprints against the grains of sand that prove the waves had once been there, long after the tide recedes.”*

*Lilly (Colleen Hoover)*

# 1. Table of Contents

<b>1. CHAPTER 1: Literature review.....</b>	<b>1</b>
1.1 Metabolic syndrome.....	1
1.1.1 Prevalence and diagnosis of the metabolic syndrome .....	1
1.2 Type 2 diabetes.....	2
1.2.1 Type 2 diabetes definition and prevalence.....	2
1.2.2 Current approved treatment options for type 2 diabetes .....	3
1.3 Non-alcoholic fatty liver disease (NAFLD).....	4
1.3.1 NAFLD definition and prevalence.....	4
1.3.2 Current treatment options for NAFLD .....	5
1.4 Physiology of glucose homeostasis and metabolism .....	6
1.4.1 Glucose absorption and blood glucose homeostasis.....	6
1.4.2 Skeletal muscle glucose metabolism: glycolysis and glycogenesis.....	6
1.4.3 White adipose tissue (WAT) glucose metabolism: glycolysis and de novo lipogenesis (DNL).....	8
1.4.4 Hepatic glucose metabolism: glycogenesis, gluconeogenesis and DNL .....	9
1.5 Physiology of lipid metabolism.....	11
1.5.1 Lipid absorption and blood lipid homeostasis .....	11
1.5.2 White adipose tissue (WAT): lipogenesis and lipolysis and adipogenesis.....	12
1.5.3 Liver: fatty acid uptake, DNL, fatty acid oxidation and export.....	15
1.6 Pathophysiology of type 2 diabetes.....	17
1.6.1 Systemic and tissue-specific insulin resistance.....	17
1.6.2 WAT insulin resistance.....	19
1.6.3 Liver insulin resistance .....	22
1.6.4 Skeletal muscle insulin resistance.....	24
1.6.5 Consequences of insulin resistance: complications of hyperglycemia .....	25
1.7 NAFLD: a disease involving a complex organ crosstalk.....	25
1.7.1 The underlying mechanisms of NAFLD: The multi-hit hypothesis.....	26
1.7.2 Progression of untreated NAFLD.....	27

1.8	Bioactive peptides and metabolic conditions .....	28
1.8.1	Definition and the role of bioactive peptides in metabolic diseases .....	28
1.8.2	Egg-derived peptides/hydrolysates and insulin resistance.....	29
1.8.3	Egg-derived peptides/hydrolysates and NAFLD .....	30
1.8.4	Previous relevant work using IRW and EWH performed by our group.....	31
<b>2.</b>	<b>CHAPTER 2: Hypothesis and objectives .....</b>	<b>33</b>
2.1	Hypothesis.....	33
2.2	Overall aims .....	33
2.3	Specific objectives.....	33
<b>3.</b>	<b>CHAPTER 3: An egg white-derived peptide enhances systemic insulin sensitivity and modulates markers of non-alcoholic fatty liver disease in obese, insulin resistant mice.....</b>	<b>38</b>
3.1	Introduction .....	41
3.2	Materials and Methods.....	42
3.2.1	Animals and Diets.....	42
3.2.2	BW, Body Composition and Sample Collection .....	47
3.2.3	Adipose Tissue Organ Culture.....	47
3.2.4	Preadipocyte Cell Culture .....	48
3.2.5	Hyperinsulinemic-Euglycemic Clamp.....	48
3.2.6	Oral Glucose Tolerance Test (OGTT) and Insulin Tolerance Test (ITT) .....	49
3.2.7	Liver Triglyceride (TG) and Cholesterol Content .....	49
3.2.8	PPAR $\gamma$ DNA Binding Activity .....	50
3.2.9	Plasma Biochemical Analysis.....	50
3.2.10	Protein Extraction and Western Blot .....	50
3.2.11	Histology.....	51
3.2.12	Quantitative PCR (qPCR).....	52
3.2.13	Statistical Analysis.....	55
3.3	Results .....	55
3.3.1	EHW Effects on WAT Lipolytic Pathway from Obese, Insulin Resistant Rats.....	55

3.3.2	Peptide 2 and Rosiglitazone Effects in HFD-Induced Obese, Insulin Resistant Mice	62
3.3.2.1	Food Intake, Body Composition and Tissue Weight.....	62
3.3.2.2	Plasma Biochemical Parameters.....	66
3.3.2.3	Glucose Homeostasis and Systemic Insulin Sensitivity .....	66
3.3.2.4	WAT Regulation by Insulin: Lipolysis and AKT .....	72
3.3.2.5	PPAR $\gamma$ Activation, Adipocyte Size and Adipogenesis Markers .....	75
3.3.2.6	Liver Characterization .....	82
3.3.2.7	Liver PPAR $\gamma$ and AT2R.....	86
3.3.2.8	Lipid Metabolism, Inflammation, and Fibrosis Genes .....	87
3.4	Discussion .....	89
<b>4.</b>	<b>CHAPTER 4: IRW (isoleucine–arginine–tryptophan) improves glucose tolerance in high-fat diet-fed C57BL/6 mice via activation of insulin signaling and AMPK pathways in skeletal muscle.....</b>	<b>98</b>
4.1	Introduction .....	101
4.2	Materials and Methods.....	102
4.2.1	Animals, Diet, and BW Measurements.....	102
4.2.2	IRW Dosage.....	104
4.2.3	Oral Glucose Tolerance and Insulin Tolerance Tests .....	104
4.2.4	Tissue Collection .....	104
4.2.5	Protein Extraction and Western Blotting .....	105
4.2.6	Plasma RAS Components and Insulin .....	105
4.2.7	RNA Sequencing and Quantitative RT-PCR (qPCR).....	106
4.2.8	Statistics and Sample Size .....	107
4.3	Results .....	108
4.3.1	Food Intake and Body Composition .....	108
4.3.2	Glucose Homeostasis and Plasma Insulin.....	110
4.3.3	Insulin Signaling and PPAR $\gamma$ Abundance .....	112
4.3.4	RAS Components.....	115
4.3.5	Skeletal Muscle Gene Expression.....	118
4.3.6	AMPK $\alpha$ Abundance and mTOR Signaling. ....	120

4.3.7	Adipose Tissue UCP-1 Abundance .....	124
4.4	Discussion .....	125
<b>5.</b>	<b>CHAPTER 5: IRW prevents high-fat diet-induced non-alcoholic fatty liver disease by preserving mitochondrial content and enhancing hepatic fatty acid oxidation capacity...</b>	<b>132</b>
5.1	Introduction .....	135
5.2	Methods.....	137
5.2.1	Animals and diet .....	137
5.2.2	BW, body composition and biological samples.....	139
5.2.3	Oral glucose tolerance test (OGTT) and fasting glucose.....	139
5.2.4	Histological analysis .....	139
5.2.5	Hepatic lipid content.....	140
5.2.6	Citrate synthase activity.....	140
5.2.7	Protein extraction and western blot.....	140
5.2.8	RNA extraction and qPCR.....	141
5.2.9	Statistical analysis and sample size.....	142
5.3	Results .....	145
5.3.1	BW and composition.....	145
5.3.2	Glucose tolerance.....	147
5.3.3	Liver lipid content and NAFLD characteristics.....	149
5.3.4	Liver lipid metabolism and mitochondrial related genes.....	151
5.3.5	Citrate Synthase activity .....	157
5.3.6	VAT adipocyte size and adipogenesis markers .....	157
5.4	Discussion .....	163
<b>6.</b>	<b>CHAPTER 6: General discussion and conclusion .....</b>	<b>174</b>
<b>7.</b>	<b>CHAPTER 7: Future perspectives .....</b>	<b>182</b>
<b>8.</b>	<b>REFERENCES.....</b>	<b>188</b>

## LIST OF TABLES

Table 3. 1. Diet composition.....	44
Table 3. 2. Peptide 2 specifications. ....	45
Table 3. 3. Primers sequences.....	53
Table 3.4. Resistin and adiponectin concentration in plasma, epididymal and retroperitoneal adipose tissue in Sprague Dawley rats treated with HFD+4% EWH for 6 weeks (Protocol 1)...	59
Table 3. 5. BW, body composition and plasma profile of C57BL/6 mice at the end of the Peptide 2 feeding trial (Protocol 2).....	65
Table 3. 6. Fibrosis assessment.....	85
Table 4. 1. Diet composition.....	103
Table 4. 2. Body composition of C57BL/6 mice after 6 weeks of LFD or HFD feeding. ....	103
Table 4. 3. Primers sequences used for RT-PCR assays.....	107
Table 4. 4. Body composition and metabolic profile of mice supplemented with IRW.....	109
Table 5. 1. Diet composition.....	138
Table 5. 2. Primers sequences.....	143

## LIST OF FIGURES

Figure 1. 1. Criteria for metabolic syndrome diagnosis according to the International Diabetes Federation. ....	2
Figure 1. 2. Blood glucose regulation and fate of glucose in the liver, skeletal muscle and white adipose tissue (WAT) .....	11
Figure 1. 3. Pathways (simplified) involved in blood lipid regulation, the fate of lipids in the liver and white adipose tissue (WAT) and the contribution of DNL to lipid homeostasis .....	17
Figure 2. 1. General study design .....	34
Figure 3. 1. Peptide 2 chromatograph.....	46
Figure 3. 2. EWH effects in WAT of Sprague Dawley rats fed EWH for 6 weeks (Protocol 1) .	57
Figure 3. 3. EWH effects in WAT of Sprague Dawley rats fed EWH for 6 weeks (Protocol 1) .	58
Figure 3. 4. Insulin tolerance test and tissues weight clamp in mice treated with Peptide 2 (Protocol 2) .....	61
Figure 3. 5. Food and water intake clamp in mice treated with Peptide 2 (Protocol 2).....	63
Figure 3. 6. Glucose tolerance clamp in mice treated with Peptide 2 (Protocol 2) .....	64
Figure 3. 7. Glucose tolerance test and hyperinsulinemic-euglycemic clamp in mice treated with Peptide 2 (Protocol 2) .....	69
Figure 3. 8. Hyperinsulinemic-euglycemic clamp and Insulin tolerance test (ITT) clamp in mice treated with Peptide 2 (Protocol 2). .....	71
Figure 3. 9. White adipose tissue (WAT) ex vivo lipolysis and protein kinase B (AKT) activation in tissues harvested from mice treated with Peptide 2 (Protocol 2).....	73
Figure 3. 10. AKT and p-AKT normalization to $\beta$ -actine. ....	74
Figure 3. 11. Retroperitoneal white adipose tissue (rWAT) and inguinal white adipose tissue (iWAT) adipogenesis markers in tissues harvested from mice treated with Peptide 2 (Protocol 2) .....	76
Figure 3. 12. Adipogenesis markers western blot.....	79
Figure 3. 13. Effect of PEP2 on 9W pre-adipocyte differentiation .....	80
Figure 3. 14. Effect of PEP2 on 9B pre-adipocyte differentiation.....	81
Figure 3. 15. Liver characterization in tissues harvested from mice treated with Peptide 2 (Protocol 2) .....	85
Figure 3. 16. Liver protein abundance in tissues harvested from mice treated with Peptide 2 (Protocol 2) .....	86
Figure 3. 17. Liver gene expression in tissues harvested from mice treated with Peptide 2 (Protocol 2).. .....	88
Figure 3. 18. Lipid metabolism gene expression in LFD and HFD groups.....	88

Figure 4. 1. Food intake measured as kcal intake per day per animal during 8 weeks of IRW treatment .....	109
Figure 4. 2. Glucose homeostasis after IRW supplementation. ....	111
Figure 4. 3. Insulin sensitivity after IRW supplementation .....	111
Figure 4. 4. Skeletal muscle insulin signaling and PPAR $\gamma$ abundance.....	113
Figure 4. 5. White adipose tissue (WAT) insulin signaling and PPAR $\gamma$ protein abundance.....	114
Figure 4. 6. Skeletal muscle renin angiotensin system components. ....	116
Figure 4. 7. Plasma renin angiotensin system components. ....	117
Figure 4. 8. Skeletal muscle gene expression of mice fed IRW for 8 weeks.....	119
Figure 4. 9. Skeletal muscle AMPK $\alpha$ , mTOR and P70 S6K protein abundance.....	121
Figure 4. 10. Retroperitoneal white adipose tissue (WAT) AMPK $\alpha$ , mTOR and P70 S6K protein abundance. ....	122
Figure 4. 11. Epididymal white adipose tissue (WAT) AMPK $\alpha$ , mTOR and P70 S6K protein abundance .....	123
Figure 4. 12. UCP-1 expression after IRW treatment.....	124
Figure 4. 13. Potential mechanisms of action of IRW to improve glucose tolerance and insulin signaling.....	130
Figure 5. 1. BW and body composition of C57BL/6 mice throughout the treatment (week 0 to week 12).....	146
Figure 5. 2. Oral glucose tolerance test (OGTT) of C57BL/6 mice at week 13 (7 weeks of treatment) .....	148
Figure 5. 3. Liver morphological characterization.....	151
Figure 5. 4. Liver lipid metabolism .....	154
Figure 5. 5. Liver AMPK protein abundance .....	154
Figure 5. 6. Liver mitochondrial related genes .....	156
Figure 5. 7. Liver mRNA expression between LFD and HFD groups .....	156
Figure 5. 8. Liver citrate synthase activity.....	157
Figure 5. 9. Epididymal white adipose tissue (eWAT) characterization .....	160
Figure 5. 10. Retroperitoneal white adipose tissue (rWAT) characterization .....	162
Figure 5. 11. Proposed mechanisms for IRW direct effect in the liver of HFD-induced obese mice to prevent diet-induced NAFLD .....	172
Figure 6. 1. Proposed mechanism of action for Peptide 2 (PEP2) and IRW.....	181
Figure 7. 1. GRP94 and AT2R protein abundance in C57BL/6 mice .....	186
Figure 7. 2. Future perspectives for the study of Peptide 2 and IRW.....	187

# 1. CHAPTER 1: Literature review

## 1.1 Metabolic syndrome

Metabolic syndrome is an umbrella term that refers to the presence of multiple co-morbidities in an individual, increasing their risk of cardiovascular disease. The co-morbidities associated with metabolic syndrome are hypertension, insulin resistance, central obesity and dyslipidemia [1].

### *1.1.1 Prevalence and diagnosis of the metabolic syndrome*

Metabolic syndrome prevalence worldwide is difficult to define due to different criteria used for diagnosis; however, it is estimated that around 25% of the global population has metabolic syndrome [2]. In Canada, the most recent data, dating back to 2014, indicates that 19% of Canadians are living with metabolic syndrome [3]. According to the criteria defined by the International Diabetes Federation, metabolic syndrome is diagnosed when an individual has central obesity and at least two more of the co-morbidities such as high triglycerides (TG), low high-density lipoprotein cholesterol, hypertension and hyperglycemia/type 2 diabetes [1]. The International Diabetes Federation thresholds used to diagnose metabolic syndrome are shown in Fig. 1.1.

Central Obesity	Triglycerides	HDL cholesterol	Blood pressure	Plasma glucose
Waist circumference measurement is ethnic specific or BMI > 30 kg/m <sup>2</sup>	≥ 1.7 mmol/l (150 mg/dl) or treatment for dyslipidemia	Males < 1.03 mmol/l (40 mg/dl) Females < 1.29 mmol/l (50 mg/dl) or treatment for dyslipidemia	Systolic ≥ 130 mmHg or Diastolic ≥ 85 mmHg or previous diagnosis of hypertension	Fasting ≥ 5.6 mmol/l (100 mg/dl) or previous type 2 diabetes diagnosis

**Figure 1. 1. Criteria for metabolic syndrome diagnosis according to the International Diabetes Federation.** BMI, body mass index. Created with Biorender.com.

## 1.2 Type 2 diabetes

### 1.2.1 Type 2 diabetes definition and prevalence

Type 2 diabetes is a metabolic condition characterized by elevated plasma glucose concentration (hyperglycemia). Hyperglycemia in type 2 diabetes may be due to impaired insulin action (insulin resistance), impaired insulin secretion/synthesis or even a combination of both factors [4]. Nevertheless, insulin resistance is considered the hallmark of 2 diabetes. Type 2 diabetes accounts for about 90% of the diabetes cases worldwide and as of 2021, 537 million of people were diagnosed with diabetes globally, a number expected to increase 46% by 2045 [4]. According to Diabetes Canada, 11.7 million (30%) of Canadians live with diabetes or pre-diabetes [5].

In Canada, diabetes is diagnosed if fasting plasma glucose  $\geq 7.0$  mmol/L, or hemoglobin A1C (HbA1c)  $\geq 6.5\%$ , or 2h plasma glucose in a 75 g oral glucose tolerance test (OGTT)  $\geq 11.1$  mmol/L, or random plasma glucose  $\geq 11.1$  mmol/L. When an individual presents impaired

fasting glucose (6.1-6.9 mmol/L), impaired glucose tolerance (7.8-11.0 mmol/L) or HbA1c 6.0%-6.4%, prediabetes is diagnosed [6].

### *1.2.2 Current approved treatment options for type 2 diabetes*

The first lines of therapy for type 2 diabetes are nutrition and physical activity therapy, also referred to as lifestyle interventions [7, 8], followed by pharmacotherapy [9, 10]. Nutrition therapy alone reduces HbA1c, improves glycemic control, reduces body weight (BW) and improves quality of life [7]. Similarly, physical activity improves cardiorespiratory outcomes, glycemic control, lipid profile and reduces the risk of cardiovascular diseases [8]. The landmark Look AHEAD randomized controlled trial used an intensive lifestyle intervention paradigm to show that the intervention participants reduced their BW and blood pressure and had improved insulin sensitivity and dyslipidemia [11]. This is supported by meta-analysis demonstrating that lifestyle interventions are beneficial for type 2 diabetes [12] even in low-income countries [13]. In addition, a 54% and 36% lower risk of developing type 2 diabetes is seen in individuals with prediabetes after 1 and 3 years of lifestyle interventions, respectively [14]. This supports the use of lifestyle interventions to manage metabolic diseases; however, because type 2 diabetes is a chronic disease, its requirement for life-long therapy and long-term adherence to lifestyle interventions is challenging [15, 16].

Pharmacotherapy should complement type 2 diabetes management from the beginning of treatment if HbA1c is  $\geq 1.5\%$  above target, or after 3 months of lifestyle interventions if the target HbA1c is not achieved [10]. The first pharmacological choice is metformin, but other categories of drugs are dipeptidyl peptidase-4 (DPP-4) inhibitors, glucagon-like peptide-1 (GLP-1) receptor agonists, sodium-glucose co-transporter (SGLT)-2-inhibitors, insulin secretagogues,

thiazolidinediones and insulin [9]. These drugs have different mechanisms of action and target organs, the discussion of which is beyond the scope of this thesis. Nevertheless, the goal of their use is to improve glycemic control and prevent complications from hyperglycemia [9].

Unfortunately, pharmacotherapy is accompanied by variable treatment adherence due to factors such as high costs [17, 18] and possible side effects, including hypoglycemic episodes and weight gain [9, 18, 19].

### **1.3 Non-alcoholic fatty liver disease (NAFLD)**

#### *1.3.1 NAFLD definition and prevalence*

NAFLD is a term referring to multiple conditions affecting the liver, ranging from simple fatty liver (hepatic steatosis) to non-alcoholic steatohepatitis (NASH), where inflammation and hepatocyte ballooning are present together with steatosis. If untreated, NASH progresses to liver cirrhosis, hepatocellular carcinoma and eventually the need for liver transplantation [20].

NAFLD is often referred to as the hepatic manifestation of the metabolic syndrome due to its high incidence in individuals with the co-morbidities under the metabolic syndrome cluster [21].

For example, among individuals with NAFLD, 42% are diagnosed with metabolic syndrome, 22% with type 2 diabetes and 51% with obesity [22]. Due to the high association between

NAFLD and other metabolic co-morbidities, a recent consensus meeting proposed to change the name to metabolic-associated fatty liver disease (MAFLD) [23]; however, in this thesis I will refer to this condition as NAFLD.

Liver biopsy (histological assessment) is the gold standard method used to diagnose NAFLD; however, because it is an invasive method hepatic steatosis is usually diagnosed using imaging (for example, ultrasound or magnetic resonance imaging). Hepatic steatosis is characterized by

lipid accumulation in the liver (> 5%) in the absence of cellular damage and without a secondary cause, such as excessive alcohol consumption, steatogenic drugs or hereditary disorders [24]. On the other hand, NASH diagnosis is made using histological analysis indicating the presence of inflammation and hepatocyte ballooning (cellular damage), with or without the presence of fibrosis [24].

A recent meta-analysis revealed that the NAFLD prevalence worldwide is 32.4%, making it one of the most prevalent liver diseases globally. This prevalence is concerning, because it is already higher than the 25% global impact initially estimated [25]. An estimated projection is that 23% of Canadians will be diagnosed with NAFLD by 2030, severely impacting the Canadian health care system [26].

### *1.3.2 Current treatment options for NAFLD*

Currently there is no approved pharmacological treatment for NAFLD. However, lifestyle interventions aiming to decrease BW and, in specific cases, bariatric surgery are indicated to treat NAFLD [27]. A decrease in BW significantly improves liver steatosis, but no improvement in fibrosis is observed with BW loss [28]. There is an intensive search for drugs that can be repurposed to treat NAFLD such as pioglitazone, a peroxisome proliferator- activated receptor gamma (PPAR $\gamma$ ) agonist [29, 30]. Moreover, other drug classes have been or are under testing in clinical trials as reviewed [31, 32], including thyroid hormones, receptor  $\beta$  agonists, lipogenesis inhibitors, fibrogenesis inhibitors, modulators of bile acid metabolism, GLP-1 agonists and dual agonists (GLP-1/glucagon receptor), and SGLT-1 receptor inhibitors. For an overview of their mechanisms of action and current clinical trials I refer the reader to excellent reviews on the topic [31, 32]. Despite these efforts, NAFLD remains without approved pharmaceutical therapy.

## 1.4 Physiology of glucose homeostasis and metabolism

### 1.4.1 *Glucose absorption and blood glucose homeostasis*

Hyperglycemia is the main symptom characterizing diabetes. Blood glucose homeostasis depends on glucose absorption and, mainly, on the integrated functional antagonism between insulin and glucagon acting on peripheral tissues. After digestion, glucose is absorbed via SGLT, which is expressed on the apical membrane of enterocytes, and crosses the basolateral membrane of enterocytes via glucose transporter (GLUT)-2 to reach the systemic circulation [33].

Ingestion of nutrients, especially glucose, stimulates the pancreas to secrete insulin, a peptide hormone produced by the  $\beta$ -cells in the islets of Langerhans. Insulin then promotes a myriad of effects in insulin-sensitive tissues, including an increase of glucose uptake, which is further converted into energy or stored for future use. On the other hand, fasting stimulates the  $\alpha$ -cells in the pancreas to secrete glucagon. Glucagon acts mainly in the liver to promote gluconeogenesis, which increases blood glucose concentration and availability for metabolism [33].

It is worth noting that insulin actions can be counter-regulated by other hormones such as adrenaline, cortisol and growth hormone, and its secretion can be modulated by leptin and GLP-1, for example [34, 35]. However, given the scope of this thesis, in the following sections I will focus on insulin-mediated glucose uptake in the skeletal muscle and white adipose tissue (WAT), including the metabolic fate of glucose in those tissues. In addition, I will address the role of glucagon in the liver to regulate blood glucose homeostasis (Fig. 1.2.).

### 1.4.2 *Skeletal muscle glucose metabolism: glycolysis and glycogenesis*

The skeletal muscle is the main tissue responsible for the blood glucose uptake, playing an important role in blood glucose homeostasis [36]. Insulin-dependent glucose uptake in skeletal

muscle is initiated when insulin binds to its receptor, which undergoes autophosphorylation and tyrosine kinase activation. The activated insulin receptor then phosphorylates the insulin receptor substrate (IRS) leading to phosphatidylinositol-3 kinase (PI3K) activation. PI3K converts phosphatidylinositol (PIP)-2 into PIP3, which activates protein kinase B (AKT). The substrate for AKT is the Akt substrate of 160 kDa (AS160), which is localized on the membrane of intracellular vesicles containing GLUT4. AS160 activation allows the translocation of GLUT4 from the vesicles to the plasma membrane. The insertion of GLUT4 into the plasma membrane facilitates glucose entrance into the muscle cells via passive diffusion [37, 38]. Once inside the skeletal muscle cells, glucose has two main fates, glycolysis or glycogenesis (Fig. 1.2).

Glycolysis is the process of breaking down glucose to generate pyruvate. The rate-limiting enzymes in the first phase of glycolysis are hexokinase, which irreversibly converts glucose into glucose-6-phosphate (G6P) and phosphofructokinase 1, which converts fructose-6-phosphate to fructose-1,6-bisphosphate [39]. During the first phase of glycolysis, adenosine triphosphate (ATP) is consumed to eventually generate glycerol 3-phosphate (G3P). The metabolism of G3P initiates the second phase of glycolysis, which generates ATP. The second phase is mainly regulated by pyruvate kinase, an enzyme that irreversibly converts phosphoenol pyruvate to pyruvate, the final product of glycolysis [39]. In the presence of oxygen (aerobic glycolysis), pyruvate enters the mitochondria, where it is then metabolized via the tricarboxylic acid cycle to generate large amounts of ATP via oxidative phosphorylation (oxphos). In the absence of oxygen (anaerobic glycolysis), pyruvate is converted in lactate, which circulates to the liver to participate in gluconeogenesis [40].

The second fate of glucose in skeletal muscle is conversion into glycogen (glycogenesis). Glycogen is the main form of glucose storage in the skeletal muscle [33]. In glycogenesis, G6P

formed during glycolysis undergoes a series of reactions to eventually form glycogen, a process catalyzed insulin-dependently by glycogen synthase [40]. Glycogen formed in the skeletal muscle is not involved in later regulation of blood glucose homeostasis, as it mainly serves as an energy substrate for the muscle cells [40], but the initial uptake of glucose from the blood by skeletal muscle cells has a great influence on blood glucose homeostasis.

It is worth mentioning that glucose uptake in skeletal muscle may occur independently of insulin signaling. For example, exercise is shown to increase GLUT4 translocation to the plasma membrane of skeletal muscle cells in both healthy individuals and individuals with type 2 diabetes [41]. AMPK signaling is also well known to lead to glucose uptake independently of insulin and 5-aminoimidazole-4-carboxamide ribonucleotide, an AMPK activator increases GLUT4 translocation to the plasma membrane enhancing glucose uptake, as reviewed [42].

#### *1.4.3 White adipose tissue (WAT) glucose metabolism: glycolysis and de novo lipogenesis (DNL)*

WAT is the main site of energy storage of lipids, mainly in the form of TG. WAT glucose uptake is insulin-dependent, via GLUT4, a similar process to what happens in skeletal muscle (section 1.4.2). Inside the adipocyte, glucose undergoes glycolysis or participates in de novo lipogenesis (DNL) (Fig. 1.2). To form lipids (lipogenesis) a glycerol backbone is necessary, and adipocytes get glycerol from the hydrolysis of TG in the circulation, which is then phosphorylated into G3P. However, adipocytes may also get G3P via more efficient pathways, such as directly from glycolysis. In addition, during excess carbohydrate intake, the pyruvate generated by glycolysis participates in fatty acid formation from a non-lipid precursor, a process named DNL, contributing to overall lipid storage [43].

In DNL, pyruvate (from glycolysis, for example) enters the mitochondria and via the tricarboxylic acid (TCA) cycle is transformed into citrate. Citrate is exported to the cytoplasm where it is converted into acetyl-CoA by ATP-citrate lyase. Acetyl-CoA is then converted into malonyl-CoA, a step catalyzed by acetyl-CoA carboxylase (ACC). The rate-limiting enzyme in DNL is fatty acid synthase (FAS), which converts malonyl-CoA into palmitate, a fatty acid that can be later modified into other fatty acids by the action of stearoyl-CoA desaturase-1 (SCD1) [44]. Fatty acids are then esterified in TG and stored in the adipocytes. Blood glucose and insulin regulate lipogenesis via carbohydrate response element binding protein (ChREBP) [45] and sterol regulatory element binding protein-1 (SREBP-1) transcription factors, respectively [44, 46]. Therefore, glucose uptake in adipocytes is involved in the regulation of blood glucose homeostasis, although to a lesser extent than skeletal muscle.

#### *1.4.4 Hepatic glucose metabolism: glycogenesis, gluconeogenesis and DNL*

The liver is a key organ involved in glucose homeostasis; however, this involvement is more related to the role of the liver in producing glucose (gluconeogenesis) than increasing glucose uptake. GLUT2 is the most expressed isoform of glucose transporter isoform in the liver, being responsible for most glucose uptake in hepatocytes during feeding periods, an action that is independent of insulin signaling [47, 48]. GLUT2 provides efficient flux of glucose inside the hepatocytes, but also exports glucose to the blood stream after gluconeogenesis. Insulin decreases the expression of GLUT2, highlighting, perhaps, a more important function in hepatic glucose efflux rather than influx [47].

Similar to skeletal muscle cells, glycolysis happens in the liver (section 1.4.2). In hepatocytes, glucose substrate for glycolysis can be from the blood circulation (feeding) or generated by

gluconeogenesis (fasting). In addition, during feeding, glycolysis generates G6P, which participates in glycogenesis (section 1.4.2). The hepatic glycogen stores are used later to increase availability of glucose in the blood through glycogenolysis, a process mainly catalyzed by glucose-6-phosphatase, which converts G6P into glucose to be exported to the blood circulation [40] (Fig. 1.2).

Glucagon is involved in inhibiting glycogenesis and stimulating glycogenolysis to promote glucose availability [49]. However, the most physiologically important role of glucagon to regulate blood glucose homeostasis is the activation of gluconeogenesis. Gluconeogenesis is the process of generating glucose from non-carbohydrates precursors, for example from lactate, amino acids and fatty acids, which are converted into pyruvate to initiate the process [40]. During fasting, the drop in blood glucose concentration stimulates the release of glucagon from the pancreas, and glucagon acts in the liver via glucagon receptor to initiate a cascade via G-coupled proteins and adenylate cyclase causing an increase in cyclic AMP (cAMP), which activates protein kinase A (PKA). PKA activation is believed to be mechanism by which glucagon increases phosphoenolpyruvate carboxykinase expression and activity in the liver. phosphoenolpyruvate carboxykinase is one of the rate-limiting enzymes in the gluconeogenic pathway, where it converts oxaloacetate (generated from pyruvate) to phosphoenolpyruvate. Through a series of reactions phosphoenolpyruvate is eventually converted into G6P, which is then converted into glucose by glucose-6-phosphatase, the rate-limiting enzyme of the last step in the gluconeogenic pathway [49]. On the other hand, during periods of feeding, insulin has a potent inhibitory action on gluconeogenesis [50], an effect that can directly affect transcription of gluconeogenic genes (for example, via forkhead box O1 (FOXO1) inhibition) [51] or occur indirectly, via insulin action in other tissues, such as by decreasing adipose tissue lipolysis [52].

In the liver, glucose can also enter the DNL pathway. Although DNL was described above in adipocytes, in the liver is where most of DNL occurs. The process is similar to what was described in section 1.4.3. culminating in hepatic lipid storage in the form of TG. Therefore, the liver participates in blood glucose regulation through many processes, mainly through modulation of glycogenesis/glycogenolysis, gluconeogenesis and DNL (Fig. 1.2).

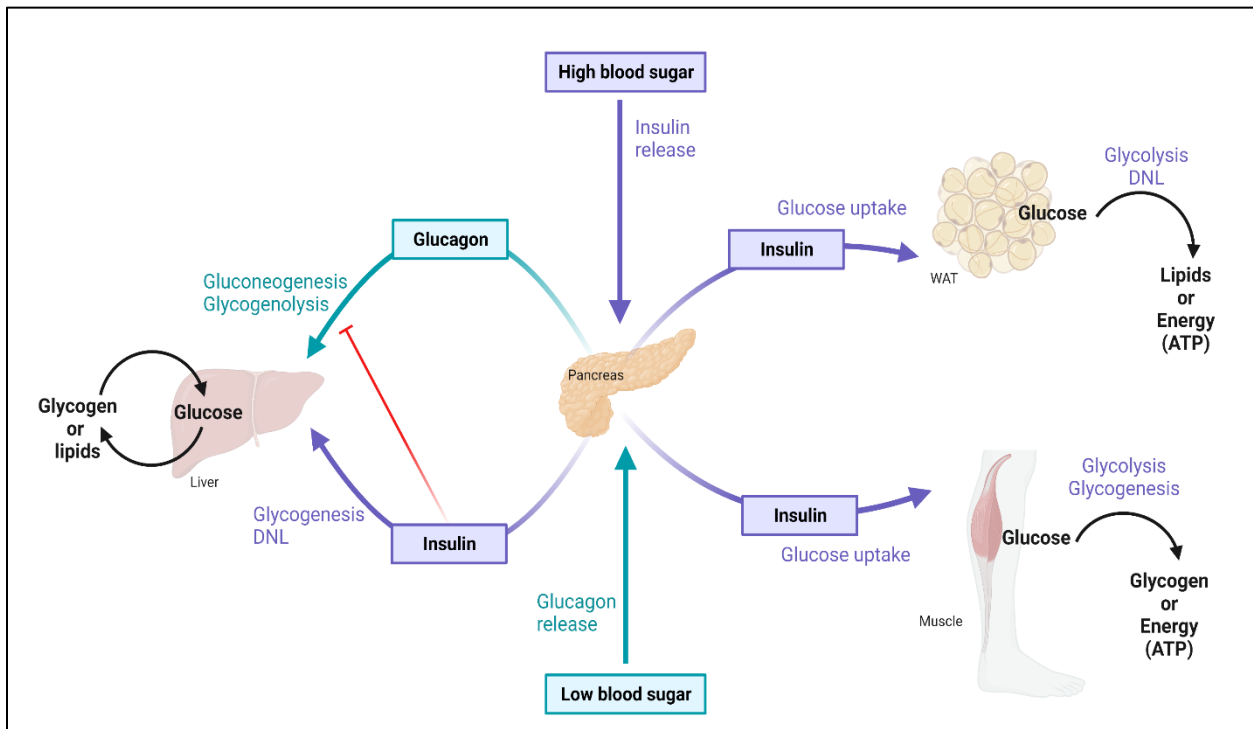


**Figure 1. 2. Blood glucose regulation and fate of glucose in the liver, skeletal muscle and white adipose tissue (WAT).** See text section 1.4.1; 1.4.2 and 1.4.3 for specific details. DNL, de novo lipogenesis. Created with Biorender.com.

## 1.5 Physiology of lipid metabolism

### 1.5.1 Lipid absorption and blood lipid homeostasis

The main form of dietary lipid ingested is TG. During the process of digestion, TGs are broken down to glycerol and fatty acids, which are absorbed by enterocytes. Inside the

enterocytes, they are re-esterified into TG and assembled into chylomicrons. Chylomicrons are then secreted by the enterocytes and enter the lymphatic system; from there they are drained by the subclavian veins into the systemic blood circulation [33, 53]. Chylomicrons are lipoproteins formed by a single phospholipid layer and proteins, with a core composed of neutral lipids (i.e., TG) and cholesterol esters. The microsomal triglyceride transfer protein (MTP) is an essential protein participating in chylomicron assembly [54]. The production of lipoproteins using lipids from endogenous sources (non-dietary lipids) happens in the liver, where very-low density lipoprotein (VLDL) is assembled and secreted into the circulation. From the circulation, lipoproteins deliver lipids to target tissues where they serve many purposes [54]. In addition, as mentioned above, excess carbohydrate intake can be converted into TG via DNL in the liver and WAT (section 1.4). Through the process of lipolysis, WAT-stored lipids are released into the circulation to be used as a fuel source by other tissues. Therefore, blood lipid homeostasis is a result of the amount of lipids absorbed by the intestinal cells and exported as chylomicrons, the uptake of lipids from the circulation in target tissues and the production and export of lipids from the liver (VLDL) and WAT (products of lipolysis). In the next sections I will focus on the lipid metabolism in WAT and in the liver.

### *1.5.2 White adipose tissue (WAT): lipogenesis and lipolysis and adipogenesis*

Lipoprotein lipase (LPL) is essential to initiate the breakdown of lipids in the circulation. LPL hydrolyses the TG from circulating lipoproteins, generating glycerol and fatty acids. While fatty acids are absorbed by adipocytes, hepatocytes and skeletal muscle cells for example, glycerol is transported to the liver where it takes part in the gluconeogenesis pathway (section 1.4.4) [53]. It is believed that most of the lipid uptake into cells is mediated by proteins. The first identified

fatty acid transporter was CD36 or fatty acid translocase [55], which is expressed by many tissues including the liver, WAT, skeletal muscle and immune cells. Other proteins involved in fatty acid uptake are fatty acid transporter proteins and very long-chain acyl-CoA synthetase. Once inside the cells, fatty acids bind to fatty acid binding proteins or are activated into acyl-CoA, a process catalyzed by acyl-CoA synthetases/ligases. After that, they are either metabolized or stored. When the amount of intracellular fatty acids exceeds the demand for cellular processes, they are stored as TG in lipid droplets (LD) [56].

The main pathway leading to TG formation and storage in adipocytes is the G3P pathway (Kennedy pathway) but the monoglyceride (MG) pathway may also be activated when intracellular lipids undergo lipolysis and MG is formed. In the G3P pathway, glucose and glycerol serve as substrates to be converted into G3P. Next, G3P is converted into phosphatidic acid through reactions catalyzed by G3P acyltransferases and acylglycerolphosphate acyltransferases, respectively. Phosphatidic acid is then converted into diglycerides (DG) by lipins. Finally, DG is converted into TG by diglyceride acyltransferases (DGATs). On the other hand, in the presence of MG, the process is shorter, and MG acyltransferases (MGATs) convert MG into DG followed by DGAT-catalyzed conversion of DG into TG [56].

LDs are considered a safe way to store lipids in a neutral form (TG) intracellularly. Lipolysis is the process through which TGs are broken down into glycerol and fatty acids to be released into the circulation [57]. LDs are coated with perilipins, proteins that maintain the structure and dynamics of LDs and the absence of perilipins in WAT leads to exacerbated lipolysis and resistance to diet-induced obesity [58, 59]. During fasting periods, with enhanced catecholamine release and  $\beta$ -adrenergic stimulation, lipolysis is activated [60, 61]. The first step in the canonical lipolysis pathway is an increase in cAMP, which activates PKA. PKA indirectly activates

adipose triglyceride lipase (ATGL), by promoting the release of comparative gene identification 58 (CGI-58), which is a coactivator of ATGL. In addition, PKA directly phosphorylates hormone-sensitive lipase (HSL) facilitating its translocation to the LD surface and also phosphorylates perilipins, which changes the LD organization to expose the lipids to the cytosolic lipases (ATGL, HSL) [62]. ATGL hydrolyses TG into DG, while HSL mainly hydrolyses DGs into MGs but can also catalyze the reaction of TG to DG. Lastly, monoacylglycerol lipase (MGL) hydrolyses MG into glycerol and fatty acids, which are exported to the blood stream [63]. It is worth mentioning that fatty acids can also be re-esterified into TG within the adipocytes, thereby adding another layer of control to regulate the amount of fatty acids released in the circulation [64].

During the fed state (postprandially, in the presence of insulin), perilipin sequesters CGI-58 and prevents HSL binding to the LD surface, thereby inhibiting lipolysis [65]. Lipolysis is strongly inhibited by insulin action, preventing the usage of endogenous energy sources, and shifting metabolism to use more glucose as fuel. Insulin inhibits lipolysis via phosphodiesterase 3B (PD3B) [66], which degrades cAMP, therefore reducing the amount of cAMP and inhibiting the canonical lipolysis cascade [63]. Despite AKT being part of the canonical insulin signaling, insulin suppression of lipolysis may happen independently of AKT [66], while insulin phosphorylation of HSL is dependent on AKT signaling [67]. Thus, WAT participates in blood lipid homeostasis by regulating lipid uptake, fatty acid release into the circulation (lipolysis) and fatty acid re-esterification.

It is important to differentiate the process of lipogenesis from adipogenesis. While lipogenesis refers to the formation of TG, adipogenesis refers to the formation of new adipocytes, through cell differentiation and maturation. The master regulator of adipogenesis is the PPAR $\gamma$ , which

acts in conjunction with CCAAT/enhancer binding protein  $\alpha$  (CEBP $\alpha$ ) to stimulate mitosis in adipose tissue [68, 69]. PPAR $\gamma$  is an adipogenic transcription factor and it also enhances lipogenic pathways to increase lipid accumulation in LD, therefore being involved in adipocyte maturation [69, 70]. Adipose tissue expansion in the context of insulin resistance will be discussed in section 1.6.

### 1.5.3 *Liver: fatty acid uptake, DNL, fatty acid oxidation and export*

The liver is a key organ involved in lipid metabolism. In terms of lipid uptake, the process occurs similarly as in WAT (section 1.5.2). As discussed above, although most of the lipids are ingested in the diet, fatty acids can also be synthesized endogenously from non-lipid precursors, such as carbohydrates, via DNL. This process happens primarily in the liver (section 1.4.4) but can also happen in WAT (section 1.4.3). The hepatic DNL contribution to the total pool of fatty acids in plasma is diet-dependent; for example, when fed diets low in fat content the rates of DNL in rodents are higher than when fed high-fat diets [71, 72]. In humans, diets high in carbohydrates enhance DNL, while high-fat diet decreases it [73, 74].

Regardless of their source (endogenous (DNL, lipolysis)/exogenous (diet)) if fatty acids exceed the liver demand for cellular process they are esterified into TG, mainly via the G3P pathway (section 1.5.2). In the liver TG will then be stored in LD or exported via VLDL. As mentioned before, insulin stimulates lipogenic pathways via SREBP-1 [44, 46].

VLDL assembly occurs in the hepatocytes, mostly in the endoplasmic reticulum (ER) and requires apolipoprotein B (apoB). Lipids for the assembly of VLDL are recruited by apoB or by MTP. Briefly, during the process of translation apoB undergoes lipidation with the help of MTP, an ER-localized protein that transfers TG to the apoB protein, initiating the clustering of TG with

apoB, forming a neutral lipid core. At the same time, regular cytosolic LDs (not associated with apoB) are being formed in the ER. This step is followed by addition of TG from the regular cytosolic LDs, giving rise to the mature VLDL particle that is exported by the liver into the circulation [54, 75]. Lipids used for VLDL assembly can be from DNL and from increased lipolysis from WAT, which increases fatty acid flux into the liver. VLDL contains many lipid species, including TG, phospholipids, and cholesterol [54].

The liver is a highly oxidative tissue and, interestingly, the master regulator of DNL, malonyl-CoA, is also the primary regulator of fatty acid oxidation. Malonyl-CoA is involved in both processes by regulating the activity of carnitine palmitoyltransferase 1 $\alpha$  (CPT1 $\alpha$ ) in the liver [76, 77]. When malonyl-CoA is decreased, such as during fasting, CPT1 $\alpha$  is more active, therefore more fatty acids undergo oxidation. During feeding periods, malonyl-CoA concentration increases, inhibiting CPT1 $\alpha$  and switching fatty acids' fate from oxidation to TG esterification and promoting DNL [76, 78]. The process of  $\beta$ -oxidation in the liver happens in the mitochondria and it generates ATP (via oxphos) and acetyl-CoA for ketone bodies. Briefly, fatty acids are converted into acyl-CoA by acyl-CoA ligases, and they enter the outer mitochondria membrane, where they are converted into acyl-carnitine by CPT1 $\alpha$  and transported through the inner mitochondria membrane by carnitine: acylcarnitine translocase. Once inside the mitochondrial matrix they are converted back to acyl-CoA to undergo oxidation. The process of oxidation starts with  $\beta$ -oxidation and the removal of carbons from the acyl-CoA generating acetyl-CoA. Next acetyl-CoA is converted into citrate by citrate synthase and oxidized to CO<sub>2</sub> via the TCA cycle [79]. Finally, flavin adenine dinucleotide (FADH) and nicotinamide adenine dinucleotide (NADH) generated from the citric acid cycle are used to generate ATP via the

electron transport chain [56, 80]. In summary, the liver is a key organ involved in blood lipid regulation, by regulating lipid uptake, oxidation, VLDL assembly and export (Fig. 1.3).

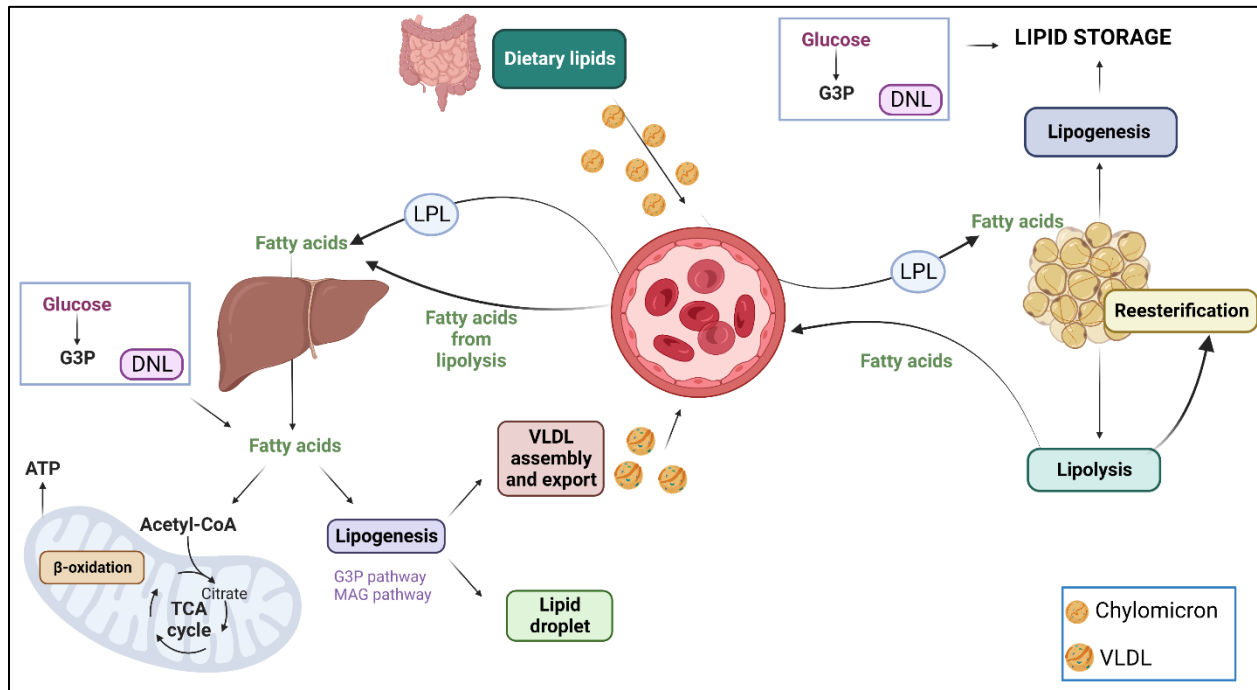


**Figure 1. 3. Pathways (simplified) involved in blood lipid regulation, the fate of lipids in the liver and white adipose tissue (WAT) and the contribution of DNL to lipid homeostasis.** See text section 1.5.2 and 1.5.3 for specific details. DNL, de novo lipogenesis; MG, monoglyceride; G3P, glycerol-3-phosphate; LPL, lipoprotein lipase. Created with Biorender.com.

## 1.6 Pathophysiology of type 2 diabetes

### 1.6.1 Systemic and tissue-specific insulin resistance

The hallmark of type 2 diabetes is insulin resistance. Insulin resistance is characterized by impaired insulin action in insulin sensitive tissues, leading to dysfunction in both glucose and lipid metabolism [81]. Therefore, it is important to consider changes happening systemically and in insulin-sensitive tissues when investigating insulin resistance.

Systemic insulin resistance refers to the whole-body impaired ability to respond to insulin action, therefore, impairing glucose and lipid homeostasis. Systemic insulin resistance in animal models is assessed by insulin tolerance tests (ITT) or by hyperinsulinemic-euglycemic clamp, the latter being the gold standard technique to assess this parameter [82]. In the ITT, if systemic insulin resistance is present, insulin administration fails to regulate glucose properly and higher plasma glucose concentration is seen for a prolonged time compared to healthy controls. While in the hyperinsulinemic-euglycemic clamp, if insulin resistance is present, insulin administration fails to suppress hepatic glucose production and fails to stimulate glucose uptake in skeletal muscle and WAT [83].

It was observed long ago that individuals with type 2 diabetes have impaired glucose disposal during the euglycemic-hyperinsulinemic clamp [83]. Moreover, hepatic glucose production is higher while plasma fatty acids is not suppressed by insulin and fatty acid oxidation is reduced [83, 84], suggesting insulin resistance. In these studies, the importance of peripheral tissues in regulating glucose disposal is emphasized. It is worth noting that not only impaired glucose disposal and hepatic glucose production account for the hyperglycemia seen in type 2 diabetes, but also a failure of  $\beta$ -cell function leading to decreased glucose-stimulated insulin secretion during the progressive stages of the disease [85, 86]. During the first stages of insulin resistance,  $\beta$ -cells secrete more insulin to compensate for the insulin resistance, thereby maintaining normoglycemia due to hyperinsulinemia. However, with time, the stress upon the cells leads to  $\beta$ -cell dysfunction, reflected as lower secretion of insulin and the onset of hyperglycemia, as reviewed [87]. Despite advancements in this field, there is evidence to support two different points of view in which 1) insulin resistance causes hyperglycemia leading to  $\beta$ -cell dysfunction or 2) hyperinsulinemia causes peripheral tissue dysfunction leading to insulin resistance; these

two situations are not mutually exclusive and may occur at the same time [88]. Nevertheless, both hypotheses culminate in hyperglycemia and dyslipidemia as major consequences of impairment in insulin signaling.

Given the underlying importance of impairment of peripheral glucose disposal and lipid metabolism to development of type 2 diabetes and related conditions, the focus of the following sections will be on insulin resistance in the WAT, liver and skeletal muscle.

### *1.6.2 WAT insulin resistance*

Obesity is a major risk factor for insulin resistance. In humans, the number of cells in subcutaneous WAT is defined during puberty, with an annual turnover of approximately 10%. Moreover, individuals with obesity and hypertrophied WAT (larger adipocytes) have a lower rate of adipogenesis, resulting in the need for old adipocytes to retain more lipids and expand even more in size [89], which is associated with detrimental effects. For example, adipose tissue expansion through hypertrophy is associated with higher plasma fasting insulin concentration and homeostatic model assessment of insulin resistance (HOMA-IR) [90]. Even in the absence of obesity, larger adipocytes are associated with increased insulin resistance and are positively correlated with inflammatory markers and lipolysis [91]. The term lipotoxicity refers to detrimental effects of excess lipid accumulation in non-adipose tissues (ectopic lipid accumulation), especially ceramides, DG, and cholesterol esters. These lipids cause inflammation, oxidative stress, mitochondrial dysfunction and insulin resistance eventually leading to cell death [92]. Impairment of WAT expansion induces lipid accumulation in non-adipose tissues [93], such as the liver and the skeletal muscle, which impairs insulin signaling via protein kinase C (PKC) activation for example, as reviewed elsewhere [81, 94].

On the other hand, prevention of PPAR $\gamma$  phosphorylation to prolong its activity improves insulin sensitivity, an effect associated with smaller adipocytes, despite similar fat mass [95]. A similar outcome is seen with troglitazone treatment, a potent PPAR agonist [96]. Moreover, enhanced insulin signaling in WAT is sufficient to restore systemic metabolic dysfunction, such as glucose intolerance and insulin resistance, and decrease hepatic lipid accumulation and WAT inflammation despite increased subcutaneous WAT mass [97]. Therefore, proper WAT expansion with preserved insulin signaling protects against ectopic lipid accumulation and systemic metabolic dysfunction. The importance of proper WAT expansion is emphasized in lipodystrophy, where insulin resistance and ectopic lipid accumulation is exacerbated, as reviewed [98].

The main systemic effects of insulin resistance in WAT are related to reduced insulin inhibition of lipolysis, impaired lipogenesis and, to a lesser extent, reduced glucose uptake [94]. For example, in 3T3-L1 adipocytes AKT silencing impairs insulin signaling and glucose uptake due to reduced GLUT4 translocation to the plasma membrane [99, 100]. In vivo, AKT ablation in WAT promotes lipodystrophy, insulin resistance and hepatic steatosis [101] and GLUT4 ablation in WAT decreases glucose uptake while inducing skeletal muscle and liver insulin resistance, glucose intolerance and hyperinsulinemia [102]. High-fat diet (HFD) feeding decreases AKT phosphorylation and increases HSL phosphorylation, leading to decreased insulin-stimulated glucose uptake and impaired insulin inhibition of lipolysis [103]. In fact, rats fed HFD have higher plasma insulin, TG, fatty acids and glycerol, suggesting increased lipolysis, effects attributed to phosphotyrosine interaction domain containing 1 (PID1), which impairs insulin action both in rodents and in 3T3-L1 cells [104]. Mice with mutated insulin receptor develop insulin resistance and, when challenged with HFD, present exacerbated WAT lipolysis,

providing extra substrate for DNL in the liver and contributing to hyperglycemia [105]. In addition, HFD-fed mice show enhanced basal lipolysis, but impaired catecholamine-stimulated lipolysis [106]. Impaired insulin inhibition of lipolysis, dysregulation of plasma fatty acids and enhanced hepatic glucose production are also seen in humans with type 2 diabetes, even independent of obesity [84, 107, 108], highlighting the close relationship between insulin resistance and lipolysis.

Despite changes in insulin's direct effect on WAT glucose and lipid metabolism, it is worth mentioning that WAT dysfunction is also related to altered secretion of adipokines, such as adiponectin and leptin. For example, decreased adiponectin is associated with increased insulin resistance, while adiponectin administration improves insulin resistance by reducing ectopic lipid accumulation and increasing lipid oxidation in the skeletal muscle [109, 110]. Leptin is involved in the regulation of food intake, glucose and lipid metabolism [111] and leptin concentration in plasma is correlated to fat mass, with obesity increasing and weight loss decreasing its plasma concentration [112]. Defective leptin physiology is present in two important animal models used in diabetes and obesity studies: the db/db mouse, which has a mutation of the leptin receptor [113] and the ob/ob mouse, which has a mutation in the gene encoding leptin, leading to leptin deficiency [114, 115]. In both cases impaired leptin signaling results in obesity and impaired glucose homeostasis leading to hyperglycemia [111]. Adipokine release and the inflammatory process during WAT expansion, although related to insulin resistance, are not the main focus of this thesis and I refer the reader to reviews on these topics [116, 117].

In summary, one of the major consequences of WAT insulin resistance is its impact on other tissues, such as inducing lipid accumulation in the liver and the skeletal muscle. Also, by

increasing fatty acid availability (due to impaired lipolysis inhibition), WAT contributes to hepatic gluconeogenesis, which affects blood glucose homeostasis.

### 1.6.3 *Liver insulin resistance*

Insulin resistance affects the liver directly and indirectly. Indirectly, WAT insulin resistance promotes excess fatty acid in the circulation, which can be captured by the liver leading to increased hepatic lipogenesis and gluconeogenesis. In addition, hyperglycemia due to impaired glucose uptake in skeletal muscle and WAT provides extra substrate for hepatic DNL. Directly, hepatic insulin resistance impairs the inhibitory action of insulin on gluconeogenesis, preventing the switch from glucose production to glucose utilization. Interestingly, although in healthy states insulin stimulates hepatic lipogenesis, one would expect that insulin resistance should then decrease this pathway. However, in obesity and type 2 diabetes a paradox is often observed, whereby hepatic insulin resistant is associated with higher activity of the lipogenic pathway, a process commonly referred to as selective insulin resistance [118].

The hypothesis of selective insulin resistance in the liver is supported by observations that despite hyperinsulinemia and impaired insulin signaling via IRS, insulin-stimulated SREBP-1 activity is enhanced in rodents [119]. In mice fed HFD, liver insulin IRS-2 is reduced, while IRS-1 is unchanged [120]. The specific liver knock out of IRS-1 or IRS-2 both induce glucose intolerance and insulin resistance, however, only IRS-1 knockout prevents hepatic lipid accumulation, decreases DNL and the expression of *Pparg*, *Fsp27* and *Cd36*, suggesting selective insulin resistance when IRS-2 is reduced and IRS-1 is intact [120]. Liver-specific deletion of both *Irs1/Irs2* induces complete insulin resistance [120]. This is consistent in obesity and type 2 diabetes models, where liver *Irs2* expression is dramatically reduced, while *Irs1* is

less affected [121]. Moreover, not only protein abundance, but insulin-stimulated IRS phosphorylation in muscle and liver is impaired in Zucker fatty rats [122]. Selective insulin resistance is also supported by observations in humans with NAFLD, where the hepatic expression of gluconeogenic genes is enhanced despite decreased *Irs2* expression, and hepatic lipid accumulation is present [123]. Moreover, the contribution DNL to hepatic lipid content is higher in obese individuals with NAFLD (40%) compared to lean (10%) and obese (20%) individuals without NAFLD. In this study, DNL is inversely correlated with hepatic and whole-body insulin sensitivity and positively correlated with plasma glucose and insulin values. In addition, weight loss is accompanied by a decreased in DNL [124].

Insulin inhibits hepatic gluconeogenesis via classical insulin signaling, in which p-AKT suppresses FOXO1 activity, therefore decreasing the activity of phosphoenolpyruvate carboxykinase and glucose-6-phosphatase, which decreases gluconeogenesis [125]. In fact, in individuals with obesity and type 2 diabetes, gluconeogenesis is exacerbated and insulin suppression of gluconeogenesis is impaired [126, 127]. Other studies in humans also support the idea of impaired inhibition of hepatic gluconeogenesis in individuals with insulin resistance [84, 108]. Failure to suppress hepatic glucose production is also seen in AKT2 knockout mouse models [128], while IRS knockout enhances expression of gluconeogenic enzymes [120], supporting evidence for the role of impaired hepatic insulin signaling in failure to suppress gluconeogenesis.

Insulin resistance is also associated with hypertriglyceridemia and lipid metabolism is impaired in individuals with type 2 diabetes [129]. A study in a subpopulation of the DiRECT trial shows that weight loss and type 2 diabetes remission decrease VLDL export, while weight re-gain in some of the individuals increases VLDL export and plasma TG [130]. Studies in

primary hepatocytes from rodents indicate that insulin inhibits apoB secretion and that hepatocytes from Zucker fatty rats have impaired insulin suppression of apoB, leading to postprandial hypertriglyceridemia [131]. Moreover, in *ob/ob* mice basal rates of VLDL production are similar to lean mice, while insulin suppression of VLDL production during a hyperinsulinemic clamp is impaired. This is associated with reduced insulin signaling [132]. Insulin may regulate VLDL secretion by inhibiting MTP via FOXO1 [133] and in HFD-induced obese mice and *db/db* mice, hypertriglyceridemia is associated with increased hepatic MTP protein abundance and FOXO1 nuclear localization [133, 134]. All of these corroborate that increased VLDL secretion downstream of insulin resistant states accounts for the hypertriglyceridemia seen in humans and rodent models of type 2 diabetes.

In summary, hepatic insulin resistance may lead to detrimental systemic and local effects, such as hypertriglyceridemia, hyperglycemia, and lipid accumulation in the liver. The role of insulin resistance in the underlying pathogenesis of NAFLD is discussed further in this thesis (section 1.7).

#### 1.6.4 *Skeletal muscle insulin resistance*

The major consequence of insulin resistance in skeletal muscle is impaired glucose uptake, which contributes to an increase in plasma glucose concentration. In type 2 diabetes impaired insulin signaling is the peripheral defect leading to hyperglycemia. Studies in rodents show that insulin signaling is impacted at different molecular sites in the skeletal muscle of obesity and type 2 diabetes models, for example AKT2 ablation in mice impairs skeletal muscle glucose uptake [128] and IRS-1 deficiency impairs insulin signaling in mice [135]. Moreover, in obese, insulin resistant mice *Irs1* and *Irs2* expression in skeletal muscle is reduced by 50% [121] and

HFD reduces skeletal muscle AKT phosphorylation [103], induces insulin resistance [136, 137] and impairs insulin-stimulated glucose uptake [138]. The disruption in insulin signaling is eventually reflected in reduced GLUT4 translocation to the plasma membrane, therefore, reducing insulin-stimulated glucose uptake in muscle, an effect seen in both rodents models of type 2 diabetes and obesity [139-141] and in humans [142], resulting in hyperglycemia.

As mentioned above, WAT insulin resistance induces ectopic lipid accumulation and increased lipid in skeletal muscle is associated with impaired insulin signaling and action [143]. Therefore, considering that the skeletal muscle is the main site of glucose disposal, insulin resistance in skeletal muscle accounts for a significant portion of the hyperglycemia in type 2 diabetes. It is clear from the sections above that the pathophysiology in type 2 diabetes is complex and involves inter-organ communication, which must be considered when interpreting any study findings.

#### *1.6.5 Consequences of insulin resistance: complications of hyperglycemia*

Uncontrolled hyperglycemia is associated with several complications, both macro and microvascular. The macrovascular complication is the increased risk for cardiovascular disease [144]. At the microvascular level, hyperglycemia is causally associated with retinopathy [145], nephropathy [146], neuropathy [147] and lower limb amputation [148]. The impact of these complications on the individual and on society emphasizes the need for optimized type 2 diabetes management for their prevention.

### **1.7 NAFLD: a disease involving a complex organ crosstalk**

NAFLD pathophysiology is a clear example of organ crosstalk, especially between the liver and WAT. However, more recently, the involvement of other organs in NAFLD pathogenesis is

becoming clearer. Moreover, the intrinsic relationship between other metabolic conditions such as obesity, type 2 diabetes, dyslipidemia and hypertension with NAFLD, makes the disease even more complex. Despite great advancements in this field, it is still unclear what drives disease progression. In the next sections I will focus on one of the most accepted hypotheses for NAFLD underlying pathophysiology and the consequences of untreated NAFLD.

### *1.7.1 The underlying mechanisms of NAFLD: The multi-hit hypothesis*

NAFLD results from the inability of the liver to properly dispose of fatty acids delivered to it or produced by DNL. The main pathways regulating lipid metabolism in the liver are uptake of fatty acids, DNL, fatty acid oxidation and VLDL secretion. The most accepted theory for NAFLD development is the multi-hit hypothesis, which accounts for many factors in disease initiation and progression, such as insulin resistance, adipokines, nutritional factors, epigenetics, gut microbiome, and genetics [149].

According to the multi-hit hypothesis, dietary habits (for example, high-fat/high-sugar diet) and genetic factors (for example, lipodystrophy) lead to a dysfunctional WAT. If WAT does not expand properly or if hypertrophy of adipocytes is exacerbated, then insulin resistance is initiated [149, 150]. The impaired capacity of WAT to retain lipids increases fatty acid availability in the circulation (hyperlipidemia) and these fatty acids can be taken up by the liver. Moreover, a dysfunctional WAT secretes pro-inflammatory molecules, such as tumor necrosis factor-alpha (TNF- $\alpha$ ) and interleukin-6 (IL-6) and decreases its secretion of adiponectin, all of which contribute to inflammation, insulin resistance and a pro-fibrotic environment [149, 150]. Adding to that, hepatic insulin resistance exacerbates DNL, contributing to the total amount of fatty acids requiring disposal by the liver. Increased fatty acids lead to TG accumulation and the formation

of toxic lipid species, causing lipotoxicity [149]. The increased fatty acid flux may increase fatty acid oxidation and elevate reactive oxygen species formation leading to mitochondria dysfunction [151]. Moreover, ER stress may occur, exacerbating the local inflammatory process. Changes in the gut microbiome seen with obesity or poor dietary habits increase pro-inflammatory cytokines and gut permeability to lipids, further affecting the liver. Lastly, genetic and epigenetic changes may enhance all of these processes, and chronic exposure to these changes leads to fibrosis development and eventually cirrhosis [149].

Many of the pathways mentioned above are, in fact, altered in NAFLD. For example, fatty acid transporter protein levels and possibly translocation are increased in patients with NAFLD compared to healthy individuals, suggesting increased capacity for fatty acid uptake [152]. DNL is exacerbated in NAFLD as mentioned above [124]. Mitochondrial function may be impacted in many instances, as reviewed [151] and ER stress is enhanced in the liver of individuals with NAFLD [153]. It is important to consider that these processes may occur concomitant with each other, and that the intensity of each process is variable across individuals with NAFLD. Nonetheless, multiple factors are involved in NAFLD pathogenesis, and many variables may be triggering disease progression, which remains to be clarified.

### *1.7.2 Progression of untreated NAFLD*

NAFLD refers to both simple steatosis and to NASH, which are reversible conditions [28]. However, if left untreated the consequences of NAFLD can be fatal. When NASH progresses to cirrhosis the advanced fibrosis leads to accumulation of non-functional hepatic tissue. In addition, cirrhosis may progress to hepatocellular carcinoma, which necessitates liver transplantation [154]. In fact, NASH has become the leading cause of hepatocellular carcinoma

in the United States of America [155]. Progression of untreated NAFLD impacts the individual's quality of life and increases health care costs associated with the disease. This highlights the need to find alternative approaches to mitigate hepatic steatosis progression to NASH.

## **1.8 Bioactive peptides and metabolic conditions**

### *1.8.1 Definition and the role of bioactive peptides in metabolic diseases*

Around 75% Canadians use a natural health product (NHP) daily [156], while 31% of people with diabetes use alternative medications to manage their disease [157]. Although there are guidelines for the use of complementary and alternative medicine for diabetes management [158], the use of NHP is not yet fully supported by clinical guidelines and practitioners due to a lack of randomized clinical trials and concerns about production and toxicity. Therefore, a process of pre-clinical study followed by clinical trials is necessary to increase the acceptability of NHP as therapies for metabolic conditions.

Under the NHP classification, among probiotics, herbal medicines and others, we encounter amino acids [159]. Peptides are short amino acid sequences and food-derived bioactive peptides (if not incorporated into foods) that can be classified as NHP. Moreover, they can potentially be classified as nutraceuticals, which are molecules with a proven physiological effect against chronic diseases that are isolated from food and sold in medicinal form [160]. Therefore, their classification depends on the form in which they are sold and consumed, and their proven beneficial effect.

Food-derived bioactive peptides are latent within the parent protein but are released after protein hydrolysis or fermentation [161, 162]. Many food proteins generate bioactive peptides, for example egg, fish, milk, soy [163]. The renin-angiotensin system (RAS) is the most studied

pathway affected by food bioactive peptides and the ability of several peptides to improve hypertension is extensively studied [164]. However, some peptides and hydrolysates also have potential to aid in the management of type 2 diabetes and obesity. Their effects range from improving insulin signaling, inflammation and lipid profile, to reducing BW or oxidative stress, as reviewed [165-167]. In addition, some protein hydrolysates promote beneficial effects in humans with type 2 diabetes by improving postprandial insulin response and glucose values, increasing plasma GLP-1, reducing HbA1c, BW and HOMA-IR [168-171].

The focus of this thesis is on egg white-derived bioactive peptides and hydrolysates. Although egg-derived hydrolysates have been tested in humans for their anti-hypertensive and cognitive effects [172-174], to my knowledge, there are no clinical trials completed or ongoing to test the beneficial effects of egg hydrolysate and peptides on insulin resistance and NAFLD.

### *1.8.2 Egg-derived peptides/hydrolysates and insulin resistance*

In preclinical models, egg-derived bioactive peptides improve obesity and insulin resistance [165]. For example, egg white hydrolysate (EWH) supplementation for 12 weeks decreases fasting plasma insulin, HOMA-IR and homeostasis model assessment of  $\beta$ -cell function (HOMA- $\beta$ ), without changes in fasting plasma glucose concentration in Zucker fatty rats [175]. In Wistar rats, 10 weeks supplementation with EWH prevents diet-induced obesity by decreasing fat mass, adipocyte size, and oxidative stress markers such as plasma malondialdehyde [176]. The same EWH (11 weeks of supplementation) decreases resistin gene expression in WAT, while enhancing the expression of genes involved in oxidative metabolism in brown adipose tissue, including *Ppargc1a*, *Cpt1b*, *Ucp1* and *Ppara*. These effects are accompanied by enhanced mitochondrial DNA and expression of mitochondria dynamics-related genes in brown adipose

tissue [177]. The authors suggest increased thermogenesis as the main mechanism observed in these studies [175, 176]. Other researchers supplemented Goto-Kakizaki rats with EWH for 6 weeks, leading to decreased BW, fasting glucose, HOMA-IR and lipid accumulation in skeletal muscle [178]. Only the prevention of ectopic lipid accumulation is reproduced in Wistar rats following the same study protocol [178]. In type 2 diabetic Nagoya-Shibata-Yasuda mice, EWH supplementation for 8 weeks improves oral glucose tolerance test (OGTT) without improvements in the ITT [179]. A recent study shows that IRW and IQW (two egg-derived bioactive peptides) supplementation for 8 weeks reduces fasting glucose and leptin while increasing adiponectin plasma concentration in diet-induced obese mice. These results are accompanied by improvements in OGTT and ITT [180]. Although improvements in metabolic parameters related to insulin sensitivity are observed in these studies, insulin signaling is not a primary outcome in any of them.

### *1.8.3 Egg-derived peptides/hydrolysates and NAFLD*

Egg peptides and hydrolysates also promote beneficial effects in NAFLD-related markers. For example, EWH supplementation for 12 weeks decreases plasma fatty acids and liver steatosis in Zucker fatty rats, together with decreased plasma malondialdehyde [181]. In Wistar rats, EWH supplementation for 8 weeks decreases diet-induced hepatic lipid accumulation and FAS activity, while increasing fat excretion in the feces [182]. In another study, EWH decreases liver cholesterol and TG accumulation and reduces the Stearoyl-CoA Desaturase (SCD) Index, while increasing cholesterol excretion in the feces of Wistar rats [183]. In Goto-Kakizaki rats, EWH decreases hepatic SCD Index without changing hepatic TG content [178]. Supplementation with EWH for 14 days prevents orotic acid-induced NAFLD in Sprague-Dawley rats, shown by

decreased hepatic TG content and serum aspartate aminotransferase. Plasma lipids are drastically decreased in orotic acid-treated animals compared to control while EWH restores hepatic VLDL secretion (measured by MTP abundance) and by increasing the formation of phospholipids in the liver to normalize circulating lipids [184]. Although EWH does not change hepatic TG during fasting, EWH tends to decrease fed state liver TG content in Nagoya-Shibata-Yasuda mice. This effect is accompanied by increased fat excretion in the feces of the animals [179]. IRW and IQW decrease gene expression of *Dgat1*, *Dgat2*, *Tnfa*, *Il6* and *Il1b* in the liver of mice supplemented for 8 weeks, but only IQW decreases hepatic cholesterol and TG accumulation [180]. These results indicate that egg hydrolysates and peptides may improve multiple aspects of NAFLD, such as an oxidative stress, inflammation and lipid accumulation, highlighting the fact that many mechanisms may be involved in these beneficial effects.

#### *1.8.4 Previous relevant work using IRW and EWH performed by our group*

Our group has extensively studied EWH and egg-derived peptides. IRW is a tripeptide (isoleucine-arginine-tryptophan) derived from ovotransferrin [185], while EWH is a mixture of bioactive peptides generated from hydrolysis of the whole egg white [186]. Both are generated after pepsin and thermolysin hydrolysis [185, 186]. Initially, they were identified as angiotensin converting enzyme (ACE) inhibitors and their effects in reducing blood pressure were shown in spontaneously hypertensive rats [186, 187]. Moreover, studies *in vitro* and *in vivo* now demonstrate their potential to decrease inflammation and oxidative stress in the cardiovascular system [186, 188-190]. Because of the crosstalk between hypertension, inflammation, obesity and insulin resistance, our group has the overarching hypothesis that IRW and EWH will also exhibit activities relevant to obesity and type 2 diabetes.

In this context, we used cell culture models to demonstrate that IRW improves angiotensin-II-induced insulin resistance in L6 myoblasts via decreasing angiotensin type 1 receptor (AT1R) protein abundance, promoting antioxidant effects and AKT phosphorylation and glucose transporter 4 (GLUT4) translocation to the plasma membrane of the cells [191]. In addition, IRW also improves TNF- $\alpha$ -induced insulin resistance in L6 cells by promoting similar effects [192]. In L6 cells and in muscle and liver of mice, IRW increases nicotinamide phosphoribosyltransferase (NAMPT), an effect accompanied by increase in sirtuin 1 (SIRT1) protein abundance in the liver [193]. SIRT1 overexpression protects against HFD-induced metabolic damage in mice [194] and decreased SIRT1 is associated with NAFLD in rats [195]. Therefore, it is worth exploring the effect of IRW on key organs involved in metabolic diseases such as skeletal muscle, WAT and liver, which is the focus of this thesis.

EWH also shows promising beneficial effects in this context. For example, EWH improves TNF- $\alpha$ -induced insulin resistance in L6 myoblasts [192] and stimulates adipocyte differentiation, adiponectin secretion, reduced inflammatory markers and sensitized preadipocytes to insulin action *in vitro* [196]. Obese, insulin resistant rats fed 4% EWH have improved glucose tolerance and insulin sensitivity, accompanied by enhanced insulin signaling in skeletal muscle and WAT, reduced adipocyte size and inflammatory markers in plasma, enhanced PPAR $\gamma$  in WAT and increased angiotensin II type 2 receptor (AT2R) protein in WAT and liver [197]. These activities of EWH led us to identify specific peptides from EWH with adipogenic effects *in vitro* [198]. However, the *in vivo* effects of these individual peptides are unknown. Therefore, investigating their activity *in vivo* is one of the objectives of this thesis.

## 2. CHAPTER 2: Hypothesis and objectives

### 2.1 Hypothesis

Based on literature review and previous work done by our group, I hypothesize that dietary supplementation with egg white-derived bioactive peptides will improve diet-induced insulin resistance and prevent NAFLD development in obese, glucose intolerant mice.

Specifically, I expect that these peptides will exert beneficial effects by improving skeletal muscle and WAT insulin signaling and by increasing hepatic lipid oxidation.

### 2.2 Overall aims

The overall aim of this thesis is to investigate the ability of specific peptides derived from the egg white to reverse HFD-induced insulin resistance in WAT and skeletal muscle and to prevent NAFLD in C57BL/6 mice.

### 2.3 Specific objectives

The specific objectives of this thesis are:

***#1 To (a) screen four different specific peptides identified in the EWH with adipogenic capacity in vitro for their ability to promote beneficial metabolic effects related to obesity and insulin sensitivity in vivo and (b) select a candidate for further characterization.***

For the completion of this specific objective, an *in vivo* study using C57BL/6 mice was conducted as exemplified in Fig. 2.1. Key outcomes were BW and body composition, glucose tolerance and insulin sensitivity. Four different EW-derived peptides previously found to

increase PPAR $\gamma$  in adipocyte cell culture [198] were screened to identify the most promising peptide to elicit *in vivo* metabolic changes. Rosiglitazone is a PPAR $\gamma$  agonist and known insulin sensitizer; therefore, a positive control group treated with rosiglitazone was included (ROSI). After the completion of this objective, I found that Peptide2 treated animals had improved insulin sensitivity and decreased inguinal and retroperitoneal fat mass. For this reason, it was selected for further characterization.

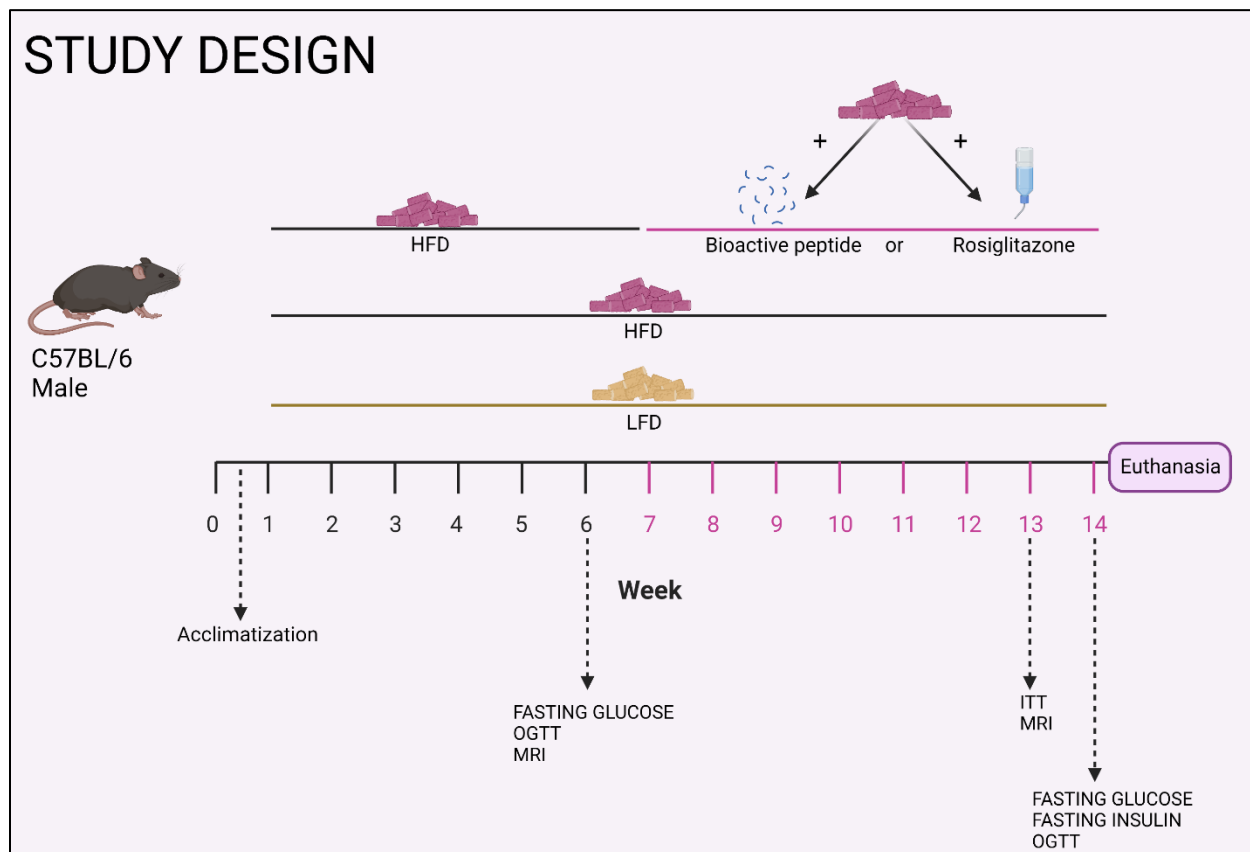


**Figure 2. 1. General study design.** LFD, low-fat diet; HFD, high-fat diet; OGTT, oral glucose tolerance test; ITT, insulin tolerance test; MRI, magnetic resonance imaging.

***#2 To identify metabolic effects and mechanistic pathways of Peptide 2 supplementation in diet induced obese-insulin resistant mice focusing on the WAT and liver.***

2a) To characterize the metabolic phenotype of mice fed HFD supplemented with Peptide 2.

2b) To evaluate WAT insulin signaling, lipolysis, adipogenesis potential and morphology.

2c) To investigate hepatic expression of genes involved in lipid metabolism and to characterize NAFLD features morphologically.

To complete objective #2a, the same study design as in objective #1 (Fig. 2.1) was conducted but comparing only Peptide 2 to HFD, low fat diet (LFD) and ROSI controls (n=8-10 animals/group). Key metabolic outcomes were glucose tolerance, insulin sensitivity and body composition. To complete objective #2b, *ex vivo* lipolysis and protein abundance of p-AKT and key target involved in adipogenesis were measured. Moreover, PPAR $\gamma$  activation and adipocyte size were investigated in WAT. For the completion of objective #2c, changes in lipid metabolism, inflammation and fibrosis gene expression in liver were measured and NAFLD features were characterized in histological samples.

***#3 To investigate the effect of IRW (a tripeptide derived from EW) on plasma RAS components, systemic insulin sensitivity and insulin signaling in skeletal muscle and WAT of obese, glucose intolerant mice.***

3a) To characterize metabolic phenotype and systemic insulin sensitivity of mice fed IRW.

3b) To quantify RAS components' plasma activity and skeletal muscle protein abundance.

3c) To investigate skeletal muscle insulin signaling, muscle synthesis pathway and AMPK $\alpha$  activation.

3d) To investigate insulin signaling, adipogenesis, AMPK $\alpha$  and thermogenesis pathways in visceral WAT.

To complete objective #3, an animal trial was conducted similarly as in objective #1 (Fig. 1.1) but changing the diet supplementation to IRW (n=8 animals/group, 45 mg/kg BW). At the end of the trial all the animals were injected with insulin intraperitoneally prior to euthanasia. For objective #3a key outcomes were glucose tolerance, insulin sensitivity and BW. To complete #3b, angiotensin II, angiotensin 1-7, ACE and ACE2 plasma activity were measured. In addition, AT1R, AT2R, angiotensin (1-7) receptor (MasR), ACE and ACE2 protein abundance in skeletal muscle was measured. For the completion of objective #3c, p-AKT, plasma membrane GLUT4, PPAR $\gamma$  and AMPK $\alpha$  protein abundance was measured in skeletal muscle. In addition, gene expression of muscle synthesis targets was analysed. To complete objective #3d, p-AKT, uncoupling protein 1 (UCP-1), PPAR $\gamma$  and AMPK $\alpha$  were measured in WAT.

***#4 To characterize the mechanisms of action of IRW in preventing HFD-induced NAFLD.***

4a) To investigate the phenotype of HFD-fed mice after IRW supplementation.

4b) To conduct a quantitative analysis of visceral adipocyte morphology and adipogenesis.

4c) To identify alterations in liver lipid accumulation and NAFLD features.

4d) To investigate hepatic lipid metabolism and mitochondrial related genes.

For objective #4, another animal trial was conducted as in objective #1 (Fig. 1.1) but changing the intervention to IRW (n=8 animals/group, 45 mg/kg BW). This animal trial was conducted in collaboration with another student in Dr. Jianping Wu's lab, who focused on skeletal muscle- and plasma-related outcomes. Main outcomes for objective #4a were body composition and OGTT. For objective #4b, adipocyte size and protein abundance of FAB4, PPAR $\gamma$ , adiponectin and perilipin 1 were measured. To complete objective #4c, NAFLD features were investigated. To complete objective #4d, the expression of genes involved in lipid metabolism and mitochondrial function were analyzed in liver tissue. In addition, p-AMPK $\beta$ , p-AMPK $\alpha$ , CPT1 $\alpha$ , p-ACC1, FAS and mitochondria oxidative phosphorylation (oxphos-complexes I-V) protein abundance was measured.

### **3. CHAPTER 3: An egg white-derived peptide enhances systemic insulin sensitivity and modulates markers of non-alcoholic fatty liver disease in obese, insulin resistant mice**

This section reflects the outcomes from experiments undertaken to address objectives #1 and #2. I participated in the study design, performed the experiments, analyzed the data, and prepared the manuscript for submission under the supervision of Dr. Catherine Chan and co-supervision of Dr. Jianping Wu. For this work I had help from Dr. Jessica Yue's, Dr. Robin Clugston's and Dr. Marcelo Mori's teams in interpreting the data and conducting the experiments related to euglycemic-hyperinsulinemic clamp, liver qPCR and *in vitro* studies, respectively. In addition, Ren Wang participated in performing the experiments as an undergraduate student under my supervision. This manuscript was published in the journal *Metabolites* in January 2023 [199]. A PDF version of the manuscript is provided in Appendix 2.

**An egg white-derived peptide enhances systemic insulin sensitivity and modulates markers of non-alcoholic fatty liver disease in obese, insulin resistant mice**

Stepheny C. de Campos Zani <sup>1,2</sup>, Ren Wang <sup>3</sup>, Hellen Veida-Silva <sup>1,2</sup>, Robin D. Clugston <sup>1</sup>, Jessica T.Y. Yue <sup>1,2,4</sup>, Marcelo A. Mori <sup>5</sup>, Jianping Wu <sup>3</sup> and Catherine B Chan <sup>1,2,3, \*</sup>

<sup>1</sup>Department of Physiology, University of Alberta, Edmonton, T6G2H7, AB, Canada; zani@ualberta.ca; hellen@ualberta.ca; clugston@ualberta.ca; jessica.yue@ualberta.ca; cbchan@ualberta.ca

<sup>2</sup>Alberta Diabetes Institute, University of Alberta, Edmonton, Alberta, Canada, Edmonton, T6G2E1, AB, Canada

<sup>3</sup>Department of Agricultural Food & Nutritional Science, University of Alberta, Edmonton, T6G1C9, AB, Canada; rwang5@ualberta.ca; jwu3@ualberta.ca

<sup>4</sup>Molecular and Cell Biology of Lipids Group, University of Alberta, Edmonton, T6G2H7, AB, Canada

<sup>5</sup>Department of Biochemistry and Tissue biology, University of Campinas, POBox 6109, Campinas, Brazil; morima@unicamp.br

\*Correspondence: cbchan@ualberta.ca; Tel.: +1-780-492-9964

## Abstract

Non-alcoholic fatty liver disease (NAFLD), the hepatic manifestation of the metabolic syndrome, is a global health problem. Currently, no pharmacological treatment is approved for NAFLD. Natural health products, including bioactive peptides, are potential candidates to aid in the management of metabolic syndrome-related conditions, including insulin resistance and obesity. In this study, we hypothesized that an egg white-derived bioactive peptide QAMPFRVTEQE (Peptide 2) would improve systemic and local WAT insulin sensitivity, thereby preventing HFD-induced exacerbation of pathological features associated with NAFLD, such as lipid droplet size and number, inflammation, and hepatocyte hypertrophy in HFD-fed mice. Similar to rosiglitazone, Peptide 2 supplementation improved systemic insulin resistance during the hyperinsulinemic-euglycemic clamp and enhanced insulin signaling in WAT, modulating *ex vivo* lipolysis. In the liver, compared with HFD-fed animals, Peptide 2 supplemented animals presented decreased hepatic cholesterol accumulation ( $p < 0.05$ ) and area of individual hepatic lipid droplet by around 50% ( $p = 0.09$ ) and reduced hepatic inflammatory infiltration ( $p < 0.05$ ) whereas rosiglitazone exacerbated steatosis. In conclusion, Peptide 2 supplementation improved insulin sensitivity and decreased hepatic steatosis, unlike the insulin-sensitizing drug rosiglitazone.

**Keywords:** Bioactive peptides; egg; metabolic syndrome; non-alcoholic fatty liver disease; type 2 diabetes

### 3.1 Introduction

Metabolic syndrome pathophysiology exemplifies a clear crosstalk between major metabolic organs, including the liver and WAT. NAFLD affects 25% of the global population and is strongly associated with obesity, type 2 diabetes/insulin resistance, and dyslipidemia. All of these conditions are a public health concern and beget socioeconomic problems [200]. Hepatic steatosis in NAFLD results from an imbalance between substrate availability (fatty acids and carbohydrates) and the hepatic capacity to dispose of fats properly. In humans, the two main sources of non-esterified fatty acids (NEFA) in the liver are WAT lipolysis and DNL [201]. DNL produces fatty acids from non-lipid precursors such as glucose or fructose and is increased in insulin resistant states [124], and plays an important role in NAFLD [202]. NAFLD may progress to NASH in which inflammation, fibrosis and cellular damage are present, then to cirrhosis and further to hepatic cancer, increasing the need for liver transplantation [201] and seriously impacting quality of life.

Lifestyle interventions (diet and physical activity) improve NAFLD, but currently no pharmacological treatment is approved for NAFLD. Several drugs, including thiazolidinediones (PPAR $\gamma$  agonists that are insulin sensitizers) are being investigated as therapies to reduce hepatic steatosis, inflammation, and fibrosis [20, 203]. However, findings are controversial [204, 205]. Natural health products and functional foods include potential candidates to aid in the management of metabolic conditions. Food-derived bioactive peptides have effects beyond their nutritive value and can modulate physiological processes promoting health benefits [206]. There are many food sources of bioactive peptides, including the egg, a universally available and consumed source of protein.

Previously, our group showed that an egg white hydrolysate (EWH) alleviates hypertension [186] and insulin resistance in rat models [197], and mimics insulin action in preadipocytes [196]. In addition, IRW, a specific peptide found in the EWH improves hypertension [187] and insulin resistance in rodents [207]. Another peptide identified in the EWH is QAMPFRVTEQE (aka Peptide 2), which mimics insulin actions to enhance PPAR $\gamma$  protein abundance and other markers of adipogenesis in preadipocyte cell culture [198] but the *in vivo* efficacy of Peptide 2 is not established.

Considering the need of new therapies for NAFLD and the crosstalk between insulin signaling, WAT and the liver, we aimed to identify specific effects of Peptide 2 diet supplementation on manifestations of the metabolic syndrome including systemic IR, WAT response to insulin and NAFLD markers, compared with the thiazolidinedione rosiglitazone. We hypothesized that Peptide 2 supplementation improves systemic and local insulin sensitivity, which in turn alleviates pathological cellular features associated with NAFLD, therefore modulating both glucose and lipid metabolism.

## **3.2 Materials and Methods**

### *3.2.1 Animals and Diets*

Protocol 1: This protocol and some results of a previous intervention trial were previously published by our group [197]. Briefly, male Sprague Dawley (SD) rats (n = 48) were fed with HFD for 6 weeks. Then, half of the animals received HFD+4% EWH with the remainder serving as HFD controls for another 6 weeks. At the end of week 12, half of the animals received an intraperitoneal injection of insulin (2 IU/kg of BW) to stimulate insulin signaling prior to euthanization using CO<sub>2</sub>. Diet composition was published elsewhere [197] and was matched for

macronutrient and energy content. Herein, we report lipolysis pathway data from WAT tissues; a full description of the rat phenotype after EWH treatment is published elsewhere [197].

Protocol 2: Male C57BL/6 mice (5 weeks old) purchased from Charles River Canada were housed 4/cage with *ad libitum* access to food and water, exposed to 12:12 h light: dark in a humidity- and temperature-controlled environment (60% humidity, 23 °C). Mice received a low-fat diet (LFD, 10% kcal fat) or a HFD (HFD, 45% kcal fat) for 6 weeks. After that, the HFD animals were divided into 3 groups: HFD only, HFD + Peptide 2 (PEP2) and HFD + rosiglitazone (ROSI) and continued receiving their respective diets for another 8 weeks. LFD animals continued receiving LFD for another 8 weeks. After a total of 14 weeks, mice either received an intraperitoneal injection of insulin (1.5 IU/kg BW) prior to euthanasia or were directly euthanized using CO<sub>2</sub>, while some mice underwent hyperinsulinemic-euglycemic clamp prior to euthanasia by ketamine. Diet composition is shown in Table 3.1. Peptide 2 was administered at 45 mg/Kg BW/day daily mixed in the diet. The characteristics of Peptide 2 are reported in Table 3.2 [198]; it was synthesized by Genscript (Piscataway, NJ, USA) with 97.9% compound purity and no terminus modifications. Peptide 2 is soluble in water, dimethyl sulfoxide and phosphate-buffered saline at a concentration  $\leq 10$  mg/mL. High performance liquid chromatography chromatogram and the mass spectra of the peptide provided by Genscript are shown in Fig. 3.1. Rosiglitazone (Sigma-Aldrich, ST. Louis, MA, USA) was administered at 2.5  $\mu\text{mol/kg}$  BW/day in the drinking water.

**Table 3. 1 Diet composition.**

	<b>LFD</b>	<b>HFD</b>	<b>HFD+PEP2</b>	<b>HFD+ROSI</b>
<b>Casein (g/Kg)</b>	210.0	245.0	245.0	245.0
<b>L-Cystine (g/Kg)</b>	3.0	3.5	3.5	3.5
<b>Corn Starch (g/Kg)</b>	445.0	85.0	85.0	85.0
<b>Maltodextrin (g/Kg)</b>	50.0	115.0	115.0	115.0
<b>Sucrose (g/Kg)</b>	160.0	200.0	200.0	200.0
<b>Lard (g/Kg)</b>	20.0	195.0	195.0	195.0
<b>Soybean Oil (g/Kg)</b>	20.0	30.0	30.0	30.0
<b>Cellulose (g/Kg)</b>	37.15	58.0	58.0	58.0
<b>Mineral Mix, AIN-93G-MX (94046) (g/Kg)</b>	35.0	43.0	43.0	43.0
<b>Calcium Phosphate, dibasic (g/Kg)</b>	2.0	3.4	3.4	3.4
<b>Vitamin Mix, AIN-93-VX (94047) (g/Kg)</b>	15.0	19.0	19.0	19.0
<b>Choline Bitartrate (g/Kg)</b>	2.75	3.0	3.0	3.0
<b>PEP2 (mg/Kg BW)</b>	n/a	n/a	45.0	n/a
<b>Rosiglitazone (<math>\mu</math>M/Kg BW in water)</b>	n/a	n/a	n/a	2.5

**Table 3. 2. Peptide 2 specifications.**

<b>Peptide 2</b>	
Amino acid sequence	QAMPFRVTEQE
Number of amino acids	11
Theoretical molecular weight (g/mol) *	1335.50
Observed molecular weight (g/mol)	1335.8
<i>Theoretical</i> isoelectric point *	4.53
Grand average of hydropathicity (GRAVY) *	-0.918
Hydrophobicity *	22
Terminus modifications	None
Net charge at pH 7.0 *	-1

\* Parameters calculated using online tools: *ProtParam (Expasy)*; *Bachem peptide calculator* and *ThermoFischer Peptide analyzing tool*. Observed molecular weight provided by *Genscript*.

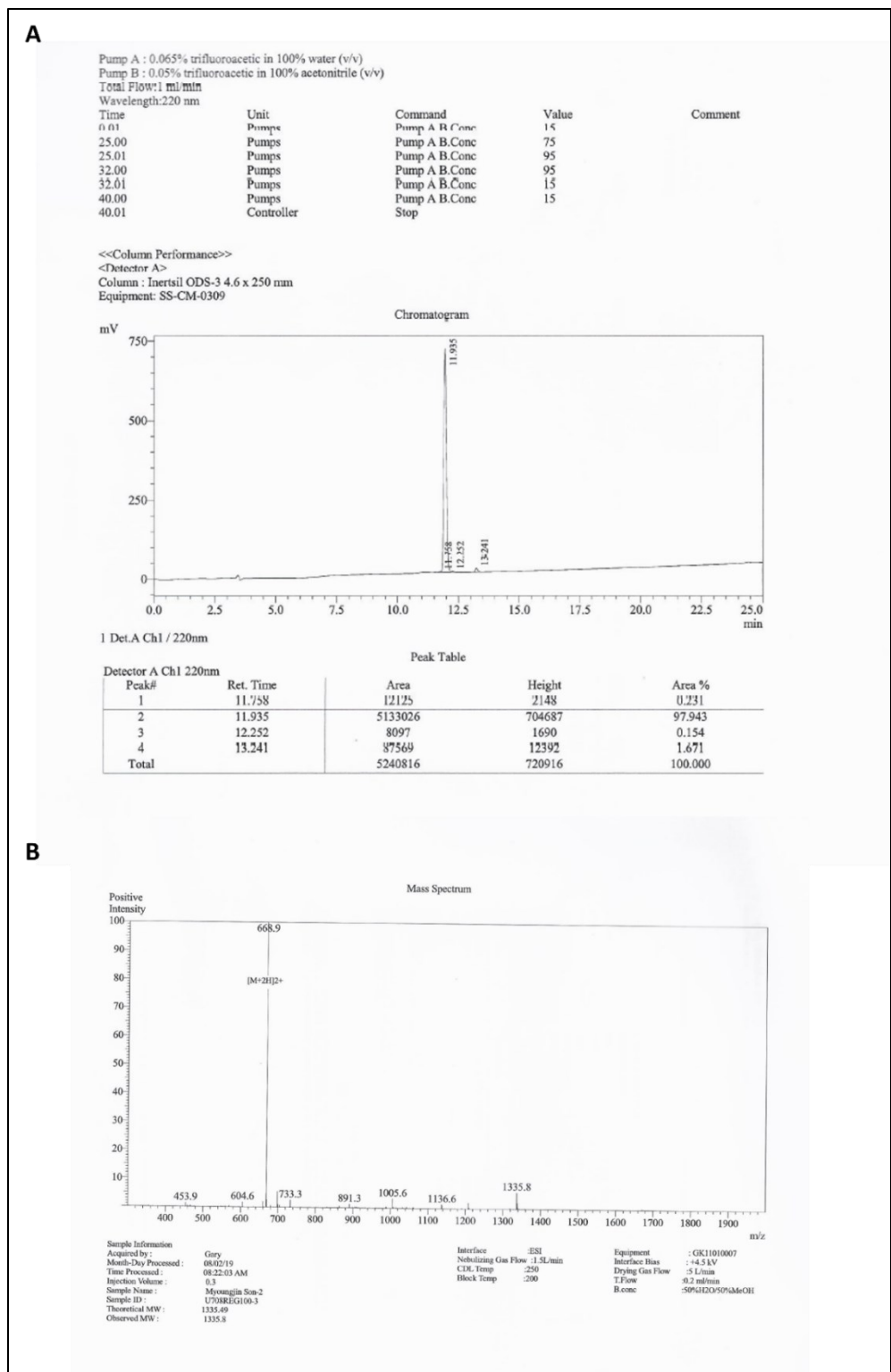


**Figure 3. 1. Peptide 2 chromatograph.** High performance liquid chromatography (A) and mass spectrometry (B).  
Provided by Genscript.

### 3.2.2 *BW, Body Composition and Sample Collection*

Mice were weighed weekly. Body composition was measured at week 14 in fasted conditions using an ECHO magnetic resonance imaging (ECHO MRI) as per manufacturer's instructions. Blood was collected by cardiac puncture into EDTA tubes and plasma was stored at  $-80^{\circ}\text{C}$  until further analysis. Liver and WAT (retroperitoneal (rWAT), epididymal (eWAT) and inguinal (iWAT)) were collected, weighed and snap frozen in liquid nitrogen. A sample of each tissue was fixed in formalin, dehydrated, and preserved in paraffin blocks for histological analysis.

### 3.2.3 *Adipose Tissue Organ Culture*

During tissue collection, a piece of approximately 100 mg each and of each fat pad (iWAT, eWAT and rWAT) were collected and washed with cold phosphate-buffered saline + 1% penicillin/streptomycin (Gibco, Waltham, MA, USA) and kept in M199 media (Sigma-Aldrich, St. Louis, MA, USA) supplemented with 50  $\mu\text{U}$  insulin (Sigma-Aldrich, St. Louis, MA, USA), 2.5 nmol/L dexamethasone (Sigma-Aldrich, St. Louis, MA, USA) and 1% penicillin/streptomycin in a cell incubator at  $37^{\circ}\text{C}$  and 5%  $\text{CO}_2$  for 24 h. After that, the media was replaced with fresh M199 supplemented only with 2.5% fatty acid-free bovine serum albumin (MP Biomedicals, Santa Ana, CA, USA). Each piece received one of the following treatments: sterile  $\text{H}_2\text{O}$  or norepinephrine (1  $\mu\text{M}$ , Sigma-Aldrich, St. Louis, MA, USA) or norepinephrine (1  $\mu\text{mol/L}$ ) + insulin (1 IU/mL) for 2 h. An aliquot of the media was collected after 2 h and kept at  $-80^{\circ}\text{C}$  for future glycerol analysis.

### 3.2.4 *Preadipocyte Cell Culture*

Preadipocytes derived from mouse inguinal WAT (9W) and from brown adipose tissue (9B) were cultured and differentiated as previously described [208]. Briefly, cells were cultured in Dulbecco's modified Eagle's medium (DMEM) containing 10% fetal bovine serum and 1% penicillin/streptomycin until confluence was reached. After that, cells were differentiated in DMEM containing 20 nmol/L insulin, 1 nmol/L triiodothyronine, 0.5 mmol/L isobutyl methylxanthine, 1  $\mu\text{mol/L}$  dexamethasone, 0.125 mmol/L indomethacin, and 2.8  $\mu\text{mol/L}$  rosiglitazone. Because we wanted to compare the effect of Peptide 2 with rosiglitazone during preadipocyte differentiation, we modified the above differentiation cocktail as follows: the control (C) received the cocktail described above, the C+PEP2 was treated with the above cocktail supplemented with 100  $\mu\text{mol/L}$  Peptide 2, the negative control (Rosi neg) received the above cocktail without rosiglitazone and the Rosi neg+PEP2 received the above cocktail without rosiglitazone but supplemented with Peptide 2 (100  $\mu\text{mol/L}$ ).

### 3.2.5 *Hyperinsulinemic-Euglycemic Clamp*

The euglycemic clamp was performed as previously described [209, 210] with the following modifications: briefly, mice were anaesthetized using ketamine (90 mg/kg BW) and xylazine (10 mg/kg BW) and underwent aseptic right jugular vein catheterization for intravenous infusions. Post-surgical BW and food intake were monitored daily. After 3–4 days (to re-establish a minimum of 90% of pre-surgical BW), the mice were fasted for 5 h and underwent a hyperinsulinemic-euglycemic clamp, in which a primed, continuous infusion of tritiated glucose (1  $\mu\text{Ci}$  bolus + 0.1  $\mu\text{Ci}$  infusion; Perkin Elmer, Waltham, MA, USA) was maintained for the duration of the experiment to assess glucose kinetics. After a basal period, the hyperinsulinemic-

euglycemic clamp was initiated with a primed, continuous infusion of insulin (3.0 mU/kg/min) for 120 min, and plasma glucose levels were maintained at a similar euglycemic level to the basal period using a variable infusion of 10% glucose solution. Plasma samples were obtained every 10 min for the measurement of glucose concentration (Analox Glucose Analyzer, Huntington beach, CA, USA) and [3-<sup>3</sup>H]-glucose specific activity. At conclusion of the clamp period, mice were euthanized using an infusion of 0.02 mL ketamine via the jugular vein, followed by decapitation.

### 3.2.6 *Oral Glucose Tolerance Test (OGTT) and Insulin Tolerance Test (ITT)*

OGTT were performed at week 13. Briefly, after overnight fasting a bolus of glucose (1 g/kg BW) was orally gavaged to mice and blood glucose was measured after 0, 15, 30, 60, 90, and 120 min from the tail vein using a glucometer (Contour<sup>®</sup>Next, Mississauga, ON, CA). ITT were performed at week 14. After 4 h fasting, mice received an intraperitoneal injection with insulin (0.75 U/Kg BW) and glucose was measured after 0, 15, 30, 60, 90, and 120 min as cited above.

### 3.2.7 *Liver Triglyceride (TG) and Cholesterol Content*

Liver TG and cholesterol were extracted using approximately 100 mg of tissue and as previously described [211]. Briefly, tissue was homogenized in 1 mL of NaCl solution. A total of 500  $\mu$ L of the extract was mixed with 2 mL of Folch solution (chloroform:methanol (2:1)), centrifuged at 3000 rpm for 10 min and the lower phase collected. Samples were dried under nitrogen and resuspended with 1 mL of 2% TritonX-100 solution in chloroform and dried under nitrogen. The dried sample was then resuspended in ddH<sub>2</sub>O and kept at -20 °C until further use.

TG and cholesterol content were measured using a commercial kit (Infinity™, Thermo Scientific, Waltham, MA, USA).

### 3.2.8 *PPAR $\gamma$ DNA Binding Activity*

Nuclear protein extraction was performed using a commercial kit (Active Motif Inc., Carlsbad, CA, USA) following the manufacturer's instructions for frozen tissue and using 100 mg of tissue for each extraction. PPAR- $\gamma$  DNA binding activity was assessed by a TransAM™ PPAR- $\gamma$  kit (Active Motif Inc., Carlsbad, CA, USA) using 10  $\mu$ g/10 $\mu$ L of nuclear protein extract following the manufacturer's instructions.

### 3.2.9 *Plasma Biochemical Analysis*

All biochemical parameters were assessed after overnight fasting (14–16 h) and using the following commercial kits or reagents as per manufacturer's instructions: mouse insulin ELISA (ALPCO, Salem, NH, USA); NEFA and liver L-type triglyceride M colorimetric assay (Wako Pure Chemical Industries Ltd., Richmond, VA, USA); adiponectin and resistin (MesoScale Discovery); non-esterified fatty acids using glycerol free reagent as standard (Sigma-Aldrich, St. Louis, MA, USA); alanine transaminase (ALT) (Abcam, Cambridge, UK). HOMA-IR was calculated using the formula: [fasting glucose (mmol/L)]  $\times$  [fasting insulin ( $\mu$ U/L)]/22.5].

### 3.2.10 *Protein Extraction and Western Blot*

All reagents were purchased from Sigma-Aldrich (Sigma-Aldrich, St. Louis, MA, USA) unless otherwise specified. Liver tissue was homogenized using a tissue homogenizer in RIPA buffer (50 mmol/L Tris HCL pH:8.0, 150 mmol/L NaCl, 0.1% Triton X-100, 0.5% sodium

deoxycholate, 0.1% SDS) supplemented with 2 µg/mL aprotinin (Calbiochem), 5 mmol/L sodium fluoride, 5 mmol/L sodium orthovanadate, and 1× protease inhibitor cocktail (FastPrep<sup>®</sup>-24, MP Biomedicals). WAT protein was extracted using an extraction kit (AT-022, Invent Biotechnologies, Plymouth, MN, USA). Lysates were stored at –80 °C for future analysis. Protein extracts were separated by SDS-PAGE 12% polyacrylamide gels as previously reported [197] and probed for p-AKT (Cell Signaling Technology (CS-4060S), AKT (CS-9272), PPAR $\gamma$  (Santa Cruz Biotechnology-SC7196), AT2R (abcam92445), p-HSL (CS-41265), HSL (abcam45422), p-PKA (CS-5661S or PKA (CS-58425) overnight before incubation with fluorescent secondary antibodies (Li-cor Biosciences) for 1 h at RT. Images were analyzed using Image Studio Lite software (Li-cor Biosciences, Lincoln, NE, USA). All the phosphorylated proteins bands were normalized to their corresponding total protein. Total proteins were normalized to either  $\beta$ -actin (Sigma-Aldrich A5441), GAPDH (SC-47724 ) or Vinculin (SC-25336).

### 3.2.11 *Histology*

Paraffin blocks of liver or WAT were cut into 5 µm sections and affixed to glass slides. Hematoxylin and eosin staining was performed as previously reported [197]. Fibrosis was assessed using Masson's trichrome staining kit (Sigma-Aldrich, St. Louis, MA, USA). Adipocyte size: 10 random photomicroscopic images of each slide (1 slide per animal) were captured using the microscope 20× objective lens and Axio Vision 4.8 software. ImageJ software “freehand selections” tool was used to measure adipocyte area (mm<sup>2</sup>) of 300 cells or 10 images per sample, whichever was reached first. Liver morphological characterization: Random photomicroscopic images (20×, Axio Vision 4.8 software, n = 3 per mouse) were taken and a researcher blinded to

group assignment used ImageJ software “freehand selections” tool to quantify LD area, cell number and inflammatory foci (a cluster with >5 immune cells). Each image was divided into 4 equal areas and the top left quadrant (standard area: 88,884.66  $\mu\text{m}^2$ ) was analyzed as a representation of the total image. In terms of LD size, there is not a defined numerical threshold for small or large LD categories. However, based on the literature, hepatic lipid accumulation was divided into three categories, macrovesicular with one large LD displacing the nucleus to the side, macrovesicular with one single small LD not displacing the nucleus and true microvesicular steatosis where several small LD occupy a hepatocyte, giving it a foamy appearance [212-214].

### 3.2.12 *Quantitative PCR (qPCR)*

Primer sequences are provided in Table 3.3 Liver RNA was extracted using the QIAGEN RNeasy Mini Plus kit following the manufacturer’s instructions and as previously described [215] with the following modifications: frozen tissue (50–100 mg) was lysed and homogenized using 1 mL of TRIzol. After 5 min at RT, 0.2 mL of chloroform per mL of TRIzol was added. Samples were shaken vigorously and incubated at RT for 3 min, followed by centrifugation at 12,000 $\times$  g for 10 min at 2–8 °C. The supernatant was collected, and the manufacturer’s instructions were followed for the remaining steps until RNA was obtained. RNA concentration and purity were measured using a Nanodrop (Thermo Fisher, Waltham, MA, USA) and cDNA synthesis was performed using the high-capacity cDNA RT kit (Applied Biosystems, Waltham, MA, USA) using 2  $\mu\text{g}$  RNA per reaction in a ProFlex PCR system thermocycler (Applied Biosystems, Waltham, MA, USA). qPCR was performed using PerfeCTa SYBR Green SuperMix ROX (Quantabio, Beverly, MA, USA) in a QuantStudio3 machine (Applied Biosystems, Waltham, MA, USA) using  $\beta$ -actin as the reference gene.

**Table 3. 3. Primers sequences.**

		<b>Primer sequence</b>
<i>Tnfa</i>	F 5' – 3' R 5' – 3'	GGTTCTCTTCACGGGACAAGGC AGAGAGGAGGTTGACTTTCTCCTG
<i>Cd36</i>	F 5' – 3' R 5' – 3'	TGGCTAAATGAGACTGGGACC ACATCACCACTCCAATCCCAAGTAAGG
<i>Fasn</i>	F 5' – 3' R 5' – 3'	CTCCGTCACTTCCAGTTAGAGCAG AGTTCAGTGAGGCGTAGTAGACAGTG
<i>Mogat1</i>	F 5' – 3' R 5' – 3'	CCTTGACCCATGGTGCCAGTT CGTCTTGTATAGTTCGTAGCCAGGAGC
<i>Ppparg</i>	F 5' – 3' R 5' – 3'	GAAGACATTCCATTCACAAGAGCTGACC GCCTGTTGTAGAGCTGGGTCTT
<i>Ppparg2</i>	F 5' – 3' R 5' – 3'	ATGCTGTTATGGGTGAACTCTGGGA CACAGAGCTGATTCCGAAGTTGGTG
<i>Ppara</i>	F 5' – 3' R 5' – 3'	CGACCTGAAAGATTCGAAACTGCAG GCGTCTTCTCGGCCATACACAAG
<i>Srebp1c</i>	F 5' – 3' R 5' – 3'	GGAGCCATGGATTGCACATTTGAAGACAT TTCCAGAGAGGAGGCCAGAGA
<i>Cpt1a</i>	F 5' – 3' R 5' – 3'	CCTACCATGGCTGGATGTTTGCAG GTATCTTTGACAGCTGGGACAGGCA
<i>Scd1</i>	F 5' – 3' R 5' – 3'	GTTCCCTCCTGCAAGCTCTACAC GCAGCCGTGCCTTGTAAGTTC
<i>Dgat2</i>	F 5' – 3' R 5' – 3'	CTGGCAAGAACGCAGTCA TTCTTCTGGACCCATCGG
<i>Actb</i>	F 5' – 3' R 5' – 3'	AGCTATGAGCTGCCTGACG TGCCACAGGATTCCATACCCAAG
<i>Atgl</i>	F 5' – 3' R 5' – 3'	TGTGGCCTCATTCTCCTAC TCGTGGATGTTGGTGGAGCT
<i>Hsl</i>	F 5' – 3' R 5' – 3'	GCT GGG CTG TCA AGC ACT GT GTA ACT GGG TAG GCT GCC AT
<i>Plin2</i>	F 5' – 3' R 5' – 3'	CTGCGGCCATGACAAGT GCTGGTTCAGAATAGGCAGTCTTT
<i>Dgat1</i>	F 5' – 3' R 5' – 3'	GAGTCTATCACTCCAGTGGG GGCGGCACCACAGGTTGACA

---

<i>ApoB</i>	F 5' – 3'	ACTGTGACTTCAATGTGGAG
	R 5' – 3'	CTGAGGCAGACAGACTTGTC
<i>Col1a1</i>	F 5' – 3'	TCAGACCTGTGTGTTCCCTACT
	R 5' – 3'	ACGGGAATCCATCGGTCAT
<i>Mttp</i>	F 5' – 3'	AGAGGACAGCTTTGTCACCG
	R 5' – 3'	TCTTCAGCTCCAATTTCTGCTTCG

---

Abbreviations: *Gene symbol* followed by its (name) and the encoded protein: *Ppara* (peroxisome proliferator-activated receptor alpha) encodes PPAR $\alpha$ ; *Pparg* (peroxisome proliferator-activated receptor gamma) encodes PPAR $\gamma$ ; *Pparg2* (peroxisome proliferator-activated receptor gamma) encodes PPAR $\gamma$ 2; *Tnfa* (tumor necrosis factor alpha) encodes TNF- $\alpha$ ; *Col1a1* (collagen type 1 alpha 1 chain) encodes pro-alpha1 chains of type 1 collagen; *Scd1* (stearoyl-Coenzyme A desaturase 1) SCD1; *Fasn* (fatty acid synthase) encodes FAS; *Srebp1c* (sterol regulatory element binding transcription factor 1c) encodes SREBP-1c; *Mogat1* (monoacylglycerol O-acyltransferase 1) encodes MGAT1; *Cd36* encodes fatty acid translocase (CD36); *Cpt1a* (carnitine palmitoyl transferase 1A) encodes CPT1 $\alpha$ ; *ApoB* (apolipoprotein B) encodes ApoB; *Mttp* (microsomal triglyceride transfer protein) encodes MTP; *Dgat1* (diglycerides O-acyltransferase 1) encodes DGAT1; *Dgat2* (diglycerides O-acyltransferase 2) encodes DGAT2; *Actb* encodes  $\beta$ -actin *Plin2* (perilipin 2) encodes PLIN2; *Hsl* (hormone sensitive lipase) encodes HSL; *Atgl* (patatin-like phospholipase domain containing 2) encodes adipose triglyceride lipase (ATGL).

### 3.2.13 Statistical Analysis

All data presented are expressed as means  $\pm$  SEM of 'n' mice as indicated in each figure description. Statistical analysis was performed using GraphPad Prism software 7.0 (GraphPad Software Inc., San Diego, CA, USA). Data were checked for normal distribution by the Shapiro–Wilk test and any identified outliers were removed. T-test was used to compare LFD to HFD (to establish insulin resistance-related differences), while one-way ANOVA was used to compare HFD groups (i.e., HFD, PEP2 and ROSI) to identify treatment effects. Two-way ANOVA was used to compare insulin regulation of AKT, PKA and HSL. Bonferroni's or Dunn's post-hoc tests were performed to assess differences between groups when a significant main effect was observed. A  $p$ -value  $\leq 0.05$  was considered statistically significant.

## 3.3 Results

### 3.3.1 EHW Effects on WAT Lipolytic Pathway from Obese, Insulin Resistant Rats

Previously we showed that 4% EWH improved glucose tolerance and insulin sensitivity, reduced adipocyte size and enhanced PPAR $\gamma$  abundance in WAT in rats [197]; thus, its effects on lipolytic enzymes in WAT was investigated here. PPAR $\gamma$  DNA binding activity was reduced by 4% EWH in eWAT ( $p < 0.01$ ), but significantly increased in rWAT ( $p < 0.01$ ) (Fig. 3.2A,B). The investigation of key enzymes involved in lipolysis by two-way ANOVA showed a significant overall diet effect ( $p < 0.05$ ) in rWAT p-PKA/PKA ratio and an overall insulin effect ( $p < 0.05$ ) in p-HSL/HSL. The post-hoc analysis revealed that 4% EHW treated animals had reduced p-HSL in rWAT after intraperitoneal injection of insulin ( $p < 0.05$ ) despite no change in phosphorylation of PKA (Fig. 3.2C,D). No changes in total PKA or HSL protein abundance were seen in rWAT (Fig. 3.3). In eWAT, two-way ANOVA revealed a significant overall diet effect

( $p < 0.05$ ) on p-PKA/PKA, while no overall effect was seen on p-HSL/HSL. No changes in p-HSL or p-PKA (Figure 3.1.2E,F) or total HSL (Fig. 3.3D) were seen in eWAT. However, total PKA abundance was reduced by 4% EWH treatment ( $p = 0.08$ ) (Fig. 3.3C). Plasma and WAT adiponectin and resistin concentrations were not different between groups (Table 3.4).

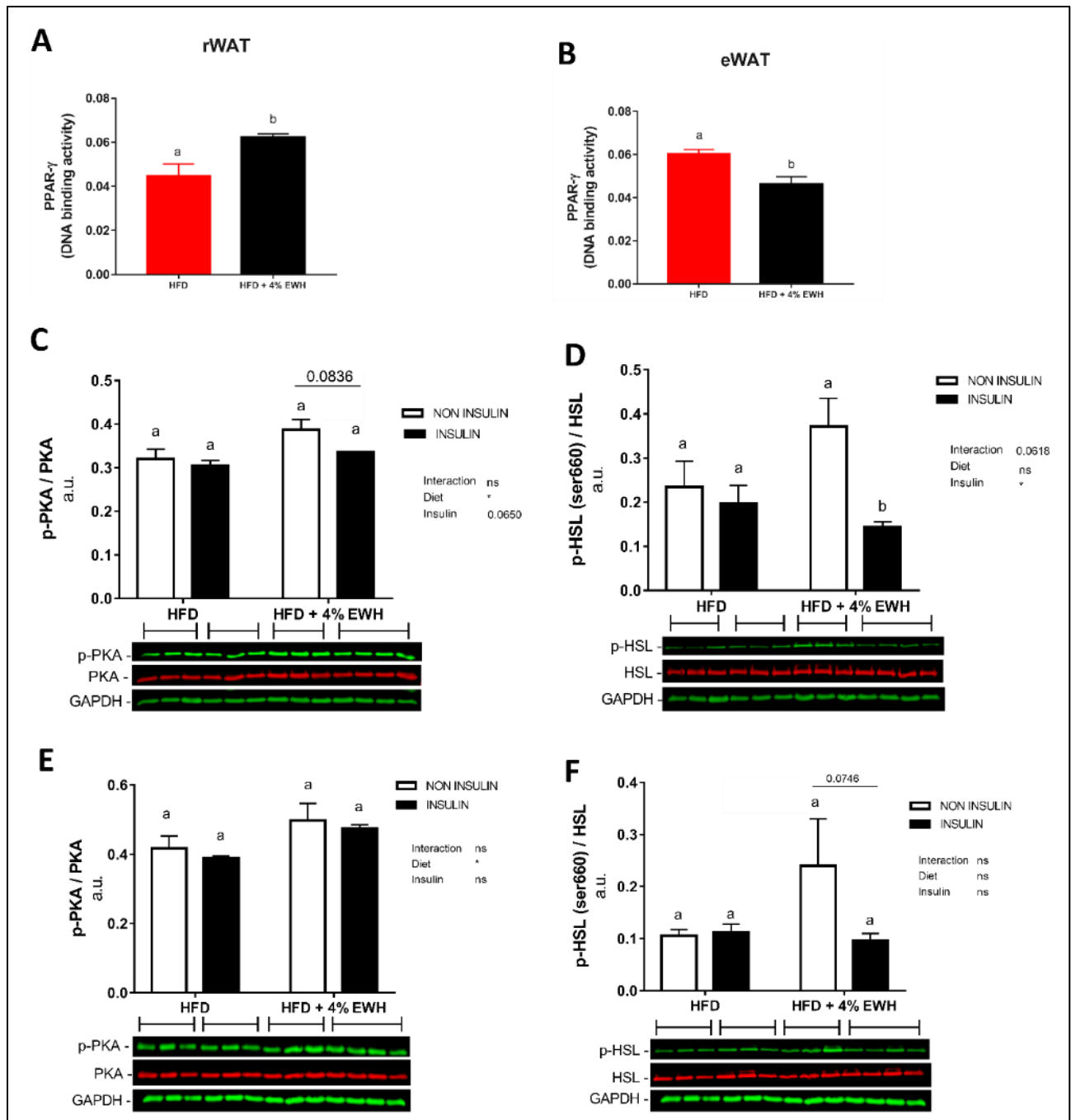


**Figure 3. 2. EWH effects in WAT of Sprague Dawley rats fed EWH for 6 weeks (Protocol 1).** PPAR $\gamma$  DNA binding activity in rWAT (A) and eWAT (B). Data expressed as mean  $\pm$  SEM and analyzed by two-tailed t-test (n = 6–7). PKA, p-PKA, HSL and p-HSL protein abundance in rWAT (C,D) and eWAT (E,F). Data expressed as mean  $\pm$  SEM and analyzed by two-way ANOVA (n = 3–4). Bars with different letters indicate  $p < 0.05$ . EWH, egg white hydrolysate; PKA, protein kinase A; PPAR $\gamma$ , Peroxisome proliferator-activated receptor gamma; HSL, hormone sensitive lipase; WAT, white adipose tissue; rWAT, retroperitoneal WAT; eWAT, epididymal WAT.

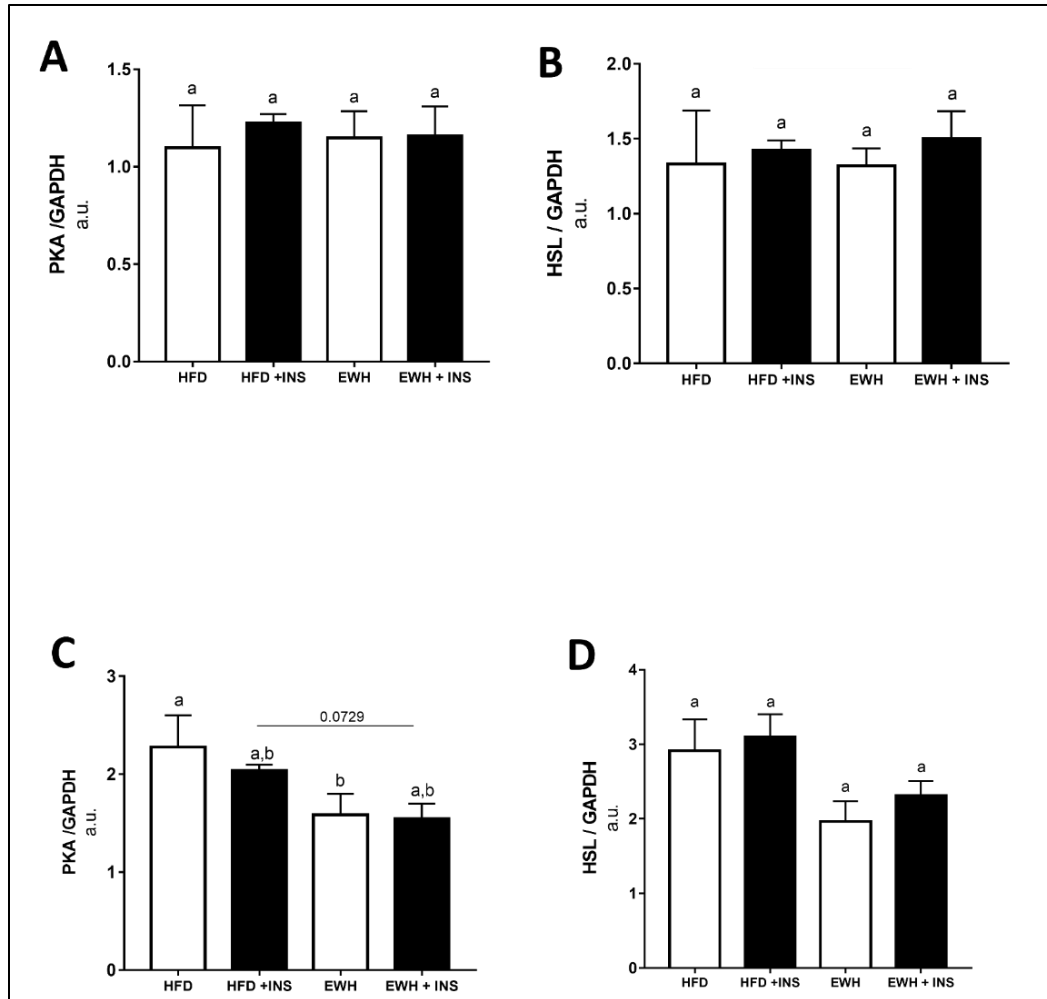


**Figure 3. 3. EWH effects in WAT of Sprague Dawley rats fed EWH for 6 weeks (Protocol 1).** PKA, p-PKA, HSL and p-HSL protein abundance in rWAT (A-B) and eWAT (C-D). Data expressed as mean + SEM and analyzed by one-way ANOVA (n=3-4). Bars with different letters indicate  $p < 0.05$ . EWH, egg white hydrolysate; PKA, protein kinase A; HSL, hormone sensitive lipase; WAT, white adipose tissue; rWAT, retroperitoneal WAT; eWAT, epididymal WAT.

**Table 3.4. Resistin and adiponectin concentration in plasma, epididymal and retroperitoneal adipose tissue in Sprague Dawley rats treated with HFD+4% EWH for 6 weeks (Protocol 1).** Data expressed as mean  $\pm$  SEM and analyzed by two tailed t-test (n = 6–7).

	HFD	HFD+4% EWH
Plasma (fasting)		
Resistin (pg/mL)	1047 $\pm$ 84.55	1011 $\pm$ 82.99
Adiponectin (ng/mL)	55,853 $\pm$ 2832	60,270 $\pm$ 7367
eWAT		
Resistin (pg/mL)	175.1 $\pm$ 15.67	166.5 $\pm$ 11.14
Adiponectin (ng/mL)	1002 $\pm$ 28.44	1044 $\pm$ 19.54
rWAT		
Resistin (pg/mL)	172.3 $\pm$ 20.14	175.1 $\pm$ 15.67
Adiponectin (ng/mL)	1033 $\pm$ 25	1026 $\pm$ 28.73

Abbreviations: HFD, high-fat diet; EWH, egg white hydrolysate; eWAT, epididymal adipose tissue; rWAT, retroperitoneal adipose tissue.

Based on these indications that 4% EWH had the potential to improve insulin-mediated suppression of lipolysis and activate PPAR $\gamma$ , a trial of 4 EWH-derived, purified peptides (Peptides 1–4) that elicited increased PPAR $\gamma$  *in vitro* [198] was initiated. From preliminary data (n=12 mice/group), insulin tolerance was improved by Peptide 2 ( $p < 0.05$ ) together with lower iWAT and rWAT weights compared to HFD (Fig. 3.4), whereas Peptides 1, 3 and 4 did not affect any WAT depot weight. Notably, Peptide 2 had the lowest and ROSI the highest liver weight. Therefore, additional experiments were performed, focusing on the effects of Peptide 2 on the insulin resistant phenotype and iWAT/rWAT lipid metabolism.

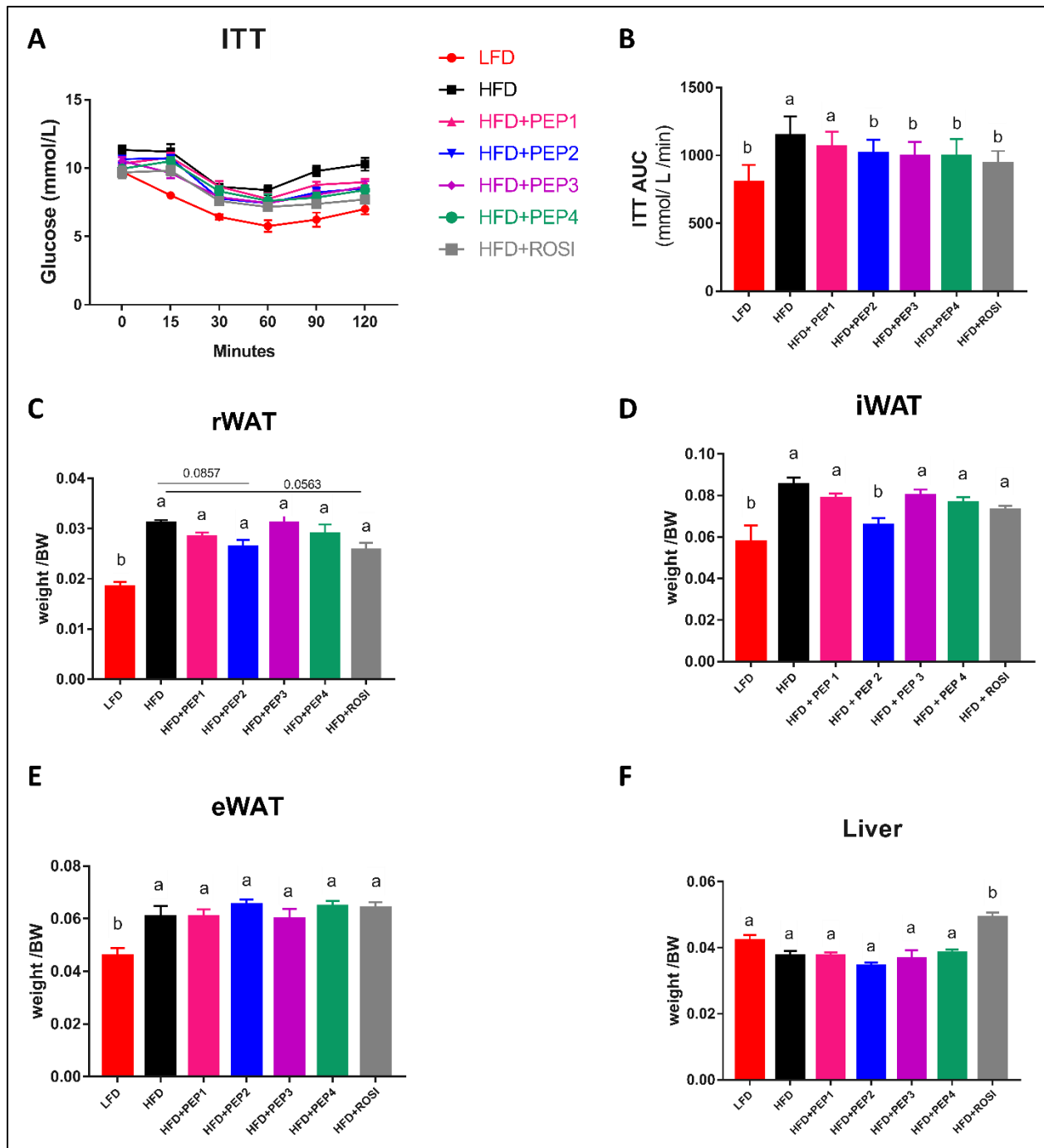


**Figure 3.4. Insulin tolerance test and tissues weight clamp in mice treated with Peptide 2 (Protocol 2).** (A-B) Insulin tolerance test (ITT) and (C-F) tissue weight after supplementation with 4 different peptides or rosiglitazone. (A) ITT, (B) ITT area under the curve (AUC), (C) rWAT, (D) iWAT, (E) eWAT and (F) liver. Data expressed as mean + SEM and analyzed by two-way ANOVA (A) or one-way ANOVA with HFD group set as control. (A-C, E) n=11-12, (D) n=9-12 and (F) n=7-12. Bars with (b) indicates p<0.05 compared to HFD group. WAT, white adipose tissue; rWAT, retroperitoneal WAT; eWAT, epididymal WAT; iWAT, inguinal WAT.

### 3.3.2 *Peptide 2 and Rosiglitazone Effects in HFD-Induced Obese, Insulin Resistant Mice*

#### 3.3.2.1 *Food Intake, Body Composition and Tissue Weight*

Food and water intake were not different between any of the groups compared to HFD animals (Fig. 3.5A–D). As expected, after 6 weeks of HFD feeding, the HFD group presented higher BW than LFD animals ( $p < 0.0001$ ) (Table 3.5) and were glucose intolerant ( $p < 0.05$ ) (Fig. 3.6). At the end of the trial, HFD group maintained higher BW and BW gain than LFD ( $p < 0.0001$ ). Initial BW was not different between all the HFD groups; however, the ROSI group had a reduced rate of BW gain than HFD group after 3 weeks of treatment leading to a reduced final BW ( $p = 0.006$ ). Peptide 2 supplementation did not influence final BW or BW gain in comparison to HFD. Body composition analysis revealed that only the LFD animals had a lower fat mass % and higher lean mass % than HFD ( $p < 0.0001$ ) (Table 3.5). Compared to HFD, LFD animals had decreased mass of all three fat pads ( $p < 0.001$ ). ROSI group presented lower rWAT mass compared to HFD ( $p = 0.0022$ ), while PEP2 animals had an intermediate rWAT mass, between ROSI and HFD groups. eWAT and iWAT did not change between all the HFD groups. The liver weight of LFD and HFD groups was not different. ROSI animals had a heavier liver than all the other HFD groups ( $p < 0.0001$ ) (Table 3.5).

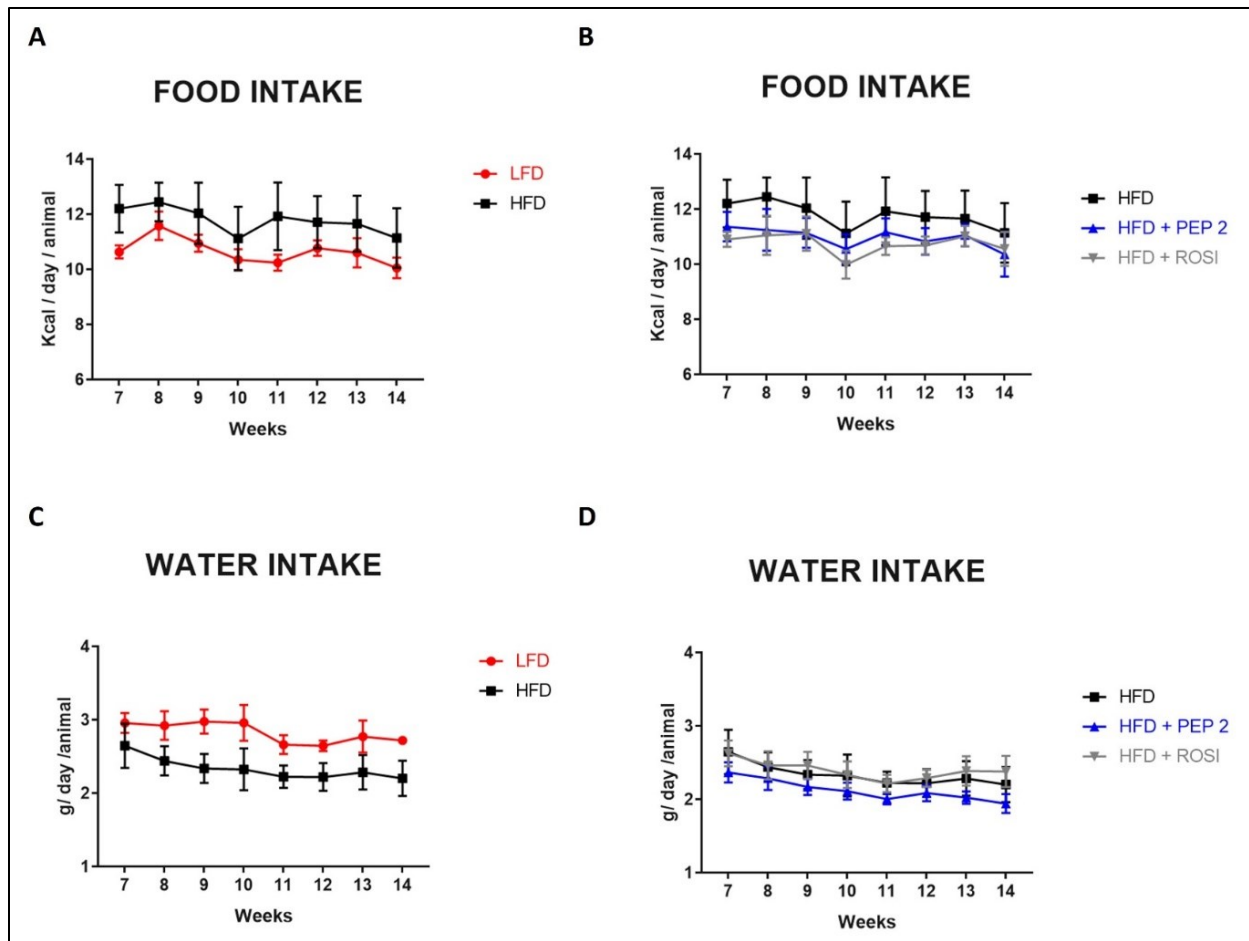


**Figure 3. 5. Food and water intake clamp in mice treated with Peptide 2 (Protocol 2).** (A and B) Food and (C and D) water intake during diet supplementation period. Data expressed as mean  $\pm$  SEM and analyzed by one-way ANOVA. HFD, high-fat diet; LFD, low fat diet; ROSI, rosiglitazone.

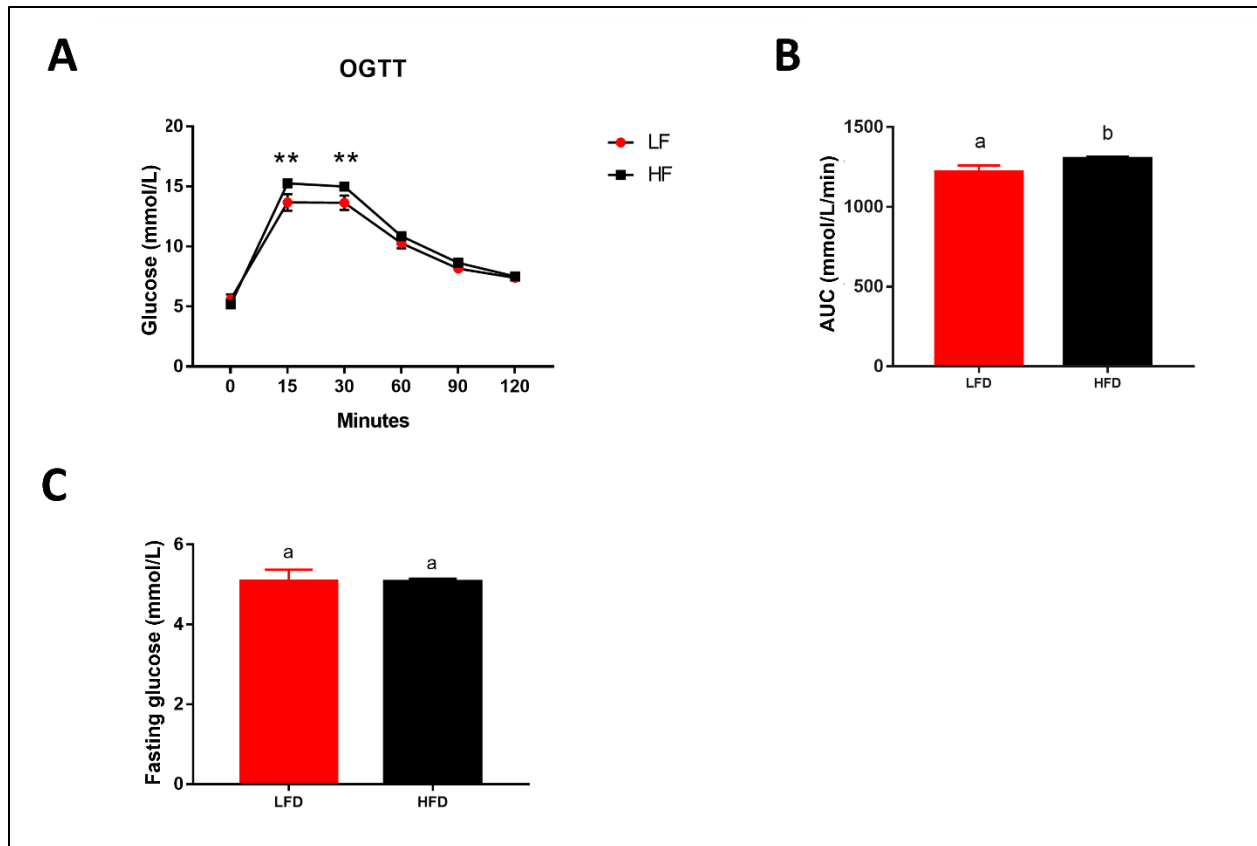


**Figure 3. 6. Glucose tolerance clamp in mice treated with Peptide 2 (Protocol 2).** (A) OGTT, (B) area under the curve (n=12 LFD and 69 HFD) and (C) fasting glucose (n=20 LFD and 101 HFD) after 6 weeks of HFD feeding. Data expressed as mean  $\pm$  SEM and analyzed by two-way ANOVA (A) or two-tailed t-test (B and C). Bars with different letters indicate  $p \leq 0.05$ . \*\*  $p < 0.01$ . HFD, high-fat diet; LFD, low fat diet.

**Table 3. 5. BW, body composition and plasma profile of C57BL/6 mice at the end of the Peptide 2 feeding trial (Protocol 2).** Data expressed as mean  $\pm$  SEM and analyzed by two-tailed t-test (LFD  $\times$  HFD) and by one-way ANOVA or Kruskal-Wallis (HFD groups). Different letters on the same row indicates  $p < 0.05$  for HFD groups. # indicates  $p \leq 0.05$  and ^ indicates  $p < 0.1$  compared to HFD.

	LFD	HFD	HFD+PEP2	HFD+ROSI
<b>Body composition (not fasted)</b>				
Initial BW (g) (week 6)	29.1 $\pm$ 0.6 #	33.9 $\pm$ 0.7 <sup>a</sup>	32.9 $\pm$ 0.6 <sup>a</sup>	33.5 $\pm$ 0.7 <sup>a</sup>
Final BW (g)	33.4 $\pm$ 0.7 #	42.5 $\pm$ 0.7 <sup>a</sup>	41.4 $\pm$ 0.5 <sup>a,b</sup>	39.4 $\pm$ 0.8 <sup>b</sup>
BW gain (%) (week 6–13)	15.4 $\pm$ 1.0 #	25.0 $\pm$ 1.3 <sup>a</sup>	26.2 $\pm$ 1.2 <sup>a</sup>	17.7 $\pm$ 1.5 <sup>b</sup>
Final fat mass (% BW)	25.6 $\pm$ 1.3 #	38.5 $\pm$ 1.1 <sup>a</sup>	38.6 $\pm$ 0.6 <sup>a</sup>	36.1 $\pm$ 1.1 <sup>a</sup>
Final lean mass (% BW)	65.9 $\pm$ 1.2 #	54.2 $\pm$ 1.0 <sup>a</sup>	54.3 $\pm$ 0.6 <sup>a</sup>	56.5 $\pm$ 1.0 <sup>a</sup>
<b>Tissue weight (g/BW)</b>				
eWAT	0.039 $\pm$ 0.0029 #	0.059 $\pm$ 0.0029 <sup>a</sup>	0.061 $\pm$ 0.0014 <sup>a</sup>	0.057 $\pm$ 0.0025 <sup>a</sup>
rWAT	0.017 $\pm$ 0.00079 #	0.028 $\pm$ 0.00084 <sup>a</sup>	0.025 $\pm$ 0.00096 <sup>a,b</sup>	0.022 $\pm$ 0.0014 <sup>b</sup>
iWAT	0.046 $\pm$ 0.0070 #	0.073 $\pm$ 0.0049 <sup>a</sup>	0.065 $\pm$ 0.0027 <sup>a</sup>	0.062 $\pm$ 0.0040 <sup>a</sup>
Liver	0.036 $\pm$ 0.0019	0.033 $\pm$ 0.0015 <sup>a</sup>	0.032 $\pm$ 0.0007 <sup>a</sup>	0.044 $\pm$ 0.0015 <sup>b</sup>
<b>Plasma (fasting)</b>				
Glucose (mmol/L)	4.5 $\pm$ 0.3 #	5.9 $\pm$ 0.3 <sup>a</sup>	5.3 $\pm$ 0.3 <sup>a</sup>	5.6 $\pm$ 0.2 <sup>a</sup>
Insulin (ng/mL)	0.5 $\pm$ 0.1 ^	1.0 $\pm$ 0.1 <sup>a</sup>	0.9 $\pm$ 0.1 <sup>a</sup>	0.6 $\pm$ 0.1 <sup>a</sup>
HOMA-IR	0.8 $\pm$ 0.2 #	2.4 $\pm$ 0.6 <sup>a</sup>	1.8 $\pm$ 0.3 <sup>a</sup>	1.9 $\pm$ 0.3 <sup>a</sup>
NEFA (mEq/L)	0.4 $\pm$ 0.02	0.4 $\pm$ 0.02 <sup>a</sup>	0.5 $\pm$ 0.03 <sup>a</sup>	0.5 $\pm$ 0.04 <sup>a</sup>
TG (mg/dL)	39.4 $\pm$ 5.6	52.6 $\pm$ 5.8 <sup>a</sup>	43.2 $\pm$ 4.2 <sup>a</sup>	41.9 $\pm$ 4.6 <sup>a</sup>
Plasma ALT (mU/mL)	8.4 $\pm$ 4.0 #	28.4 $\pm$ 27.1 <sup>a</sup>	24.9 $\pm$ 15.1 <sup>a</sup>	20.9 $\pm$ 13.5 <sup>a</sup>
<b>Liver content (mg/g tissue)</b>				
TG	46.8 $\pm$ 2.3 #	71.5 $\pm$ 11.0 <sup>a</sup>	57.6 $\pm$ 6.7 <sup>a</sup>	132.7 $\pm$ 12.1 <sup>b</sup>
Cholesterol	2.4 $\pm$ 0.2	2.1 $\pm$ 0.2 <sup>a</sup>	1.3 $\pm$ 0.1 <sup>b</sup>	1.8 $\pm$ 0.1 <sup>a</sup>

Abbreviations: ALT, alanine aminotransferase; BW, body weight; eWAT, epididymal white adipose tissue (WAT); HFD, high-fat diet; HOMA-IR, homeostatic model assessment of insulin resistance; iWAT, inguinal WAT; LFD, low fat diet; NEFA, non-esterified fatty acids; rWAT, retroperitoneal WAT; TG, triglycerides.

### 3.3.2.2 Plasma Biochemical Parameters

Fasted LFD animals had lower blood glucose concentration than HFD ( $p < 0.001$ ), while no statistical difference was seen between the HFD groups. No statistical difference was seen in fasting plasma insulin concentration between any of the groups, despite a considerable reduction in LFD ( $p < 0.1$ ) and ROSI groups compared to HFD. This was accompanied by a lower HOMA-IR in LFD animals compared to HFD ( $p = 0.024$ ) but no differences between HFD groups. No changes were seen regarding plasma lipid profile (NEFA and TG) between any of the groups (Table 3.5).

### 3.3.2.3 Glucose Homeostasis and Systemic Insulin Sensitivity

In vivo tests confirmed that at week 14 HFD animals were glucose intolerant compared to LFD animals ( $p = 0.015$ ) (Fig. 3.7A,C), and that the ROSI group had improved glucose tolerance compared to HFD group ( $p < 0.05$ ) (Fig. 3.7B,C, right). Two-way ANOVA analysis show a significant treatment  $\times$  time interaction ( $p < 0.0001$ ) and a significant effect of diet ( $p = 0.0437$ ) among the HFD groups. However, despite changes in the OGTT curve and AUC, the incremental AUC was not different between groups (Fig. 3.7D). This is likely because fasting glucose concentration in the OGTT was significantly lower in the LFD group compared to HFD (Fig. 3.7E, left).

During the hyperinsulinemic-euglycemic clamp LFD, ROSI and PEP2 groups had improved insulin sensitivity compared to HFD ( $p < 0.05$ ) (Fig. 3.7 F–I and Fig. 3.8). Plasma glucose during the hyperinsulinemic-euglycemic clamp was not different among the groups (Fig. 3.7F). Similarly, there was no difference in plasma insulin during the clamp procedure (Fig. 3.7G), both validating the clamp technique. Insulin resistance of the HFD group was indicated by the lower

glucose infusion rate (GIR) ( $p < 0.001$ ) (Fig. 3.7H, left) and higher glucose production during the clamp than LFD ( $p = 0.005$ ) (Fig. 3.7I, left). Moreover, GIR was higher in PEP2 ( $p = 0.0047$ ) and ROSI ( $p = 0.0013$ ) compared to HFD (Fig. 3.7H, right). In addition, glucose production was reduced in the PEP2 group compared to HFD ( $p = 0.015$ ), while ROSI showed an intermediate effect (Fig. 3.7I, right). When comparing basal vs. clamp glucose production within group, glucose production was only suppressed in the PEP2 group, with a similar pattern in the LFD group (Fig. 3.8A). Insulin-stimulated glucose disposal was higher in the LFD ( $p = 0.038$ ) and ROSI ( $p = 0.06$ ) groups compared to HFD and although it was also numerically higher in the PEP2 group, no significance was seen (Fig. 3.8B). Improvement in insulin sensitivity after PEP2 and ROSI treatment was confirmed during the insulin tolerance test (Fig. 3.8C–I).

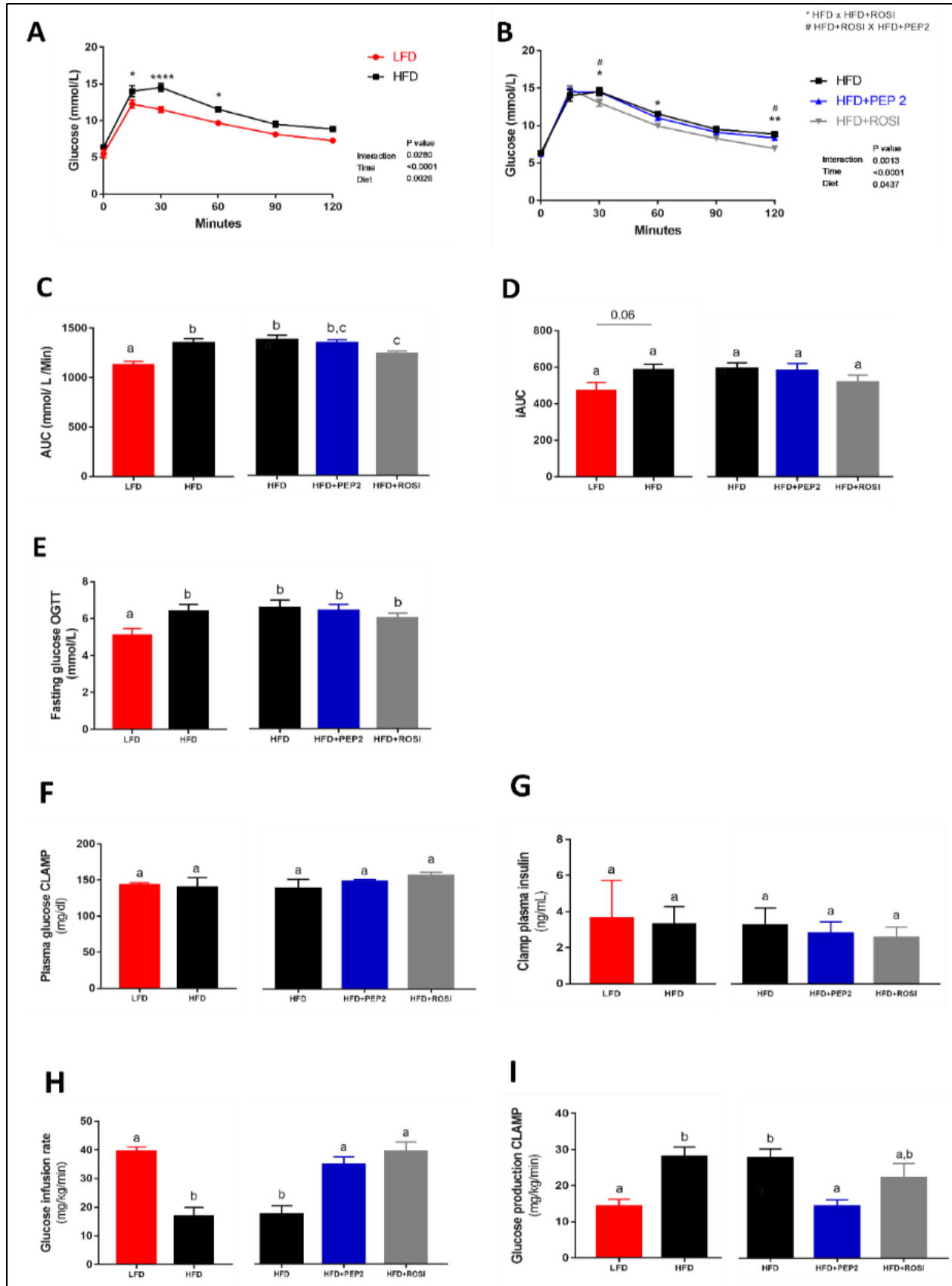


**Figure 3. 7. Glucose tolerance test and hyperinsulinemic-euglycemic clamp in mice treated with Peptide 2 (Protocol 2).** (A,B) Glucose tolerance test (OGTT), (C) OGTT area under the curve (AUC), (D) OGTT incremental AUC, (E) overnight fasting glucose on OGTT day (n = 11–12). Data expressed as mean  $\pm$  SEM and analyzed by two-tailed t-test (LFD vs. HFD) and by one-way ANOVA or Kruskal-Wallis (HFD groups) or two-way ANOVA. In the hyperinsulinemic-euglycemic clamp: (F) plasma glucose concentration; (G) plasma insulin; (H) glucose infusion rate and (I) glucose production. Data expressed as mean  $\pm$  SEM of n = 4–7 and analyzed by two-tailed t-test (LFD vs. HFD) or by one-way ANOVA (HFD groups). Bars with different letters indicate  $p < 0.05$ . \* and # indicate  $p < 0.05$ ; \*\* indicates  $p < 0.01$ ; \*\*\*\* indicates  $p < 0.0001$ .

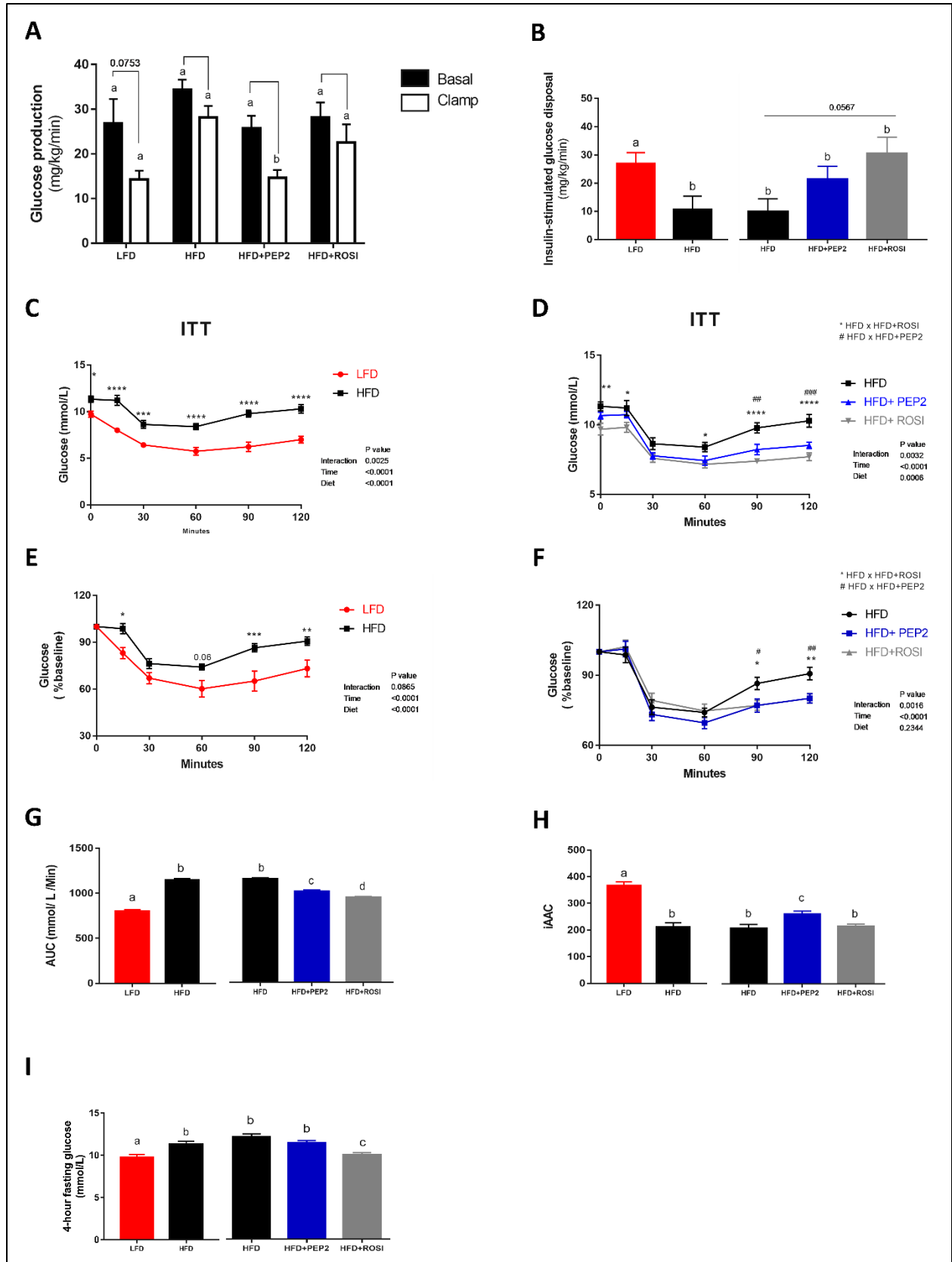


**Figure 3. 8. Hyperinsulinemic-euglycemic clamp and Insulin tolerance test (ITT) clamp in mice treated with Peptide 2 (Protocol 2).** (A) within group glucose production comparison at basal state and during clamp; (B) insulin stimulated glucose disposal. Data expressed as mean  $\pm$  SEM. Figure A and B (LFD x HFD) were analyzed by two tailed t test and figure B (HFD groups) analyzed by one-way ANOVA (n=4-7). (C/D) ITT LFD x HFD and ITT HFD groups (n=11-12); (E/F) insulin tolerance test (ITT) as % of baseline blood glucose concentration (n=11-12), (G) ITT AUC, (H) ITT incremental area above the curve (AAC) and (I) 4-hour fasting glucose on ITT day (n=12). Data expressed as mean  $\pm$  SEM and analyzed by two-way ANOVA (C-F) and by two tailed t test (LFD x HFD) or by one-way ANOVA (HFD groups) (G-I). \* Indicates  $p \leq 0.05$ , \*\* $p < 0.01$ , \*\*\*  $p < 0.001$  \*\*\*\* $p < 0.0001$ . HFD, high-fat diet; LFD, low fat diet; ROSI, rosiglitazone. BW, body weight; HFD, high-fat diet; LFD, low fat diet; ROSI, rosiglitazone. Bars with different letters indicate  $p \leq 0.05$ .

#### 3.3.2.4 WAT Regulation by Insulin: Lipolysis and AKT

Tissue collected from fasted HFD animals had impaired norepinephrine-stimulated lipolysis *ex vivo* in eWAT and iWAT (Fig. 3.9A,B), while in rWAT lipolysis stimulation occurred in all the groups, despite HFD having a lower magnitude of stimulation (Fig. 3.9C). Two-way ANOVA diet overall effect was significant in rWAT and iWAT ( $p < 0.05$ ), but not in eWAT. The overall stimulatory effect was significant in all three fat pads ( $p < 0.05$ ). Interestingly, none of the groups showed suppression of lipolysis by insulin in the eWAT (Fig. 3.9A), but the lack of suppression of lipolysis by insulin in HFD was rescued by Peptide 2 in both iWAT (Fig. 3.9B) and rWAT (Fig. 3.9C). ROSI normalized lipolysis suppression in iWAT (Fig. 3.9B) but not in rWAT (Fig. 3.9C). Because only rWAT and iWAT demonstrated rescued suppression of lipolysis, we investigated insulin regulation of the lipolytic pathway only in these two fat pads. rWAT and iWAT exhibited enhanced AKT phosphorylation after insulin stimulation in LFD, PEP2 and ROSI but not in HFD groups, with an overall effect of insulin in both fat pads, but a dietary overall effect only in iWAT (Fig. 3.9D,E and Fig. 3.10).

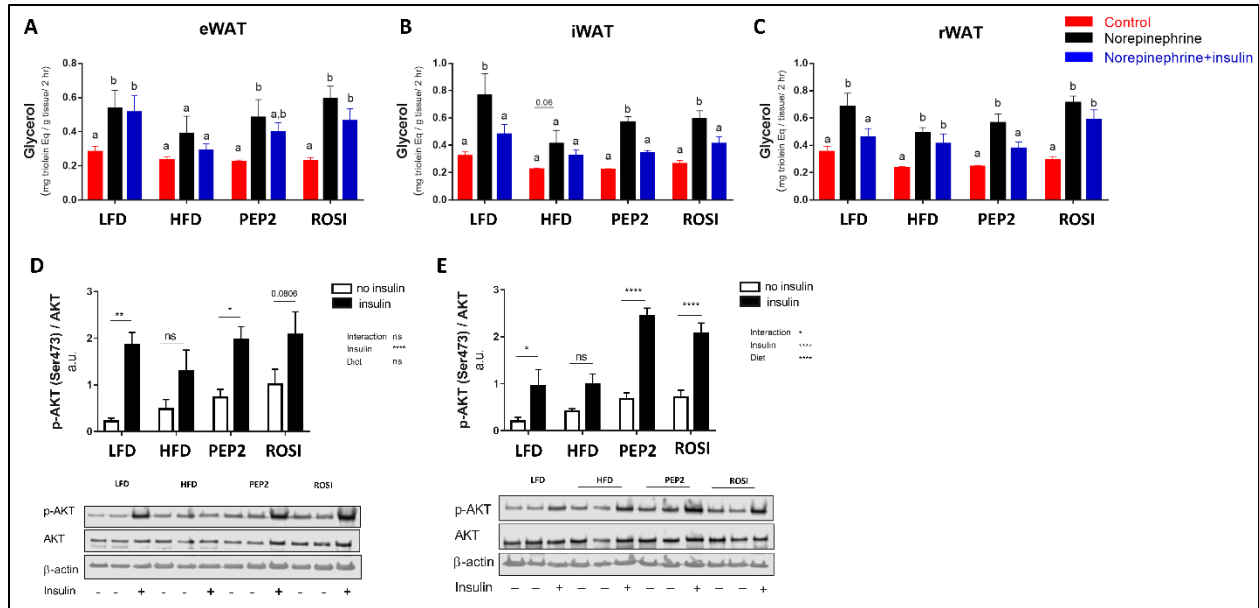


**Figure 3.9. White adipose tissue (WAT) ex vivo lipolysis and protein kinase B (AKT) activation in tissues harvested from mice treated with Peptide 2 (Protocol 2).** Lipolysis ex-vivo in (A) eWAT (n = 5–6), (B) iWAT (n = 5–6) and (C) rWAT (n = 4–6). (D) rWAT p-AKT/AKT (n = 6) and (E) iWAT p-AKT/AKT (n = 6). Data expressed as mean ± SEM and analyzed by two-way ANOVA (D,E). Bars with different letters and \* indicate  $p \leq 0.05$ ; \*\*  $p < 0.01$  and \*\*\*\*  $p < 0.0001$ . HFD, high-fat diet; rWAT, retroperitoneal WAT; eWAT, epididymal WAT, iWAT inguinal WAT; LFD, low fat diet; ROSI, rosiglitazone.

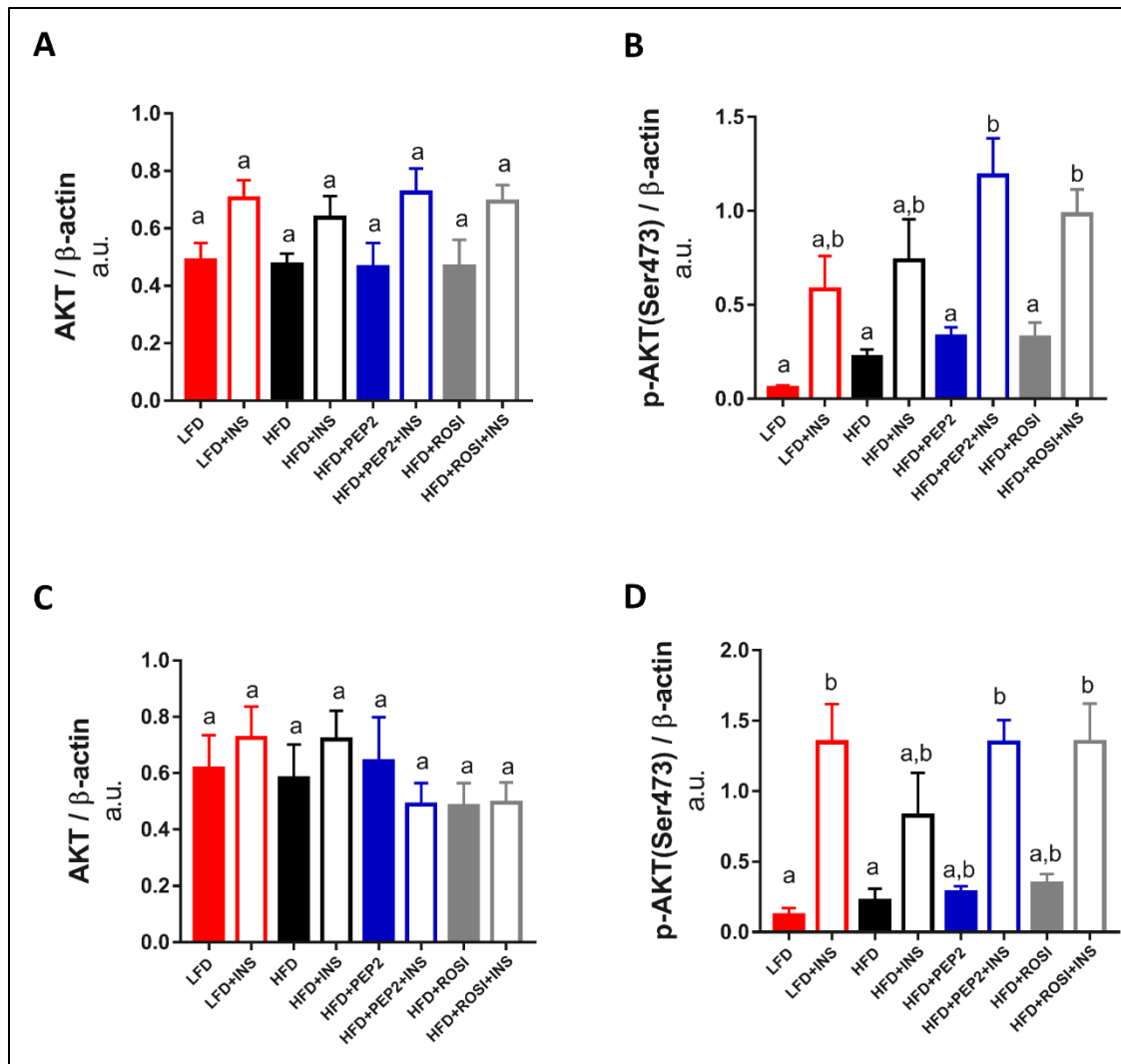


**Figure 3. 10. AKT and p-AKT normalization to  $\beta$ -actin.** (A) rWAT AKT/ $\beta$ -actin; (B) rWAT p-AKT/  $\beta$ -actin; (C) iWAT AKT/ $\beta$ -actin; (D) iWAT p-AKT/ $\beta$ -actin. Data expressed as mean  $\pm$  SEM of n=6 mice. Data analyzed by one-way ANOVA or Kruskal-Wallis. Bars with different letters indicate  $p \leq 0.05$ . HFD, high-fat diet; LFD, low fat diet; rWAT, retroperitoneal WAT; eWAT, epididymal WAT; iWAT, inguinal WAT; ROSI, rosiglitazone.

### 3.3.2.5 PPAR $\gamma$ Activation, Adipocyte Size and Adipogenesis Markers

Despite being increased 40–50% in PEP2 and ROSI groups, PPAR $\gamma$  protein abundance in rWAT did not reach statistical significance (Fig. 3.11A). However, PPAR $\gamma$  activation was increased in LFD ( $p = 0.016$ ) and ROSI ( $p = 0.49$ ) groups compared to HFD, but not in PEP2 (Fig. 3.11B). Image analysis revealed no differences in average adipocyte size or distribution in the rWAT (Fig. 3.11C and Fig. 3.12, respectively) in any diet group. In iWAT, total PPAR $\gamma$  protein abundance was similar between groups (Fig. 3.11E) and PPAR $\gamma$  activation was not different between groups (Fig. 3.11F). The average adipocyte size in LFD group was smaller than HFD ( $p = 0.048$ ) (Fig. 3.11, left). However, no changes were seen among the HFD groups (Fig. 3.11G, right). The distribution curve showed reduced percentage of larger adipocytes ( $>0.017 \text{ mm}^2$ ) in the LFD compared to HFD ( $p < 0.05$ ) (Fig. 3.12). Protein abundance of markers of adipogenesis, including adiponectin, perilipin-1, fatty-acid binding protein 4 and fatty acid synthase were similar between HFD groups in both rWAT and iWAT (Fig. 3.12). In addition, we tested the effect of Peptide 2 during the differentiation of cultured pre-adipocytes derived from both subcutaneous (9W) and brown (9B) adipose tissue pads from mice. However, no major effects were observed in terms of adipogenesis, lipolysis, lipogenesis, and WAT browning (Fig. 3.13 and Fig. 3.14).

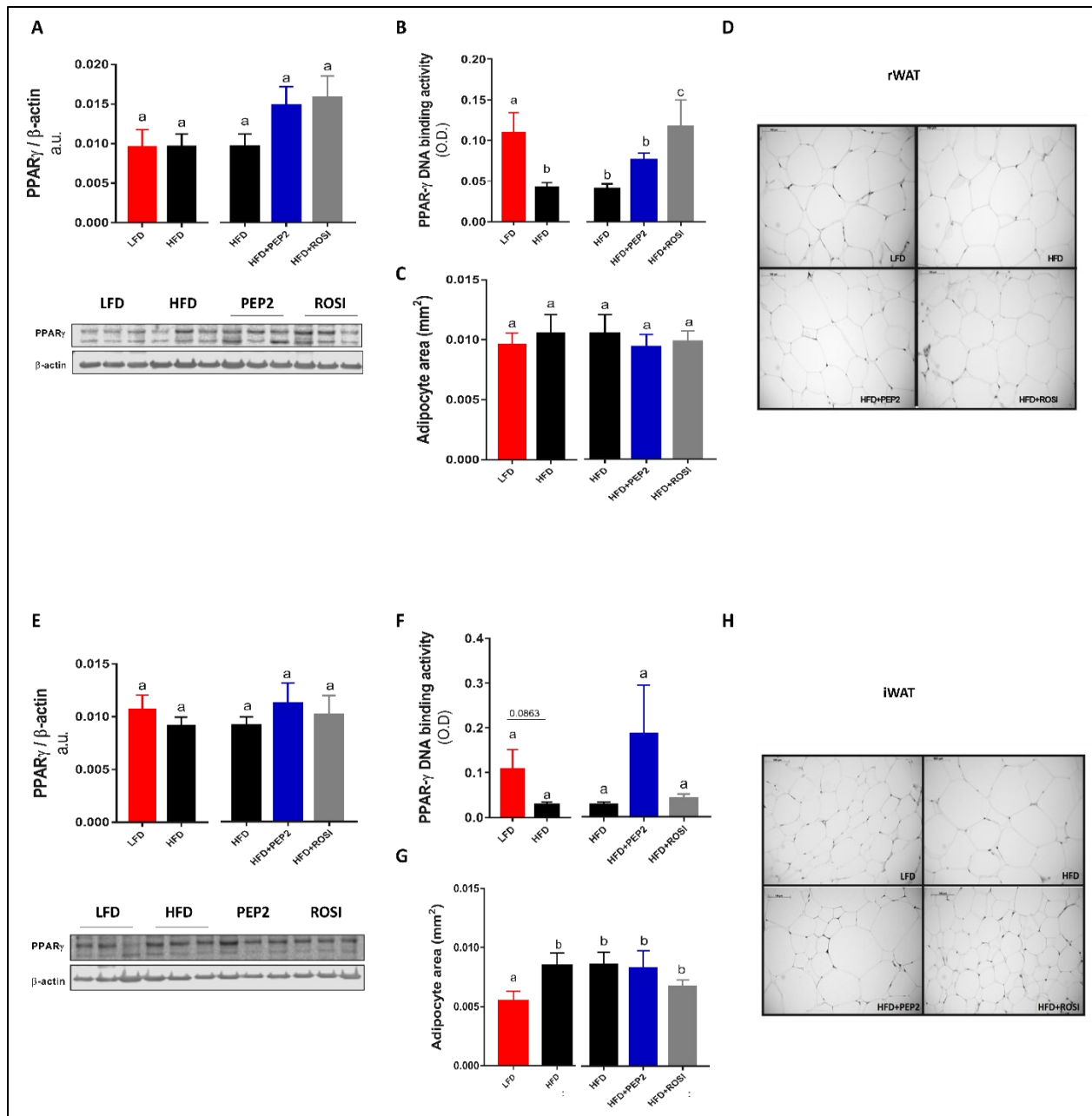


**Figure 3. 11. Retroperitoneal white adipose tissue (rWAT) and inguinal white adipose tissue (iWAT) adipogenesis markers in tissues harvested from mice treated with Peptide 2 (Protocol 2).** (A) PPAR $\gamma$  protein abundance in rWAT; (B) PPAR $\gamma$  DNA binding activity in rWAT (n = 5–6); (C) adipocytes mean area in rWAT (n = 4); (D) representative image in rWAT; (E) PPAR $\gamma$  protein abundance in iWAT; (F) PPAR $\gamma$  DNA binding activity in iWAT (n = 5–6); (G) adipocytes mean area in iWAT (n = 4); (H) representative image in iWAT. Data expressed as mean  $\pm$  SEM and analyzed by two tailed t-test (LFD vs. HFD) and by one-way ANOVA or Kruskal–Wallis (HFD groups). Bars with different letters indicates  $p \leq 0.05$ . HFD, high-fat diet; LFD, low fat diet; rWAT, retroperitoneal

WAT; eWAT, epididymal WAT; iWAT, inguinal WAT; PPAR $\gamma$ , peroxisome proliferator activated receptor gamma; ROSI, rosiglitazone.

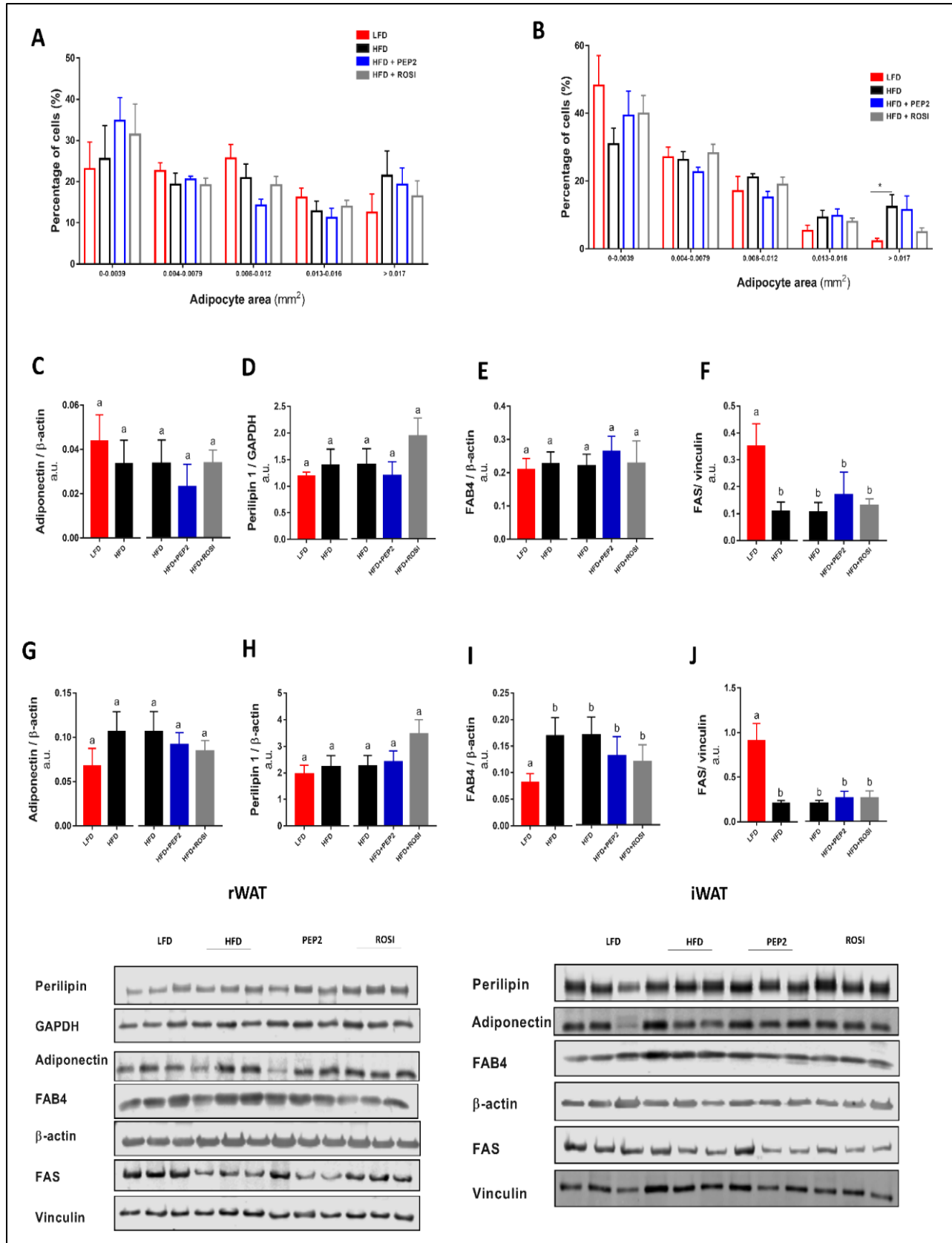


**Figure 3. 12. Adipogenesis markers western blot.** (A) adipocyte size distribution in rWAT (n=4) and (B) adipocyte size distribution in iWAT (n=4). (C) Adiponectin rWAT, (D) Perilipin-1 rWAT, (E) Fatty acid binding protein-4 (FAB4) rWAT, (F) Fatty-acids synthase (FAS) rWAT, (G) Adiponectin iWAT, (H) Perilipin-1 iWAT, (I) Fatty acid binding protein-4 (FAB4) iWAT, (J) Fatty-acids synthase (FAS) iWAT. Data expressed as mean  $\pm$  SEM of n=5-6 mice and analyzed by two-tailed t-test (LFD x HFD) or by one-way ANOVA or Kruskal-Wallis (HFD groups). Bars with different letters indicate p<0.05. HFD, high-fat diet; LFD, low fat diet; rWAT, retroperitoneal WAT; eWAT, epididymal WAT; iWAT, inguinal WAT; ROSI, rosiglitazone.

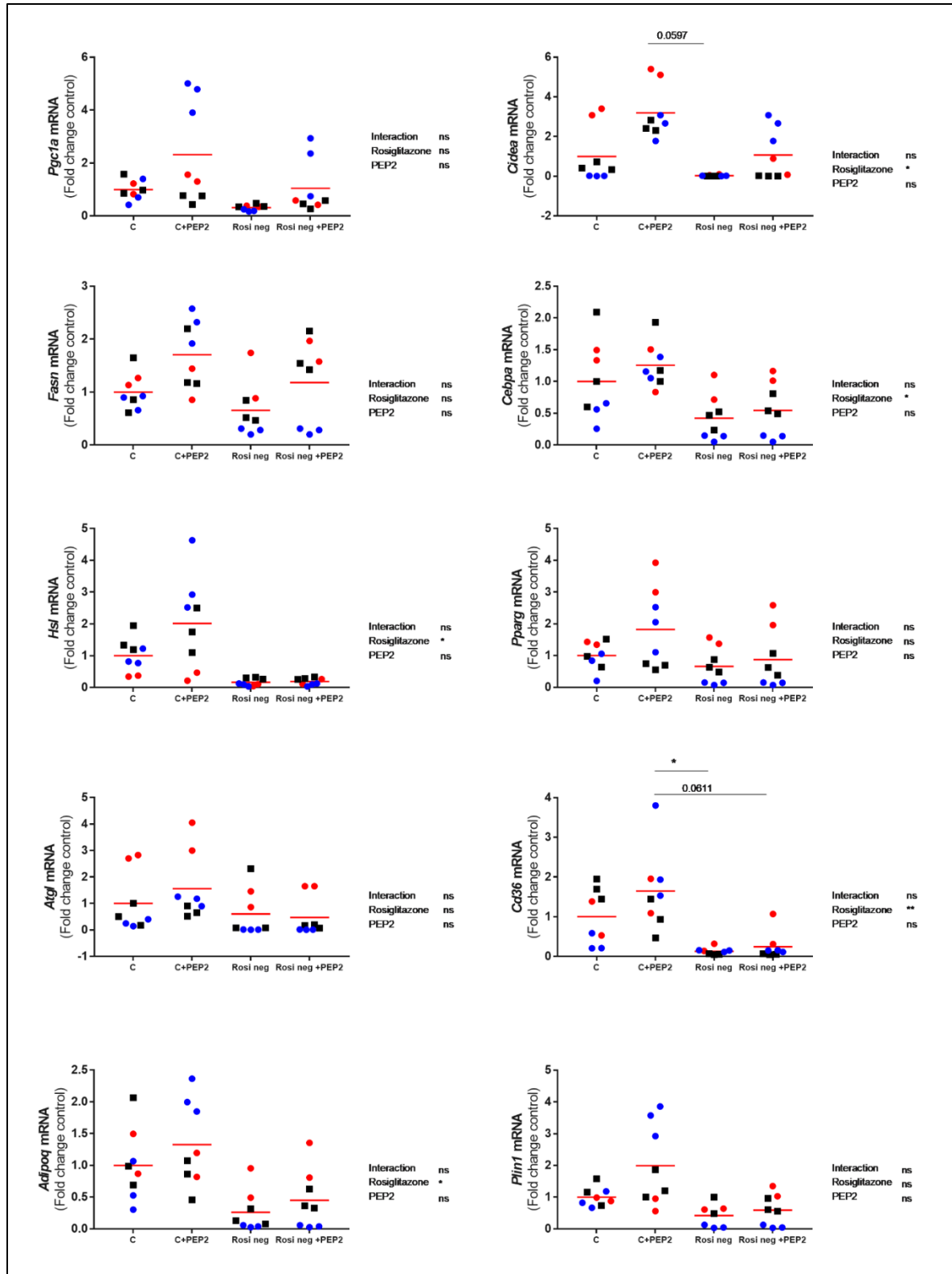


Figure 3. 13. Effect of PEP2 on 9W pre-adipocyte differentiation. Data expressed as grand mean of fold change compared to control. Data analyzed by two-way ANOVA. Different colors indicate biological replicates.

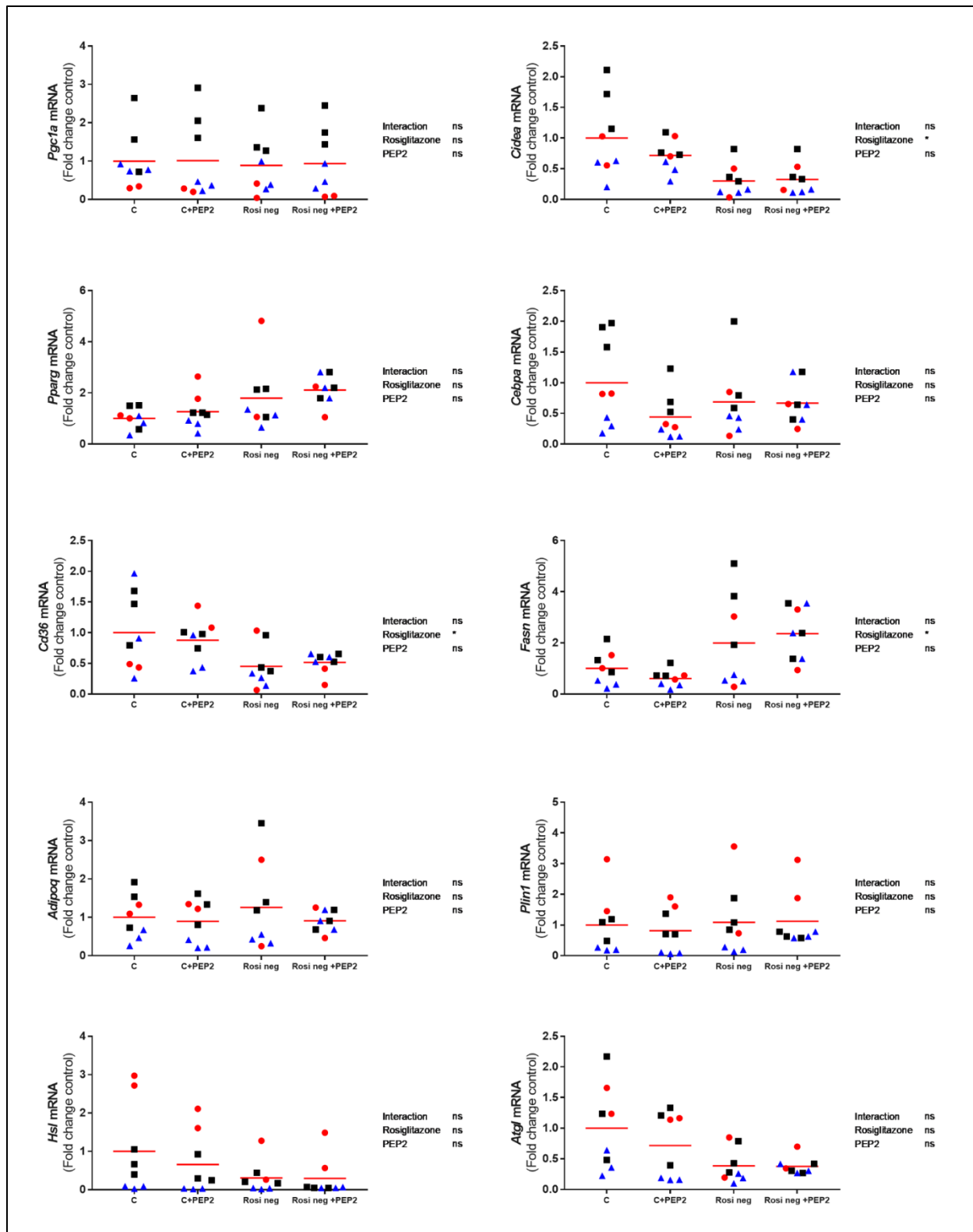
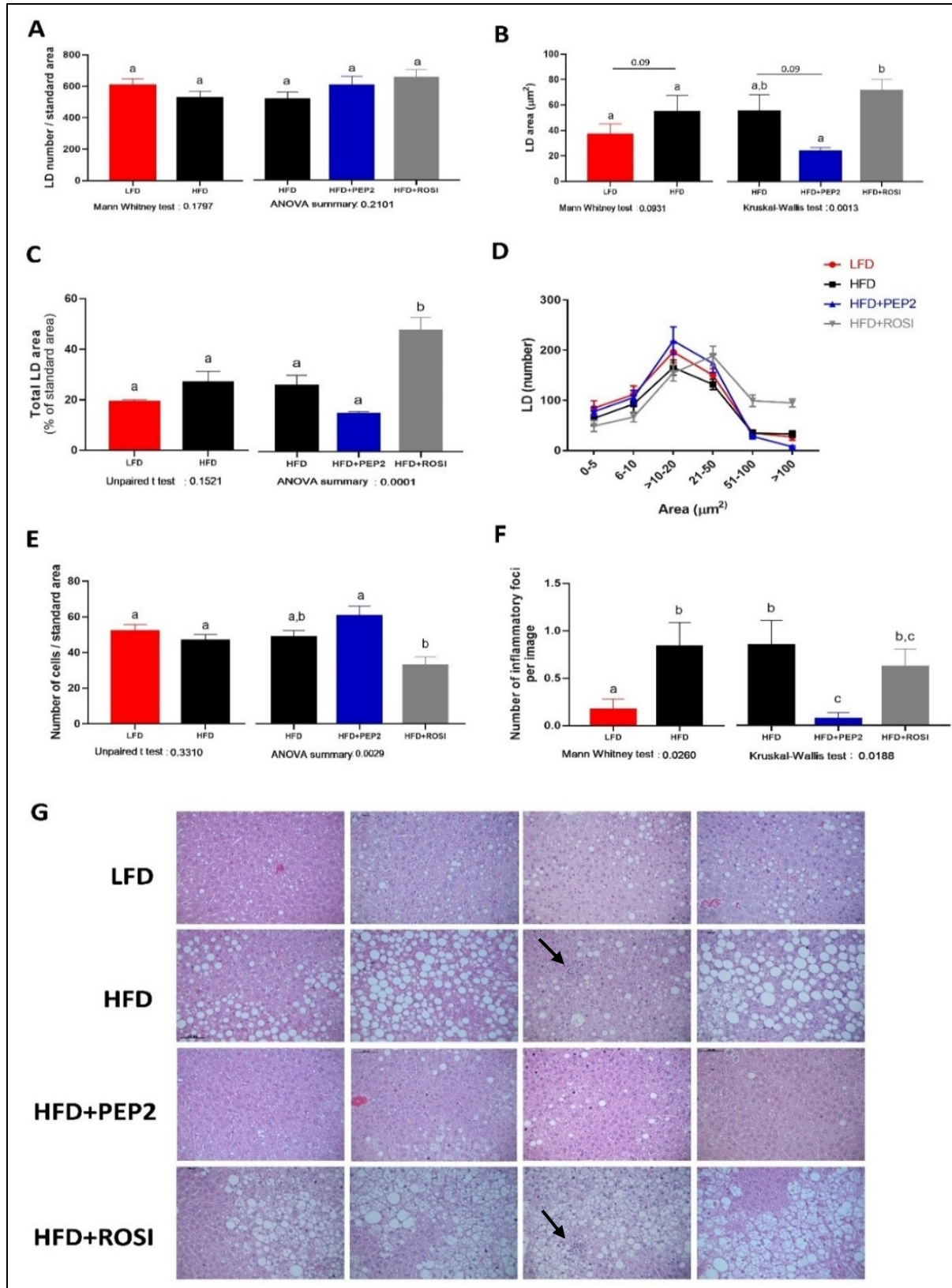


Figure 3. 14. Effect of PEP2 on 9B pre-adipocyte differentiation. Data expressed as grand mean of fold change compared to control. Data analyzed by two-way ANOVA. Different colors indicate biological replicates.

### 3.3.2.6 Liver Characterization

Morphological characterization of LD showed no differences between LFD and HFD groups in terms of total LD number (Fig. 3.15A, left) and total LD area (Fig. 3.15C, left), but LFD had 30–40% smaller individual LD area ( $p = 0.09$ ) (Fig. 3.15B, left). Among HFD groups, despite a similar number of LD in all the groups (Fig. 3.15A, right), ROSI had a similar individual LD area to HFD and an increased total LD area ( $p < 0.04$ ) (Fig. 3.15B,C, right, respectively). PEP2 had smaller individual LD area compared to ROSI ( $p < 0.0043$ ), and around 50% smaller area compared to HFD ( $p = 0.09$ ) (Fig. 3.15B, right). In addition, PEP2 had 40–50% smaller total LD area compared to HFD, but while the ANOVA showed a  $p = 0.0001$  suggesting an overall treatment effect, no statistical difference was observed between these groups (Fig. 3.15C, right,  $p = 0.2$ ). Albeit not statistically significant, the qualitative analysis of the images revealed that most of the animals had visibly less liver fat (first, second and fourth panel on Fig. 3.15G) while the minority did not (third panel Fig. 3.15G). These differences were also reflected by the distribution curve (Fig. 3.15D), which emphasized the right-shift in LD area as well as more abundant LD  $> 50 \mu\text{m}^2$  in area in the ROSI livers. Regarding hepatocyte size, no difference between LFD and HFD was observed, but PEP2 had a higher number of cells per area than ROSI ( $p = 0.0024$ ), indicative of less hypertrophy (Fig. 3.15E, right). Moreover, PEP2 and LFD exhibited fewer inflammatory foci compared to HFD ( $p = 0.026$ ), while ROSI had an intermediate effect (Fig. 3.15F, right). The differences seen in hepatic TG content (Table 3.5) and LD characterization are supported by the representative images, where we observed smaller LD, less area covered in LD and reduced inflammatory foci presence in LFD and PEP2 groups, while ROSI exhibited most of the image covered in LD (Fig. 3.15G). Hepatic cholesterol content was lower in the PEP2 group compared to HFD ( $p = 0.02$ ) and ROSI ( $p = 0.038$ ) groups, but not

different between LFD and HFD (Table 3.5). Plasma ALT was not different among the HFD groups, but LFD had lower plasma ALT concentration than HFD animals (Table 3.5). Collagen staining to identify fibrosis revealed no presence of collagen within the hepatic parenchyma in almost all the samples. However, the samples from ROSI group had at least 1 image out of 19 with presence of weak collagen staining. One sample in the LFD group exhibited marked collagen staining, which was attributed to a random finding of fibrosis (Table 3.6).



**Figure 3. 15. Liver characterization in tissues harvested from mice treated with Peptide 2 (Protocol 2).** (A) total LD number (n = 6); (B) average individual LD area (n = 6); (C) average area covered by LD (n = 6); (D) LD distribution by size (n = 6); (E) number of cells per liver area analyzed (n = 6); (F) average inflammatory foci per image (n = 5–6); (G) liver representative images. Data expressed as mean ± SEM and analyzed by two tailed t-test (LFD vs. HFD) and by one-way ANOVA or Kruskal–Wallis (HFD groups). Arrows indicate inflammatory foci. Bars/lines with different letters indicates  $p \leq 0.05$ . LD, lipid droplet; HFD, high-fat diet; LFD, low fat diet; ROSI, rosiglitazone.

**Table 3. 6. Fibrosis assessment.**

<b>GROUPS</b>	<b>Number of images POSITIVE FOR FIBROSIS (REVIEWER 1)</b>	<b>Number of images POSITIVE FOR FIBROSIS (REVIEWER 2)</b>	<b>FINAL AVERAGE</b>
<b>LFD-29</b>	0/19	0/19	0/19
<b>LFD-31</b>	0/19	0/19	0/19
<b>LFD-F6</b>	17/19	19/19	18/19
<b>HFD-35</b>	0/19	0/19	0/19
<b>HFD-63</b>	0/19	0/19	0/19
<b>HFD-F17</b>	1/19	0/19	0.5/19
<b>PEP2-43</b>	0/19	0/19	0/19
<b>PEP2-F16</b>	0/19	0/19	0/19
<b>PEP2-F35</b>	0/19	2/19	1/19
<b>ROSI-25</b>	0/19	1/19	0.5/19
<b>ROSI-27</b>	0/19	0/19	0/19
<b>ROSI-53</b>	1/19	0/19	0.5/19

### 3.3.2.7 Liver PPAR $\gamma$ and AT2R

Hepatic PPAR $\gamma$  abundance was similar between all groups (Fig. 3.16A). Interestingly, angiotensin II-type 2 receptor (AT2R) protein abundance was enhanced 2-fold ( $p=0.0004$ ) in the PEP2 group compared to HFD (Fig. 3.16B, right).

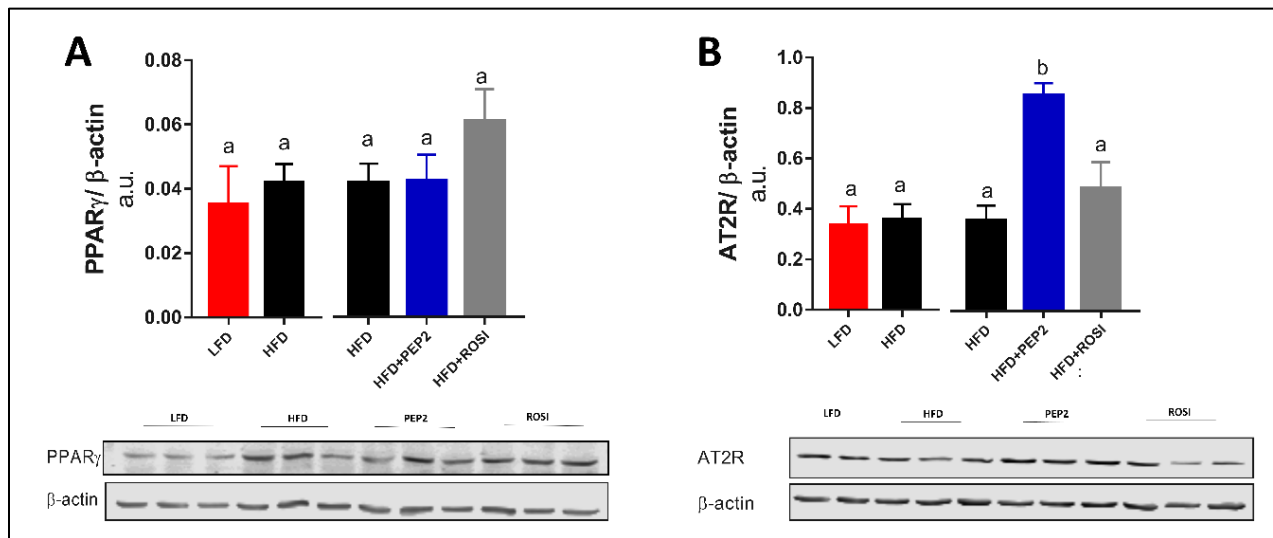


**Figure 3. 16. Liver protein abundance in tissues harvested from mice treated with Peptide 2 (Protocol 2).** (A) PPAR $\gamma$  protein abundance and (B) AT2R. Data expressed as mean  $\pm$  SEM of  $n = 5-6$  mice. Data analyzed by two-tailed t-test (LFD vs. HFD) and by one-way ANOVA or Kruskal-Wallis (HFD groups). Bars with different letters indicates  $p \leq 0.05$ . PPAR $\gamma$ , peroxisome proliferator-activated receptor gamma; AT2R, angiotensin II type 2 receptor.

### 3.3.2.8 Lipid Metabolism, Inflammation, and Fibrosis Genes

mRNA expression of PPAR alpha (*Ppara*), gamma (*Pparg*) and gamma2 (*Pparg2*) was not different among the HFD groups (Fig. 3.7A). Although pro-inflammatory gene *Tnfa* was not different among the HFD groups, a trend of reduced *Colla1* ( $p = 0.055$ ), a marker of fibrosis, was observed in PEP2 compared with ROSI (Fig. 3.17B). Among the several genes involved in lipid metabolism analyzed, only *Mogat1* showed a significant difference, with a 3-fold increase in the PEP2 group compared to HFD ( $p = 0.0017$ ), and an approximately 1.5-fold increase compared to ROSI ( $p = 0.0494$ ) (Fig. 3.17C). No changes were seen in selected genes that encode LD-associated proteins or that are involved in lipolysis (Fig. 3.17D). No difference in any of the analyzed genes was observed between LFD and HFD (Fig. 3.18).

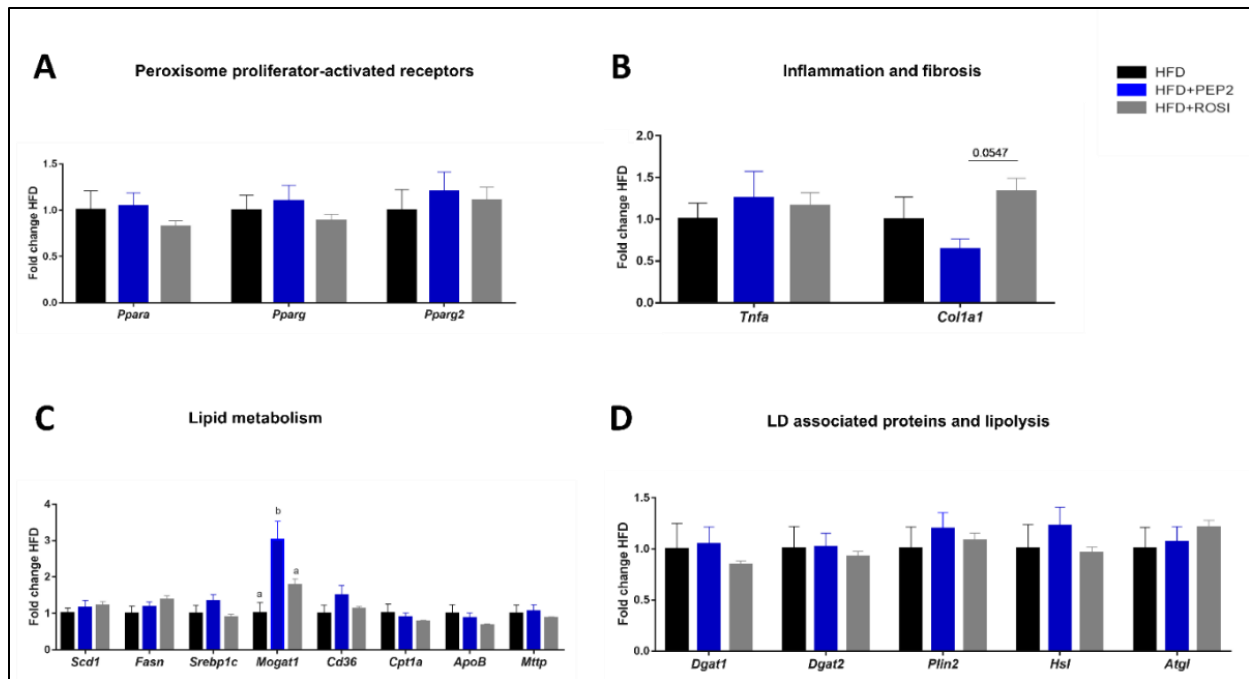


**Figure 3. 17. Liver gene expression in tissues harvested from mice treated with Peptide 2 (Protocol 2).** (A) Peroxisome proliferator-activated receptors; (B) inflammation and fibrosis related genes; (C) lipid metabolism related genes and (D) LD associated proteins and lipolysis related genes. Data expressed as mean  $\pm$  SEM of fold change of HFD control (n = 7–8) and analyzed by one-way ANOVA or Kruskal–Wallis test. Data normalized to  $\beta$ -actin gene expression. Bars with different letters indicates  $p \leq 0.05$ . LD, lipid droplet.

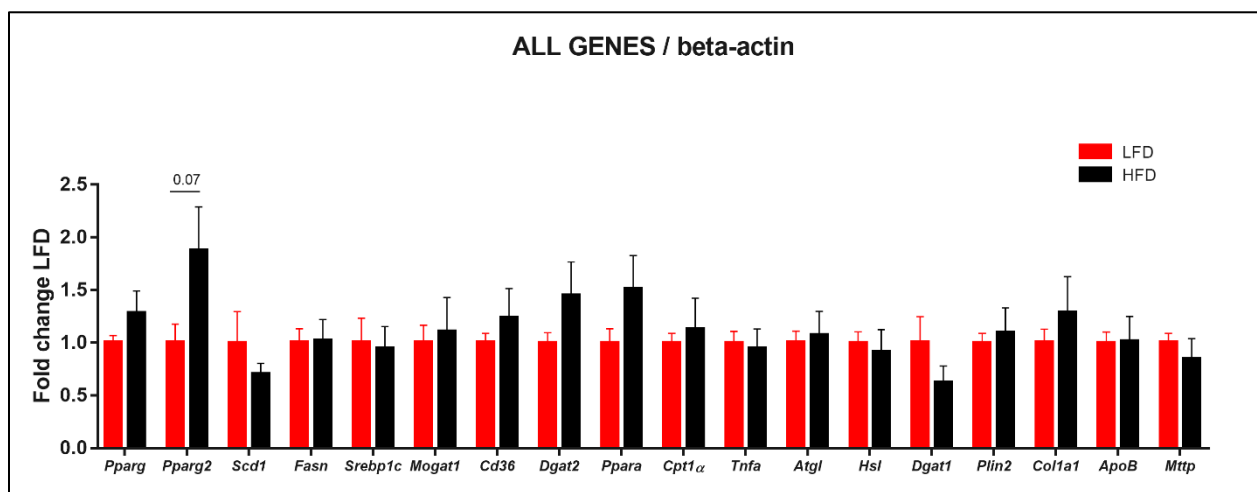


**Figure 3. 18. Lipid metabolism gene expression in LFD and HFD groups.** Data expressed as mean  $\pm$  SEM of fold change of LFD control and analyzed by two tailed t test (n=7). Data normalized to  $\beta$ -actin gene expression. HFD, high-fat diet; LFD, low fat diet.

### 3.4 Discussion

The prevalence of NAFLD, obesity and type 2 diabetes are increasing in parallel. In fact, because of the relationship between hepatic steatosis and metabolic diseases, there is a movement to change the parameters used for diagnosis of NAFLD and a name change to metabolic-associated fatty liver disease (MAFLD) is also proposed [23]; however, we have used NAFLD as the chosen abbreviation. Bioactive peptides have potential to aid in the management of metabolic diseases because they can modulate physiological processes [206] either in conjunction with pharmacological treatments or as novel, stand-alone approaches for conditions without approved pharmacotherapy, such as NAFLD. In this study, we hypothesized that diet supplementation with Peptide 2 would improve systemic and local insulin resistance and consequently, modulate features of NAFLD in HFD-induced obese-insulin resistance mice. We found that Peptide 2 supplementation: (1) improved systemic insulin resistance during the hyperinsulinemic-euglycemic clamp; (2) rescued insulin-regulated lipolysis in rWAT and iWAT, despite no change in adipocyte size or BW; (3) reduced hepatic lipid accumulation while increasing monoacylglycerol O-acyltransferase 1 (*Mogat1*) gene expression in the liver; and (4) reduced hepatic inflammatory infiltration.

EWH is a mixture of bioactive peptides shown before to improve insulin resistance and reduce adipocyte size in rodents [197]. Herein, we showed that PPAR $\gamma$  activation was enhanced in rWAT of EWH supplemented animals, which was accompanied by a better response to insulin in terms of suppression of enzymes involved in lipolysis in rWAT as well as increased p-AKT [197]. Another possibility is that HFD reduced baseline p-HSL/HSL ratio, which was restored by EWH leading to the insulin suppression of p-HSL observed. Nevertheless, these findings led us

to hypothesize that the metabolic improvements seen *in vivo* were due to modulation of PPAR $\gamma$  in WAT, similar to the action of thiazolidinediones, which would induce adipogenesis and promote the appearance of more insulin sensitive adipocytes [116] improving systemic insulin sensitivity. We then asked if there were specific peptides from the EWH mixture that could modulate PPAR $\gamma$  abundance and an *in vitro* screening revealed that a few peptides were able to mimic insulin effect of enhancing PPAR $\gamma$  in preadipocytes [198], which led us to investigate their effects *in vivo*. The peptide with greater potential based on our screening (Fig. 3.4) was Peptide 2 and we further evaluated its effects in obese, insulin resistant mice focusing on WAT and the liver.

Insulin resistance is a key feature of type 2 diabetes, and it plays a significant, multi-factorial role in the development of NAFLD [216]. Insulin resistance in WAT leads to impaired suppression of lipolysis, which increases NEFA delivered to the liver whereas hepatic insulin resistance impairs the suppression of gluconeogenesis [216]. Egg-derived peptides and hydrolysates were shown before to improve insulin sensitivity in rodents [175, 197, 207] but relative contributions of hepatic versus non-hepatic tissues were not evaluated. Therefore, we first investigated the potential of Peptide 2 supplementation to reduce insulin resistance using a hyperinsulinemic-euglycemic clamp, the gold standard technique for this outcome measurement. We observed that LFD, PEP2 and ROSI groups had lower insulin resistance compared to HFD group. Although rosiglitazone, a known insulin sensitizer, was expected to reduce insulin resistance, this is the first study showing that dietary supplementation with Peptide 2 improves insulin resistance, despite no changes in glucose tolerance or BW. Moreover, suppression of endogenous glucose production during clamp was stronger in the PEP2 and LFD groups compared to HFD, consistent with better hepatic insulin sensitivity. This improvement in insulin

resistance was supported by a reduced HOMA-IR in the LFD group, but despite a decrease in PEP2 group HOMA-IR, it was not statistically significant. Not only systemic insulin sensitivity was improved by Peptide 2 supplementation but WAT insulin signaling was also rescued. The normalized regulation of lipolysis by insulin would be predicted to reduce NEFA delivery to the liver. Taken together, these results suggest that the improvement in systemic insulin sensitivity in the PEP2 group could be in part because of a decreased spillover of lipids from WAT to non-adipose tissues due to a better hormonal regulation of lipolysis.

We then asked if the improvement in WAT insulin signaling was associated with PPAR $\gamma$  activation. PPAR $\gamma$  regulates adipogenesis and has an important role in glucose and lipid metabolism. We previously showed that Peptide 2 increased PPAR $\gamma$  protein in adipocyte cell culture [198]. However, we did not see higher PPAR $\gamma$  activation in any of the fat pads tested. This was accompanied by no overall changes in WAT adipocyte size or adipogenesis markers among HFD group, substantiated by no effect in adipogenesis markers during preadipocyte differentiation of mouse-derived cells in culture. On the other hand, we observed increased activation of PPAR $\gamma$  in rWAT of ROSI animals. Therefore, the effects of Peptide 2 are different from rosiglitazone, supporting a PPAR $\gamma$  independent mechanism of action. We conclude at this point that Peptide 2 acts to improve insulin signaling independently of PPAR $\gamma$ , at least in the models used in this study; therefore, other mechanisms need to be investigated.

Ongoing efforts seek to validate the use of insulin sensitizers, such as thiazolidinediones for the treatment of NAFLD. However, findings are controversial, with most of the benefits seen with pioglitazone rather than rosiglitazone [204, 205]. In rodents, rosiglitazone plays a dual role depending on the level of hepatic PPAR $\gamma$  expression [217]. For example, in mice with low hepatic expression of PPAR $\gamma$ , rosiglitazone protects against lipid accumulation while in obese

mice with elevated PPAR $\gamma$ , rosiglitazone exacerbates hepatic steatosis [217]. In fact, PPAR $\gamma$  is a key up-regulator of hepatic steatosis in HFD-induced obese mice treated with rosiglitazone [218]. Similarly, in this study we showed that the ROSI group, although more insulin-sensitive, exhibited higher liver weight and TG content compared to HFD, whereas PEP2 did not worsen HFD-induced hepatic steatosis. PPAR $\gamma$  is mainly expressed in adipose tissue, but it is also expressed in the liver [219] and its expression is enhanced in the liver of HFD fed animals [217, 218]. Similarly to the literature, in our study HFD feeding tended to increase hepatic *Pparg2* gene expression and PPAR $\gamma$  protein compared to the LFD group, but neither PEP2 nor ROSI groups affected *Pparg* or *Pparg2* mRNA. However, albeit not significant, we saw a trend to increase hepatic PPAR $\gamma$  protein abundance in the ROSI group compared to HFD control. Peptide 2 supplementation did not increase PPAR $\gamma$  protein abundance above the HFD-induced effect. Although we did not measure hepatic PPAR $\gamma$  DNA binding activity, the results suggest that Peptide 2 may not be directly activating hepatic PPAR $\gamma$ , suggesting a difference in mechanism from rosiglitazone.

In NAFLD, progression to NASH is characterized by increased LD size, hepatocyte hypertrophy and inflammation [20, 201]. Surprisingly, the ROSI group exhibited a true microvesicular steatosis mixed with macrovesicular steatosis, while PEP2 and HFD groups appeared to have macrovesicular steatosis, which is considered more pathological [212-214]. However, PEP2 tended to decrease LD area compared to HFD. Therefore, PEP2 group presented a macrovesicular steatosis with small LD vs. macrovesicular steatosis with large LD in the HFD group. The importance of LD size is highlighted by findings showing that macrovesicular steatosis is linked to fibrosis and microcirculation impairment in rodents [220, 221] and fibrogenesis in humans [212]. Moreover, the extent of macrovesicular steatosis can impact liver

transplantation and graft survival in humans [213]. Other food-derived peptides reduce LD size, for example pepsin-generated EWH supplementation reduces the number and size of LD in rats, accompanied by a decrease in plasma inflammatory and oxidative stress markers [181]. In addition, supplementation with a peptide derived from sweet lupine (GPETAFLR) improves hepatic steatosis and reduces TG content. The mechanism of action suggested was through PPAR $\alpha$  and uncoupling protein 1 (UCP1) activation and reduced hepatic expression of fatty-acid synthase gene (*Fasn*) and inflammatory markers, but only mRNA levels were measured, not their activity [222]. In another study, the improvement in NAFLD seen after potato-derived peptide (DIKTNKPVIF) supplementation is accredited to 5'-adenosine monophosphate-activated protein kinase (AMPK) activation and decreased inflammatory markers [223]. We find no changes in gene expression of *Ppara* or *Fasn* after Peptide 2 supplementation. Therefore, the mechanism behind the effect of PEP2 supplementation to modulate hepatic LD size is unclear. Decrease in BW is associated with improvements in NAFLD; being an important confounding factor when evaluating an interventional study. However, we observed modulation of LD size by Peptide 2 independently of changes in BW. In the studies mentioned above, one of them reported similar final BW but a lower eWAT mass [181], while the other reported decreased BW [222] and one did not report BW measurements [223]. It is worth noting that several peptides reduce hepatic lipid accumulation; however, whether it is a protein (amino-acid)-related or a peptide-specific effect remains to be determined.

The observed improvement in liver morphology was independent of hepatic TG content, which was not significantly different between PEP2 and HFD groups, but a decrease in cholesterol content was seen between HFD and PEP2 groups. This is similar to Song et al. [224], who report a reduction of the hepatic total cholesterol content after quinoa supplementation but

no difference between HFD and quinoa supplemented groups in terms of hepatic TG [224]. They attribute the improvement in NAFLD in part to changes in hepatic phospholipids, such as increased lysophosphatidylcholine and pantothenic acid, and decreased phosphatidylcholine and dioleoylphosphatidylcholine [224]. Indeed, impairment of cholesterol metabolism may be the key driver to large LD formation, rather than TG metabolism [212]. Despite higher hepatic TG content in the ROSI group, lack of change in plasma ALT indicates no further liver damage on top of that induced by HFD. Therefore, rather than only LD size or amount, its lipid composition also plays a key role in causing hepatic damage.

Inflammation and fibrosis are important markers to evaluate NAFLD progression to NASH. Peptide 2 supplementation attenuated the density of hepatic inflammatory foci consistent with the parent EWH hydrolysate decreasing plasma inflammatory markers. In the same study, an increase in AT2R was seen in WAT and liver [197]. Moreover, the hydrolysate reduced blood pressure in rats by modulating the RAS, including reduction of angiotensin II-type 1 receptor and induction of AT2R abundance in the aorta of rats [186]. AT2R is not only involved in the modulation of blood pressure by opposing angiotensin II-type 1 receptor activity, but its stimulation is associated with reno- and cardio-protective effects, anti-inflammatory and antifibrotic action, among others as extensively reviewed elsewhere [225]. In fact, RAS modulation is linked to hepatic fibrosis in rodents and humans with NAFLD [226, 227]. In addition, AT2R has antifibrotic action in the liver of mice [228] and plays a role in blood flow regulation [229, 230]. When we evaluated the presence of collagen staining as an indication of fibrosis, we found no presence of collagen in most of the samples. This may be because 14 wk of 45% HFD is insufficient to induce marked inflammation and fibrosis. Although *Coll1a1* mRNA was increased after 19 wk of 60% HFD, only at 50 wk of dietary intervention was fibrosis seen

in histological analysis [231]. Considering that macrovesicular steatosis with large LD impairs hepatic blood flow [220] and our finding that PEP2 had the highest hepatic AT2R and lowest mRNA expression of type 1 collagen, we speculate that AT2R up-regulation may be a mechanism by which PEP2 decreases inflammation and fibrosis over a longer-term of NAFLD but further research is needed to confirm this speculation. Conversely, ROSI did not induce AT2R or suppress collagen gene expression, differentiating its hepatic effects from PEP2.

Many pathways underlie hepatic lipid accumulation including increased delivery of NEFA to the liver following WAT lipolysis, decreased fatty acid oxidation, increased DNL or decreased VLDL secretion [201]. Although differences in gene expression involved in glucose and lipid metabolism occur between hepatocytes displaying large and small LD in the liver [232], surprisingly the mRNA expression patterns in our study are similar between ROSI and HFD groups. This does not exclude the role of ROSI in modulating lipid metabolism pathways since we did not measure the activity of the related enzymes. The only difference observed between PEP2 and HFD group was higher *Mogat1* gene expression in the PEP2 group. *Mogat1* encodes the mannosylglycoprotein N-acetyl-glucosaminyl transferase 1 (MGAT1), which catalyzes TG synthesis via the monoacylglycerol O-acyltransferase pathway. The role of MGAT1 in liver steatosis is controversial, with some studies showing that silencing of hepatic MGAT1 improves steatosis and blood glucose levels [233, 234]. Conversely, others demonstrate that MGAT1 knockout in liver does not improve hepatic steatosis, liver TG content, insulin sensitivity or glucose tolerance in HFD-fed mice [235]. Moreover, hepatic overexpression of MGAT1 does not increase liver TG content in HFD mice but does in LFD animals [235]. In our study using fasted animals, we found reduced LD size concomitant with higher *Mogat1* gene expression, but no other direct target of PPAR $\gamma$  had increased expression. Intriguingly, increased hepatic *Mogat1*

expression and MGAT activity occur after prolonged fasting with higher fat oxidation, and are both dependent and independent of *Ppara* expression, suggesting that MGAT1 regulates the hepatic fasting response [236]. This is consistent with the reduced LD size found in our study. We did not see altered *Ppara* gene expression, and we did not measure its activity directly, therefore, further investigation is needed to elucidate the role of Peptide 2 in hepatic lipid metabolism and its relationship to MGAT1.

Because our intended use of rosiglitazone was as a positive control for insulin sensitization and PPAR $\gamma$  agonism, differences in the hepatic phenotype versus PEP2 were unexpected. Our results suggest that, in contrast to rosiglitazone, Peptide 2 does not activate PPAR $\gamma$  in vivo, and, in conditions of HFD-induced obesity and insulin resistance, Peptide 2 does not worsen HFD-induced hepatic steatosis. Rather, Peptide 2 supplementation improves insulin resistance and rescues insulin-regulated lipolysis in WAT while tending to reduce LD area, decreasing inflammation, and possibly preventing fibrosis, crucial processes to prevent NAFLD progression to NASH.

We note that a HFD containing 45% kcal fat is not commonly used to generate NASH animal models, with most of the diet-induced models receiving a high-fat/high sugar diet. Thus, less hepatic inflammation and fibrosis in our model was observed compared with the available literature [237, 238]. The peptide was administered mixed in the animals' diet, which does not allow for precise specification of the dose of peptide received by each animal. On the other hand, this dietary intervention has advantages over daily gavage for chronic studies in terms of reducing stress in the animals, which worsens insulin resistance, our main outcome. It is important to note that oxidative stress can also be involved in hepatic steatosis progression to NASH and that several food-derived peptides exert antioxidant activity as recently reviewed

[239]. In future research, it would be worth exploring the antioxidant activity of Peptide 2 as a possible mechanism of preventing disease progression. In addition, it would be relevant to test Peptide 2 bioavailability and absorption pathways, including ability to modulate cell tight junction proteins. Lastly, all our data reflect the overnight fasting state which, compared to fed state, may yield a different gene expression pattern and less pronounced effects in some of the outcomes reported.

In conclusion, this study shows for the first time that Peptide 2 diet supplementation improves insulin resistance in HFD-induced obese and insulin resistant mice, while at the same time preventing further exacerbation of HFD-induced NAFLD features independently of BW. On the other hand, rosiglitazone-treated mice, despite having improved IR, exhibited worse hepatic steatosis if administered together with HFD. Therefore, compared to rosiglitazone, Peptide 2 promotes more beneficial effects on the combined outcomes of insulin resistance, WAT dysfunction and hepatic steatosis.

**Institutional Review Board Statement:** The animal study protocol was approved by the Animal Care and Use Committee of the University of Alberta (Protocol# 1472) in accordance with guidelines issued by the Canadian Council on Animal Care.

**Acknowledgments:** We would like to thank Bryan Lum, Samantha Kinney, and Dr. Herver Brunetta for their skilled assistance during the clamp experiments, qPCR, and cell culture experiments, respectively.

**Conflicts of Interest:** The authors declare no conflicts of interest.

#### **4. CHAPTER 4: IRW (isoleucine–arginine–tryptophan) improves glucose tolerance in high-fat diet-fed C57BL/6 mice via activation of insulin signaling and AMPK pathways in skeletal muscle**

This section presents the outcomes from experiments done to address objective #3. It reflects work done in collaboration with Dr. Myoungjin Son and Dr. Khushwant S. Bhullar. For this study, I performed the experiments in WAT, analyzed all the data, and wrote the manuscript's first and last draft. The manuscript was edited by Dr. Catherine Chan and Dr. Jianping Wu. This manuscript was published in the journal *Biomedicines* in May 2022 [207]. A PDF version of this manuscript is provided in Appendix 2.

**IRW (isoleucine–arginine–tryptophan) improves glucose tolerance in high-fat diet-fed C57BL/6 mice via activation of insulin signaling and AMPK pathways in skeletal muscle**

Stephany C. de Campos Zani <sup>1</sup>, Myoungjin Son <sup>2</sup>, Khushwant S. Bhullar <sup>2,3</sup>, Catherine B. Chan <sup>1,2</sup>, and Jianping Wu <sup>2\*</sup>

<sup>1</sup>Department of Physiology, University of Alberta, Edmonton, Alberta Canada, T6G2H7;  
zani@ualberta.ca; cbchan@ualberta.ca

<sup>2</sup>Department of Agricultural Food & Nutritional Science, University of Alberta, Edmonton, Alberta, Canada, T6G2P5; mjson0823@gmail.com; jw3@ualberta.ca

<sup>3</sup>Department of Pharmacology, University of Alberta, Edmonton, Alberta, Canada, T6G2H7;  
bhullar@ualberta.ca

\*Correspondence: jw3@ualberta.ca; Tel.: +1-780-492-6885; Fax: +1-780-492-4346

## Abstract

IRW (isoleucine–arginine–tryptophan) has antihypertensive and anti-inflammatory properties in cells and animal models and prevents angiotensin-II- and tumor necrosis factor (TNF)- $\alpha$ -induced insulin resistance *in vitro*. We investigated the effects of IRW on body composition, glucose homeostasis and insulin sensitivity in a HFD-induced insulin resistant model. C57BL/6 mice were fed HFD for 6 weeks, after which IRW was incorporated into the diet (45 or 15 mg/kg BW) until week 14. IRW45 (at a dose of 45 mg/kg BW) reduced BW ( $p = 0.0327$ ), fat mass gain ( $p = 0.0085$ ), and preserved lean mass of HFD mice ( $p = 0.0065$ ), concomitant with enhanced glucose tolerance and reduced fasting glucose ( $p < 0.001$ ). In skeletal muscle, IRW45 increased insulin-stimulated AKT phosphorylation ( $p = 0.0132$ ) and GLUT translocation ( $p < 0.001$ ). Angiotensin 2 receptor (AT2R) ( $p = 0.0024$ ), phosphorylated AMPK $\alpha$  ( $p < 0.0124$ ) and PPAR $\gamma$  ( $p < 0.001$ ) were enhanced in skeletal muscle of IRW45-treated mice, as was the expression of genes involved in myogenesis. Plasma angiotensin converting enzyme-2 (ACE2) activity was increased ( $p = 0.0016$ ). IRW improves glucose tolerance and body composition in HFD-fed mice and promotes glucose uptake in skeletal muscle via multiple signaling pathways, independent of ACE inhibition.

**Keywords:** ACE; bioactive peptides; IRW; insulin resistance; obesity

## 4.1 Introduction

The pathophysiology of metabolic syndrome is complex, involving obesity, insulin resistance, dyslipidemia, and hypertension, but oxidative stress and inflammation also contribute to its progression [240]. Metabolic syndrome also involves overactivation of the RAS, which is linked to obesity and insulin resistance [241]. Besides the systemic RAS, an independent local RAS in skeletal muscle [242] influences insulin responsiveness [229]. ACE inhibitors or AT1R blockers reduce insulin resistance in animal models and improve insulin sensitivity in humans [243-245], supporting the link between RAS and insulin resistance. In addition, RAS blockade reverses the deleterious effect of exogenous angiotensin II on skeletal muscle mitochondria and improves glycemic control in mice [246].

Food-derived bioactive peptides exert effects beyond their nutritional value and modulate physiological parameters in different tissues [247]. Previous research demonstrated the beneficial effects of egg-derived peptides and hydrolysates on glucose tolerance [197], adipogenic capacity [198], and osteoblast differentiation [248]. Some egg-derived bioactive peptides are ACE inhibitors [249] and ameliorate insulin resistance and glucose intolerance [165]. Of particular interest is the ovotransferrin-derived, ACE inhibitory peptide [185] tripeptide IRW (isoleucine–arginine–tryptophan), which exhibits anti-inflammatory and antioxidant effects in endothelial cells [188, 190], reduces blood pressure in rodents [187, 250], and improves angiotensin II- or TNF- $\alpha$ -induced insulin resistance in a skeletal muscle cell line [191, 192]. However, whether IRW has glucoregulatory properties *in vivo* is unknown.

In this study, we investigated the insulin sensitizing effects of IRW *in vivo* using a HFD-induced obese-insulin resistant mouse model. Because of the intimate crosstalk between obesity,

hypertension, and insulin resistance, we hypothesized that IRW supplementation improves glucose intolerance by inhibiting RAS locally in skeletal muscle to improve insulin signaling.

## 4.2 Materials and Methods

### 4.2.1 Animals, Diet, and BW Measurements

The animal experimental protocol was approved by the Animal Care and Use Committee of the University of Alberta (Protocol# 1472) in accordance with guidelines issued by the Canadian Council on Animal Care and followed the ARRIVE guidelines. Thirty-two male 4-week-old C57BL/6 mice were purchased from Charles River Canada (St. Constant, QC, Canada) and housed 2 per cage with *ad libitum* access to standard food and water, a 12:12-h cycle of light:dark with 60% humidity and 23 °C temperature. Eight mice were fed with low fat diet (LFD, 10% kcal from fat, Envigo, Indianapolis, IN, USA, TD06415) and the remainder with HFD (45% kcal from fat, Envigo TD110675) for 6 weeks. Diet composition is shown in Table 4.1. The initial 6 weeks of HFD were used to induce obesity, confirmed by at least a 20% increase in BW and significantly higher fat mass and lower lean mass compared to LFD-fed animals (Table 4.2). Animals were then divided into 4 groups: LFD control, HFD control, high dose IRW + HFD (IRW45; at a dose of 45 mg/kg BW), low dose IRW + HFD (IRW15; at a dose of 15 mg/kg BW) (n = 8/group). These diets continued for another 8 weeks with *ad libitum* access to food and water. In total, mice consumed HFD for 14 weeks to induce obesity and glucose intolerance [251]. Food consumption was measured once every 3 days and BW twice weekly. Body composition was evaluated using magnetic resonance imaging (MRI, Echo MRI™, Echo Medical Systems LLC, Houston, TX, USA) at week 6 and week 14.

**Table 4. 1. Diet composition.**

	<b>LFD</b>	<b>HFD</b>	<b>IRW15</b>	<b>IRW45</b>
<b>Casein (g/kg)</b>	210.0	245.0	245.0	245.0
<b>L-Cystine (g/kg)</b>	3.0	3.5	3.5	3.5
<b>Corn Starch (g/kg)</b>	445.0	85.0	85.0	85.0
<b>Maltodextrin (g/kg)</b>	50.0	115.0	115.0	115.0
<b>Sucrose (g/kg)</b>	160.0	200.0	200.0	200.0
<b>Lard (g/kg)</b>	20.0	195.0	195.0	195.0
<b>Soybean Oil (g/kg)</b>	20.0	30.0	30.0	30.0
<b>Cellulose (g/kg)</b>	37.15	58.0	58.0	58.0
<b>Mineral Mix, AIN-93G-MX (94046) (g/kg)</b>	35.0	43.0	43.0	43.0
<b>Calcium Phosphate, dibasic (g/kg)</b>	2.0	3.4	3.4	3.4
<b>Vitamin Mix, AIN-93-VX (94047) (g/kg)</b>	15.0	19.0	19.0	19.0
<b>Choline Bitartrate (g/kg)</b>	2.75	3.0	3.0	3.0
<b>IRW (mg/kg BW)</b>	n/a	n/a	15	45

**Table 4. 2. Body composition of C57BL/6 mice after 6 weeks of LFD or HFD feeding.**

	<b>LFD (n=7-8)</b>	<b>HFD (n=24)</b>
<b>BW gain (g)</b>	8.37±1.0 <sup>a</sup>	9.23±0.4 <sup>a</sup>
<b>Fat mass %</b>	22.25 ± 1.5 <sup>a</sup>	29.94 ± 0.7 <sup>b</sup>
<b>Lean mass %</b>	70.26 ± 1.5 <sup>a</sup>	63.14 ± 0.7 <sup>b</sup>

Abbreviations: BW, body weight; LFD, low fat diet; HFD, high-fat diet.

#### 4.2.2 *IRW Dosage*

The estimated doses of IRW used were 45 mg/kg BW and 15 mg/kg BW. The dosages were selected based on previous studies done by our group in spontaneous hypertensive rats [187, 250] and cell line studies [185, 188]. The peptide was administered mixed in the animals' diet starting at week 7 of the 14-week trial, and the animals had ad libitum access to food and water. IRW was synthesized by Genscript (Piscataway, NJ, USA) with  $\geq 98\%$  purity.

#### 4.2.3 *Oral Glucose Tolerance and Insulin Tolerance Tests*

At weeks 12 and 13, respectively, ITT and OGTT were performed [252] with the following modifications: For ITT, 1.5 IU/kg BW insulin was injected intraperitoneally. For OGTT, 70% glucose solution was used, and 1 g of glucose/kg BW was given via oral gavage. In both cases, blood glucose was measured for up to 2 h. Blood glucose was measured from the tail vein using a Contour®Next glucometer (Mississauga, ON, Canada). OGTT was the primary outcome assessed in this study.

#### 4.2.4 *Tissue Collection*

At week 14, all animals were fasted for 16 h and injected with insulin (2 IU/kg BW) intraperitoneally to stimulate insulin signaling 10 min prior to euthanasia. Animals were euthanized using CO<sub>2</sub> and blood was collected via cardiac puncture. Plasma, gastrocnemius skeletal muscle and WAT from retroperitoneal and epididymal depots were collected, snap frozen, and stored at  $-80\text{ }^{\circ}\text{C}$  until further analysis.

#### 4.2.5 *Protein Extraction and Western Blotting*

Total protein from skeletal muscle was extracted using a lysis buffer containing phosphatase and protease inhibitors. WAT total protein extraction was performed using a commercial kit (Invent Biotechnologies Inc., Plymouth, MA, USA). Plasma membrane protein was extracted using a commercial kit (Thermo Fisher Scientific, Waltham, MA, USA)[191]. Total protein content was measured using the bicinchoninic acid assay. Western blotting was performed as previously [197] with the following modifications: a 9% sodium dodecyl sulfate polyacrylamide gel electrophoresis was run and protein was transferred to a nitrocellulose membrane, which was incubated overnight with antibodies against p-AKT (Cell Signaling Technology, Beverly, MA, USA), AKT (Santa Cruz Biotechnologies Inc., Dallas, TX, USA), GLUT4 (Abcam, Toronto, ON, Canada), ACE, ACE2, AT1R, AT2R, Mas receptor, PPAR- $\gamma$ , mammalian target of rapamycin (mTOR), p-mTOR, AMPK $\alpha$ , p-AMPK $\alpha$  (Thr172), P70 S6 kinase (S6K), p-P70 S6K (Thr389), uncoupling protein (UCP)-1 (Sigma, St. Louis, MO, USA),  $\beta$ -actin (Sigma) and glyceraldehyde-3-phosphate dehydrogenase (GAPDH). After incubating with appropriate fluorescent-conjugated secondary antibodies (Li-cor Biosciences, Lincoln, NE, USA) for 1 h at room temperature, protein bands were quantified by densitometry using Image Studio Lite 5.2 (Li-Cor Biosciences).

#### 4.2.6 *Plasma RAS Components and Insulin*

Plasma concentrations of RAS components were quantified by mouse specific commercial ELISAs: ACE (Aviva System, San Diego, CA, USA), ACE2 (Abcam), angiotensin II (Enzo Life Sciences, Burlington, ON, Canada), angiotensin (1–7) (Aviva System).

#### 4.2.7 *RNA Sequencing and Quantitative RT-PCR (qPCR)*

Total RNA was extracted from skeletal muscle using TRIzol reagent (Invitrogen, Life Technologies Inc., Burlington, ON, Canada) and quantified by measuring the absorbance at 260 nm and purity assessed by the A260/280 ratio. Total RNA (500 ng, with RNA integrity number > 8 for all samples) was used for the preparation of RNAseq libraries with the NEBNext Ultra II Directional RNA Library Prep Kit from Illumina (NEB, Mississauga, ON, Canada). Enriched mRNA was reverse-transcribed, and second-strand cDNA synthesis was performed. Double-stranded cDNAs were A-tailed to enable adapter ligation and, finally, libraries were indexed by 15 PCR cycles. Libraries were sequenced on a NextSeq 500 instrument (Illumina), following a paired-end 150 cycle protocol. Deregulated transcripts were annotated using the BioMart database from Ensembl (EMBL-EBI Hinxton, Cambridgeshire, UK).

For qPCR, cDNA was synthesized from 1 µg total RNA using the High-Capacity cDNA Reverse Transcription Kit (Thermo Fisher Scientific, Waltham, MA, USA). mRNA expression of target genes was determined by real-time qPCR using GAPDH as the endogenous control. All of the qPCR experiments and analyses were conducted using the MIQE guidelines.[253] The primers were designed based on the genomic sequence deposited in GenBank are described in Table 4.3.

**Table 4. 3. Primers sequences used for RT-PCR assays.**

<b>Gene</b>	<b>Forward Primer</b>	<b>Reverse Primer</b>
<b><i>Rbm5</i></b>	TTGTAATCTGAGTCCC GCCG	CATGGGTGGTATGTTTTAAGGGA
<b><i>Mdm2</i></b>	CCACAGACTAACGACTCGACC	TTTTTGAGGCCCTACTGCGA
<b><i>Dlg1</i></b>	AGATCGCATCATATCGGTGAA	TCAAAACGACTGTACTCTTCGG
<b><i>Myom1</i></b>	CAGATGTGTGGCCTCAACTGA	TCGGATTGACTTTGCTCCT
<b><i>Aspn</i></b>	CTCCAATGTGTGGGTAGGGG	GCACCTGGATCCTAACCCCTC
<b><i>Pparg</i></b>	GGGAAAGACCAGCAACAACC	GCAGTGAAGAATCGGACCT
<b><i>Plin2</i></b>	GAAGGACGTGCAAACAGAAAGG	CTGGGCTATCACGTGGCTCG
<b><i>Lpl</i></b>	GGGAAAGGACTCAGCAGTGTT	TAGGTGGAGGCCACTTCAAGA
<b><i>Cebpa</i></b>	CCCTTGCTTTTTGACCTCC	TGCCCCCATTCTCCATGAAC
<b><i>Gapdh</i></b>	TGAAATGTGCACGCACCAAG	GGGAAGCAGCATTTCAGGTCT

Abbreviations: *Rbm5*, RNA binding motif 5; *Mdm2*, nuclear-localized E3 ubiquitin ligase; *Dlg1*, Discs large homolog 1; *Myom1*, myomesin 1; *Aspn*; asporin; *Pparg*, eraxisome proliferator- activated receptor gamma; *Plin2*, perilipin2; *Lpl*, lipoprotein lipase; *Cebpa*, CCAAT enhancer binding protein A; *Gapdh*, glyceraldehyde-3-phosphate dehydrogenase.

#### 4.2.8 Statistics and Sample Size

All data presented were expressed as mean  $\pm$  SEM of 5–8 mice from each treatment group as indicated in the figure and table legends. Statistical analysis was performed using GraphPad Prism 7.0 (San Diego, CA, USA). Outliers indicated by the statistical software were removed prior to data evaluation. Data were evaluated by one-way ANOVA, Kruskal–Wallis’ test, or two-way ANOVA when appropriate. HFD group was set as the control group for all the analysis because our intention was to evaluate the impact of a HFD supplemented with peptide compared

to HFD alone. For RNA sequencing, transcripts were considered differentially expressed when they had a corrected  $p$ -value  $< 0.05$ . Post hoc analysis was done using Bonferroni's or Dunn's test.  $p$ -value was considered significant if  $< 0.05$ .

### 4.3 Results

#### 4.3.1 Food Intake and Body Composition

No sustained differences in food intake were detected between the groups (Fig. 4.1). At week 14 the LFD group had lower BW than the HFD group ( $p < 0.001$ ). Of the peptide treatments, only the high dose of IRW (IRW45) reduced final BW ( $p = 0.0327$ ) and both absolute (g) and relative (%) BW gain ( $p < 0.001$ ). Moreover, the IRW45 group presented lower absolute (g) ( $p < 0.001$ ) and relative (%) fat mass gain ( $p = 0.0085$ ), and less relative (%) lean mass loss ( $p = 0.0065$ ) compared to the HFD group (Table 4.4). BW and composition changes were not seen with IRW15.

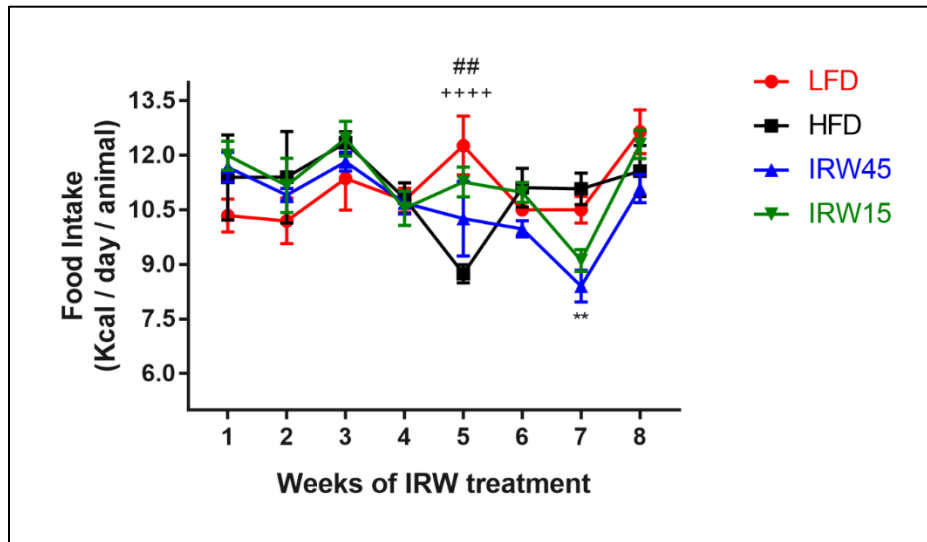


**Figure 4. 1. Food intake measured as kcal intake per day per animal during 8 weeks of IRW treatment.** Data expressed as mean  $\pm$  SEM of n = 8 mice. Analysis by two-way ANOVA followed by Bonferroni's post-hoc comparison test. \*\* p<0.01 between IRW45 and HFD. ## p<0.01 between IRW15 and HFD. ++++ p<0.0001 between LFD and HFD.

**Table 4. 4. Body composition and metabolic profile of mice supplemented with IRW.** Analysis by one-way ANOVA followed by Bonferroni's post hoc test (lean mass change, fasting glucose initial) or Kruskal–Wallis's test followed by Dunn's post-hoc test. Data expressed as mean  $\pm$  SEM of n = 7–8 mice. Values in the same row represented by different letters are statistically different ( $p \leq 0.05$ ) compared to HFD control.

	LFD	HFD	IRW45	IRW15
<b>Body composition</b>				
BW week 6 (g)	28.1 $\pm$ 0.8 <sup>a</sup>	31.3 $\pm$ 0.7 <sup>a</sup>	30.9 $\pm$ 0.9 <sup>a</sup>	31.7 $\pm$ 1.0 <sup>a</sup>
BW week 14 (g)	35.0 $\pm$ 0.7 <sup>a</sup>	41.6 $\pm$ 0.8 <sup>b</sup>	36.9 $\pm$ 0.5 <sup>a</sup>	40.4 $\pm$ 1.0 <sup>b</sup>
BW gain (g) (week 6–14)	7.0 $\pm$ 0.2 <sup>a</sup>	10.2 $\pm$ 0.3 <sup>b</sup>	6.0 $\pm$ 0.6 <sup>a</sup>	8.6 $\pm$ 0.6 <sup>b</sup>
BW gain (% of week 6)	25.1 $\pm$ 1.2 <sup>a</sup>	32.8 $\pm$ 1.3 <sup>b</sup>	19.9 $\pm$ 2.3 <sup>a</sup>	27.5 $\pm$ 2.2 <sup>b</sup>
Fat mass gain (g)	3.9 $\pm$ 0.5 <sup>a</sup>	7.0 $\pm$ 0.3 <sup>b</sup>	3.6 $\pm$ 0.4 <sup>a</sup>	6.1 $\pm$ 0.4 <sup>b</sup>
Fat mass gain (% BW)	8.2 $\pm$ 1.1 <sup>b</sup>	9.5 $\pm$ 0.8 <sup>b</sup>	4.8 $\pm$ 0.9 <sup>a</sup>	8.9 $\pm$ 0.9 <sup>b</sup>
Lean mass change (g)	0.8 $\pm$ 0.3 <sup>a</sup>	2.6 $\pm$ 0.1 <sup>b</sup>	2.0 $\pm$ 0.1 <sup>b</sup>	2.3 $\pm$ 0.2 <sup>b</sup>
Lean mass change (% BW)	-7.8 $\pm$ 1.0 <sup>b</sup>	-9.2 $\pm$ 0.7 <sup>b</sup>	-5.0 $\pm$ 0.9 <sup>a</sup>	-7.9 $\pm$ 0.9 <sup>b</sup>
<b>Metabolic profile</b>				
Fasting glucose week 6 (mmol/L)	4.5 $\pm$ 0.06 <sup>a</sup>	4.7 $\pm$ 0.3 <sup>a</sup>	5.0 $\pm$ 0.3 <sup>a</sup>	4.7 $\pm$ 0.2 <sup>a</sup>
Fasting glucose week 14 (mmol/L)	4.8 $\pm$ 0.1 <sup>a</sup>	6.3 $\pm$ 0.4 <sup>b</sup>	4.4 $\pm$ 0.2 <sup>a</sup>	5.7 $\pm$ 0.2 <sup>b</sup>

Abbreviations: BW, body weight; LFD, low fat diet; HFD, high-fat diet.

### 4.3.2 Glucose Homeostasis and Plasma Insulin

The IRW45 group had lower fasting blood glucose beginning at week 9 of treatment compared to the HFD group (Fig. 4.2A) and two-way ANOVA analysis showed significant interaction ( $p < 0.001$ ) and diet effects ( $p < 0.001$ ). At week 14, the LFD and IRW45 groups had lower fasting blood glucose ( $p < 0.001$ ) compared to the HFD (Table 4.4). Two-way ANOVA showed a diet effect on OGTT ( $p = 0.001$ ). Both doses of IRW lowered circulating glucose at 15 and 30 min compared with HFD (Fig. 4.2B). The area under the curve (AUC) was lower in the LFD ( $p < 0.001$ ) and IRW45 ( $p = 0.0195$ ) compared to the HFD group (Fig. 4.2C). Despite changes in ITT when expressed as absolute glucose concentrations (Fig. 4.3), no significant differences between the groups were observed when data were adjusted to baseline blood glucose concentration (Fig. 4.2D).

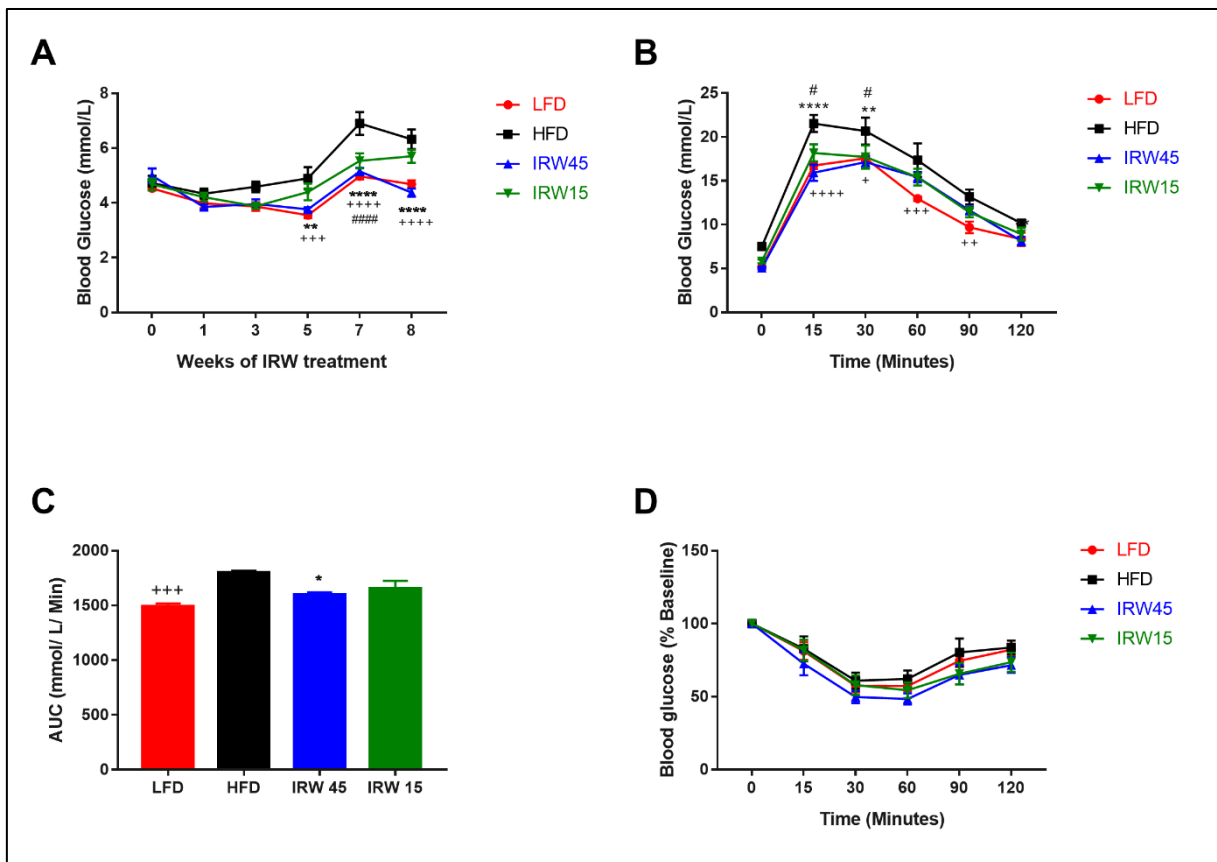


**Figure 4. 2. Glucose homeostasis after IRW supplementation.** (A) Fasting glucose over time (n = 6–8), (B) Oral glucose tolerance test (OGTT) (n = 6–8). (C) Area under the curve (AUC) for OGTT (n = 5–8). (D) Insulin tolerance test (ITT) as percentage of the baseline glucose values (n = 8). Data expressed as mean  $\pm$  SEM and analyzed by two-way ANOVA (A,C,D) or one-way ANOVA (B) followed by Bonferroni's post-hoc comparison test. \* p < 0.05, \*\* p < 0.01 and \*\*\*\* p < 0.0001 between IRW45 and HFD. # p < 0.05 and ##### p < 0.0001 between IRW15 and HFD. + p < 0.05, ++ p < 0.01, +++ p < 0.001 and ++++ p < 0.0001 between LFD and HFD.

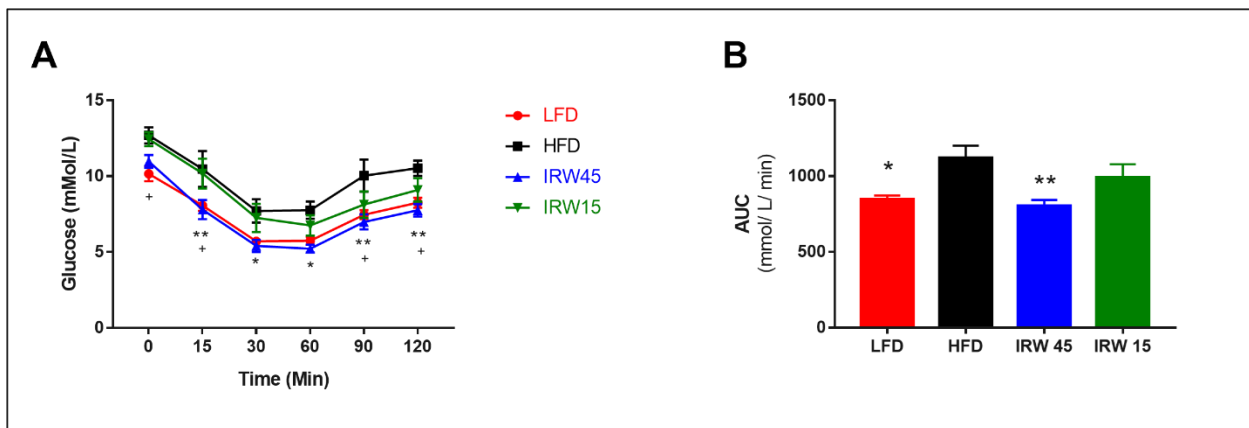


**Figure 4. 3. Insulin sensitivity after IRW supplementation.** (A) Insulin tolerance test (ITT) and (B) Area under the curve (AUC) for ITT after 8 weeks of IRW supplementation (n = 8). Data expressed as mean  $\pm$  SEM and analyzed by two-way ANOVA (A) or one-way ANOVA (B) followed by Bonferroni's post-hoc comparison test. \* p < 0.05 and \*\* p < 0.01 between IRW45 and HFD. + p < 0.05 between LFD and HFD.

### 4.3.3 *Insulin Signaling and PPAR $\gamma$ Abundance*

Insulin-stimulated phosphorylation of AKT (Ser473) in muscle was higher in LFD ( $p = 0.0196$ ) and IRW45 ( $p = 0.0132$ ) compared to the HFD group, whereas IRW15 was non-significantly increased (Fig. 4.4A). Consistent with this result, GLUT 4 translocation to the plasma membrane in skeletal muscle was ~4-fold higher in the IRW45 ( $p < 0.001$ ) and 2-fold higher in IRW15 ( $p = 0.04$ ) compared to the HFD group, as shown by the ratio of membrane GLUT4/cytosol GLUT4 (Fig. 4.4B). In addition, PPAR $\gamma$  abundance was 15–17-fold higher in LFD ( $p = 0.0013$ ) and IRW45 ( $p < 0.001$ ) compared to HFD (Fig. 4.4C). In both retroperitoneal and epididymal WAT, no changes in AKT phosphorylation or PPAR $\gamma$  abundance were seen following IRW supplementation (Fig. 4.5A–F).

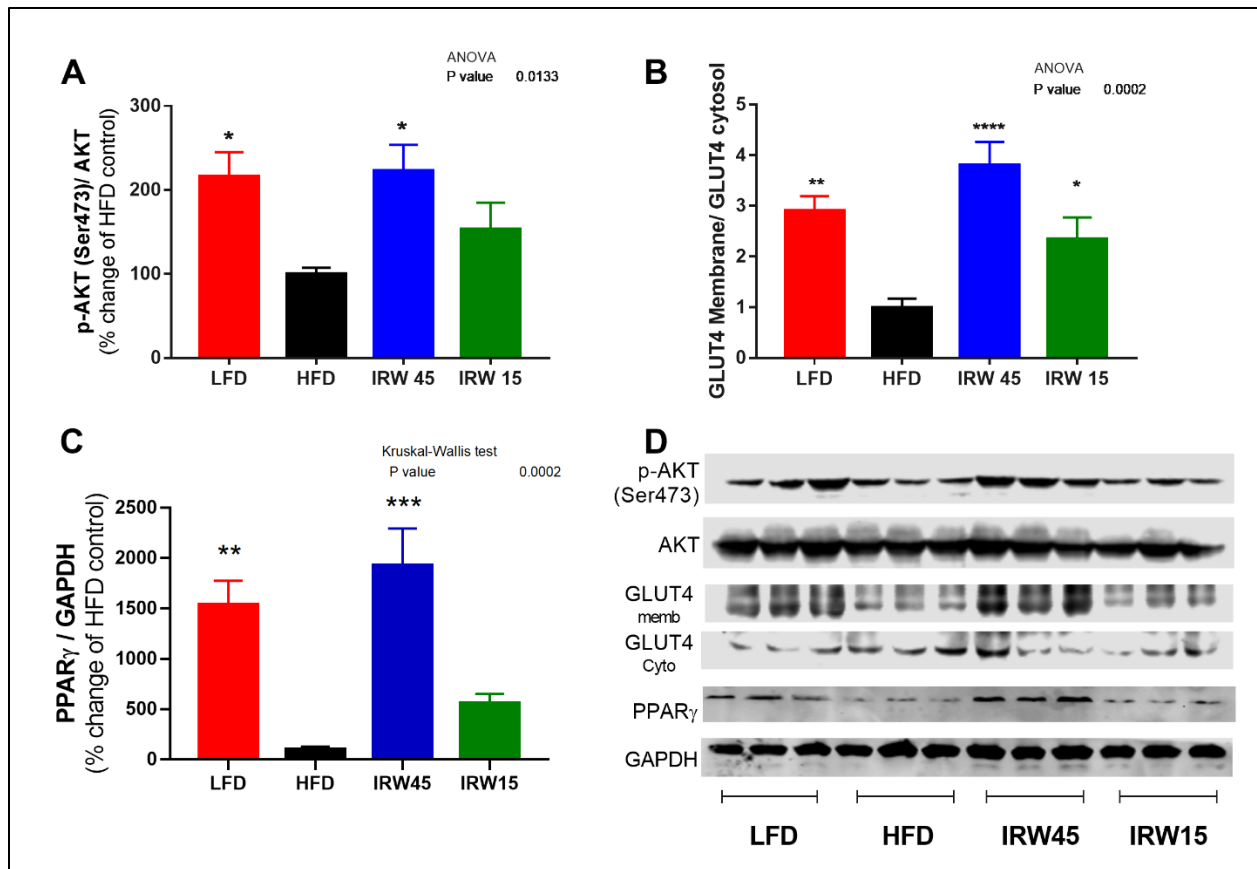


**Figure 4. 4. Skeletal muscle insulin signaling and PPAR $\gamma$  abundance.** (A) p-AKT, (B) GLUT4 membrane/cytosol, (C) PPAR $\gamma$ , and (D) representative blots. p-AKT was normalized to total AKT. GLUT4 is expressed as a ratio of membrane to cytosolic GLUT4. PPAR $\gamma$  was normalized to GAPDH. Data expressed as mean  $\pm$  SEM of  $n = 6$ . Analysis by one-way ANOVA followed by Bonferroni's post-hoc test or Kruskal-Wallis followed by Dunn's post-hoc test. \*  $p < 0.05$ , \*\*  $p < 0.01$  \*\*\*  $p < 0.001$  and \*\*\*\*  $p < 0.0001$  versus HFD. AKT, Protein kinase B; PPAR $\gamma$ , Peroxisome proliferator-activated receptor gamma; GLUT4, glucose transporter 4.

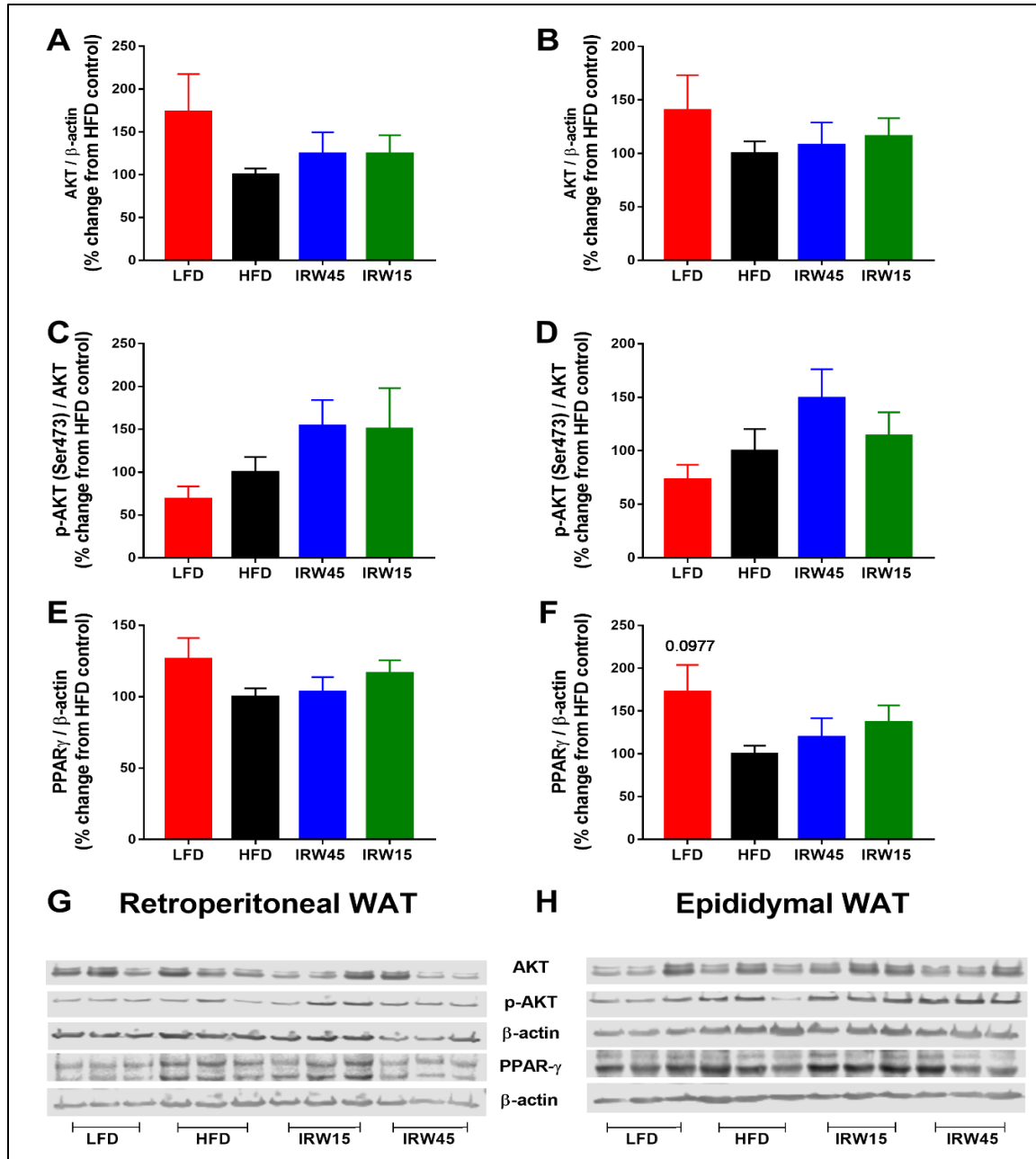


**Figure 4.5. White adipose tissue (WAT) insulin signaling and PPAR $\gamma$  protein abundance.** Retroperitoneal WAT (A)AKT, (C) p-AKT (E) PPAR $\gamma$  and (G) representative blots. Epididymal WAT (B)AKT, (D) p-AKT, (F) PPAR $\gamma$  and (H) representative blots. p-AKT protein band was normalized to total AKT. PPAR $\gamma$  protein band was normalized to  $\beta$ -actin as the loading control. Data expressed as mean  $\pm$  SEM of n= 6 mice. Analysis by one-way ANOVA followed by Bonferroni's post-hoc test; or Kruskal-Wallis test followed by Dunn's post hoc test when appropriate.  $p < 0.01$  versus HFD indicated over bars. AKT, protein kinase B; PPAR $\gamma$ , Peroxisome proliferator-activated receptor gamma.

#### 4.3.4 *RAS Components*

In skeletal muscle, there were no significant differences in ACE2, AT1R, and Mas receptor between the groups (Fig. 4.6B,C,F). However, a lower ACE abundance in LFD ( $p = 0.0259$ ), IRW15 ( $p = 0.0157$ ), and IRW45 ( $p = 0.0113$ ) groups was observed compared to HFD (Fig. 4.6A). In addition, AT2R abundance increased almost 3-fold in the IRW45 group compared to HFD ( $p = 0.0024$ ) (Fig. 4.6D). The plasma ACE activity was similar between groups (Fig. 4.7A). Although ANOVA analysis identified an overall effect ( $p = 0.01$ ) on plasma angiotensin II, post-hoc analysis showed no significant differences between groups (Fig. 4.7C). Whereas ACE2 activity was highest in the IRW45 group ( $p = 0.0016$ ) (Fig. 4.7B) and plasma Ang (1–7) plasma concentration was not increased by IRW compared to the HFD (Fig. 4.7D).

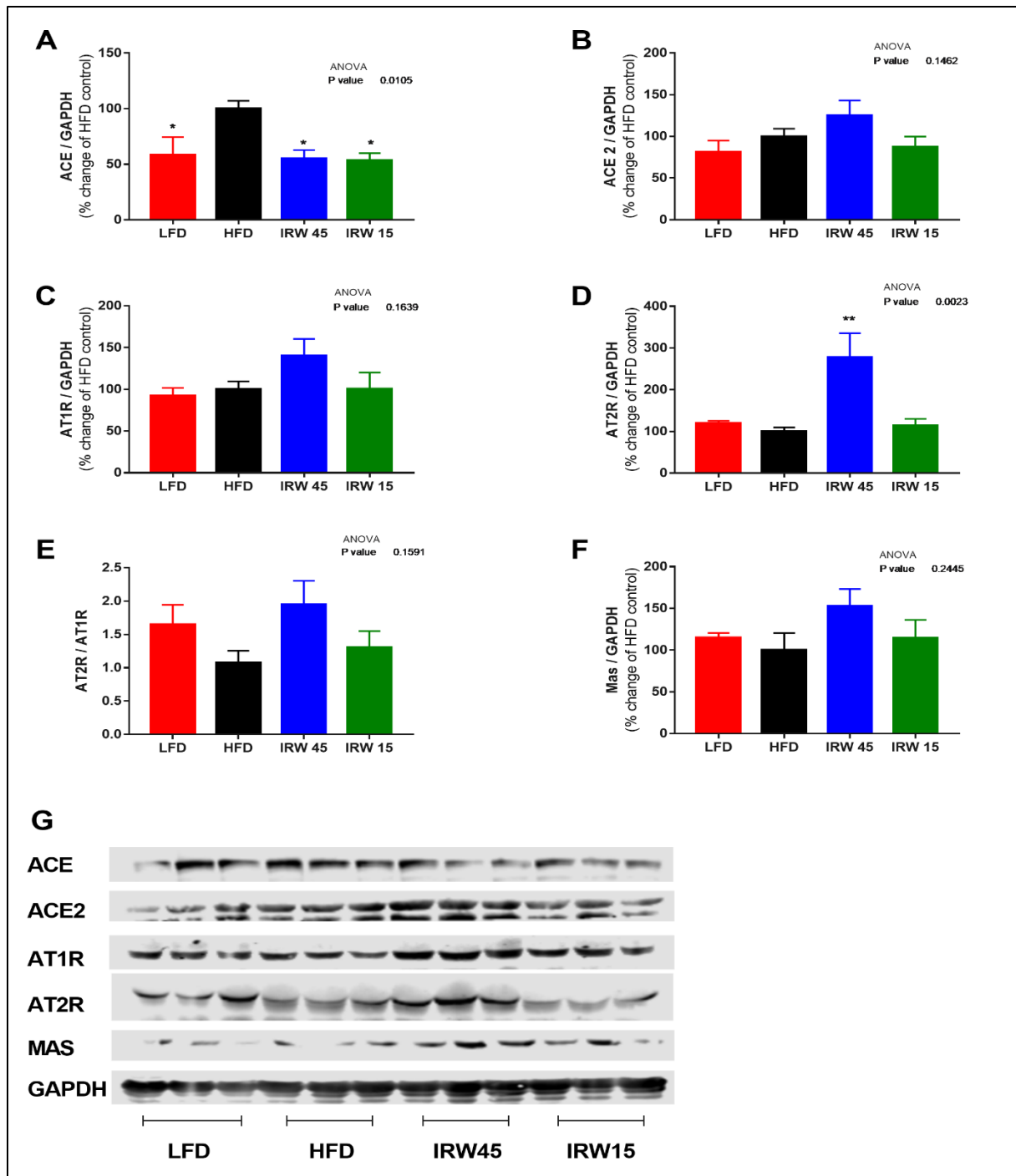


**Figure 4.6. Skeletal muscle renin angiotensin system components.** (A) ACE, (B) ACE2, (C) AT1R, (D) AT2R, (E) AT2R/AT1R ratio, (F) Mas receptor, and (G) representative blot. ACE, ACE2, AT1R, AT2R, and Mas were normalized to GAPDH. Data expressed as mean  $\pm$  SEM of  $n = 5-6$  mice. Analysis by one-way ANOVA followed by Bonferroni's post-hoc test. \*  $p < 0.05$  and \*\*  $p < 0.01$  versus HFD. ACE, angiotensin converting enzyme; ACE2, angiotensin converting enzyme 2; AT1R, angiotensin receptor type 1; AT2R, angiotensin receptor type 2.

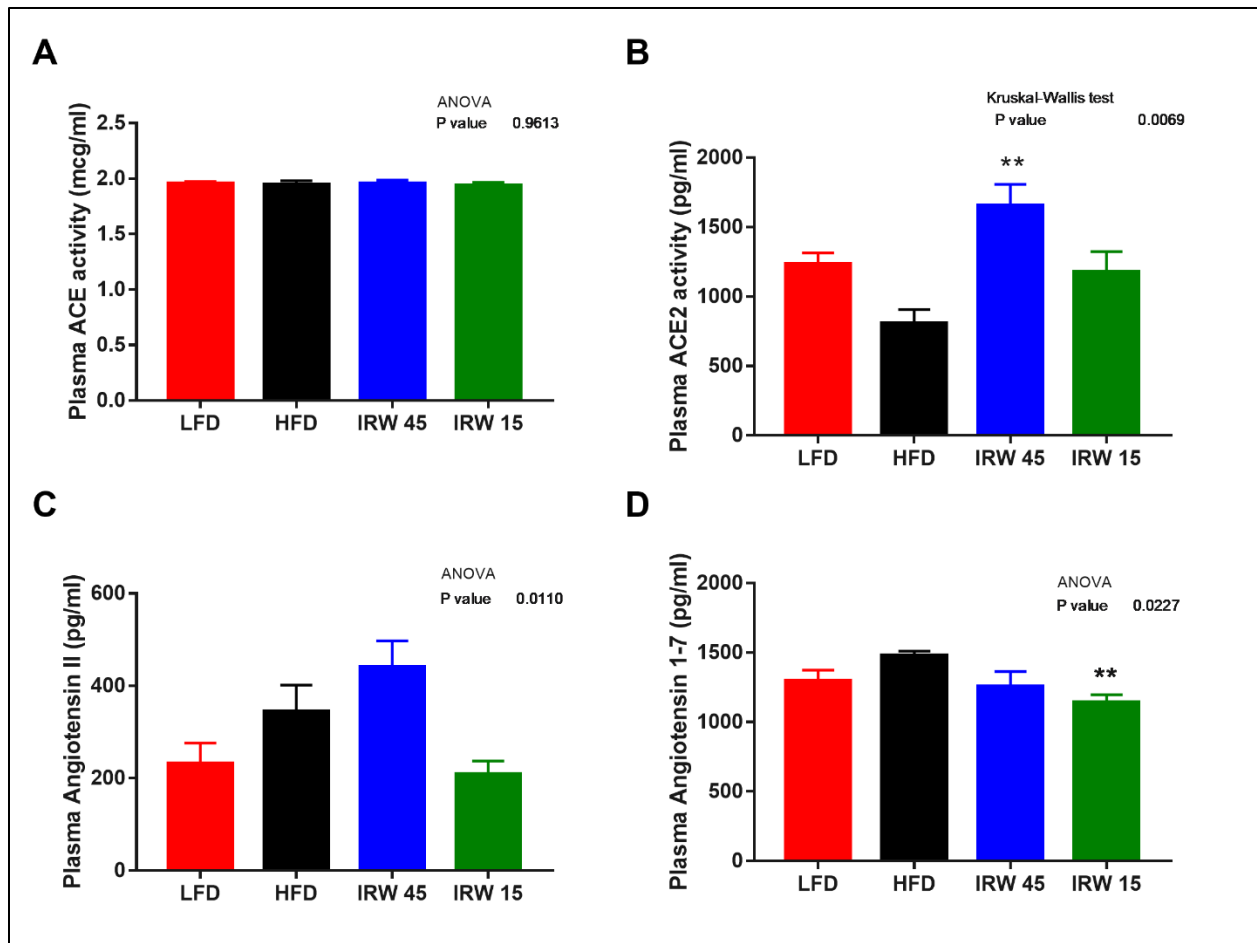


**Figure 4. 7. Plasma renin angiotensin system components.** (A) Plasma angiotensin converting enzyme (ACE), (B) Plasma angiotensin converting enzyme 2 (ACE2), (C) Plasma angiotensin II, and (D) Plasma angiotensin (1–7). Data expressed as mean  $\pm$  SEM of n = 4–7 mice. Analysis by one-way ANOVA followed by Bonferroni’s post-hoc comparison test or Kruskal–Wallis followed by Dunn’s post hoc test when appropriate. \*\* p < 0.01 versus HFD.

#### 4.3.5 Skeletal Muscle Gene Expression

RNA sequencing of gastrocnemius muscle transcripts revealed that IRW45 elicited a generally higher abundance of transcripts related to muscle synthesis (Fig. 4.8A). qPCR validation identified *Rbm5* ( $p = 0.0094$ ), *Mdm2* ( $p = 0.0094$ ), *Dlg1* ( $p < 0.001$ ), and *Myom1* ( $p < 0.001$ ) genes upregulated and *Aspn* ( $p < 0.001$ ) downregulated by IRW45 compared to the HFD group (Fig. 4.8B). For PPAR $\gamma$  related genes, IRW45 significantly enhanced the expression of *Pparg* ( $p = 0.0112$ ) and *Lpl* ( $p < 0.001$ ) but not *Plin2* or *Cebpa* (Fig. 4.8C). However, it should be noted that the expression of *Plin2* and *Cebpa* were 15 and ~50-fold higher in HFD and IRW45 than LFD.

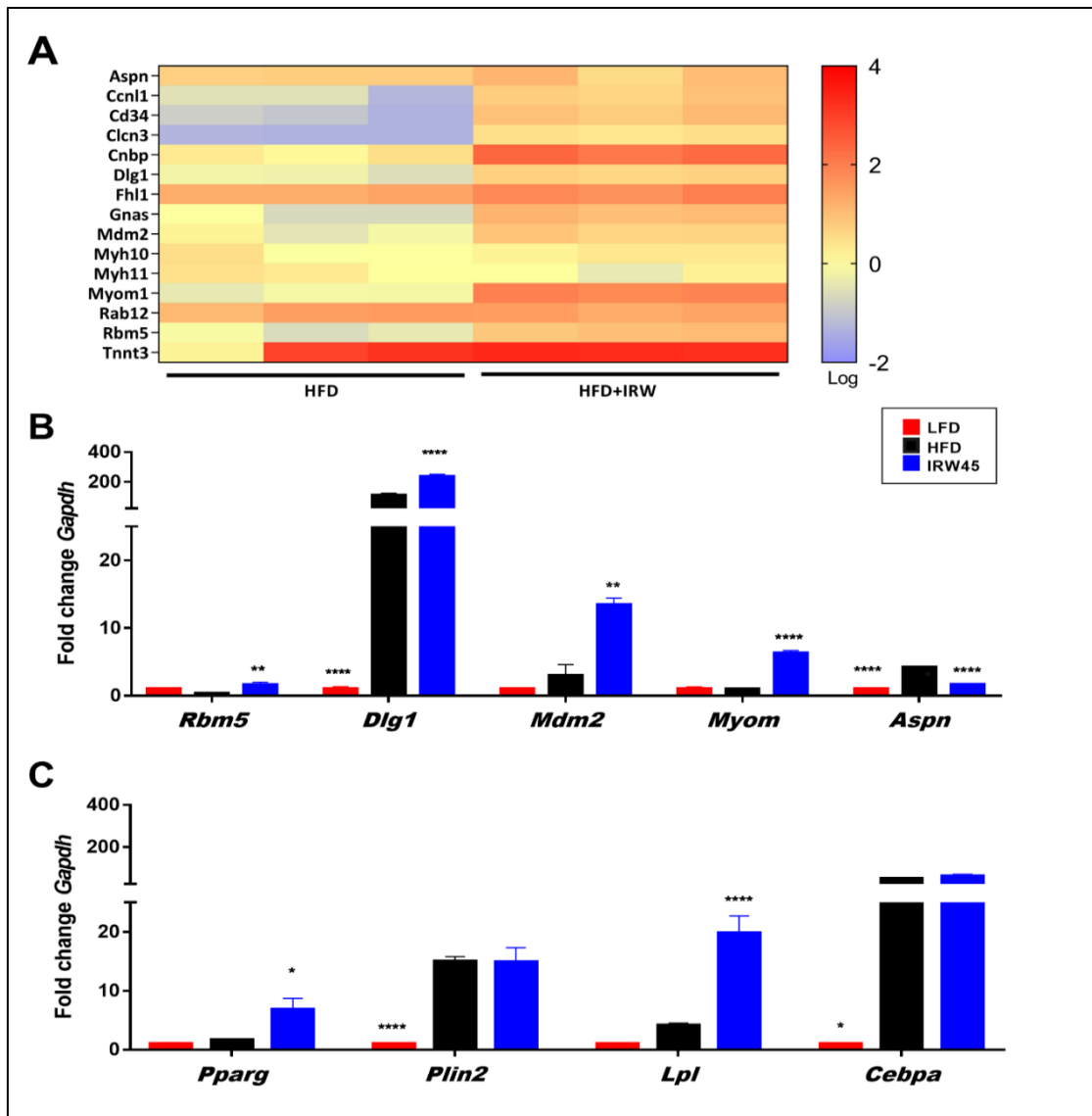


**Figure 4. 8. Skeletal muscle gene expression of mice fed IRW for 8 weeks.** (A) Heatmap showing the abundance of major genes involved in muscle synthesis modulated by IRW45 determined by RNA sequencing. (B) Rbm5, Mdm2, Dlg1, Myom1, and Aspn qPCR validation of IRW in vivo using gastrocnemius skeletal muscle. Data expressed as mean  $\pm$  SEM of n = 5 mice. (C) Pparg, Plin2, Cebpa and Lpl qPCR validation using gastrocnemius skeletal muscle. Data expressed as mean  $\pm$  SEM of n = 5 mice. Analysis by one-way ANOVA followed by Bonferroni's post-hoc comparison test or Kruskal–Wallis followed by Dunn's post hoc test when appropriate. \* p < 0.05, \*\* p < 0.01, and \*\*\*\* p < 0.0001 versus HFD.

#### 4.3.6 *AMPK $\alpha$ Abundance and mTOR Signaling.*

IRW45 treatment elicited a ~10-fold increase in AMPK $\alpha$  phosphorylation (Thr172) relative to total AMPK $\alpha$  in skeletal muscle compared to HFD ( $p < 0.0124$ ) (Fig. 4.9A), with no change in total AMPK $\alpha$  (Fig. 4.9B). ANOVA indicated an overall diet effect in p-AMPK $\alpha$  over GAPDH (Fig. 4.9C), consistent with findings in Fig. 4.9A. No changes in total or phosphorylated AMPK $\alpha$  abundance in retroperitoneal or epididymal WAT were observed after IRW supplementation (Fig. 4.10 and 4.11, respectively).

Phosphorylated (Ser2448) mTOR relative to total mTOR had an overall significant increase ( $p = 0.003$ ) in skeletal muscle, but the post-hoc analysis revealed no statistical significance between IRW45 and HFD ( $p = 0.2332$ ), while in IRW15 p-mTOR (Ser2448) was increased ( $p < 0.0138$ ) (Fig. 4.9D). Total mTOR was not affected (Fig. 4.9E); however, p-mTOR was statistically increased by IRW45 ( $p < 0.001$ ) (Fig. 4.9F). The downstream p70 S6K protein phosphorylation trended to elevated IRW45 relative to total p70 S6K (Fig. 4.9G,  $p = 0.2075$ ) and 3-fold relative to GAPDH (Fig. 4.9I,  $p = 0.15$ ); however, total p70 S6K protein was significantly increased ( $p < 0.045$ ) in IRW45 compared to HFD (Fig. 4.9H). In WAT, no changes were seen in total and phosphorylated mTOR or p70 S6K in both retroperitoneal and epididymal WAT (Fig. 4.10 and Fig. 4.11, respectively).

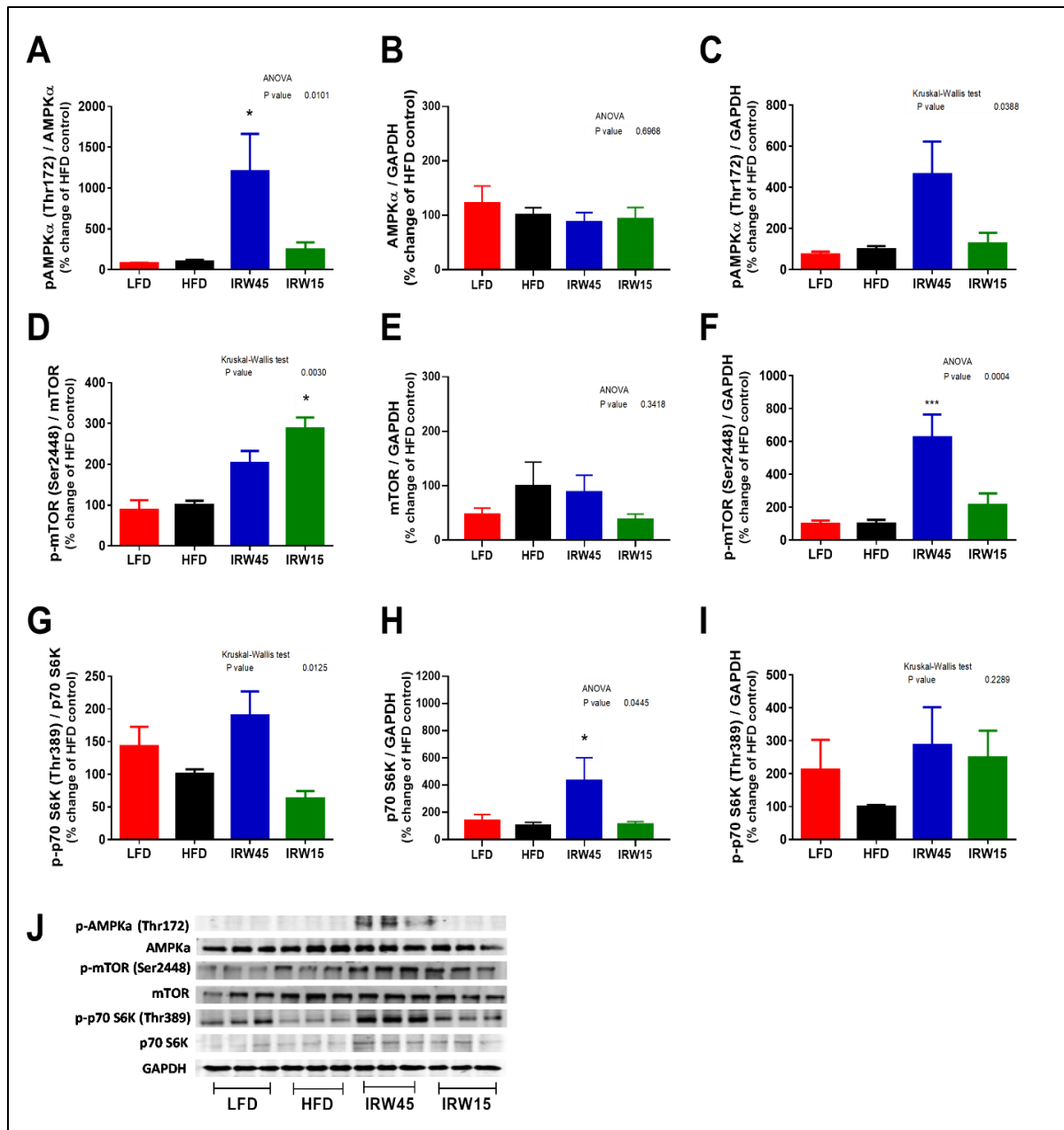


**Figure 4. 9. Skeletal muscle AMPK $\alpha$ , mTOR and P70 S6K protein abundance.** (A) p-AMPK $\alpha$ /AMPK $\alpha$ . (B) AMPK $\alpha$ /GAPDH. (C) p-AMPK $\alpha$ /GAPDH. (D) p-mTOR/mTOR. (E) mTOR/GAPDH. (F) p-mTOR/GAPDH. (G) p-P70 S6K / P70 S6K. (H) P70 S6K/GAPDH. (I) p-P70 S6K/GAPDH and (J) representative blots. Data expressed as mean  $\pm$  SEM of n = 5–6 mice. Analysis by one-way ANOVA followed by Bonferroni's post-hoc comparison test or Kruskal–Wallis followed by Dunn's post hoc test when appropriate. \*  $p < 0.05$  and \*\*\*  $p < 0.001$  versus HFD. AMPK, 5' AMP-activated protein kinase; mTOR, mammalian target of rapamycin; P70 S6K, Ribosomal protein S6 kinase beta-1.

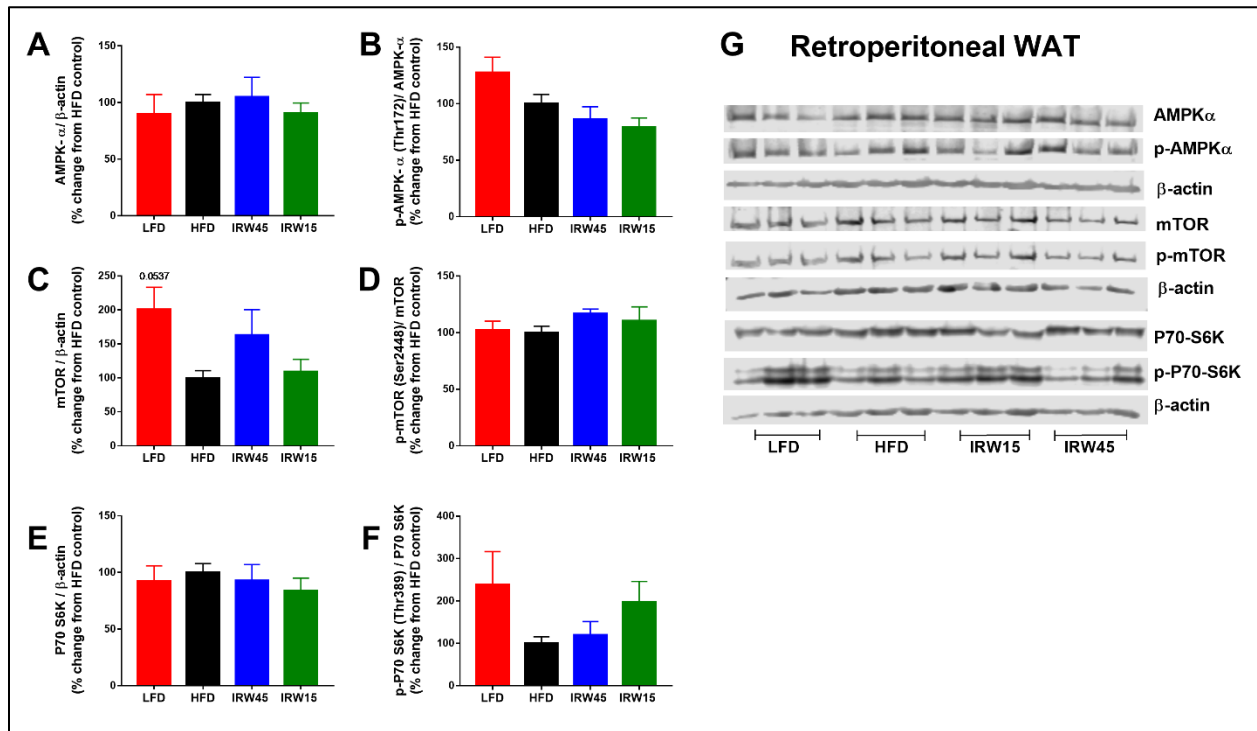


**Figure 4. 10. Retroperitoneal white adipose tissue (WAT) AMPK $\alpha$ , mTOR and P70 S6K protein abundance.** (A) AMPK $\alpha$ , (B) p-AMPK $\alpha$  (C) mTOR, (D) p-mTOR, (E) P70 S6K, (F) p-P70 S6K and (G) representative blots. Phospho proteins were normalized by their respective total protein. Total protein was normalized to  $\beta$ -actin as the loading control. Data expressed as mean  $\pm$  SEM of n = 6 mice. Analysis by one-way ANOVA followed by Bonferroni's post-hoc test; or Kruskal-Wallis test followed by Dunn's post hoc test when appropriate. AMPK, 5'-AMP-activated protein kinase; mTOR, mammalian target of rapamycin; P70 S6K, ribosomal protein S6 kinase beta-1.

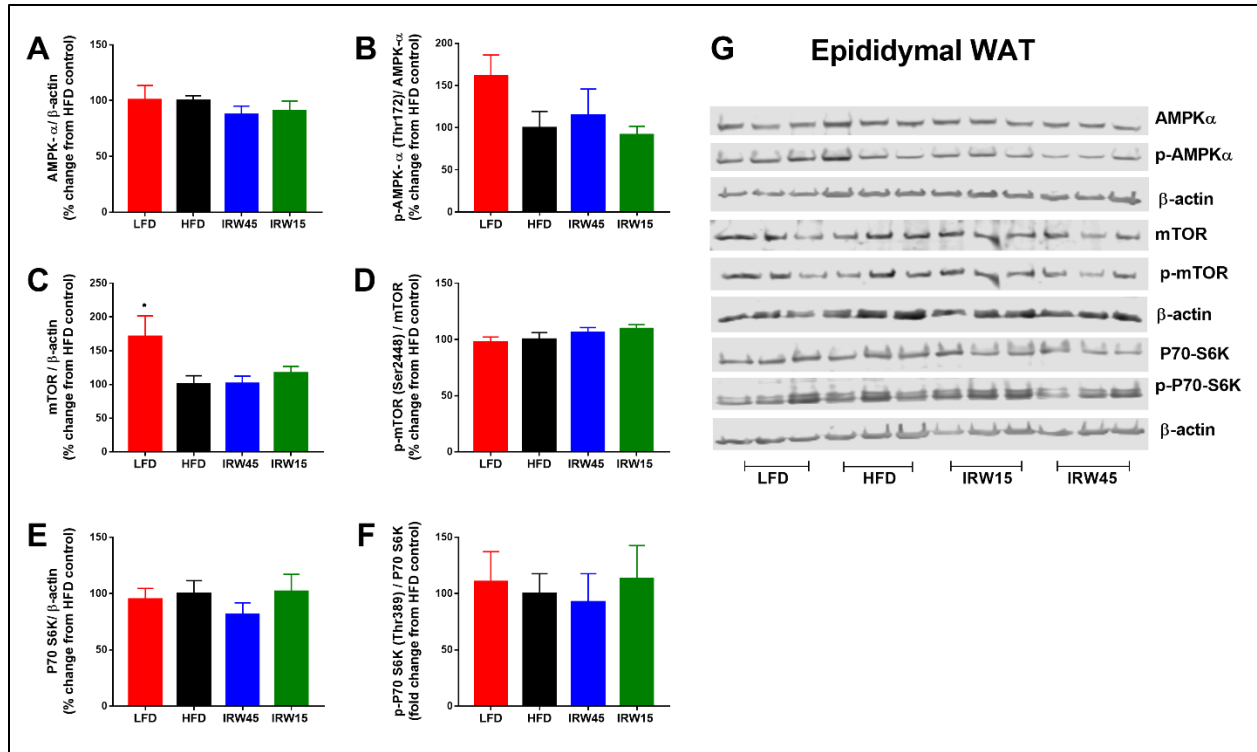


**Figure 4. 11. Epididymal white adipose tissue (WAT) AMPK $\alpha$ , mTOR and P70 S6K protein abundance.** (A) AMPK $\alpha$ , (B) p-AMPK $\alpha$  (C) mTOR, (D) p-mTOR, (E) P70 S6K, (F) p-P70 S6K and (G) representative blots. Phospho proteins were normalized by their respective total protein. Total protein was normalized to  $\beta$ -actin as the loading control. Data expressed as mean  $\pm$  SEM of  $n = 6$  mice. Analysis by one-way ANOVA followed by Bonferroni's post-hoc test; or Kruskal-Wallis test followed by Dunn's post hoc test when appropriate. \*  $p < 0.05$  versus HFD. AMPK, 5' AMP-activated protein kinase; mTOR, mammalian target of rapamycin; P70 S6K, ribosomal protein S6 kinase beta-1. \*  $p < 0.05$  versus HFD.

### 4.3.7 Adipose Tissue UCP-1 Abundance

The investigation of UCP-1 abundance in retroperitoneal and epididymal WAT is shown in Fig. 4.12. UCP-1 was decreased by HFD compared with LFD and this was significant in epididymal WAT ( $p < 0.0188$ ) (Fig. 4.12B). IRW15 and IRW45 exhibited intermediate abundance in epididymal WAT.

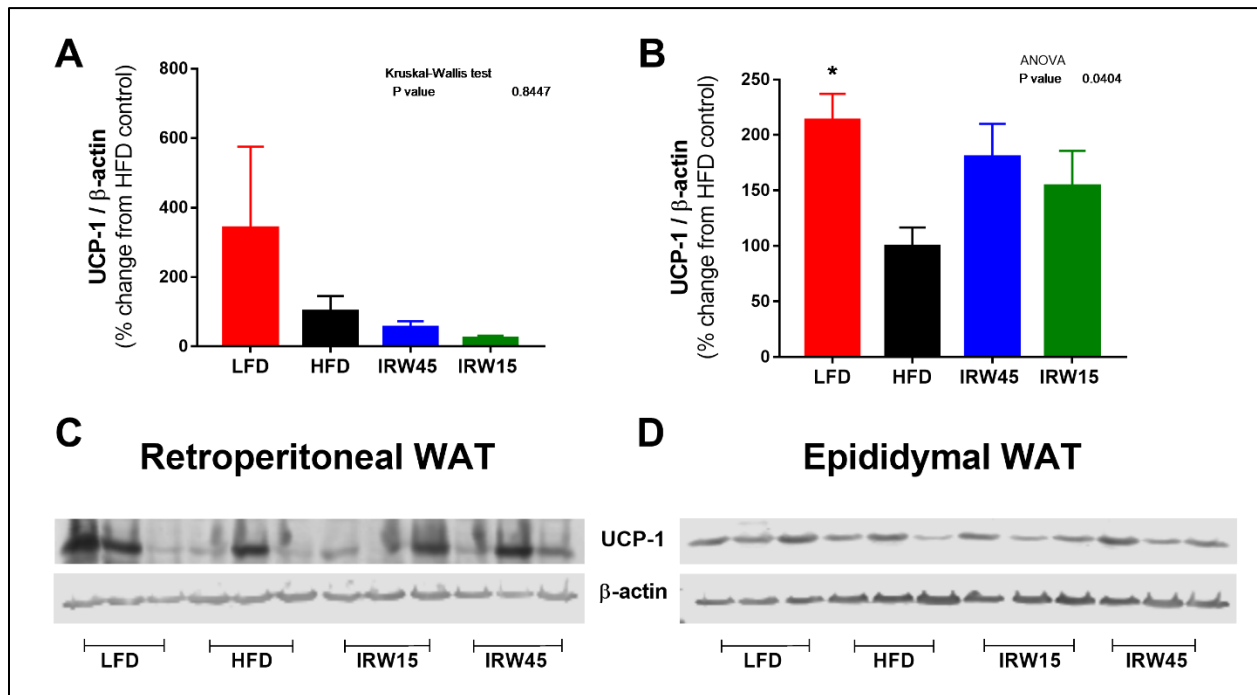


**Figure 4. 12. UCP-1 expression after IRW treatment.** WAT UCP-1 protein abundance. Retroperitoneal WAT UCP-1 (A) and representative blot (C). Epididymal WAT UCP-1 (B) and representative blot (D). UCP-1 was normalized to  $\beta$ -actin. Data expressed as mean  $\pm$  SEM of  $n = 5-6$  mice. Analysis by one-way ANOVA followed by Bonferroni's post-hoc test or Kruskal-Wallis followed by Dunn's post hoc test when appropriate. \*  $p < 0.05$  versus HFD. UCP, uncoupling protein.

#### 4.4 Discussion

Natural health products [254] are used by a wide range of the population but their efficacy in managing complex metabolic diseases is still debated. Despite that, food-derived bioactive peptides exhibit positive physiological effects related to metabolic diseases and their complications [165, 166, 255]. IRW is an ovotransferrin-derived bioactive peptide previously shown to exert antihypertensive and anti-inflammatory effects [187, 190]. In addition, *in vitro*, IRW presented antioxidant effects and improved insulin signaling [191, 192]. In this study, using an obese, insulin resistant rodent model we demonstrated that IRW supplementation at a dose of 45 mg/kg BW: (1) prevented BW and fat mass gain during HFD treatment while protecting lean body mass; (2) improved glucose tolerance and fasting blood glucose; and (3) enhanced insulin-dependent and -independent signaling governing glucose uptake in skeletal muscle. IRW15 was not as effective as IRW45, illustrating dose dependence. For this reason, the discussion is focused on IRW45 findings. Contrary to our hypothesis, these activities of IRW did not appear to involve the inhibition of local RAS.

As previously demonstrated [187, 250], IRW retained biological activity *in vivo* possibly because we mixed IRW into the HFD, which may have protected it from degradation by digestive enzymes [256]. However, IRW can be degraded into the dipeptide IR in simulated gastrointestinal digestion, which decreases its ACE inhibitory activity drastically *in vitro* [185]. We did not calculate the concentration or characterize the bioactive form reaching the bloodstream in the current study and we cannot exclude the possibility of the dipeptide IR being bioactive *in vivo*, therefore it is only a speculation. Nevertheless, IRW at a dosage of 45 mg/kg BW promoted enhanced glucose homeostasis. This dosage is comparable to other studies investigating the role of small molecules, natural products or bioactive peptides in cardio-

metabolic conditions using rodent models. For example, AdipoRon, a small-molecule agonist of adiponectin receptor is used at 50 mg/kg BW [257], curcumin at 100 mg/kg BW [258], soy  $\beta$ -conglycin at 10% of diet (*w/w*) [259] and the di-peptide (Trp-His) at dosages ranging between 10–100 mg/kg BW [260, 261]. Moreover, metformin is used at 200 mg/kg BW in rodent models of diabetes [262, 263].

In this study, IRW45 improved both fasting and insulin-stimulated glucose indices. Similarly, an egg white hydrolysate improved glucose tolerance and insulin sensitivity in HFD rats [197]. In Zucker Fatty rats, egg white hydrolysate treatment lowered fasting insulin but not glucose concentrations, resulting in reduced HOMA-IR and HOMA- $\beta$  indices [175]. Although our ITT study shows that IRW45 treatment improved insulin sensitivity compared to the HFD group, the significance was lost after adjustment for baseline blood glucose concentration, suggesting that the effects observed were dependent on differences in fasting blood glucose concentration.

Glucose uptake in skeletal muscle occurs via insulin-dependent and -independent pathways. Insulin activates the PI3K-AKT cascade leading to translocation of GLUT4 to the plasma membrane, and thus increases glucose uptake [38], which was demonstrated in skeletal muscle of IRW45 treated animals compared to the HFD. However, because ITT was not different between groups, insulin-independent pathways may also play a role. AMPK activation, such as in muscle contraction, enhances GLUT4 translocation [264] and increases glucose entry independently of insulin [265]. Indeed, AMPK $\alpha$  phosphorylation in skeletal muscle of IRW45 animals was significantly increased. Both AKT and AMPK pathways could contribute to improved glucose tolerance observed in IRW45 mice. We also acknowledge the possibility of enhanced basal AKT phosphorylation by IRW directly. In this study, only insulin-stimulated animals were included, which did not allow for this latter analysis.

We initially hypothesized that IRW-mediated improvements in insulin signaling would be associated with reduced local RAS activity, based on previous studies [185, 187, 250, 266]. Despite IRW being an ACE inhibitor *in vitro* [185], we found no effect of IRW on systemic ACE activity in this insulin resistant model, similar to previous results using IRW in SHR rats [250]. However, IRW reduced ACE protein abundance in skeletal muscle, which might contribute to lower local ACE activity. Moreover, plasma ACE2 activity was increased in our study, consistent with previous studies showing that oral IRW supplementation enhanced circulating ACE2 abundance and activity [250], and ACE2 protein expression in the aorta of SHR rats [266]. ACE2 antagonizes the actions of angiotensin II, thereby reducing blood pressure, and reducing CVD risk through angiotensin (1–7)/Mas receptor axis as reviewed [267]. Interestingly, in this study angiotensin (1–7) was not increased by IRW treatment.

In skeletal muscle, modulation of AT1R and AT2R regulates insulin action locally, with systemic AT2R blockade impairing insulin-stimulated AKT phosphorylation, whole body glucose uptake, and muscular microvascular function, while systemic AT1R blockade restores muscle insulin signaling [229]. AT2R opposes the effects of AT1R activation in blood vessels with their interplay regulating blood flow and glucose utilization in skeletal muscle [268]. In our study, IRW45 increased AT2R abundance in skeletal muscle. Similarly, we previously showed that egg hydrolysate enhanced AT2R abundance in WAT and liver, and improved glucose tolerance [197]. Possibly, increased AT2R abundance in skeletal muscle tissue permits increased binding of angiotensin II to AT2R in the capillary endothelium, thus improving blood flow to facilitate insulin access to muscle cells and enhancing glucose uptake. Moreover, IRW may directly activate AT2R in muscle cells, which we speculate may improve glucose transport via

AMPK and PPAR $\gamma$  activation. Despite no clear direct link between AT2R and AMPK yet being demonstrated, RAS modulation improves glucose tolerance and uptake via AMPK [269, 270].

In some tissues, such as WAT, AT2R is linked to PPAR $\gamma$  as evidenced by PPAR $\gamma$  mRNA and activation being enhanced by AT2R agonists [271] and egg white hydrolysate concomitantly increased AT2R and PPAR $\gamma$  abundance [197]. Thiazolidinediones (TZDs) are PPAR $\gamma$  agonists and cause insulin sensitizing effects by enhancing skeletal muscle glucose uptake, reducing liver glucose output, and affecting WAT physiology [272]. PPAR $\gamma$  agonists potentiate AKT phosphorylation in WAT and skeletal muscle [273] and specific deletion of PPAR $\gamma$  in skeletal muscle of mice induces insulin resistance [274]. In insulin resistant hamsters, PPAR $\gamma$  RNA expression in skeletal muscle is downregulated, along with other genes regulated by PPAR $\gamma$  such as *Ppargc1a*, *Lpl*, and *Adipoq* (adiponectin) genes [275]. In this study, IRW45 treatment upregulated *Pparg* and *Lpl* in skeletal muscle while increasing PPAR $\gamma$  protein abundance, suggesting that IRW may upregulate a cassette of PPAR $\gamma$ -related genes as part of its metabolic activity.

Despite similar caloric intake, IRW45 improved body composition by reducing BW and fat mass gain, while protecting lean mass. In humans, the reduction of whole-body fat mass after an exercise intervention was associated with increased insulin sensitivity index [276]. Recently, an extract from rice hulls decreased fat mass by suppressing adipogenic genes in epididymal WAT and liver while enhancing AMPK $\alpha$  protein, consistent with increased fatty acid oxidation [277]. However, neither AMPK $\alpha$  nor PPAR $\gamma$  abundance changed in visceral WAT after IRW treatment. We also investigated whether UCP-1 protein abundance in WAT could have been induced by IRW, since it might explain reduced fat mass because AT2R activation was previously shown to induce UCP-1 in epididymal WAT [278] and brown adipose tissue [279]. We found that

compared with LFD, UCP-1 was reduced in HFD epididymal WAT, similar to other findings [280]. IRW45 treatment tended to increase UCP-1 but not as strongly as expected if thermogenesis was the main route eliciting fat mass loss. The mechanism by which IRW reduced fat mass is still unclear and other pathways deserve investigation, including the effect of IRW in the subcutaneous adipose tissue, which is more prone to browning than visceral depots [281, 282].

Skeletal muscle synthesis is a key indicator of metabolic health and is regulated by insulin [283]. Upregulation of genes involved in muscle synthesis was induced by IRW. Primarily, mTOR activation is modulated by nutrients and, once activated, is involved in protein and lipid synthesis [284]. However, despite increased AMPK phosphorylation and expression of muscle synthesis genes in skeletal muscle, phosphorylation of mTOR (Ser2448) by IRW was not dose-dependent nor correlated with phosphorylation of the downstream S6K P70. Nevertheless, the gene upregulation observed after IRW supplementation indicates a possible ability of IRW to trigger myogenesis pathways, which may be related to our observation of protected lean body mass. Alternatively, IRW may be acting independently of mTOR to promote these effects.

In summary, IRW reduced BW and fat mass gain while improving glucose tolerance and insulin sensitivity in HFD mice. We identified several mechanisms of action for IRW in skeletal muscle and, to a lesser extent, WAT (Fig. 4.13) that were independent of ACE inhibition. Pathways influenced by IRW include the AKT-GLUT4 and AMPK $\alpha$ -GLUT4, which both enhance glucose uptake in skeletal muscle, while activation of the AT2R-PPAR $\gamma$  pathway could improve insulin sensitivity. Furthermore, IRW may reduce inflammation [192, 250], contributing to insulin sensitization. Because the liver regulates fasting glucose homeostasis, IRW may also improve liver insulin sensitivity during fasting, leading to better glucose tolerance. IRW effects

in the liver are currently being investigated by our group. Thus, IRW has the potential to exert beneficial effects on glucose homeostasis, making it a strong candidate to be further studied in the context of metabolic diseases.

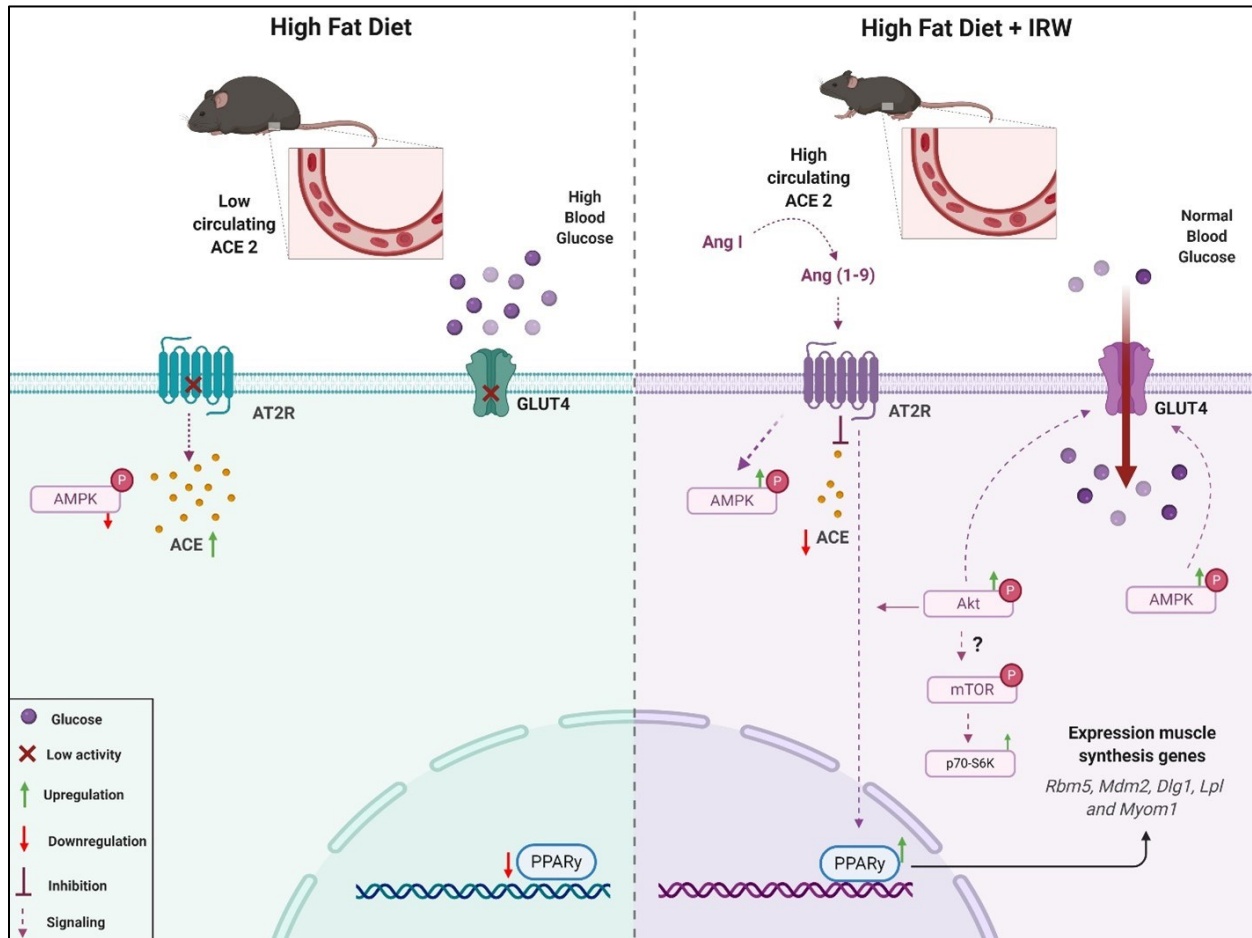


**Figure 4. 13. Potential mechanisms of action of IRW to improve glucose tolerance and insulin signaling.** HFD activates the classical RAS arm to increase ACE, which may be counteracted by IRW via AT2R. In blood, IRW stimulates ACE2, which can produce Angiotensin (1-9) leading to direct activation of AT2R. This increase in AT2R may induce AMPK phosphorylation and neutralize the increased abundance of ACE. In addition, AMPK facilitates insulin-independent glucose uptake by skeletal muscle. AT2R may also trigger PPAR $\gamma$ , leading to transcription of myogenesis genes. Further, IRW-stimulated p-AKT increases glucose uptake via GLUT4. p-AKT plays a significant physiological role in insulin-stimulated glucose uptake and activates mTOR and p70-S6K, however IRW involvement in this pathway requires further clarification.

**Institutional Review Board Statement:** The animal study protocol was approved by the Animal Care and Use Committee of the University of Alberta (Protocol# 1472) in accordance with guidelines issued by the Canadian Council on Animal Care.

**Acknowledgments:** We sincerely thank Nicole Coursen for the help with the animal trial and Juan Jovel and the genomics core facility for their assistance with the RNA sequencing.

**Conflicts of Interest:** The authors declare no conflict of interest.

**5. CHAPTER 5: IRW prevents high-fat diet-induced non-alcoholic fatty liver disease by preserving mitochondrial content and enhancing hepatic fatty acid oxidation capacity.**

This section shows the outcomes after completion of objective #4. I performed experiments, data analysis, visualization and wrote the first draft of the manuscript. The *in vivo* study was performed in collaboration with Xu Jiang. In addition, Emily Berg was involved in performing some of the experiments. Moreover, I was fortunate to be able to supervise several undergraduate students who helped in performing the experiments shown including Alexandra Knox, Evan Ackroyd and Aaron Getachew. This manuscript has not been submitted for publication yet.

**IRW prevents high-fat diet induced non-alcoholic fatty liver disease by preserving mitochondrial content and enhancing hepatic fatty acid oxidation capacity.**

Stepheny C. de Campos Zani <sup>1,2</sup>, Emily Berg <sup>1,2</sup>, Xu Jiang <sup>3</sup>, Alexandra Knox<sup>4</sup>, Evan Ackroyd<sup>1</sup>, Aaron Getachew<sup>1</sup>, Jianping Wu <sup>3</sup> and Catherine B Chan <sup>1,2,3, \*</sup>

<sup>1</sup>Department of Physiology, University of Alberta, Edmonton, T6G2H7, AB, Canada.

<sup>2</sup>Alberta Diabetes Institute, University of Alberta, Edmonton, T6G2E1, AB, Canada.

<sup>3</sup>Department of Agricultural Food & Nutritional Science, University of Alberta, Edmonton, T6G1C9, AB, Canada.

<sup>4</sup>Faculty of Pharmacy and Pharmaceutical Sciences, University of Alberta, Edmonton, Canada, University of Alberta, Edmonton, T6G2H7, AB, Canada

\*Correspondence: [cbchan@ualberta.ca](mailto:cbchan@ualberta.ca); Tel.: +1-780-492-9964

## Abstract

NAFLD is a disease considered as the hepatic manifestation of the metabolic syndrome. Its recent rise as a public health concern, complex underlying pathophysiology and poorly understood triggers for disease progression have created a situation in which NAFLD remains without approved pharmacological treatment, with lifestyle modifications being the only therapy. Alternative approaches, including natural health products, functional foods and food-derived bioactive peptides can aid in the management of metabolic conditions including hypertension, obesity and insulin resistance. IRW is a tripeptide with ACE-inhibitory properties produced from the egg white protein ovotransferrin. Previous studies reveal that IRW supplementation elicits antihypertensive effects, improves whole body insulin resistance and skeletal muscle insulin signaling, and glucose tolerance, while reducing BW gain. In this study, we hypothesized that IRW45 supplementation would prevent HFD-induced NAFLD by modulating hepatic lipid metabolism. We find that although both IRW45 and rosiglitazone improve insulin resistance, only IRW45 prevents HFD-induced NAFLD. IRW45 decreases hepatic TG content and LD size compared to HFD ( $p = 0.015$ ,  $p = 0.0012$ , respectively) and ROSI (both  $p < 0.0001$ ). This is accompanied by a trend to increased hepatic *Ppargc1a* ( $p = 0.08$ ) gene expression and upregulated expression of *Cd36* ( $p = 0.013$ ) compared to HFD. Moreover, IRW45 increases the hepatic mitochondrial complexes ( $p < 0.05$ ), p-AMPK $\alpha$  ( $p < 0.05$ ) and has a trend to increase p-ACC ( $p = 0.06$ ) protein abundance compared to HFD. Therefore, IRW45 prevents diet-induced NAFLD, in part by enhancing the expression of genes involved in mitochondrial biogenesis, the abundance of mitochondria complexes and increasing the capacity for lipid oxidation, while possibly decreasing DNL under HFD challenge.

**Key words:** IRW, non-alcoholic fatty liver disease, mitochondria, bioactive peptides.

## 5.1 Introduction

NAFLD currently affects 25% of the population worldwide and continues to increase in prevalence [285]. NAFLD is a term used to refer to fatty liver (hepatic steatosis) or to NASH, in which inflammation, cell damage and fibrosis are present. NAFLD is highly associated with comorbidities within the metabolic syndrome cluster, such as obesity, dyslipidemia and insulin resistance; in fact, NAFLD is considered the hepatic manifestation of the metabolic syndrome [20].

Many pathways lead to hepatic lipid accumulation, such as increased non-esterified fatty acid (NEFA) availability in the blood, increased hepatic NEFA uptake, DNL, decreased fatty acid oxidation or reduced very low density lipoprotein secretion [201]. In addition, inflammation, oxidative stress, fibrosis and mitochondrial dysfunction are involved in the progression of liver steatosis to NASH [286, 287]. The most accepted theory for NAFLD pathogenesis is the multi-hit hypothesis. Briefly, it states that increased caloric intake leads to obesity and WAT insulin resistance. Insulin resistance impairs lipolysis inhibition in WAT, increasing NEFA availability in the circulation, which can travel to and be taken up by the liver. Moreover, insulin resistance is associated with WAT dysfunction leading to inflammation and secretion of inflammatory cytokines from WAT. In the liver, insulin resistance induces exaggerated DNL, which combined with the extrahepatic influx of NEFA causes lipid accumulation and lipotoxicity (damage caused by lipid mediators). This in turn initiates mitochondrial dysfunction, reactive oxygen species production and ER stress. In addition, according to this theory the gut microbiome, genetics and epigenetics factors also play a role in disease initiation and progression [149]. With chronic exposure to these detrimental effects, cellular damage and inflammation occur, leading to

NASH. NASH can progress to fibrosis causing liver cirrhosis, and eventually hepatocellular carcinoma and the need for liver transplantation [20, 149, 201].

Lifestyle modifications (diet and physical activity) leading to weight loss are the first line of therapy for NAFLD [27]. Despite a global effort to find a pharmacological therapy for NAFLD, many clinical trials failed to advance to the next phase due to null results or adverse side effects. For instance, the peroxisome proliferator-activated receptor (PPAR) agonist, elanafibranor, failed to improve NASH after 72 weeks of treatment [288]. Null results were also observed with a fibroblast-growth factor analog [289] and a caspase inhibitor [290]. Although a recent meta-analysis showed that a thiazolidinedione drug (pioglitazone) improves NAFLD in clinical trials [30], thiazolidinedione usage comes with severe side-effects including weight gain and increased risk for cardiovascular disease [291, 292]. There are still clinical trials focusing on NASH and drug repurposing in progress, for example, trials using semaglutide and tirzepatide, which are currently used for obesity and diabetes treatment, respectively [286]. Nevertheless, currently there is no approved pharmacological treatment for NAFLD.

There is an increasing focus on the potential role of food-derived bioactive peptides to complement the management of metabolic diseases as reviewed elsewhere [163, 293]; however, the number of studies validating *in vitro* findings in animal models or in clinical trials is small. Based on previous evidence from our group, IRW (isoleucine-arginine-tryptophan) holds potential to ameliorate metabolic syndrome conditions *in vivo*. We showed that IRW, an egg white-derived bioactive peptide with ACE inhibitory activity *in vitro* [185], which increased ACE2 activity *in vivo* [250], improved glucose tolerance and insulin signaling in skeletal muscle [207] and decreased blood pressure [187, 250] in rodents. Moreover, IRW modulated skeletal muscle glucose homeostasis in an insulin-independent manner, via AMPK $\alpha$  activation

[207]. In cell culture, IRW reversed TNF- $\alpha$ -induced insulin resistance in a skeletal muscle cell line [192] and attenuated the inflammatory response in endothelial cells [188]. As NAFLD patients exhibit insulin resistance and inflammation in addition to fatty liver, an ideal pharmacological treatment would improve insulin resistance and modulate hepatic lipid metabolism, e.g., by increasing fatty acid oxidation via AMPK activation and preserving mitochondria function. Therefore, a possible role for IRW in NAFLD management is plausible. In this study we hypothesized that IRW would prevent HFD-induced hepatic steatosis in mice by modulating lipid metabolism and preventing hepatic mitochondrial dysfunction.

## 5.2 Methods

### 5.2.1 *Animals and diet*

This study was approved by the Animal Care and Use Committee of the University of Alberta (Protocol #1472) in accordance with guidelines issued by the Canadian Council on Animal Care. Male C57BL/6 mice age 5 weeks (Charles River Canada, St. Constant, QC, Canada) were fed low-fat diet (LFD (10% kcal fat) or HFD (45% kcal fat) for 6 weeks to induce obesity and glucose intolerance [199]. After that, animals receiving HFD were randomly assigned to continue receiving only HFD or HFD supplemented with IRW at 45 mg/Kg BW (IRW45) in their diet or HFD + rosiglitazone at 2.5  $\mu$ mol/Kg BW in their drinking water (ROSI) for 8 weeks. Rosiglitazone was added as a positive control for PPAR $\gamma$  agonism. LFD group received the same diet throughout the entire period. Mice had ad libitum access to food and water and were housed 4 per cage with a 12:12 light cycle, 60% humidity and 23 °C temperature. After a total of 14 weeks, after overnight fasting half the animals were injected with (2 IU/kg BW) insulin or saline, then after 10 minutes animals were euthanized using CO<sub>2</sub>. IRW was synthesized by Genscript

(Piscataway, NJ, USA) and the dosage selected was based on a previous study by our group [207]. Rosiglitazone was purchased from Sigma-Aldrich (St. Louis, MA, USA). Diet composition is shown in Table 5.1.

**Table 5. 1. Diet composition**

	<b>LFD</b>	<b>HFD</b>	<b>IRW45</b>	<b>ROSI</b>
<b>Casein (g/Kg)</b>	210.0	245.0	245.0	245.0
<b>L-Cystine (g/Kg)</b>	3.0	3.5	3.5	3.5
<b>Corn Starch (g/Kg)</b>	445.0	85.0	85.0	85.0
<b>Maltodextrin (g/Kg)</b>	50.0	115.0	115.0	115.0
<b>Sucrose (g/Kg)</b>	160.0	200.0	200.0	200.0
<b>Lard (g/Kg)</b>	20.0	195.0	195.0	195.0
<b>Soybean Oil (g/Kg)</b>	20.0	30.0	30.0	30.0
<b>Cellulose (g/Kg)</b>	37.15	58.0	58.0	58.0
<b>Mineral Mix, AIN-93G-MX (94046) (g/Kg)</b>	35.0	43.0	43.0	43.0
<b>Calcium Phosphate, dibasic (g/Kg)</b>	2.0	3.4	3.4	3.4
<b>Vitamin Mix, AIN-93-VX (94047) (g/Kg)</b>	15.0	19.0	19.0	19.0
<b>Choline Bitartrate (g/Kg)</b>	2.75	3.0	3.0	3.0
<b>IRW (mg/Kg BW)</b>	n/a	n/a	45.0	n/a
<b>Rosiglitazone (<math>\mu</math>M/Kg BW in water)</b>	n/a	n/a	n/a	2.5

Abbreviations: BW, body weight; n/a, not applicable

### 5.2.2 *BW, body composition and biological samples*

Animals were weighed weekly throughout the study. At week 14, body composition was assessed in overnight-fasted mice using ECHO magnetic resonance imaging (ECHO MRI) (Echo Medical Systems LLC, Houston, TX, USA). Blood was collected via cardiac puncture after euthanasia. Liver, epididymal (eWAT) and retroperitoneal (rWAT) adipose tissues were collected, snap frozen in liquid nitrogen and stored at  $-80^{\circ}\text{C}$ . In addition, a sample of each tissue was fixed with buffered formalin and preserved in paraffin blocks for histological analysis.

### 5.2.3 *Oral glucose tolerance test (OGTT) and fasting glucose*

At week 13, all the animals underwent an OGTT as previously described [199]. Briefly, a bolus of glucose (1g/kg BW) was orally gavaged to overnight-fasted mice and blood glucose measured from the tail vein using a glucometer (Contour<sup>®</sup>Next, Mississauga, ON, CA) at 0-, 15-, 30-, 60-, 90-, and 120-min. Fasting blood glucose was measured after overnight fasting from the tail vein.

### 5.2.4 *Histological analysis*

Paraffin blocks were cut in 5  $\mu\text{m}$  sections and the prepared slides stained for hematoxylin & eosin as previously reported [199]. Liver characterization: 3 random photomicroscopic images per mice were taken by one researcher (20 $\times$ , Axio Vision 4.8 software) and a second researcher blinded to group allocation used the ImageJ software “freehand selections” tool to quantify LD area. Cell number and inflammatory foci (clusters with  $>5$  immune cells) were counted. Each image was divided into 4 equal quadrants and the top left section analyzed. Adipose tissue characterization: 10 random photomicroscopic images per animal were taken (20 $\times$  objective lens

and Axio Vision 4.8 software). Adipocyte area ( $\text{mm}^2$ ) was measured using the ImageJ software “freehand selections” tool. A total of 300 cells or 10 images per sample was measured, whichever was reached first.

#### 5.2.5 *Hepatic lipid content*

Liver lipid content was extracted as previously described [199, 211]. Briefly, 100mg of tissue was homogenized in 1 mL of NaCl solution. Half of the homogenate (500 $\mu$ l) was mixed with 2 mL of Folch solution (chloroform: methanol (2:1)), centrifuged at 3000 rpm for 10 min and the lower phase collected. Dried samples were resuspended in 1 mL of 2% TritonX-100 solution in chloroform and dried under nitrogen one more time. The final sample was resuspended in ddH<sub>2</sub>O and kept at  $-20\text{ }^\circ\text{C}$  until further analysis. Liver TG and cholesterol content were measured using commercial kits (Infinity<sup>TM</sup>, Thermo Scientific, Waltham, MA, USA).

#### 5.2.6 *Citrate synthase activity*

Hepatic citrate activity was measured in liver lysate using a commercial kit specific for rodents (MAK193, Sigma-Aldrich, St. Louis, MA, USA). 30 mg of tissue was homogenized in 300  $\mu$ l of assay buffer and 25  $\mu$ l of sample was used in each well following the manufacturer’s protocol.

#### 5.2.7 *Protein extraction and western blot*

WAT protein extraction was performed using a commercial kit (AT-022, Invent Biotechnologies, Plymouth, MN, USA), using 100 mg of tissue. Liver protein extracts were obtained using lysis buffer (50 mmol/L Tris HCL pH:8.0, 150 mmol/L NaCl, 0.1% Triton X-

100, 0.5% sodium deoxycholate, 0.1% SDS) supplemented with protease and phosphatase inhibitors (2 µg/mL aprotinin (Calbiochem), 5 mmol/L sodium fluoride, 5 mmol/L sodium orthovanadate, and 1X protease inhibitor cocktail (FastPrep<sup>®</sup>-24, MP Biomedicals)). Protein extracts were stored at -80°C. Thawed samples were separated using an SDS-PAGE 8% or 12% polyacrylamide gels, transferred to nitrocellulose membranes and probed overnight at 4°C for PPAR $\gamma$  (CS2435), perilipin 1 (CS9349), fatty acid synthase (FAS) (CS3180), adiponectin (CS2789), oxphos (ab110413), fatty acid binding protein 4 (FAB4) (CS2120), acetyl-CoA carboxylase (ACC) (CS3676); p-ACC (Ser79) (CS11818), carnitine palmitoyl transferase 1 $\alpha$  (CPT1 $\alpha$ ) (CS97361), AMP-activated protein kinase  $\beta$  (AMPK $\beta$ ) (CS12063), p-AMPK $\beta$  (Ser108) (CS23021), p-AMPK $\alpha$  (Thr172) (C2531S), AMPK $\alpha$  (CS2603S) and  $\beta$ -actin (Sigma-Aldrich A5441). The next day membranes were incubated with fluorescent secondary antibodies (Li-cor Biosciences) for 1 h at room temperature. Images were captured using Li-cor scanners and analyzed using Image Studio Lite software (Li-cor Biosciences, Lincoln, NE, USA). Bands that were below of the quantification threshold were given a value of 0 (zero). Total proteins were normalized to  $\beta$ -actin and phosphorylated proteins were normalized to their respective total protein.

### 5.2.8 RNA extraction and qPCR

RNA extraction was performed using the QIAGEN RNeasy Mini Plus kit following the manufacturer's instructions, with the following modifications as previously described [199]: 5-100 mg of frozen tissue was homogenized using 1 mL of TRIzol and after 5 min at RT, 0.2 mL of chloroform per mL of TRIzol was added. Samples were incubated at room temperature for 3 min, followed by centrifugation at 12,000  $\times$  g for 10 min at 2–8 °C. The supernatant was

collected, and the manufacturer's instructions were followed for the remaining steps. RNA concentration was measured using a Nanodrop (Thermo Fisher, Waltham, MA, USA) and cDNA synthesis was performed using the high-capacity cDNA RT kit (Applied Biosystems, Waltham, MA, USA) using 2 µg RNA per reaction. qPCR was performed using PerfeCTa SYBR Green SuperMix ROX (Quantabio, Beverly, MA, USA) in a QuantStudio3 machine (Applied Biosystems, Waltham, MA, USA) using cyclophilin A as the reference gene. Primer sequences are provided in Table 5.2.

#### 5.2.9 *Statistical analysis and sample size*

A sample size of  $n = 4$  (non- or insulin-injected) to 8 (all mice)/group was used in this study as specified in the figure captions. Data are presented as means  $\pm$  SEM. Statistical analysis was performed using GraphPad Prism software 7.0 (GraphPad Software Inc., San Diego, CA, USA). LFD was compared to HFD group using a two tailed t-test to identify glucose intolerance-related differences. HFD, HFD+IRW and HFD+ROSI groups were compared using one-way ANOVA followed by Bonferroni's post-hoc test to study treatment effects (IRW and rosiglitazone). OGTT was analyzed using 2-way ANOVA followed by Bonferroni's post-hoc test. Data were checked for normal distribution by the Shapiro–Wilk test and any identified outliers were removed. Data that did not follow a normal distribution was log-transformed prior to the statistical analysis. A  $p$ -value  $\leq 0.05$  was considered statistically significant and a  $p$ -value  $< 0.1$  was considered a trend.

**Table 5. 2. Primers sequences.**

		<b>Primer sequence</b>
<i>Mtp</i>	F 5' – 3' R 5' – 3'	AGAGGACAGCTTTGTCACCG TCTTCAGCTCCAATTTCTGCTTCG
<i>Cd36</i>	F 5' – 3' R 5' – 3'	TGGCTAAATGAGACTGGGACC ACATCACCCTCCAATCCCAAGTAAGG
<i>Fasn</i>	F 5' – 3' R 5' – 3'	CTTCCGTCCTCCAGTTAGAGCAG AGTTCAGTGAGGCGTAGTAGACAGTG
<i>Pparg</i>	F 5' – 3' R 5' – 3'	GAAGACATTCCATTCACAAGAGCTGACC GCCTGTTGTAGAGCTGGGTCTT
<i>Pparg2</i>	F 5' – 3' R 5' – 3'	ATGCTGTTATGGGTGAAACTCTGGGA CACAGAGCTGATTCCGAAGTTGGTG
<i>Ppara</i>	F 5' – 3' R 5' – 3'	CGACCTGAAAGATTCGGAAACTGCAG GCGTCTTCTCGGCCATACACAAG
<i>Srebp1c</i>	F 5' – 3' R 5' – 3'	GGAGCCATGGATTGCACATTTGAAGACAT TTCCAGAGAGGAGGCCAGAGA
<i>Cpt1a</i>	F 5' – 3' R 5' – 3'	CCTACCATGGCTGGATGTTTGCAG GTATCTTTGACAGCTGGGACAGGCA
<i>Acaca</i>	F 5' – 3' R 5' – 3'	CCTGAAGACCTTAAAGCCAATGC CCAGCCCACACTGCTTGTA
<i>Acacb</i>	F 5' – 3' R 5' – 3'	TTCCCCAGCCAGCAGATAG TGAAGAAGACCTCTCGGTCC
<i>Cidea</i>	F 5' – 3' R 5' – 3'	GCCGTGTTAAGGAATCTGCTG TGCTCTTCTGTATCGCCCAGT
<i>Sod1</i>	F 5' – 3' R 5' – 3'	AACCAGTTGTGTTGTCAGGAC TCCTGCACTGGTACAGCCTT
<i>Opa1</i>	F 5' – 3' R 5' – 3'	TCTCAGCCTTGCTGTGTCAGAC TTCCGTCTCTAGGTTAAAGCGCG
<i>Vdac1</i>	F 5' – 3' R 5' – 3'	CTCCCACATACGCCGATCTT AAGCCGTAGCCCTTGGTGAAG
<i>Mfn1</i>	F 5' – 3' R 5' – 3'	CCAGGTACAGATGTCACCACAGAGC TTGGAGAGCCGCTCATTACCT
<i>Mfn2</i>	F 5' – 3' R 5' – 3'	GTGGAATACGCCAGTGAGAAGC CAACTTGCTGGCACAGATGAGC
<i>Bax</i>	F 5' – 3' R 5' – 3'	GGAGCTGCAGAGGATGATTGCT AAGTAGAAGAGGGCAACCACGC
<i>Pparg1a</i>	F 5' – 3'	GAATCAAGCCACTACAGACACCG

	R 5' – 3'	AGGCTTCATAGCTGTCGTACCTG
<i>Ppia</i>	F 5' – 3'	TGGCTATAAGGGTTCCTCCTTTACAG
	R 5' – 3'	GCCAGGACCTGTATGCTTTAGGATG

---

Abbreviations: *Gene symbol* followed by its (name) and the encoded protein: *Mttp* (microsomal triglyceride transfer protein) encodes MTP; *Cd36* encodes fatty acid translocase (CD36); *Fasn* (fatty acid synthase) encodes FAS; *Pparg* (peroxisome proliferator-activated receptor gamma) encodes PPAR $\gamma$ ; *Pparg2* (peroxisome proliferator-activated receptor gamma) encodes PPAR $\gamma$ 2; *Ppara* (peroxisome proliferator-activated receptor alpha) encodes PPAR $\alpha$ ; *Srebp1c* (sterol regulatory element binding transcription factor 1c) encodes SREBP-1c; *Cpt1a* (carnitine palmitoyl transferase 1A) encodes CPT1 $\alpha$ ; *Acaca* (acetyl-CoA carboxylase alpha) encodes ACC1; *Acacb* (acetyl-CoA carboxylase beta) encodes ACC2; *Cidea* (cell death-inducing DNA fragmentation factor-like effector A) encodes CIDEA; *Sod1* (Superoxide dismutase 1) encodes SOD1; *Opal* (mitochondrial dynamin like GTPase) encodes OPA1; *Vdac1* (Voltage-Dependent Anion-Selective Channel Protein 1 ) encodes VDAC1; *Mfn1* (Mitofusin-1) encodes MFN1; *Mfn2* (Mitofusin-2) encodes MFN2; *Bax* (bcl-2-like protein 4) encodes BAX; *Ppargc1a* (PPARG coactivator 1 alpha) encodes PCG1 $\alpha$ ; *Ppia* (Peptidylprolyl isomerase A) encodes cyclophilin A.

## 5.3 Results

### 5.3.1 *BW and composition*

HFD animals gained more weight during the first 6 weeks prior to the peptide supplementation than LFD fed animals (Fig. 5.1A). At week 6, at the start of the peptide supplementation, no differences in BW among the HFD groups were observed (Fig. 5.1B and C). At week 12, the final BW of LFD ( $p < 0.0001$ ) and IRW45 ( $p = 0.0003$ ) groups were lower than HFD groups, while the ROSI group had similar final BW as HFD (Fig. 5.1D). This was due to lower absolute fat mass in the LFD ( $p < 0.0001$ ) and slight, but not statistically lower mass in the IRW45 group, compared to HFD. No differences in lean mass were observed (Fig. 5.1J).

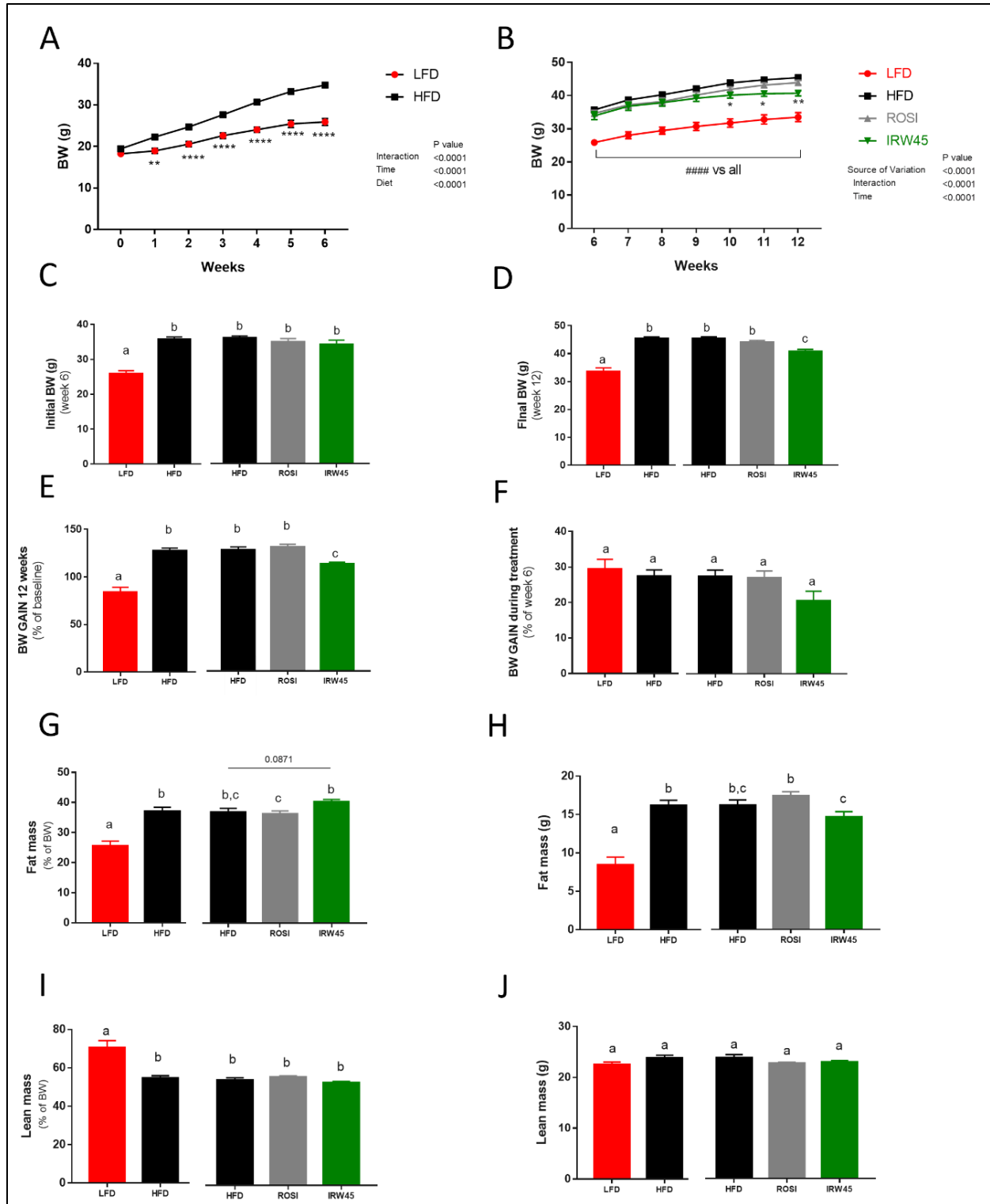


**Figure 5. 1. BW and body composition of C57BL/6 mice throughout the treatment (week 0 to week 12).** (A) BW before peptide supplementation; (B) BW during peptide supplementation and rosiglitazone treatment; (C) initial BW before peptide supplementation (week 6); (D) final BW after peptide supplementation (week 12); (E) BW gain

throughout the study (week 0 to week 12); (F) BW gain during peptide supplementation (week 6 to week 12); (G) relative fat mass; (H) absolute fat mass; (I) relative lean mass and (J) absolute lean mass. Data expressed as mean  $\pm$  SEM of  $n = 8$  mice/group and analyzed by 2-way ANOVA (A and B), two-tailed t-test (LFD x HFD) or one-way ANOVA (HFD groups). Different letters indicate  $p \leq 0.05$ .

### 5.3.2 *Glucose tolerance*

After 7 weeks of IRW treatment, glucose tolerance in the HFD group was impaired compared with LFD ( $p = 0.007$ ) (Fig. 5.2A and C, left). ROSI ( $p = 0.05$ ) and IRW45 ( $p = 0.02$ ) groups presented improved glucose tolerance compared with HFD as shown in Fig. 5.2B and by the area under the curve (AUC) (Fig. 5.2C, right). No changes were seen in the incremental AUC (iAUC) among groups (Fig. 5.2D). Differences in AUC but not iAUC are consistent with fasting blood glucose concentration being lower in the LFD ( $p = 0.007$ ), ROSI ( $p = 0.03$ ) and IRW45 ( $p = 0.002$ ) groups compared to HFD (Fig. 5.2E).

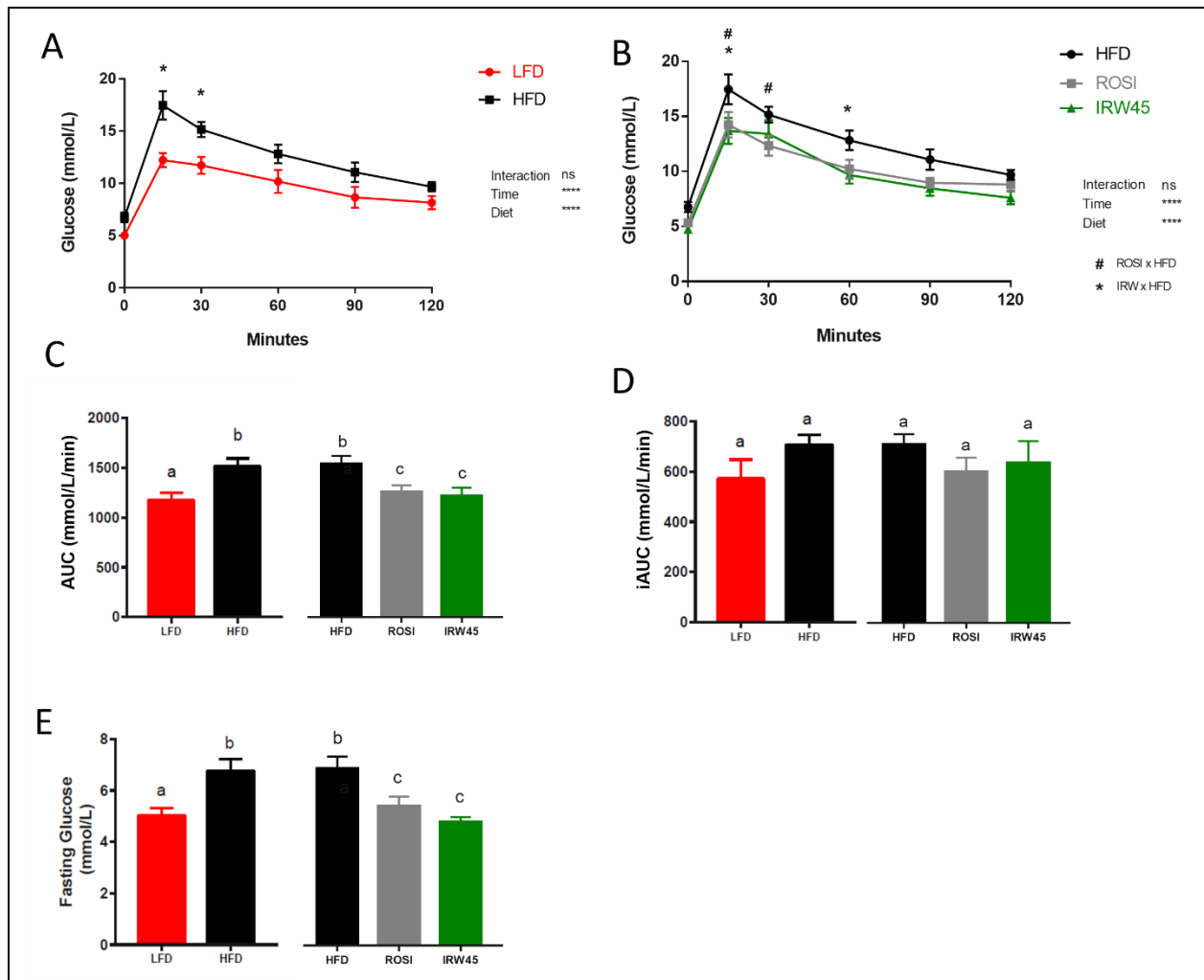


**Figure 5. 2. Oral glucose tolerance test (OGTT) of C57BL/6 mice at week 13 (7 weeks of treatment).** (A) LFD vs HFD OGTT curve; (B) HFD groups OGTT curve; (C) area under the curve (AUC) for OGTT; (D) incremental AUC for OGTT; (E) fasting blood glucose. Data expressed as mean  $\pm$  SEM of  $n=8$  mice/group and analyzed by 2-way ANOVA (A and B), two-tailed t-test (LFD vs HFD) or one-way ANOVA (HFD groups). Different letters indicate  $p \leq 0.05$  in panels C-E. \* and # indicate  $p \leq 0.05$  and \*\*\*\* indicates  $p \leq 0.0001$  in panels A and B.

### 5.3.3 *Liver lipid content and NAFLD characteristics*

Liver weight was not different between LFD and HFD (Fig. 5.3A, left). The ROSI group exhibited ~50% increased liver weight compared to HFD and IRW45 ( $p < 0.0001$ ) (Fig. 5.3A, right). Liver TG was decreased in LFD ( $p = 0.0031$ ) and IRW45 ( $p = 0.015$ ) groups compared to HFD, while ROSI had increased liver TG content versus HFD ( $p = 0.016$ ) and IRW45 ( $p < 0.0001$ ) groups (Fig. 5.3B). In addition, there was a trend for IRW45 to decrease liver cholesterol content compared to HFD and ROSI ( $p = 0.06$ , Fig. 5.3C, right) but no differences were observed among the other groups. Quantitative analysis of the LD number in liver histological samples showed a trend ( $p = 0.08$ ) in HFD to have more LD than LFD (Fig. 5.3D, left). IRW45 presented a similar LD number as HFD, but ROSI had ~50% more LD than HFD ( $p = 0.006$ ) and IRW45 groups ( $p = 0.001$ ) (Fig. 5.3D, right). LFD ( $p = 0.005$ ) and IRW45 ( $p = 0.0012$ ) had a smaller LD area than HFD, while ROSI had a similar LD area to HFD (Fig. 5.3E). Overall, both LFD ( $p = 0.002$ ) and IRW45 ( $p = 0.014$ ) groups had less area of the total image covered by LD compared to HFD (Fig. 5.3F), while ROSI had more area covered by LD than IRW45 and HFD groups ( $p < 0.0001$ ) (Fig. 5.3F, right). These data are supported by the qualitative assessment of the histological samples (Fig. 5.3I). No treatment changes were observed in terms of cell size (Fig. 5.3G) and inflammatory foci (Fig. 5.3H). The distribution of LD by number and size is shown in Fig. 5.3J, supporting that HFD exhibited a right shift in LD area that was even more exaggerated in ROSI.

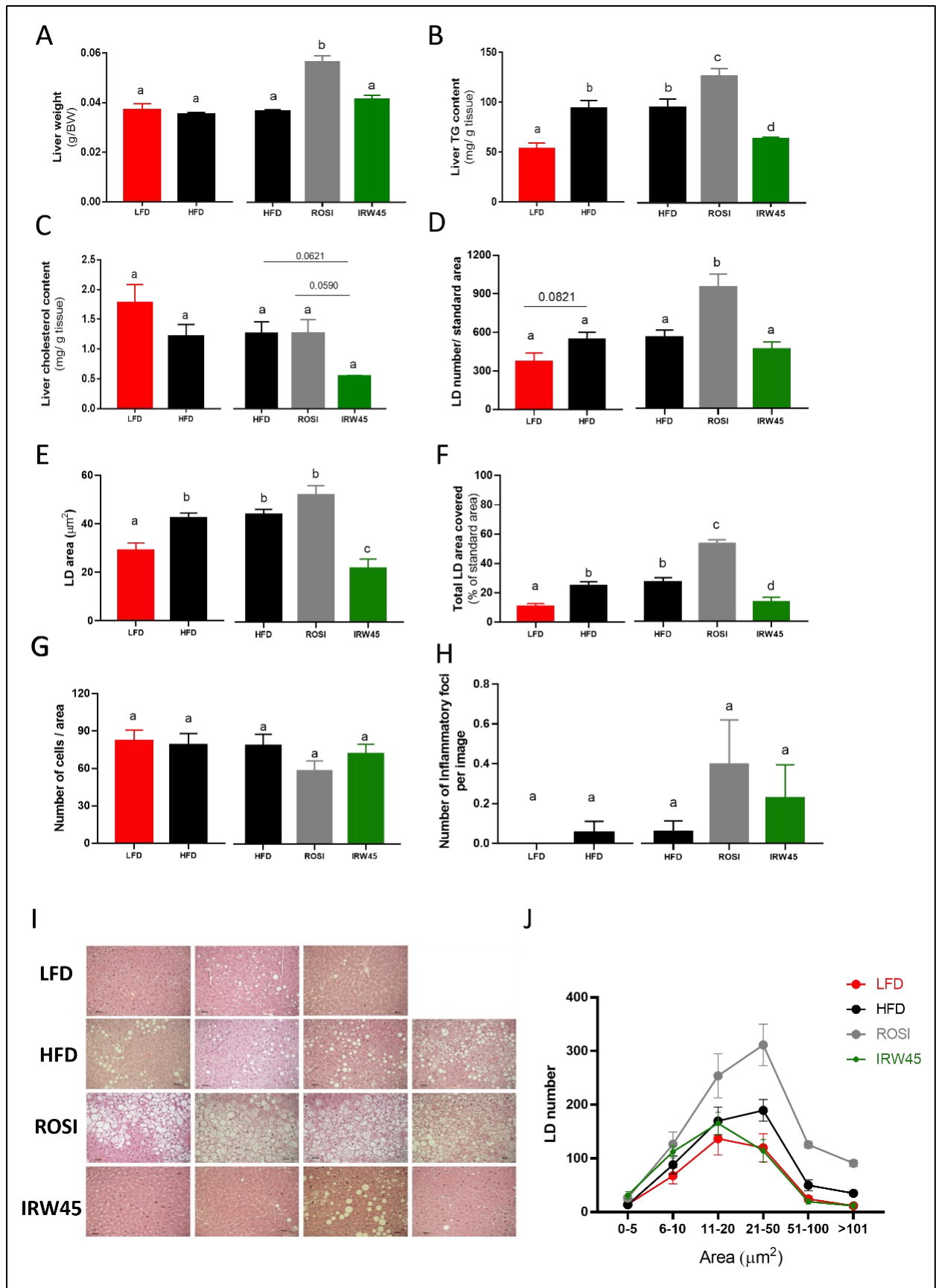


**Figure 5. 3. Liver morphological characterization.** (A) liver weight; (B) liver triglyceride content; (C) liver cholesterol content; (D) lipid droplet average number; (E) lipid droplet average area; (F) percentage area of the image covered by lipid droplets; (G) number of cells per area analyzed; (H) number of inflammatory foci per image analyzed; (I) histological representative images and (J) distribution of lipid droplets by size and number. Data expressed as mean  $\pm$  SEM of n=8 mice (A) or n = 6 (B-H, J) and analyzed by two-tailed t-test (LFD vs HFD) or one-way ANOVA (HFD groups). Different letters indicate  $p \leq 0.05$ .

#### 5.3.4 Liver lipid metabolism and mitochondrial related genes

Measurement of hepatic expression of genes involved in lipid metabolism revealed that *Cd36* and *Cidea* expression was upregulated 2-fold and more than 15-fold in the IRW45 ( $p = 0.013$  and  $0.0027$ , respectively) and ROSI ( $p = 0.071$  and  $0.001$ , respectively) groups compared to HFD, respectively. On the other hand, *Cpt1a*, *Mttp* and *Acaca* gene expression was downregulated in the IRW45 ( $p = 0.017$ ,  $0.0135$  and  $0.029$ , respectively) group compared to HFD (Fig. 5.4A). Despite a 50% reduction in *Pparg2* expression, it did not reach statistical significance when IRW45 was compared to HFD but had a strong trend to be lower than the ROSI group ( $p = 0.06$ ) (Fig. 5.4A). Western blot was conducted to determine if changes in gene expression were confirmed at the protein level. While FAS protein abundance showed a trend ( $p = 0.099$ ) to be higher in the IRW45 group, western blot of other key proteins involved in lipid metabolism (CPT1 $\alpha$ , PPAR $\gamma$  and total ACC) were not different among the HFD groups (Fig. 5.4B-D, right and 5.4F). This suggests that some of the differences observed in mRNA expression did not correspond to the protein being translated in the IRW45 group or that post-transcriptional regulation may limit protein abundance in this group. p-ACC protein abundance was enhanced in the IRW45 group compared to ROSI ( $p = 0.006$ ) and had a strong trend to be increased when compared to HFD ( $p = 0.06$ ) (Fig.5.4E). AMPK subunits were probed to examine a potential insulin-independent regulation of lipid metabolism. p-AMPK $\beta$  and total AMPK $\beta$  protein abundance did not change between LFD and HFD, nor among the HFD

treatment groups (Fig. 5.5A-C). p-AMPK $\alpha$ /AMPK $\alpha$  was similar between IRW45 and HFD groups but was increased in IRW45 compared to ROSI ( $p < 0.01$ ) (Fig. 5.5D); similarly, p-AMPK $\alpha$ / $\beta$ -actin was significantly higher in IRW45 compared to the other groups ( $p < 0.05$ ) (Fig. 5.5F). PPAR $\gamma$  protein abundance and both *Pparg* and *Pparg2* were decreased in the LFD compared to HFD ( $p < 0.05$ ) (Fig. 5.4D and Fig. 5.7A). In addition, FAS was enhanced in LFD compared to HFD (Fig. 5.4A, left), while the other proteins and the expression of other genes were not different between LFD and HFD groups (Fig. 5.4C,E-G and Fig. 5.7A).

Mitochondrial-related genes *Vdac1* ( $p = 0.01$ ) and *Mfn1* ( $p = 0.06$ ) were downregulated in IRW45 compared to HFD (Fig. 5.6A), while *Opal* showed a trend ( $p = 0.098$ ) to be reduced in IRW45 in comparison to HFD. ROSI had reduced *Vdac1* compared to HFD ( $p = 0.036$ ). Both *Bax* and *Ppargc1a* gene expression was upregulated in the ROSI compared to HFD ( $p = 0.025$  and  $0.048$ , respectively), while IRW45 showed a trend ( $p = 0.087$ ) to increased *Ppargc1a* gene expression compared to HFD. The protein abundance of mitochondrial complexes V, IV, III and II were increased in the IRW45 group compared to HFD ( $p < 0.05$ ) (Fig. 5.6B-E, right) and Complex I showed a consistent, similar trend to be increased in the IRW45 ( $p = 0.07$ ) (Fig. 5.6F, right). Expression of mitochondrial genes in the LFD group compared with HFD is shown in Fig. 5.7B with no differences observed.

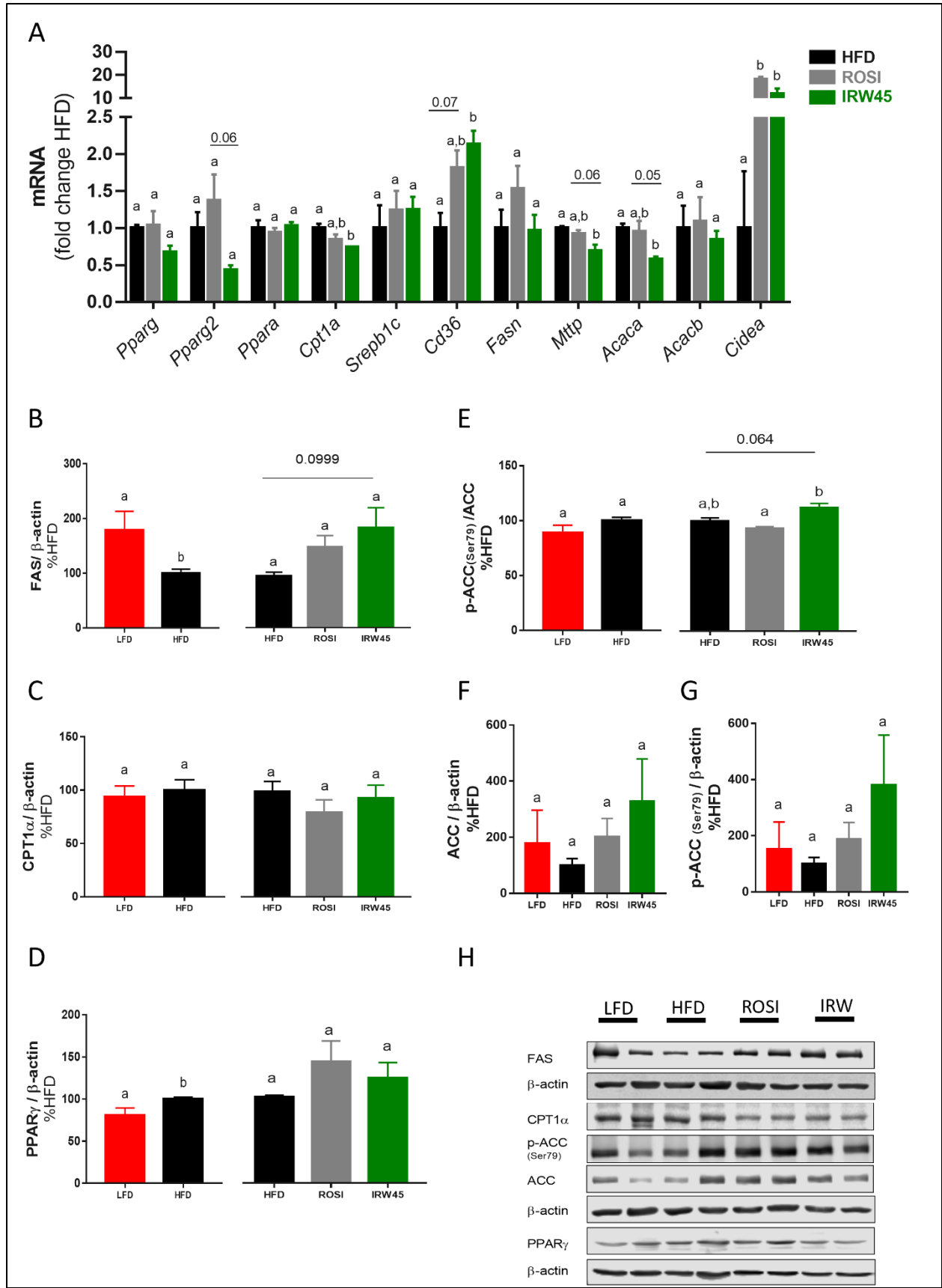


**Figure 5. 4. Liver lipid metabolism.** (A) Liver mRNA expression of genes involved in lipid metabolism (n = 4); Protein abundance (n = 8) of (B) FAS; (C) CPT1 $\alpha$ ; (D) PPAR $\gamma$ ; (E) p-ACC/ACC (n = 4 non-insulin-injected); (F) ACC and (G) p-ACC and (H) western blot representative images. Total proteins were normalized to  $\beta$ -actin and phosphorylated proteins were normalized to their total protein. Data analyzed by two-tailed t-test (LFD vs HFD) or one-way ANOVA (HFD groups). Different letters indicate  $p \leq 0.05$ .

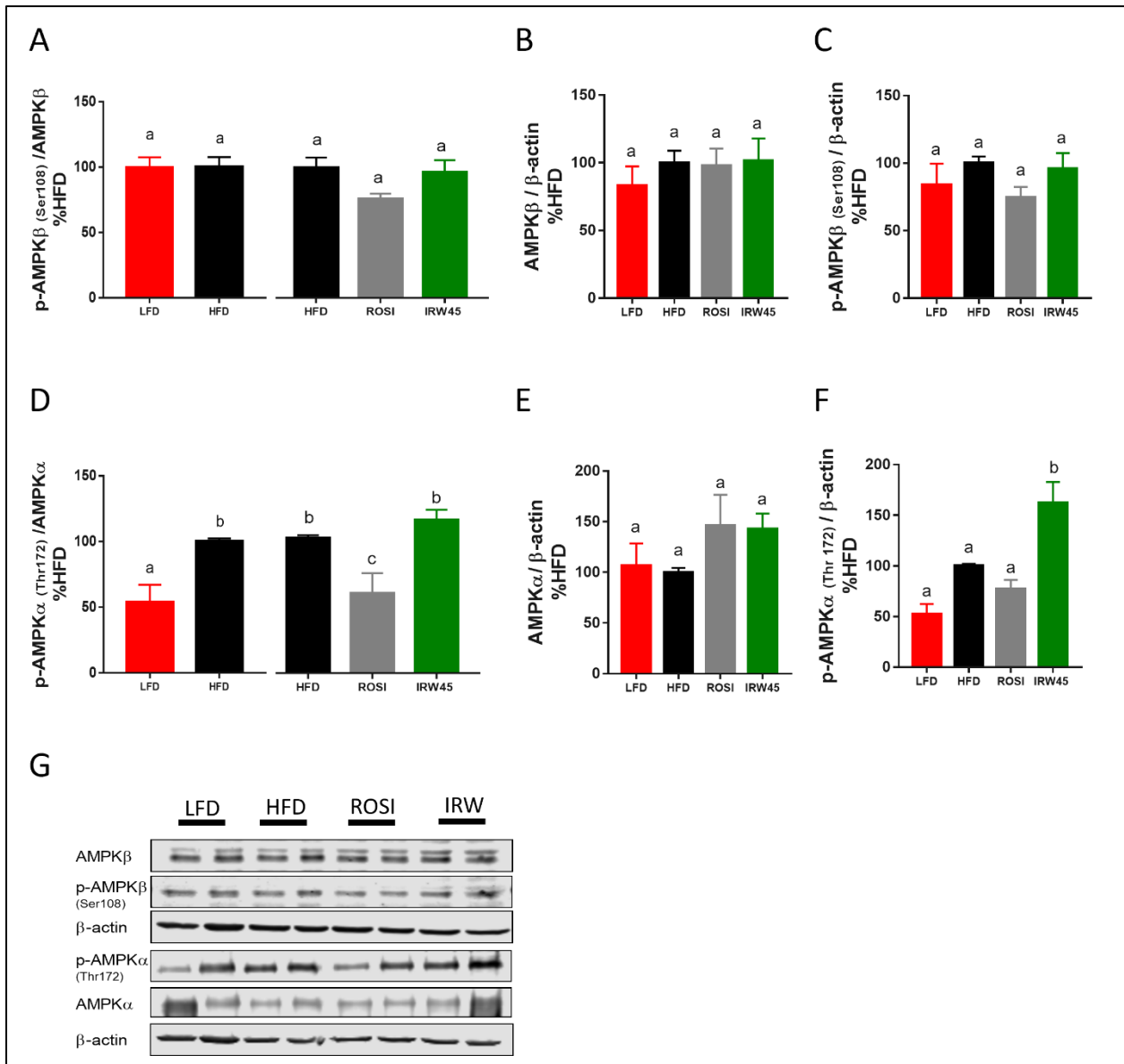


**Figure 5. 5. Liver AMPK protein abundance.** (A) p- AMPK $\beta$ / AMPK $\beta$ ; (B) AMPK $\beta$ ; (C) P-AMPK $\beta$ ; (D) p-AMPK $\alpha$ / AMPK $\alpha$ ; (E) AMPK $\alpha$  and (F) p-AMPK $\alpha$ . proteins were normalized to  $\beta$ -actin. Data expressed as mean  $\pm$  SEM of n = 4 non-insulin-injected mice. Data analyzed by one-way ANOVA. Different letters indicate  $p \leq 0.05$ .

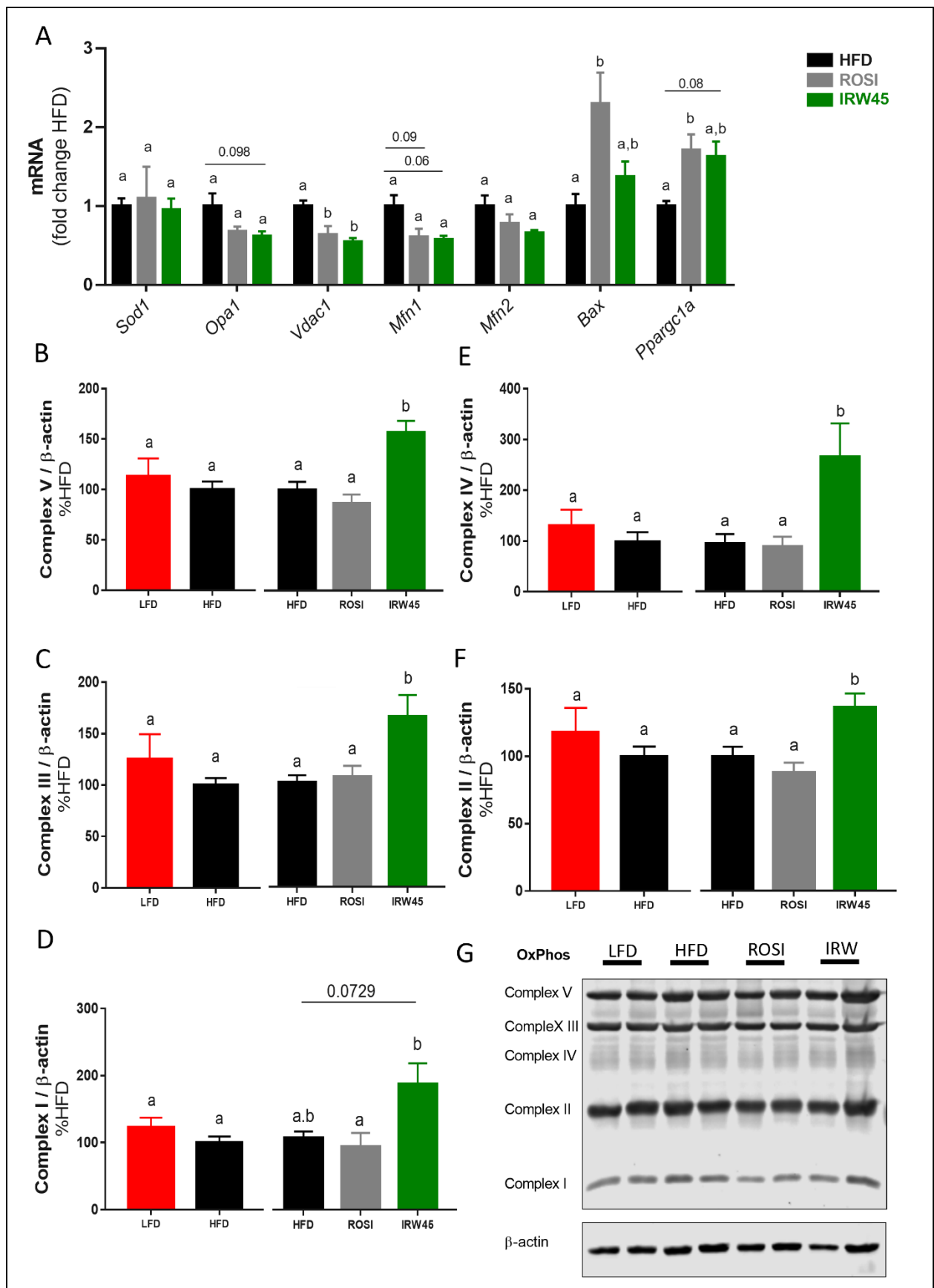


**Figure 5. 6. Liver mitochondrial related genes.** (A) Liver mRNA expression of genes involved in mitochondrial function; (B) mitochondrial complex V protein abundance; (C) mitochondrial complex IV protein abundance; (D) mitochondrial complex III protein abundance; (E) mitochondrial complex II protein abundance; (F) mitochondrial complex I protein abundance and (G) western blot representative image. Proteins were normalized to  $\beta$ -actin. Data expressed as mean  $\pm$  SEM of  $n = 4$  (A) and  $n=8$  (B-G). Data analyzed by two-tailed t-test (LFD x HFD) or one-way ANOVA (HFD groups). Different letters indicate  $p \leq 0.05$ .

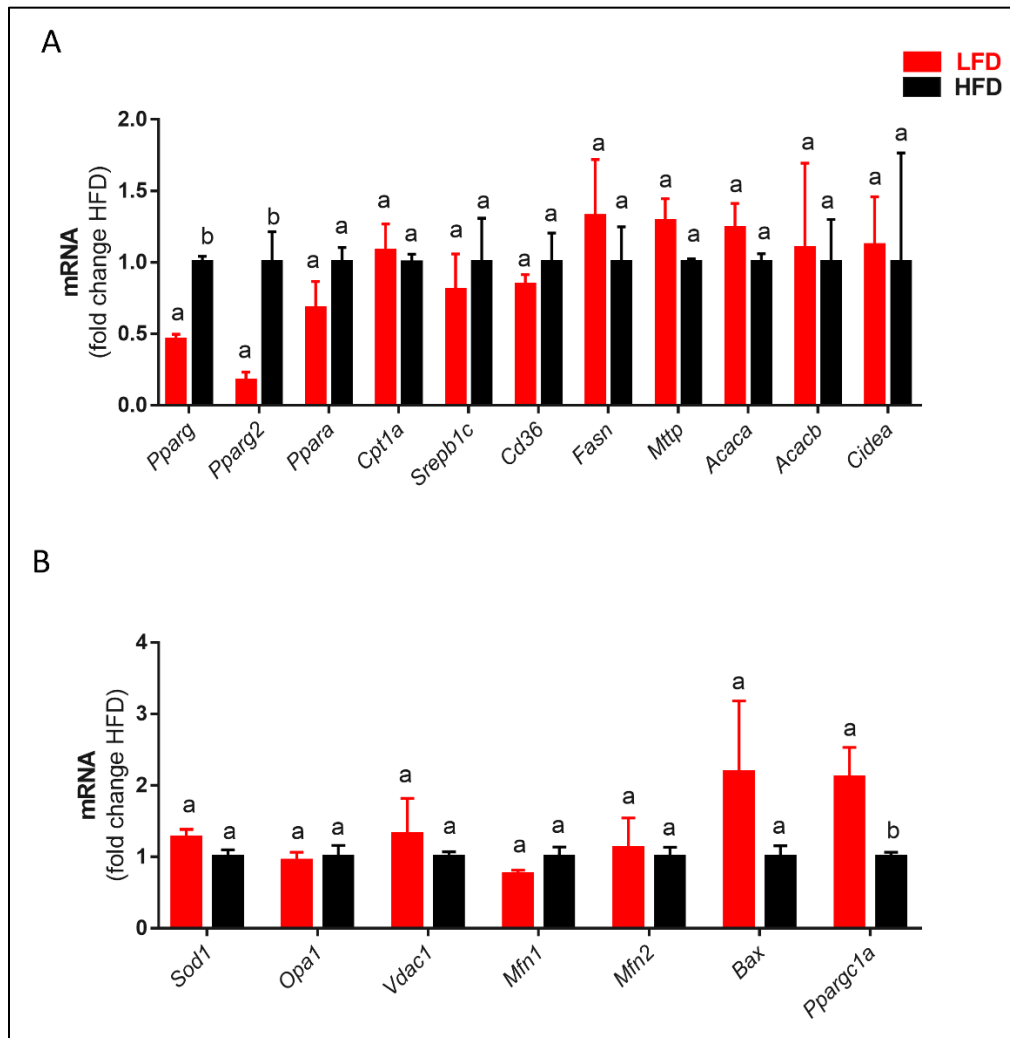


**Figure 5. 7. Liver mRNA expression between LFD and HFD groups.** (A) Liver mRNA expression of genes involved in lipid metabolism; (B) liver mRNA expression of mitochondrial genes. Data expressed as mean  $\pm$  SEM of  $n = 4$  and analyzed by two-tailed t-test. Different letters indicate  $p \leq 0.05$ .

### 5.3.5 Citrate Synthase activity

Citrate synthase activity was similar between LFD and HFD groups (Fig. 5.8, left) whereas IRW45 had higher citrate synthase activity than HFD ( $p = 0.0037$ ) and a trend to higher ( $p = 0.06$ ) compared to ROSI (Fig. 5.8, right).

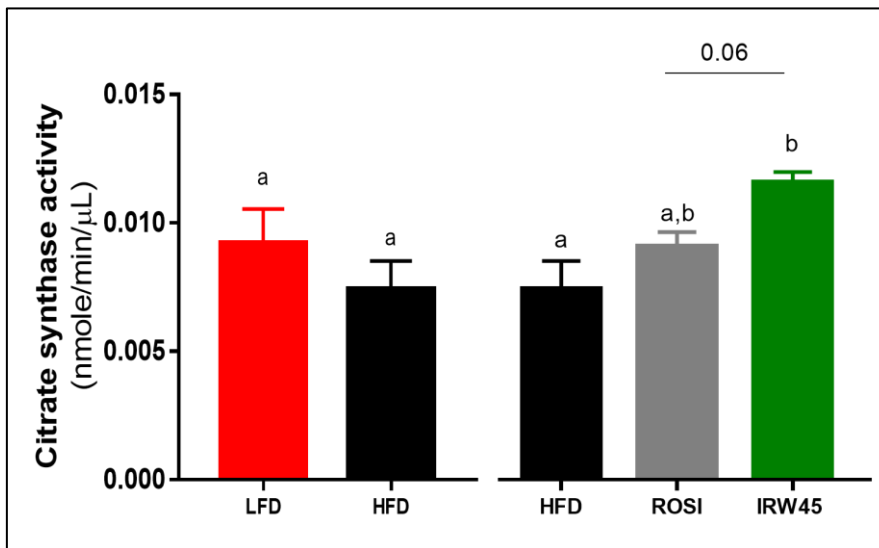


**Figure 5. 8. Liver citrate synthase activity.** Data expressed as mean  $\pm$  SEM of  $n = 7$  and analyzed by two-tailed t-test (LFD vs HFD) or one-way ANOVA (HFD groups). Different letters indicate  $p \leq 0.05$ .

### 5.3.6 VAT adipocyte size and adipogenesis markers

LFD had lower eWAT mass than HFD ( $p = 0.0014$ ) (Fig. 5.9A, left), while ROSI and IRW45 groups had increased eWAT mass compared with HFD ( $p < 0.001$ ) (Fig. 5.9A, right). LFD had lower adipocyte size than HFD ( $p = 0.01$ ) (Fig. 5.9B, left), while ROSI and IRW45 had similar adipocyte size as HFD (Fig. 5.9B, right). Protein abundance of perilipin 1, FAB4 and adiponectin were not statistically different between LFD and HFD groups, despite 4-fold higher adiponectin in the LFD group ( $p = 0.1$ ) (Fig. 5.9C-G). PPAR $\gamma$  protein abundance was increased

in the eWAT of LFD animals compared to HFD animals ( $p = 0.007$ ) (Fig. 5.9E, left). Among the HFD treatment groups no changes in perilipin 1, FAB4, PPAR $\gamma$  or adiponectin were observed (Fig. 5.9C-G), but a trend to increased PPAR $\gamma$  protein abundance was seen in ROSI groups vs HFD ( $p = 0.09$ ) (Fig. 5.9E, left). Representative images of the western blots and adipocyte size in eWAT are shown in Fig. 5.9G and H, respectively.

In terms of rWAT, LFD animals, as expected, had a lower fat mass, which was below the detection limit of the scale. Among the HFD groups no changes were seen in rWAT mass (Fig. 5.10A). Adipocyte size and adipogenesis markers were not different between LFD and HFD (Fig. 5.10C-E, left), nor among HFD groups (Fig. 5.10C-E, right). Adiponectin showed a trend to be higher in the LFD group compared to HFD ( $p = 0.09$ ) and was increased in the IRW45 group compared to HFD ( $p = 0.032$ ) (Fig. 5.10F). Representative images of the western blots and adipocyte size in rWAT are shown in Fig. 5.10G and H, respectively.

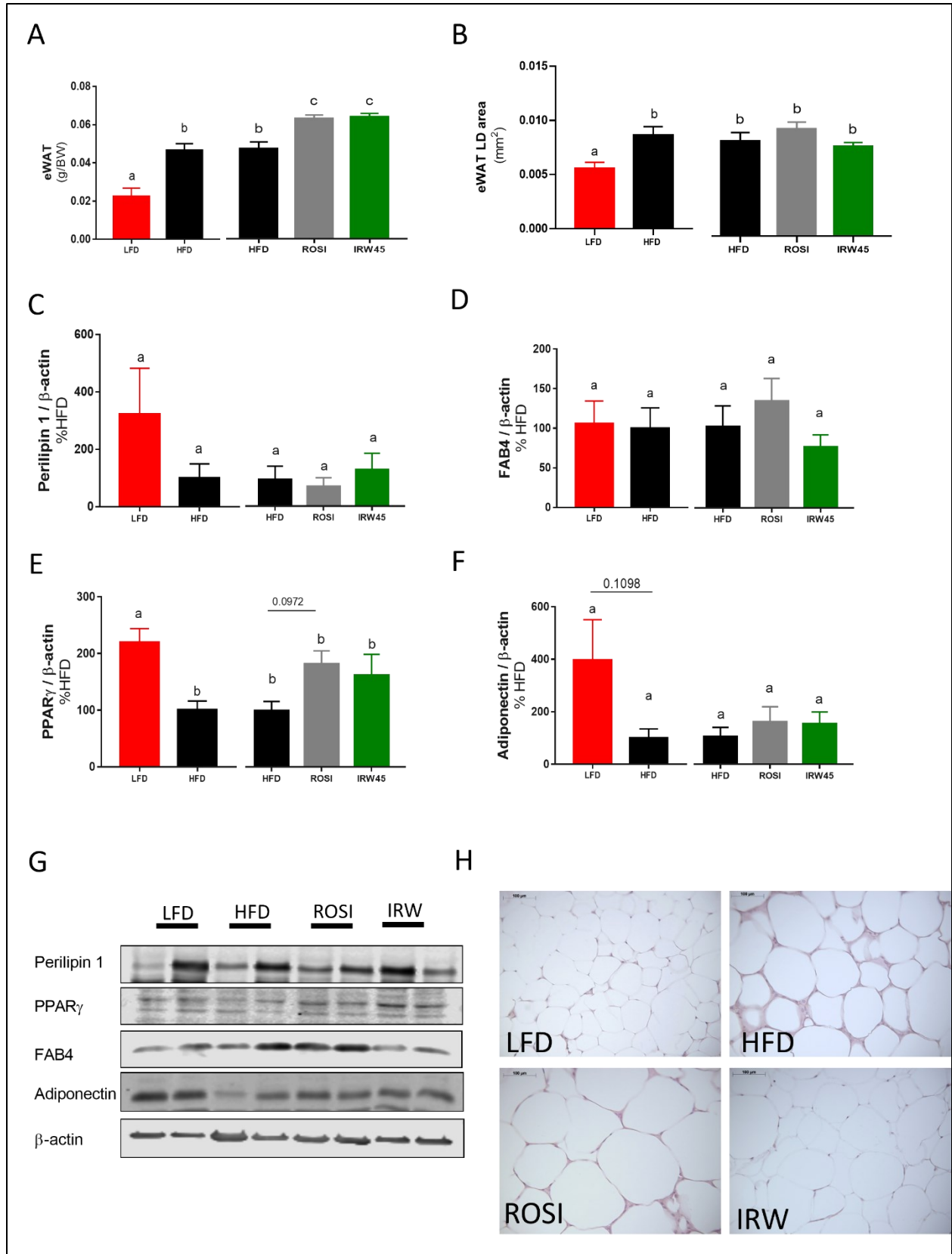


**Figure 5. 9. Epididymal white adipose tissue (eWAT) characterization.** (A) eWAT weight; (B) eWAT lipid droplet average area; (C) perilipin 1 protein abundance; (D) FAB4 protein abundance; (E) PPAR $\gamma$  protein abundance; (F) adiponectin protein abundance; (G) western blot representative images and (H) histological analysis representative images. Total proteins were normalized to  $\beta$ -actin. Data expressed as mean  $\pm$  SEM of n = 8 (A) or n = 6 (B) or n = 4 non-insulin-injected mice (C-F). Data analyzed by two-tailed t-test (LFD vs HFD) or one-way ANOVA (HFD groups). Different letters indicate  $p \leq 0.05$ . FAB4, fatty acid binding protein 4; PPAR $\gamma$ , peroxisome proliferator-activated receptor gamma.

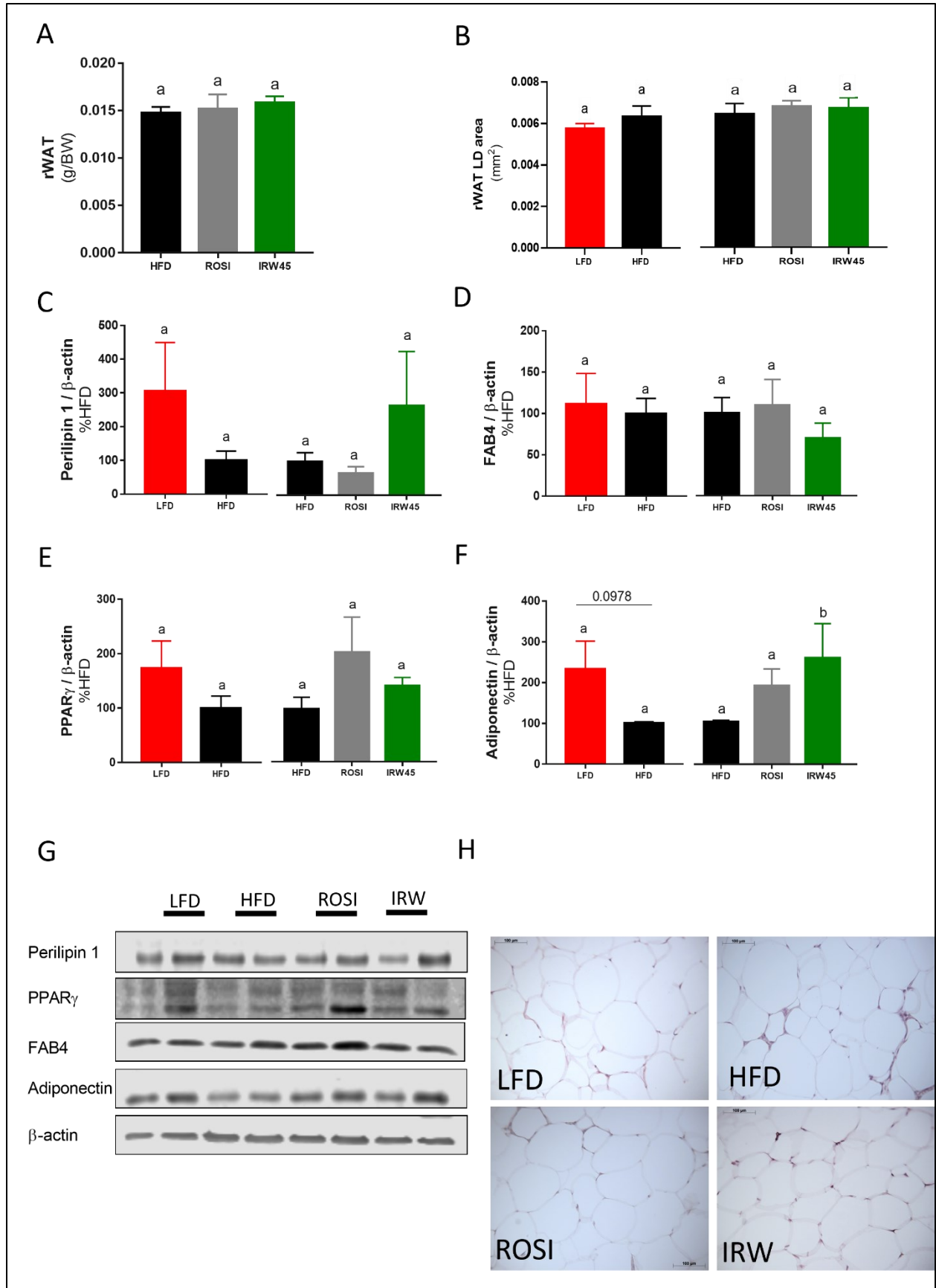


**Figure 5. 10. Retroperitoneal white adipose tissue (rWAT) characterization.** (A) rWAT weight; (B) rWAT lipid droplet average area; (C) perilipin 1 protein abundance; (D) FAB4 protein abundance; (E) PPAR $\gamma$  protein abundance; (F) adiponectin protein abundance; (G) western blot representative images and (H) histological analysis representative images. Total proteins were normalized to  $\beta$ -actin. Data expressed as mean  $\pm$  SEM of n = 8 (A) or n = 6 (B) or n=4 non-insulin-injected mice (C-F). Data analyzed by two-tailed t-test (LFD vs HFD) or one-way ANOVA (HFD groups). Different letters indicate  $p \leq 0.05$ . FAB4, fatty acid binding protein 4; PPAR $\gamma$ , peroxisome proliferator-activated receptor  $\gamma$ .

## 5.4 Discussion

The complex pathophysiology of NAFLD and the lack of understanding about the triggers leading to the onset of NASH complicates the development of therapeutic targets to treat this condition. Thus, NAFLD currently remains without approved pharmacological treatment. While diet and exercise are recommended to decrease BW and improve hepatic steatosis [27], there is keen interest to find novel approaches to complement NAFLD management. The underlying pathogenesis of NAFLD involves multiple detrimental “hits” in an organ crosstalk manner, including insulin resistance in WAT, increased influx of lipids in the liver and DNL, decreased lipid oxidation and export of VLDL. These ultimately cause inflammation, impairment in mitochondria dynamics, ER stress and apoptosis, which culminates in hepatic steatosis, inflammation and NASH [20, 149]. We show in this study that a small peptide derived from the egg ovotransferrin protein, namely IRW (isoleucine-arginine-tryptophan), prevented HFD-induced hepatic steatosis, in part by increasing the capacity for fatty acid oxidation via increased abundance of mitochondrial complexes, enzymes involved in fatty acid oxidation and citrate synthase activity. We previously showed that IRW45 improved skeletal muscle insulin signaling and glucose tolerance in HFD-induced obese mice [207], therefore, IRW could be a novel therapy to manage metabolic conditions and prevent one of the first (insulin resistance) and later hits (mitochondrial dysfunction) involved in NAFLD progression.

IRW45 improved histological and biochemical features in the liver of obese, glucose intolerant mice. IRW45-treated mice had parallel decreases in hepatic TG content, hepatic LD size and LD-covered area compared to HFD, supporting an improvement in hepatic steatosis. On the other hand, rosiglitazone-treated animals had worsened hepatic TG accumulation and LD-covered area. Therefore, even though both IRW45 and rosiglitazone improved glucose

homeostasis and insulin resistance in our previous experiments [199, 207], only IRW45 prevented HFD-induced liver steatosis. Differently from its effects in humans, rosiglitazone treatment in mice induces hepatic lipid accumulation via PPAR $\gamma$  activation in the liver [217, 218], which is consistent with our findings. Because we previously saw an increase in skeletal muscle PPAR $\gamma$  protein abundance in IRW45-treated animals [207], we wanted to further investigate the mechanism by which IRW45 prevents hepatic steatosis and differentiate it from the effects promoted by rosiglitazone.

Initially we thought that IRW45 might reduce lipid uptake by the liver, thereby preventing hepatic lipid accumulation, while increasing lipid accumulation in the WAT, as a safer storage depot to prevent metabolic complications [294, 295]. However, despite an increase in eWAT in the IRW45 and ROSI groups compared to HFD, absolute fat mass was not different between the IRW45 group compared to HFD at the end of the study. In fact, BW was marginally reduced in the IRW45 group. In addition, the ROSI group had no differences compared to HFD in terms of BW and fat mass. Moreover, individual adipocyte size did not change among the HFD-treated groups, nor did the adipogenesis markers. This suggests that lipid accumulation in WAT is similar among the groups and that IRW45 is probably not inducing adipogenesis to prevent hepatic lipid accumulation. It is worth noting that in the rWAT, adiponectin protein abundance was higher in the IRW45 group compared to HFD, which may contribute to IRW45's beneficial effects, since adiponectin agonists are shown to improve NASH in rodents [296], and plasma adiponectin is inversely correlated hepatic lipid accumulation in humans [297].

We hypothesized that IRW would modulate hepatic lipid metabolism and mitochondrial function to prevent NAFLD. Although IRW modulated lipid metabolism it seems that, contrary to our initial hypothesis, it was not due to decreased fatty acid uptake because both IRW45 and

ROSI groups had upregulated hepatic expression of genes involved in lipid uptake (*Cd36*) and downregulated expression of genes involved in VLDL assembly (*Mttp*) and in the transport of fatty acids into the mitochondria (*Cpt1a*). In addition, gene expression of targets involved in DNL were downregulated or unchanged in the IRW45 group compared to HFD (*Acaca* and *Fasn*, respectively). However, total protein content of CPT1 $\alpha$  and ACC (encoded by *Acaca*) was similar among the groups, while FAS protein abundance showed a trend to be increased in the IRW45 group. Moreover, ACC phosphorylation (Ser79) was increased by IRW45. ACC is a rate-limiting enzyme in DNL and its inhibition by AMPK $\alpha$ -mediated phosphorylation of Ser79 is essential to decrease lipogenesis by reducing malonyl-CoA synthesis, thus decreasing hepatic lipid accumulation [298]. Therefore, enhanced p-ACC in the IRW45 group suggests decreased lipogenesis in this group, which could contribute, in part, to the lower hepatic TG content and smaller LD. Despite a suggested increase in hepatic lipid uptake by the qPCR results, image analysis and protein results support the hypothesis of less lipid accumulation in the IRW45 group.

We then investigated other pathways that could be working to decrease hepatic lipid accumulation, despite increased uptake, such as fatty acid oxidation. AMPK $\alpha$  is a known lipid metabolism regulator and its activation, besides leading to inhibition of lipogenesis, also induces fatty acid uptake. Via AMPK $\alpha$ -catalyzed phosphorylation of ACC, malonyl-CoA availability is decreased, which relieves inhibition of the rate-limiting enzyme shuttling fatty acid into the mitochondria, CPT1 $\alpha$ . Therefore, more fatty acids can enter cells and be directed for  $\beta$ -oxidation as reviewed elsewhere [299]. Here we showed that liver *Cd36* expression was increased in IRW45 group, suggesting increased fatty acid uptake. Moreover, we previously found that in skeletal muscle of HFD-fed animals, IRW45 supplementation increased p-AMPK $\alpha$ , an effect not

seen in WAT [207]. In this study, hepatic p-AMPK $\alpha$  /AMPK $\alpha$  ratio did not change between IRW45 and HFD group, but it was increased compared to ROSI group. Interestingly, p-AMPK $\alpha$ / $\beta$ -actin ( $p < 0.05$ ) and AMPK $\alpha$ / $\beta$ -actin (not statistically significant) were more than 50% higher in the IRW45 group compared to HFD, suggesting a greater initial capacity for AMPK $\alpha$  activation (for example,  $V_{max}$ ), which in turn increases the capacity for activating AMPK $\alpha$ -related targets. In fact, in another study, compared to HFD alone, IRW45 increased hepatic silent mating-type information regulation 2 homolog 1 (SIRT1) protein abundance, a protein known to interact with AMPK $\alpha$  [193]. This effect was accompanied by increased NAMPT and forkhead box O3 (FOXO3) protein content in the liver and increased nicotinamide adenine dinucleotide (NAD<sup>+</sup>) concentration in the liver and in plasma [193], consistent with improved metabolic regulation and possibly enhanced mitochondrial oxidative phosphorylation in the IRW45-supplemented mice. This is supported by our findings that citrate synthase activity was increased in the IRW45 group, which may indicate enhanced hepatic oxidative metabolism. The role of NAMPT and SIRT1 in NAFLD is already shown, for example, SIRT1 is decreased in models of HFD-induced NAFLD [195], while overexpression of SIRT1 prevents hepatic TG accumulation and inflammation [194, 300]. On the other hand, pharmacological inhibition of NAMPT worsens hepatic TG accumulation via SIRT1/AMPK $\alpha$  in a HFD-induced hepatic steatosis model [301]. In addition, NAD<sup>+</sup> deficiency induces hepatic steatosis, inflammation, fibrosis and apoptosis in HFD-fed mice, therefore contributing to the progression to NASH [302]. All of this provide evidence that IRW45 may prevent HFD-induced hepatic steatosis by improving the function of the NAMPT/SIRT1/AMPK $\alpha$  pathway.

SIRT1 also interacts with AMPK $\alpha$  and induces PGC1 $\alpha$  activation, which is a key factor in mitochondrial biogenesis [303]. Mitochondrial dysfunction is implicated in NAFLD

development and progression [304]. Moreover, HFD decreases mitochondrial complexes (oxphos) and therefore, reduces capacity for fatty acid oxidation and increases lipid accumulation, processes involved in the progression of NAFLD [305, 306]. In addition, *Ppargc1a* overexpression *in vitro* and *in vivo* increases fatty acid oxidation, decreases hepatic TG accumulation and circulating TG concentration [307]. Our observation of decreased *Mttp* gene expression, together with a trend for increased hepatic *Ppargc1a* mRNA and increased content of mitochondrial complexes in the IRW45 compared to HFD, is consistent with the literature. This indicates increased mitochondrial content in the IRW45 group and a higher capacity for fatty acid oxidation leading to reduced hepatic lipid accumulation, as observed.

Mitochondrial dynamics is another factor under debate in relation to NAFLD [308]. Mitochondrial fission and fusion are essential mechanisms to prevent mitochondrial dysfunction and a balance between these processes maintains healthy mitochondrial function. The process of mitochondrial fusion is regulated mainly by mitofusin-1 and OPA1 and occurs when mitochondria function is impaired, acting as a protective mechanism to prevent further damage and maintain mitochondrial homeostasis [309]. Increased fusion leads to enlarged mitochondria, a characteristic seen in the liver of individuals with NAFLD [310, 311] and liver-specific deletion of OPA1 prevents methionine-choline-deficient diet-induced hepatic damage and mitochondrial enlargement [312]. Conversely, others found that HFD decreases mitofusin-1 [313]. Moreover, mitofusin-2 plays a key role in transferring lipid between the endoplasmic reticulum and mitochondria, and a role for decreased mitofusin-2 in NAFLD progression is suggested [314]. We found decreased *Mfn1* and a trend for decreased *Opal* gene expression in the liver of IRW45-treated animals compared to HFD, and no changes in terms of *mfn2* expression. These results are consistent with a compensatory effect occurring in the HFD group,

whereby mitochondrial fusion is used as a mechanism to stem the increased lipid influx into the liver and prevent further HFD-mediated mitochondrial damage. Conversely, IRW45 treatment enhanced mitochondria content and function, as indicated by higher oxphos enzymes and citrate synthase activity, which accommodated the extra lipid influx and relieved the stress imposed by the HFD, feeding back to lower expression of *Mfn1* and *Opal*. This is also consistent with the increased lipid accumulation in the ROSI group, which could reflect more lipid storage via PPAR $\gamma$  activation as a protective mechanism against fat deposition in skeletal muscle. Fat accumulation without induction of mitochondria activity would not result in mitochondrial damage but would increase hepatic lipid deposition, as observed. Moreover, *Vdac1* mRNA was upregulated in the HFD group. VDAC1 regulates many cellular processes including calcium transport, energy metabolism, apoptosis and inflammation (inducing cytokine release) [315]. Therefore, enhanced expression of *Vdac1* in the HFD group may indicate impaired mitochondrial homeostasis, including impaired mitophagy and inflammatory processes. However, future functional assays must be done to investigate mitochondrial membrane potential, permeability, biogenesis, morphological aspects and stability to fully elucidate the role of IRW in this context.

Interestingly, *Cidea* gene expression was drastically increased in the IRW45 and ROSI groups compared to HFD. Cell death-inducing DNA fragmentation factor- $\alpha$ -like effectors A (*Cidea*) is a lipid droplet-associated protein. Its expression is regulated by PGC1 $\alpha$  [316] and its hepatic expression is elevated during NAFLD [317]. PPAR $\alpha$  agonists increase *Cidea* expression in the liver [318, 319] and in WAT [320]. Moreover, PPAR $\gamma$ -dependent hepatic steatosis increases *Cidea* expression independently of PPAR $\alpha$ , whereas choline deficiency-induced steatosis (which is independent of PPAR $\gamma$  activation) does not [318]. This suggests that both PPAR $\alpha$  and PPAR $\gamma$

can directly enhance *Cidea* transcription and is consistent with the *Cidea* overexpression in the ROSI group because rosiglitazone is a potent PPAR $\gamma$  agonist. In the liver, *Pparg2* gene expression had a strong trend ( $p = 0.06$ ) to be lower in the IRW group compared to ROSI group, and our histological analysis is consistent with IRW45 not activating hepatic PPAR $\gamma$ . However, *Cidea* expression was more than 15-fold higher in the IRW45 group as well. Because PPAR $\alpha$  enhances *Cidea* transcription, it is possible that IRW45 is enhancing fatty acid oxidation via PPAR $\alpha$  activation. This would explain, in part, the differences between IRW45 and ROSI groups. However, *Ppara* expression did not change among the groups and PPAR transcriptional activation was not investigated in this study. Although *Cidea* and *Cidec/FSP27* are induced during liver steatosis, it was recently reported that *Cidea* expression is reduced during the progression from hepatic steatosis to NASH [317]. Thus, it raises the possibility of HFD animals being in a more advanced stage of progression to NASH compared to IRW45 and ROSI.

We cannot ignore the effect of IRW45 in decreasing BW gain, which may indirectly improve NAFLD. As mentioned before, lifestyle changes improve NAFLD mainly through decreased BW [27]. In this study, IRW45 decreased BW and fat mass (both by approximately 9%) of HFD-induced obese, glucose intolerant mice independently of changes in food intake, consistent with previous results using IRW45 [207]. Moreover, we consistently observed improvements in OGTT and fasting blood glucose concentration ([207] and this study), demonstrating that IRW45-supplemented animals exhibit a healthier metabolic phenotype compared to HFD animals. In contrast, although rosiglitazone improved OGTT and fasting glucose, it promoted no changes in BW in this study, which is partially consistent with the well-known side-effect of thiazolidinedione to induce weight gain in humans [321-323], and consistent with the controversial effect of rosiglitazone on BW in studies using rodent models [218, 324, 325].

Our findings are, in part, consistent with a recent study published by Liu et al. [180]. In their study, IRW supplementation for 3 weeks decreased blood glucose concentration, improved glucose tolerance and insulin resistance, without changes in plasma TG concentration [180]. Moreover, IRW decreased the expression of inflammatory genes in the liver, together with downregulation of *Dgat1* and *Dgat2* gene expression, supporting the reduced liver TG seen in our study. However, the decrease in liver TG in their study was not statistically significant. Despite no changes in BW, relative eWAT and iWAT mass was reduced by IRW. The authors attributed many of the effects of IRW to changes in the gut microbiota [180]. The differences seen between our studies may be due to the supplementation period, 8 weeks *versus* 3 weeks. Moreover, we used a dosage of approximately 45mg/Kg BW based on weekly food intake and BW, while they used a fixed dosage of 0.03 g/L of water. In addition, the authors did not specify the dosage based on BW and water intake nor provide the diet macronutrient content, making it difficult to compare the trials. Nevertheless, in both trials IRW reduces the metabolic complications of HFD, and together suggest that a longer period of supplementation may be required for IRW to promote significant changes in BW and liver TG accumulation.

This is the first study showing that IRW, a small peptide that improves skeletal muscle insulin signaling, is also protective against HFD-induced NAFLD. Although research is still needed to fully elucidate the complete mechanism of action of IRW in this respect, we present evidence that IRW supplementation improves NAFLD via both an enhancement in insulin signaling in skeletal muscle as previously reported [207], and a possible effect in the liver leading to increased capacity for fatty acid uptake and oxidation by preserving mitochondrial content and function. Together, these mechanisms would reduce the substrates for DNL and increase fatty acid oxidation to ameliorate HFD-induced NAFLD. It is worth mentioning that the effects

observed after IRW supplementation are, in part, similar to the effects observed with thyroid receptor  $\beta$ -agonists, which have been used in clinical trials to treat NAFLD and promote increased hepatic fatty acid uptake and oxidation, enhanced mitochondrial biogenesis and energy expenditure, and modulation of cholesterol and bile acid metabolism, as reviewed [31]. In addition, a recent study using another tripeptide named DT-109 (Gly-Gly-Leu) shows that daily gavage of DT-109 for 12 weeks (mice) and 5 months (nonhuman primates) improves NAFLD by inducing fatty acid oxidation, increasing antioxidant capacity through glutathione biosynthesis and modulating bile acid metabolism [326]. The most effective dosage of DT-109 was 450 mg/Kg/day in mice [326], which is 10-fold higher than the IRW dosage used in our study.

Our study has some limitations, for example the transcriptional activation of PPARs was not investigated and we did not directly measure fatty acid flux or oxidation. In addition, our dietary model, although efficient in promoting hepatic steatosis, is not an established model of NASH and the interpretation of the results should be taken with care if translated in the context of NASH.

In conclusion, while both IRW45 and rosiglitazone improved glucose tolerance and insulin resistance in previous studies [199, 207], our data indicate that IRW45 uniquely acts in the liver to protect against NAFLD by preserving mitochondrial content. This in turn enhances mitochondria oxidative capacity potentially leading to increased fatty acid oxidation, while decreasing lipogenesis and VLDL assembly, all of which prevent HFD-induced NAFLD (Fig. 5.11). On the other hand, the evidence for rosiglitazone is consistent with activation of hepatic PPAR $\gamma$ , which induces lipogenic pathways and lipid accumulation as a mechanism to protect against lipid-induced insulin resistance in skeletal muscle and improve systemic insulin

sensitivity. Therefore, while both IRW45 and ROSI improve whole body insulin sensitivity, IRW45 has a protective effect against hepatic steatosis while rosiglitazone worsens the HFD-induced lipid accumulation in the liver. The proposed mechanisms of the direct action of IRW in the liver to promote the observed effects are shown in Fig. 5.11.

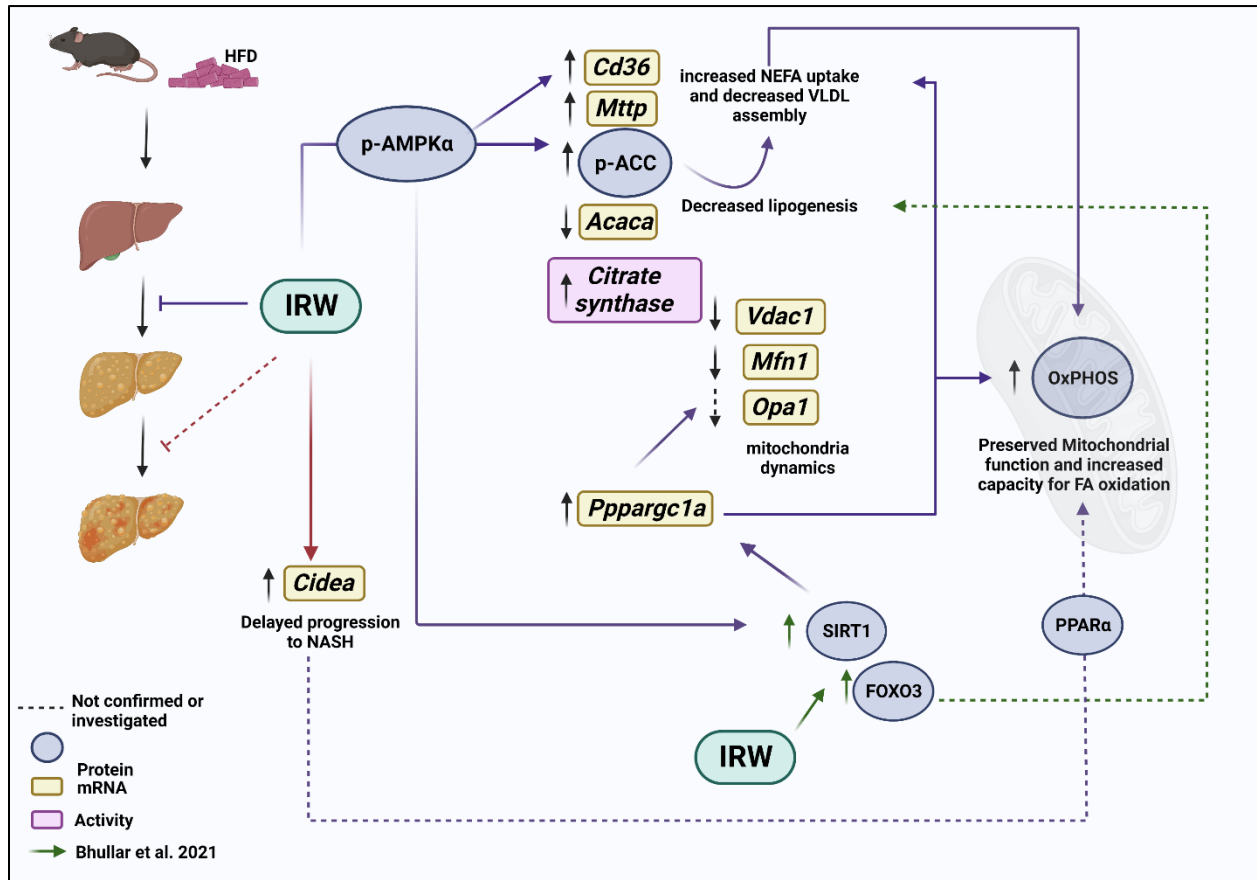


**Figure 5. 11. Proposed mechanisms for IRW direct effect in the liver of HFD-induced obese mice to prevent diet-induced NAFLD.** See text section 5.5 for details. Created with biorender.com.

**Institutional Review Board Statement:** The animal study protocol was approved by the Animal Care and Use Committee of the University of Alberta (Protocol# 1472) in accordance with guidelines issued by the Canadian Council on Animal Care.

**Acknowledgments:** We sincerely thank Dr. Robin Clugston for providing the expertise and equipment necessary to conduct this study.

**Conflicts of Interest:** The authors declare no conflict of interest.

## 6. CHAPTER 6: General discussion and conclusion

In this thesis I provide evidence that two egg-derived bioactive peptides, IRW and Peptide 2 improve metabolic dysfunction in HFD-induced obese, glucose intolerant mice. Several pathways and tissues involved in the complex pathophysiology of insulin resistance and NAFLD were identified. The data generated in this thesis expands our knowledge of the beneficial effects of egg-derived bioactive peptide supplementation in metabolic conditions and supports further investigations to clarify their mechanisms of action and guide future clinical trials.

The RAS was not the focus of this thesis, but it may be related to the mechanisms of action of the peptides as discussed further below. In addition to the RAS being the major system regulating the water-salt balance in the body [33, 327], it is also related to insulin resistance [328]. Briefly, the system is initiated by renin, which converts angiotensinogen into angiotensin I. The activity of ACE converts angiotensin I into angiotensin II. Angiotensin II promotes its activity through AT1R and AT2R. These receptors have opposing effects with AT1R causing vasoconstriction and increasing blood pressure [327, 329] and AT2R decreasing fibrosis, inflammation and causing vasodilation [329, 330]. Angiotensin II can be further converted into angiotensin 1-7 by ACE2. In addition, angiotensin I can be converted in angiotensin 1-9 by ACE2. Angiotensin 1-7 acts via MasR and ACE2/angiotensin 1-7/MasR is considered the protective arm of the RAS pathway (Fig. 6.1) [331]. Angiotensin II has other functions to regulate blood pressure, such as to stimulate aldosterone and vasopressin release [33]. Despite its main function to regulate blood pressure, RAS is also linked to insulin resistance. For example, exposure of tissues to elevated concentrations of angiotensin II induces insulin resistance [332]. AT1R receptor blockers, such as losartan, improve insulin resistance and prevent NAFLD [333, 334] and ACE inhibitors improve insulin resistance [335, 336], while AT2R activation increases

adipogenesis and improves insulin resistance [337]. The beneficial effect of RAS blockade in improving insulin resistance is also seen in humans [328].

In chapter 3, I presented the first study *in vivo* using Peptide 2. In that study we show that diet supplementation with Peptide 2 improves systemic insulin resistance in obese glucose intolerant mice. This is accompanied by enhanced insulin signaling and restored hormonal regulation of lipolysis in WAT, decreased hepatic LD size, cholesterol content and inflammatory infiltrate. As previously discussed, impaired lipolysis is intrinsically related to insulin resistance and NAFLD [20, 149]. We initially thought that Peptide 2 would exert its effects similarly to rosiglitazone, via PPAR $\gamma$  activation in WAT. However, although our initial hypothesis was supported by evidence *in vitro* [198], beneficial effects of Peptide 2 *in vivo* were observed without changes in BW, PPAR $\gamma$  activation or adipogenesis markers in WAT, suggesting another mechanism of action. We demonstrated that AT2R protein abundance is enhanced in the liver of the Peptide 2-supplemented animals and, given the beneficial effects of AT2R activation in fibrosis and insulin resistance [225, 228], we speculate that Peptide 2 may be exerting its effects through AT2R activation in the liver, differently from rosiglitazone (chapter 3). However, despite a beneficial systemic and local effects in metabolic dysfunction, the full mechanism of action of Peptide 2 remains to be elucidated (Fig. 6.1).

A larger body of research has accumulated with IRW and several beneficial effects of IRW *in vitro* and in spontaneous hypertensive rats are known (section 1.8) [338]. However, the studies presented here are the first to describe the effect of IRW supplementation *in vivo* to modulate glucose homeostasis by improving insulin signaling and insulin-independent glucose uptake in skeletal muscle (chapter 4) and to show a protective effect of IRW against HFD-induced NAFLD (chapter 5).

In these studies, we provide evidence that IRW supplementation reduces blood fasting glucose concentration and improves glucose tolerance. In skeletal muscle (chapter 4), IRW supplementation ameliorates insulin resistance by improving insulin signaling and increasing p-AMPK $\alpha$ , resulting in increased GLUT4 abundance in the plasma membrane, suggesting enhanced insulin-dependent and -independent glucose uptake. This alone could be sufficient to correct HFD-induced hyperglycemia in this model, as observed. We did not investigate oxidative pathways in skeletal muscle, but enhanced p-AMPK $\alpha$  together with enhanced PPAR $\gamma$  could also be activating fatty acid uptake, lipogenesis and oxidation in skeletal muscle, which would reduce fat mass, improve insulin sensitivity (chapter 4) and decrease hepatic lipid accumulation (chapter 5). However, this line of inquiry remains to be investigated (Fig. 6.1).

Interestingly, we also show increase mRNA expression of genes related to cell growth and muscle synthesis, which is consistent with preserved lean mass in IRW-supplemented animals. However, no changes in the classical muscle synthesis pathways mediated by mTOR are seen, suggesting that other mechanisms might be in place to preserve lean mass in these mice. It is worth noting that all these effects in skeletal muscle occurred independently of local RAS inhibition. Nevertheless, increase in AT2R abundance in muscle and plasma ACE2 activity led us to hypothesise that IRW may be acting through AT2R in skeletal muscle to induce beneficial effects (chapter 4). IRW activation of AT2R still requires further investigation.

In chapter 5, we show evidence that IRW prevents HFD-induced NAFLD. The prevention of NAFLD may be due to improved p-AMPK $\alpha$  signaling and enhanced fatty acid oxidation, while at the same time preserving mitochondria dynamics and content, or enhanced biogenesis (which remains to be investigated). In general, IRW decreases hepatic TG content, increases mRNA of markers for fatty acid uptake in the liver, enhances capacity for fatty acid oxidation by

increasing oxphos content, increases citrate synthase activity and decreases mRNA of a gene involved in VLDL secretion. Therefore, we conclude that IRW is improving insulin resistance and preventing NAFLD by increasing the capacity to oxidize fatty acids (possibly in both the liver and skeletal muscle), thereby preventing lipotoxicity and decreasing hyperlipidemia (not investigated). IRW effects on WAT, in terms of adipogenesis were minimal, and the evidence does not support that IRW is directly affecting WAT expansion, rather, the effects seen in WAT, such as increased adiponectin, may be an indirect consequence of overall improved metabolic function.

The exact mechanisms by which IRW prevents NAFLD are still not clarified. We have evidence from these and other studies that IRW improves signaling through the p-AMPK $\alpha$ /SIRT1/PGC1 $\alpha$  pathway in the liver (this thesis and reference [193]), however, we do not know how IRW is acting upstream of these pathways or if indirectly affecting them. Nonetheless, we have some speculations about possible upstream pathways leading to the beneficial effects of IRW. For example, IRW is known to increase ACE2 activity. IRW increases ACE2 mRNA expression and decreases AT1R mRNA expression in the aorta of HFD-fed mice. Moreover, IRW increases p-AMPK $\alpha$  and SIRT1 protein abundance in the aorta [339]. Although ACE2 protein abundance is not enhanced in skeletal muscle, plasma ACE2 activity is increased (chapter 5). In addition, IRW increases the plasma concentration of angiotensin 1-7 and MasR protein abundance in the aorta of spontaneous hypertensive rats [250]. In this thesis, the RAS components were not investigated in the liver of HFD-fed mice, however, it is possible that IRW may be acting through MasR activation to improve NAFLD. In fact, MasR activation was attributed to a beneficial effect of liraglutide in NAFLD. Liraglutide activates the ACE2/Angiotensin 1-7/MasR via PI3K/AKT pathway leading to NAFLD improvement [340]. In

addition, MasR activation stimulates lipophagy and fatty acid oxidation [341] and angiotensin 1-7 improves NAFLD via MasR by upregulating mitochondrial function, while MasR deletion increases TG accumulation, gluconeogenesis markers and reduced oxphos abundance in the liver of mice. On the other hand, MasR overexpression and treatment with angiotensin 1-7 in hepatocytes decreases lipid accumulation, increases p-AKT and p-AMPK protein abundance [342]. The relationship between RAS and AMPK is already reported in the literature, with AMPK activation balancing the RAS towards a beneficial arm via ACE2/angiotensin 1-7/MasR pathway, as reviewed [343]. All of this supports a proposed mechanism of action of IRW in the liver to improve HFD-induced NAFLD via MasR (Fig 6.1). Measurement of MasR and RAS components mRNA expression in the liver of IRW-supplemented animals is already under investigation by our group.

Another mechanism by which IRW could be reducing hepatic lipid accumulation could be mediated by glucagon. Arginine (R) is a potent glucagon secretagogue [344] and a constituent amino acid of IRW. In individuals with NAFLD, glucagon inhibition of VLDL secretion is impaired [345]. Moreover, glucagon is involved in AMPK $\alpha$  signaling and fatty acid oxidation [346]. The importance of arginine in the IRW activity is shown *in vitro*, where IRW, IRA and IR prevent insulin resistance in L6 cells, but not arginine alone, IAW or ARW. In fact, it suggests that IR may be the biologically active sequence of the peptide [347]. Therefore, it is plausible that IRW may be promoting improvements in the liver indirectly, by stimulating glucagon secretion (Fig. 6.1).

An interesting finding in these studies is that Peptide 2 and IRW both improve insulin sensitivity similarly to rosiglitazone. However, rosiglitazone treatment together with HFD feeding worsens diet-induced NAFLD in both studies, while the peptides protect against

NAFLD. This suggests that the mechanism of action of the peptides differ from that of rosiglitazone. For example, rosiglitazone acts via PPAR $\gamma$  activation in WAT, preventing ectopic lipid accumulation (except during HFD feeding in rodents [217]), adipokine secretion and improving systemic insulin resistance [348]. On the other hand, Peptide 2 and IRW are not exerting their effects by activating PPAR $\gamma$  in WAT. For instance, Peptide 2 improves WAT insulin signaling and response to insulin without changing PPAR $\gamma$  activation. In the liver Peptide 2 reduces lipid accumulation, an effect that may be a consequence of improved WAT insulin response but also an action via AT2R, which is increased in the liver of supplemented animals. On the other hand, IRW seems to have little effect on WAT but influences the physiology of the skeletal muscle and liver. In the skeletal muscle, AT2R and PPAR $\gamma$  abundance is increased, which could contribute to the insulin-sensitizing effects of IRW, but also through an effect via AMPK $\alpha$ . In the liver, IRW may be acting via AT2R or via MasR to activate AMPK $\alpha$ /SIRT1/PGC1 $\alpha$  to increase capacity for fatty acid oxidation and mitochondrial biogenesis.

The difference between IRW vs Peptide 2 in WAT insulin sensitization could be related to the amino acid sequence and length of the peptides because these properties influence bioactivity and bioavailability [349]. For example, ACE inhibitory peptides are usually short and the presence of certain amino acids, including tryptophan, isoleucine and arginine increases the chance of them binding to ACE [350]. Moreover, our group showed before that IRW amino acid sequence IR may be essential for its biological activity related to insulin-stimulated glucose uptake (further discussed in chapter 7). Therefore, the differences in amino acid sequence and length between Peptide 2 and IRW may contribute to their different effects in WAT. This is an important finding because of the preponderance of research investigating ACE-related

bioactivity of peptides and justifies new lines of investigation of ACE-independent bioactivities. There is a chance that peptides are improving vascular function via RAS to improve insulin signaling. Many factors related to vascular function associate with insulin action as reviewed elsewhere, suggesting that vascular dysfunction can be both a inducer and a consequence of insulin resistance [351]. For example, the ability of insulin to cross the endothelial barrier affects its action in peripheral tissues as shown by delayed action of insulin to stimulate glucose uptake in obesity and type 2 diabetes [352, 353]. On the other hand, hyperinsulinemia impairs vasodilation [354]. The link between vascular function and insulin resistance appears to be partially related to changes in nitric oxide action [351].

In conclusion, this work provides evidence that dietary supplementation with egg-derived peptides improves diet-induced insulin resistance and NAFLD in a rodent model of obesity and glucose intolerance. Further studies are needed to completely understand how the peptides are exerting these beneficial effects, nonetheless, improved metabolic dysfunction is observed with both peptides.

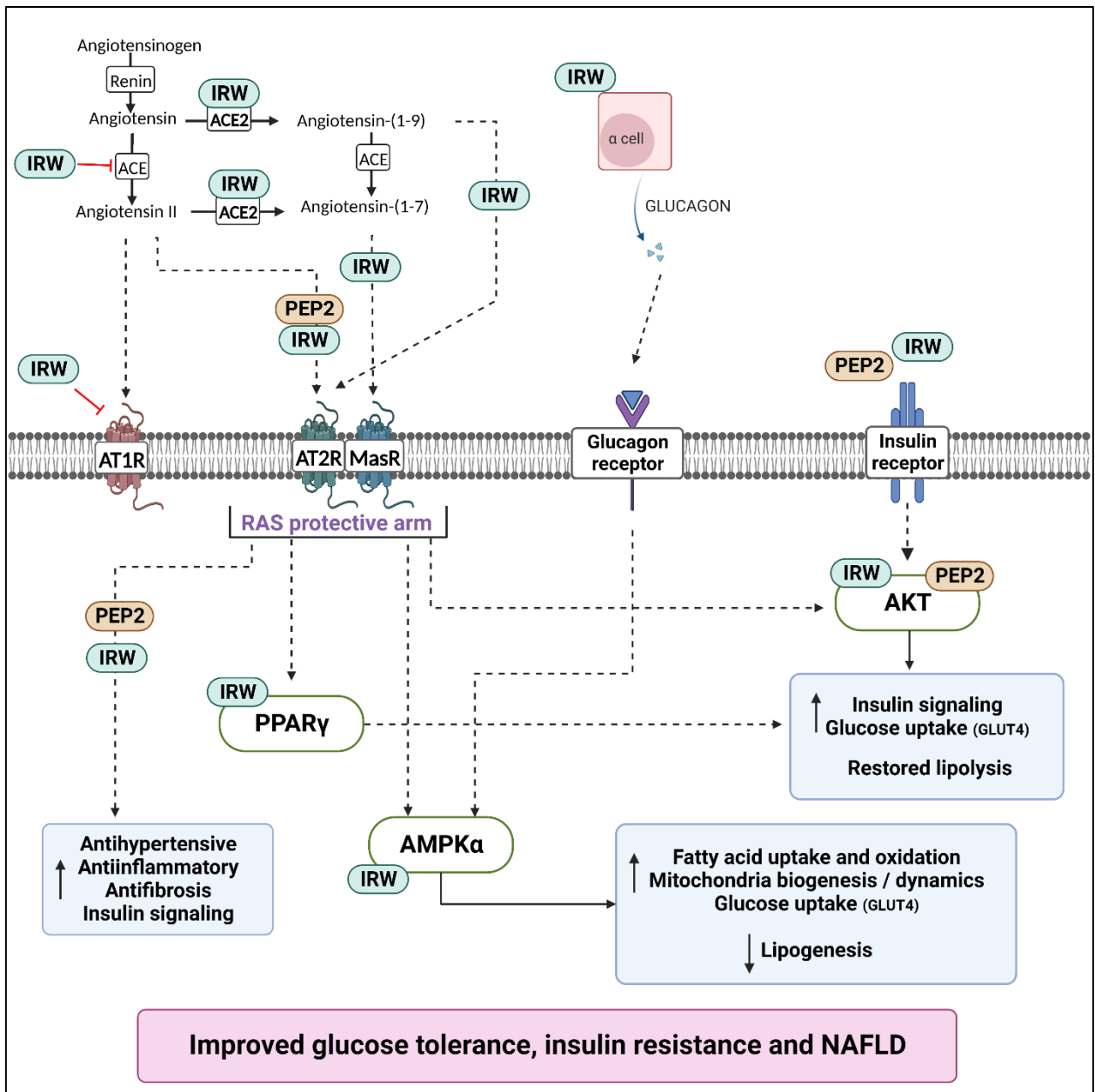


**Figure 6. 1. Proposed mechanism of action for Peptide 2 (PEP2) and IRW.** See text for more details. ACE, angiotensin converting enzyme; ACE2, angiotensin converting enzyme 2; AT1R, angiotensin II type 1 receptor; AT2R, angiotensin II type 2 receptor; MasR, Mas receptor/angiotensin 1-7 receptor; RAS, renin angiotensin system; AKT, protein kinase B; AMPK $\alpha$ , 5' AMP-activated protein kinase; NAFLD, non-alcoholic fatty liver disease.

## 7. CHAPTER 7: Future perspectives

Although the experiments performed in this thesis answer many questions about how Peptide 2 and IRW improve insulin resistance and NAFLD, the underlying mechanisms of action by which they act remain only partially elucidated. The following paragraphs, in no particular order, highlight some of the future investigations proposed to clarify their mechanism of action related to insulin resistance and NAFLD (Fig. 71).

First, it is important to study the bioavailability of the peptides to investigate if they are absorbed intact and if they are reaching the target tissues via the bloodstream. So far, based on in vitro studies, we know that IRW transits Caco-2 cells intact (paracellularly and via peptide transporter 1) and that IRW is also digested into dipeptides [185, 355]; however, no in vivo studies have yet been conducted to assess plasma concentration of these peptides. No bioavailability studies, in vivo or in vitro using Peptide 2 have been performed yet.

As discussed in chapter 6 (Fig. 6.1), we believe that the peptides may be acting through multiple receptors to exert beneficial effects. One priority is to investigate MasR and RAS components (AT2R) expression and activity in the liver of peptide-supplemented animals. Preliminary data shows that AT2R protein abundance is increased in the liver of IRW45 supplemented animals (Fig. 7.1 D). Establishing the dependence of the peptides on these receptors could be accomplished in vitro by knocking out MasR or AT2R in HepG2 or L6 cells and measuring changes in key proteins involved in fatty acid oxidation and insulin signaling. Moreover, it could be assessed dynamically, by stimulating lipid accumulation and glucose uptake in those cells in the presence or absence of the peptide. The use of receptor antagonists, for example AT2R antagonists (PD123319 or EMA401) [356, 357] or MasR antagonists (A779) [358] could also be used in vitro and in vivo together with peptide administration to answer

questions regarding the dependence of the peptides on those receptors' activation. AT2R [359] and MasR [360] knockout mice are viable and could also be used to elucidate this question in vivo. Using a liver -or skeletal muscle-specific knockout of these receptors would give more accurate insight about tissue-specific actions of the peptides, rather than a global knockout model. Moreover, given the fact that IRW modulates ACE2 activity in SHR rats [250] , it is possible that the beneficial effects on insulin signaling might be a consequence of vascular function. Therefore, investigating markers of vascular function in plasma, e.g., vascular cell adhesion protein 1 (VCAM1), intercellular adhesion molecule 1 (ICAM1) or nitric oxide or using doppler ultrasound in vivo to blood flow could be employed. In terms of the discussed potential effect of IRW on glucagon secretion, it could be evaluated in vitro using islets and measuring glucagon in the media, but also in vivo by measuring plasma concentration of glucagon after acute IRW feeding and during fasting, since chronic administration of the peptide could be inducing long-term changes (gene transcription) and modulating fasting responses.

I propose that it is important to differentiate the effects observed with peptide supplementation from a protein (amino acid) effect *in vivo*. On that note, IRW and its derivatives IRA and IR prevent TNF $\alpha$ -induced insulin resistance in L6 cells, an effect that is not seen with individual amino acids that are part of the peptide, nor with other derivatives of IRW [347]. The peptides prevents the TNF $\alpha$ -induced increase in p-IRS (Ser) and decrease in p-IRS (Tyr) and p-AKT phosphorylation [347]. Moreover, IQW, another egg-derived peptide does not improve angiotensin II-induced insulin resistance in vitro, while IRW does [191]. This suggests that the sequence IR may be responsible for the biological activity of the peptide [347] and highlights the importance of amino acid sequence in the peptide's bioactivity. In vivo, IRW and both derivatives (IRA and IR) improve glucose tolerance and insulin signaling in skeletal muscle,

while only IRW and IRA enhance p-AMPK $\alpha$  and AT2R protein abundance in muscle [361]. No parallel studies comparing Peptide 2 were performed (and would be more complicated because of its 11-amino acid structure). Thus, previous work with IRW suggests that the metabolic improvement observed is not an amino acid effect [361]. I propose comparing the in vivo dietary effect of the peptides with their derivatives and single amino acids and investigating the postprandial blood concentration of the amino acids and their effect in the liver. This would strengthen the findings presented in this thesis.

Although not statistically significant, Peptide 2 decreased plasma TG during fasting and other food bioactive peptides decrease fat absorption. For example, EWH supplementation reduces ectopic lipid accumulation in association with increased lipid content in the feces of rats compared to casein [182, 183]. Similarly, soy hydrolysate [362] and both soy and potato peptides [363] increase fecal lipid content in rodents compared to casein. It would be interesting to measure plasma lipid profile combined with measurements of fecal lipid content to provide a complete overview of the peptide's effects on lipid absorption and plasma lipid concentration to support the results presented here. In addition, measuring fatty acid flux using labeled palmitate, for example, or investigating fatty acid oxidation by measuring mitochondria oxygen consumption using oxygraphy would strength the findings of this project related to lipid metabolism.

Based on preliminary results, we saw enhanced glucose-regulated protein 94 (GRP94) protein abundance in the liver but not WAT of IRW-supplemented animals (Fig. 7.1 A-C). GRP94 is a ER chaperone that prevents the accumulation of misfolded proteins, thereby preventing an exacerbated unfolded protein response and regulating cell homeostasis [364]. GRP94 is decreased in NASH compared to controls [365] and ER stress is involved in the multi-hit

hypothesis for NAFLD pathogenesis (section 1.7). Therefore, it would be interesting to study ER chaperones and ER stress in the liver of IRW-supplemented animals to test the hypothesis that IRW prevents ER stress by upregulating destruction of misfolded proteins. Conversely, it is possible that this is an indication of increased ER stress. An initial assessment of ER chaperone protein abundance in the liver of IRW-supplemented animals is already underway in our laboratory.

Lastly, moving forward towards future clinical application of the peptides in metabolic disease management, evaluation of their effect in humans is essential. Many food-derived bioactive peptides have been used in clinical trials [366] and based on our group's cell and rodent studies (section 1.8, chapter 3, 4 and 5), we anticipate that the peptides can be safely ingested. However, as reviewed by our group, many challenges exist regarding the translation of food-derived bioactive peptides from basic science to clinical trials, such as country-specific regulations, low bioavailability, lack of randomized clinical trials, high cost of bioactive peptide production and palatability [366]. Therefore, the first step in this journey, following establishment of their safety, would be to design a randomized clinical trial to investigate the effect of these peptides in humans while continuing to elucidate their mechanism of action. This would validate their role in metabolic disease management and increase their chances of being implemented in the functional food / natural health product market (Fig. 7.2).

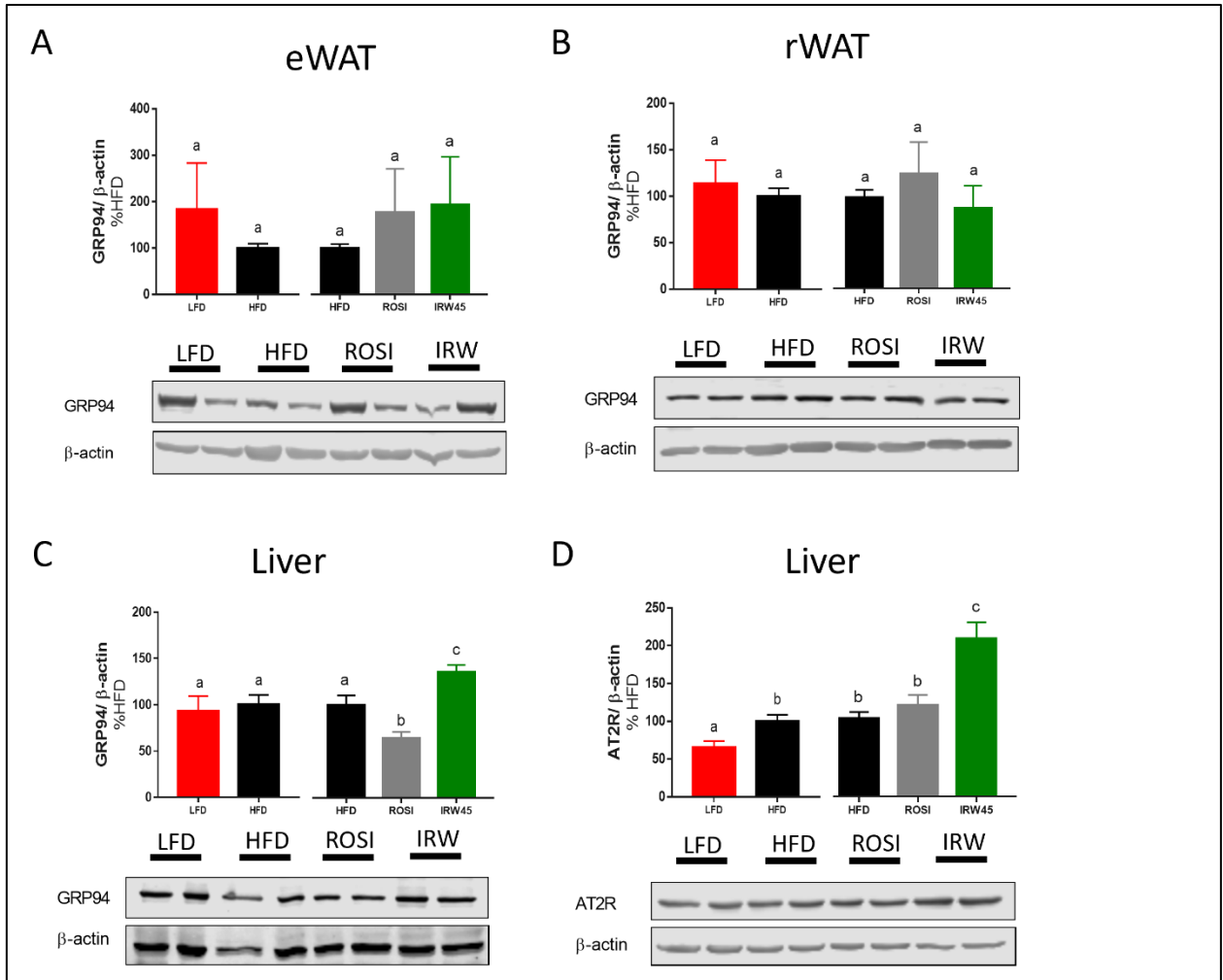


**Figure 7. 1. GRP94 and AT2R protein abundance in C57BL/6 mice.** (A) eWAT GRP94 protein abundance; (B) rWAT GRP94 protein abundance, (C) liver GRP94 protein abundance and (D) AT2R protein abundance. Total proteins were normalized to  $\beta$ -actin. Data expressed as mean + SEM of  $n = 4$  (non-injected mice for A and B) and  $n = 8$  (C). Data analyzed by two-tailed t-test (LFD vs HFD) or one-way ANOVA (HFD groups). Different letters indicate  $p < 0.05$ .

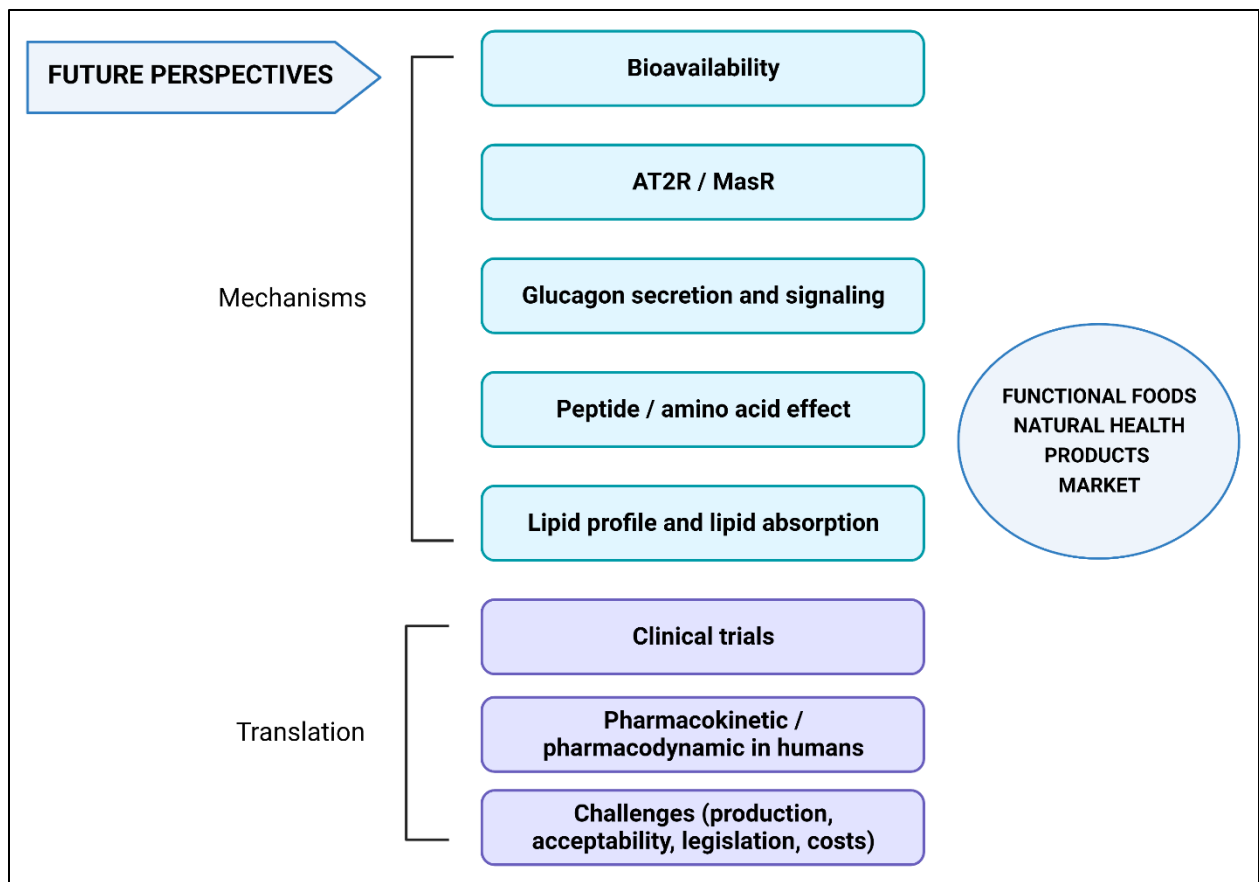


**Figure 7. 2. Future perspectives for the study of Peptide 2 and IRW.** See text for details. AT2R, angiotensin II type 2 receptor; MasR, Mas receptor/angiotensin 1-7 receptor.

## 8. REFERENCES

1. Alberti, K.G., P. Zimmet, and J. Shaw, Metabolic syndrome--a new world-wide definition. A Consensus Statement from the International Diabetes Federation. *Diabet Med*, 2006; 23: p. 469-480 DOI: 10.1111/j.1464-5491.2006.01858.x.
2. Saklayen, M.G., The Global Epidemic of the Metabolic Syndrome. *Curr Hypertens Rep*, 2018; 20: p. 12 DOI: 10.1007/s11906-018-0812-z.
3. Rao, D.P., S. Dai, C. Lagace, et al., Metabolic syndrome and chronic disease. *Chronic Dis Inj Can*, 2014; 34: p. 36-45.
4. International Diabetes Federation, *IDF Diabetes Atlas 10th ed.* 2021: Brussels, Belgium.
5. Diabetes in Canada: Backgrounder. Diabetes Canada 2022; Available from: <https://www.diabetes.ca/advocacy---policies/advocacy-reports/national-and-provincial-backgrounders/diabetes-in-canada>.
6. Punthakee, Z., R. Goldenberg, and P. Katz, Definition, Classification and Diagnosis of Diabetes, Prediabetes and Metabolic Syndrome. *Can J Diabetes*, 2018; 42 Suppl 1: p. S10-S15 DOI: 10.1016/j.jcjd.2017.10.003.
7. Sievenpiper, J.L., C.B. Chan, P.D. Dworatzek, et al., Nutrition Therapy. *Can J Diabetes*, 2018; 42 Suppl 1: p. S64-S79 DOI: 10.1016/j.jcjd.2017.10.009.
8. Sigal, R.J., M.J. Armstrong, S.L. Bacon, et al., Physical Activity and Diabetes. *Can J Diabetes*, 2018; 42 Suppl 1: p. S54-S63 DOI: 10.1016/j.jcjd.2017.10.008.
9. Lipscombe, L., G. Booth, S. Butalia, et al., Pharmacologic Glycemic Management of Type 2 Diabetes in Adults. *Can J Diabetes*, 2018; 42 Suppl 1: p. S88-S103 DOI: 10.1016/j.jcjd.2017.10.034.
10. Lipscombe, L., S. Butalia, K. Dasgupta, et al., Pharmacologic Glycemic Management of Type 2 Diabetes in Adults: 2020 Update. *Can J Diabetes*, 2020; 44: p. 575-591 DOI: 10.1016/j.jcjd.2020.08.001.
11. Look, A.R.G. and R.R. Wing, Long-term effects of a lifestyle intervention on weight and cardiovascular risk factors in individuals with type 2 diabetes mellitus: four-year results of the Look AHEAD trial. *Arch Intern Med*, 2010; 170: p. 1566-1575 DOI: 10.1001/archinternmed.2010.334.
12. Jonas, D.E., K. Crotty, J.D.Y. Yun, et al., Screening for Prediabetes and Type 2 Diabetes: Updated Evidence Report and Systematic Review for the US Preventive Services Task Force. *JAMA*, 2021; 326: p. 744-760 DOI: 10.1001/jama.2021.10403.
13. Sagastume, D., I. Siero, E. Mertens, et al., The effectiveness of lifestyle interventions on type 2 diabetes and gestational diabetes incidence and cardiometabolic outcomes: A systematic review and meta-analysis of evidence from low- and middle-income countries. *EClinicalMedicine*, 2022; 53: p. 101650 DOI: 10.1016/j.eclinm.2022.101650.
14. Glechner, A., L. Keuchel, L. Affengruber, et al., Effects of lifestyle changes on adults with prediabetes: A systematic review and meta-analysis. *Prim Care Diabetes*, 2018; 12: p. 393-408 DOI: 10.1016/j.pcd.2018.07.003.
15. Katsaridis, S., M.G. Grammatikopoulou, K. Gkiouras, et al., Low Reported Adherence to the 2019 American Diabetes Association Nutrition Recommendations among Patients with Type 2 Diabetes Mellitus, Indicating the Need for Improved Nutrition Education and Diet Care. *Nutrients*, 2020; 12 DOI: 10.3390/nu12113516.

16. MacDonald, C.S., M. Ried-Larsen, J. Soleimani, et al., A systematic review of adherence to physical activity interventions in individuals with type 2 diabetes. *Diabetes Metab Res Rev*, 2021: p. e3444 DOI: 10.1002/dmrr.3444.
17. Azharuddin, M., M. Adil, M. Sharma, et al., A systematic review and meta-analysis of non-adherence to anti-diabetic medication: Evidence from low- and middle-income countries. *Int J Clin Pract*, 2021: p. e14717 DOI: 10.1111/ijcp.14717.
18. Polonsky, W.H. and R.R. Henry, Poor medication adherence in type 2 diabetes: recognizing the scope of the problem and its key contributors. *Patient Prefer Adherence*, 2016: 10: p. 1299-1307 DOI: 10.2147/PPA.S106821.
19. Phung, O.J., J.M. Scholle, M. Talwar, et al., Effect of noninsulin antidiabetic drugs added to metformin therapy on glycemic control, weight gain, and hypoglycemia in type 2 diabetes. *JAMA*, 2010: 303: p. 1410-1418 DOI: 10.1001/jama.2010.405.
20. Godoy-Matos, A.F., W.S. Silva Junior, and C.M. Valerio, NAFLD as a continuum: from obesity to metabolic syndrome and diabetes. *Diabetol Metab Syndr*, 2020: 12: p. 60 DOI: 10.1186/s13098-020-00570-y.
21. Marchesini, G., M. Brizi, G. Bianchi, et al., Nonalcoholic fatty liver disease: a feature of the metabolic syndrome. *Diabetes*, 2001: 50: p. 1844-1850 DOI: 10.2337/diabetes.50.8.1844.
22. Younossi, Z.M., A.B. Koenig, D. Abdelatif, et al., Global epidemiology of nonalcoholic fatty liver disease-Meta-analytic assessment of prevalence, incidence, and outcomes. *Hepatology*, 2016: 64: p. 73-84 DOI: 10.1002/hep.28431.
23. Eslam, M., P.N. Newsome, S.K. Sarin, et al., A new definition for metabolic dysfunction-associated fatty liver disease: An international expert consensus statement. *J Hepatol*, 2020: 73: p. 202-209 DOI: 10.1016/j.jhep.2020.03.039.
24. Chalasani, N., Z. Younossi, J.E. Lavine, et al., The diagnosis and management of nonalcoholic fatty liver disease: Practice guidance from the American Association for the Study of Liver Diseases. *Hepatology*, 2018: 67: p. 328-357 DOI: 10.1002/hep.29367.
25. Riazi, K., H. Azhari, J.H. Charette, et al., The prevalence and incidence of NAFLD worldwide: a systematic review and meta-analysis. *Lancet Gastroenterol Hepatol*, 2022: 7: p. 851-861 DOI: 10.1016/S2468-1253(22)00165-0.
26. Swain, M.G., A. Ramji, K. Patel, et al., Burden of nonalcoholic fatty liver disease in Canada, 2019-2030: a modelling study. *CMAJ Open*, 2020: 8: p. E429-E436 DOI: 10.9778/cmajo.20190212.
27. Sebastiani, G., K. Patel, V. Ratziu, et al., Current considerations for clinical management and care of non-alcoholic fatty liver disease: Insights from the 1st International Workshop of the Canadian NASH Network (CanNASH). *Can Liver J*, 2022: 5: p. 61-90 DOI: 10.3138/canlivj-2021-0030.
28. Koutoukidis, D.A., N.M. Astbury, K.E. Tudor, et al., Association of Weight Loss Interventions With Changes in Biomarkers of Nonalcoholic Fatty Liver Disease: A Systematic Review and Meta-analysis. *JAMA Intern Med*, 2019: 179: p. 1262-1271 DOI: 10.1001/jamainternmed.2019.2248.
29. Sookoian, S. and C.J. Pirola, Repurposing drugs to target nonalcoholic steatohepatitis. *World J Gastroenterol*, 2019: 25: p. 1783-1796 DOI: 10.3748/wjg.v25.i15.1783.
30. Zhao, Y., W. Zhao, H. Wang, et al., Pioglitazone on nonalcoholic steatohepatitis: A systematic review and meta-analysis of 15 RCTs. *Medicine (Baltimore)*, 2022: 101: p. e31508 DOI: 10.1097/MD.00000000000031508.

31. Prikhodko, V.A., N.N. Bezborodkina, and S.V. Okovityi, Pharmacotherapy for Non-Alcoholic Fatty Liver Disease: Emerging Targets and Drug Candidates. *Biomedicines*, 2022: 10 DOI: 10.3390/biomedicines10020274.
32. Shao, Y., S. Chen, L. Han, et al., Pharmacotherapies of NAFLD: updated opportunities based on metabolic intervention. *Nutr Metab (Lond)*, 2023: 20: p. 30 DOI: 10.1186/s12986-023-00748-x.
33. Silverthorn, D.U., *Human physiology: an integrated approach*. 6th ed. 2013: Pearson.
34. Fu, Z., E.R. Gilbert, and D. Liu, Regulation of insulin synthesis and secretion and pancreatic Beta-cell dysfunction in diabetes. *Curr Diabetes Rev*, 2013: 9: p. 25-53.
35. Smith, U., S. Attvall, J. Eriksson, et al., The insulin-antagonistic effect of the counterregulatory hormones--clinical and mechanistic aspects. *Adv Exp Med Biol*, 1993: 334: p. 169-180.
36. Shulman, G.I., D.L. Rothman, T. Jue, et al., Quantitation of muscle glycogen synthesis in normal subjects and subjects with non-insulin-dependent diabetes by <sup>13</sup>C nuclear magnetic resonance spectroscopy. *N Engl J Med*, 1990: 322: p. 223-228 DOI: 10.1056/NEJM199001253220403.
37. White, M.F., The insulin signalling system and the IRS proteins. *Diabetologia*, 1997: 40 Suppl 2: p. S2-17.
38. Zhou, X., P. Shentu, and Y. Xu, Spatiotemporal regulators for insulin-stimulated GLUT4 vesicle exocytosis. *J Diabetes Res*, 2017: 2017: p. 1683678 DOI: 10.1155/2017/1683678.
39. Patil, N., O. Howe, P. Cahill, et al., Monitoring and modelling the dynamics of the cellular glycolysis pathway: A review and future perspectives. *Mol Metab*, 2022: 66: p. 101635 DOI: 10.1016/j.molmet.2022.101635.
40. Dashty, M., A quick look at biochemistry: carbohydrate metabolism. *Clin Biochem*, 2013: 46: p. 1339-1352 DOI: 10.1016/j.clinbiochem.2013.04.027.
41. Kennedy, J.W., M.F. Hirshman, E.V. Gervino, et al., Acute exercise induces GLUT4 translocation in skeletal muscle of normal human subjects and subjects with type 2 diabetes. *Diabetes*, 1999: 48: p. 1192-1197 DOI: 10.2337/diabetes.48.5.1192.
42. Musi, N. and L.J. Goodyear, AMP-activated protein kinase and muscle glucose uptake. *Acta Physiologica Scandinavica*, 2003: 178: p. 337-345 DOI: 10.1046/j.1365-201X.2003.01168.x.
43. Guo, X., H. Li, H. Xu, et al., Glycolysis in the control of blood glucose homeostasis. *Acta Pharmaceutica Sinica B*, 2012: 2: p. 358-367 DOI: 10.1016/j.apsb.2012.06.002.
44. Ameer, F., L. Scanduzzi, S. Hasnain, et al., De novo lipogenesis in health and disease. *Metabolism*, 2014: 63: p. 895-902 DOI: 10.1016/j.metabol.2014.04.003.
45. Herman, M.A., O.D. Peroni, J. Villoria, et al., A novel ChREBP isoform in adipose tissue regulates systemic glucose metabolism. *Nature*, 2012: 484: p. 333-338 DOI: 10.1038/nature10986.
46. Assimacopoulos-Jeannet, F., S. Brichard, F. Rencurel, et al., In vivo effects of hyperinsulinemia on lipogenic enzymes and glucose transporter expression in rat liver and adipose tissues. *Metabolism*, 1995: 44: p. 228-233 DOI: 10.1016/0026-0495(95)90270-8.
47. Leturque, A., E. Brot-Laroche, and M. Le Gall, GLUT2 mutations, translocation, and receptor function in diet sugar managing. *Am J Physiol Endocrinol Metab*, 2009: 296: p. E985-992 DOI: 10.1152/ajpendo.00004.2009.

48. Karim, S., D.H. Adams, and P.F. Lalor, Hepatic expression and cellular distribution of the glucose transporter family. *World J Gastroenterol*, 2012; 18: p. 6771-6781 DOI: 10.3748/wjg.v18.i46.6771.
49. Jiang, G. and B.B. Zhang, Glucagon and regulation of glucose metabolism. *Am J Physiol Endocrinol Metab*, 2003; 284: p. E671-678 DOI: 10.1152/ajpendo.00492.2002.
50. Hatting, M., C.D.J. Tavares, K. Sharabi, et al., Insulin regulation of gluconeogenesis. *Ann N Y Acad Sci*, 2018; 1411: p. 21-35 DOI: 10.1111/nyas.13435.
51. I, O.S., W. Zhang, D.H. Wasserman, et al., FoxO1 integrates direct and indirect effects of insulin on hepatic glucose production and glucose utilization. *Nat Commun*, 2015; 6: p. 7079 DOI: 10.1038/ncomms8079.
52. Mittelman, S.D., Y.Y. Fu, K. Rebrin, et al., Indirect effect of insulin to suppress endogenous glucose production is dominant, even with hyperglucagonemia. *J Clin Invest*, 1997; 100: p. 3121-3130 DOI: 10.1172/JCI119867.
53. Boron, W.F. and E.L. Boulpaep, *Medical physiology: a cellular and molecular approach*. Updated edition ed. 2005, United States of America: Elsevier Saunders.
54. McLeod, R.S. and Z. Yao, Chapter 16 - Assembly and Secretion of Triglyceride-Rich Lipoproteins, in *Biochemistry of Lipids, Lipoproteins and Membranes (Sixth Edition)*, N.D. Ridgway and R.S. McLeod, Editors. 2016, Elsevier: Boston. p. 459-488.
55. Abumrad, N.A., M.R. el-Maghrabi, E.Z. Amri, et al., Cloning of a rat adipocyte membrane protein implicated in binding or transport of long-chain fatty acids that is induced during preadipocyte differentiation. Homology with human CD36. *J Biol Chem*, 1993; 268: p. 17665-17668.
56. Lehner, R. and A.D. Quiroga, Chapter 5 - Fatty Acid Handling in Mammalian Cells, in *Biochemistry of Lipids, Lipoproteins and Membranes (Sixth Edition)*, N.D. Ridgway and R.S. McLeod, Editors. 2016, Elsevier: Boston. p. 149-184.
57. Jarc, E. and T. Petan, Lipid Droplets and the Management of Cellular Stress. *Yale J Biol Med*, 2019; 92: p. 435-452.
58. Martinez-Botas, J., J.B. Anderson, D. Tessier, et al., Absence of perilipin results in leanness and reverses obesity in *Lepr(db/db)* mice. *Nat Genet*, 2000; 26: p. 474-479 DOI: 10.1038/82630.
59. Tansey, J.T., C. Sztalryd, J. Gruia-Gray, et al., Perilipin ablation results in a lean mouse with aberrant adipocyte lipolysis, enhanced leptin production, and resistance to diet-induced obesity. *Proc Natl Acad Sci U S A*, 2001; 98: p. 6494-6499 DOI: 10.1073/pnas.101042998.
60. Arner, P., Catecholamine-induced lipolysis in obesity. *Int J Obes Relat Metab Disord*, 1999; 23 Suppl 1: p. 10-13 DOI: 10.1038/sj.ijo.0800789.
61. Arner, P., Human fat cell lipolysis: biochemistry, regulation and clinical role. *Best Pract Res Clin Endocrinol Metab*, 2005; 19: p. 471-482 DOI: 10.1016/j.beem.2005.07.004.
62. Clifford, G.M., C. Londos, F.B. Kraemer, et al., Translocation of hormone-sensitive lipase and perilipin upon lipolytic stimulation of rat adipocytes. *J Biol Chem*, 2000; 275: p. 5011-5015 DOI: 10.1074/jbc.275.7.5011.
63. Lafontan, M. and D. Langin, Lipolysis and lipid mobilization in human adipose tissue. *Prog Lipid Res*, 2009; 48: p. 275-297 DOI: 10.1016/j.plipres.2009.05.001.
64. Edens, N.K., R.L. Leibel, and J. Hirsch, Mechanism of free fatty acid re-esterification in human adipocytes in vitro. *J Lipid Res*, 1990; 31: p. 1423-1431.

65. Sztalryd, C. and D.L. Brasaemle, The perilipin family of lipid droplet proteins: Gatekeepers of intracellular lipolysis. *Biochim Biophys Acta Mol Cell Biol Lipids*, 2017: 1862: p. 1221-1232 DOI: 10.1016/j.bbalip.2017.07.009.
66. DiPilato, L.M., F. Ahmad, M. Harms, et al., The Role of PDE3B Phosphorylation in the Inhibition of Lipolysis by Insulin. *Mol Cell Biol*, 2015: 35: p. 2752-2760 DOI: 10.1128/MCB.00422-15.
67. Choi, S.M., D.F. Tucker, D.N. Gross, et al., Insulin regulates adipocyte lipolysis via an Akt-independent signaling pathway. *Mol Cell Biol*, 2010: 30: p. 5009-5020 DOI: 10.1128/MCB.00797-10.
68. Rosen, E.D., C.J. Walkey, P. Puigserver, et al., Transcriptional regulation of adipogenesis. *Genes Dev*, 2000: 14: p. 1293-1307.
69. Tontonoz, P., E. Hu, and B.M. Spiegelman, Stimulation of adipogenesis in fibroblasts by PPAR gamma 2, a lipid-activated transcription factor. *Cell*, 1994: 79: p. 1147-1156 DOI: 10.1016/0092-8674(94)90006-x.
70. Tontonoz, P. and B.M. Spiegelman, Fat and beyond: the diverse biology of PPARgamma. *Annu Rev Biochem*, 2008: 77: p. 289-312 DOI: 10.1146/annurev.biochem.77.061307.091829.
71. Delgado, T.C., D. Pinheiro, M. Caldeira, et al., Sources of hepatic triglyceride accumulation during high-fat feeding in the healthy rat. *NMR Biomed*, 2009: 22: p. 310-317 DOI: 10.1002/nbm.1327.
72. Duarte, J.A., F. Carvalho, M. Pearson, et al., A high-fat diet suppresses de novo lipogenesis and desaturation but not elongation and triglyceride synthesis in mice. *J Lipid Res*, 2014: 55: p. 2541-2553 DOI: 10.1194/jlr.M052308.
73. Luukkonen, P.K., S. Sadevirta, Y. Zhou, et al., Saturated Fat Is More Metabolically Harmful for the Human Liver Than Unsaturated Fat or Simple Sugars. *Diabetes Care*, 2018: 41: p. 1732-1739 DOI: 10.2337/dc18-0071.
74. Sevastianova, K., A. Santos, A. Kotronen, et al., Effect of short-term carbohydrate overfeeding and long-term weight loss on liver fat in overweight humans. *Am J Clin Nutr*, 2012: 96: p. 727-734 DOI: 10.3945/ajcn.112.038695.
75. Shelness, G.S. and J.A. Sellers, Very-low-density lipoprotein assembly and secretion. *Curr Opin Lipidol*, 2001: 12: p. 151-157 DOI: 10.1097/00041433-200104000-00008.
76. McGarry, J.D., G.F. Leatherman, and D.W. Foster, Carnitine palmitoyltransferase I. The site of inhibition of hepatic fatty acid oxidation by malonyl-CoA. *J Biol Chem*, 1978: 253: p. 4128-4136.
77. McGarry, J.D., G.P. Mannaerts, and D.W. Foster, A possible role for malonyl-CoA in the regulation of hepatic fatty acid oxidation and ketogenesis. *J Clin Invest*, 1977: 60: p. 265-270 DOI: 10.1172/JCI108764.
78. Foster, D.W., The role of the carnitine system in human metabolism. *Ann N Y Acad Sci*, 2004: 1033: p. 1-16 DOI: 10.1196/annals.1320.001.
79. Martinez-Reyes, I. and N.S. Chandel, Mitochondrial TCA cycle metabolites control physiology and disease. *Nat Commun*, 2020: 11: p. 102 DOI: 10.1038/s41467-019-13668-3.
80. Houten, S.M., S. Violante, F.V. Ventura, et al., The Biochemistry and Physiology of Mitochondrial Fatty Acid beta-Oxidation and Its Genetic Disorders. *Annu Rev Physiol*, 2016: 78: p. 23-44 DOI: 10.1146/annurev-physiol-021115-105045.

81. Petersen, M.C. and G.I. Shulman, Mechanisms of Insulin Action and Insulin Resistance. *Physiol Rev*, 2018: 98: p. 2133-2223 DOI: 10.1152/physrev.00063.2017.
82. Bowe, J.E., Z.J. Franklin, A.C. Hauge-Evans, et al., Metabolic phenotyping guidelines: assessing glucose homeostasis in rodent models. *J Endocrinol*, 2014: 222: p. G13-25 DOI: 10.1530/JOE-14-0182.
83. DeFronzo, R.A., R. Gunnarsson, O. Bjorkman, et al., Effects of insulin on peripheral and splanchnic glucose metabolism in noninsulin-dependent (type II) diabetes mellitus. *J Clin Invest*, 1985: 76: p. 149-155 DOI: 10.1172/JCI111938.
84. Groop, L.C., R.C. Bonadonna, S. DelPrato, et al., Glucose and free fatty acid metabolism in non-insulin-dependent diabetes mellitus. Evidence for multiple sites of insulin resistance. *J Clin Invest*, 1989: 84: p. 205-213 DOI: 10.1172/JCI114142.
85. Brunzell, J.D., R.P. Robertson, R.L. Lerner, et al., Relationships between fasting plasma glucose levels and insulin secretion during intravenous glucose tolerance tests. *J Clin Endocrinol Metab*, 1976: 42: p. 222-229 DOI: 10.1210/jcem-42-2-222.
86. Perley, M.J. and D.M. Kipnis, Plasma insulin responses to oral and intravenous glucose: studies in normal and diabetic subjects. *J Clin Invest*, 1967: 46: p. 1954-1962 DOI: 10.1172/JCI105685.
87. Prentki, M. and C.J. Nolan, Islet beta cell failure in type 2 diabetes. *J Clin Invest*, 2006: 116: p. 1802-1812 DOI: 10.1172/JCI29103.
88. Czech, M.P., Insulin action and resistance in obesity and type 2 diabetes. *Nat Med*, 2017: 23: p. 804-814 DOI: 10.1038/nm.4350.
89. Spalding, K.L., E. Arner, P.O. Westermark, et al., Dynamics of fat cell turnover in humans. *Nature*, 2008: 453: p. 783-787 DOI: 10.1038/nature06902.
90. Eriksson-Hogling, D., D.P. Andersson, J. Backdahl, et al., Adipose tissue morphology predicts improved insulin sensitivity following moderate or pronounced weight loss. *Int J Obes (Lond)*, 2015: 39: p. 893-898 DOI: 10.1038/ijo.2015.18.
91. Acosta, J.R., I. Douagi, D.P. Andersson, et al., Increased fat cell size: a major phenotype of subcutaneous white adipose tissue in non-obese individuals with type 2 diabetes. *Diabetologia*, 2016: 59: p. 560-570 DOI: 10.1007/s00125-015-3810-6.
92. Engin, A.B., What Is Lipotoxicity? *Adv Exp Med Biol*, 2017: 960: p. 197-220 DOI: 10.1007/978-3-319-48382-5\_8.
93. Bays, H., L. Mandarino, and R.A. DeFronzo, Role of the adipocyte, free fatty acids, and ectopic fat in pathogenesis of type 2 diabetes mellitus: peroxisomal proliferator-activated receptor agonists provide a rational therapeutic approach. *J Clin Endocrinol Metab*, 2004: 89: p. 463-478 DOI: 10.1210/jc.2003-030723.
94. Morigny, P., M. Houssier, E. Mouisel, et al., Adipocyte lipolysis and insulin resistance. *Biochimie*, 2016: 125: p. 259-266 DOI: 10.1016/j.biochi.2015.10.024.
95. Rangwala, S.M., B. Rhoades, J.S. Shapiro, et al., Genetic modulation of PPARgamma phosphorylation regulates insulin sensitivity. *Dev Cell*, 2003: 5: p. 657-663 DOI: 10.1016/s1534-5807(03)00274-0.
96. Okuno, A., H. Tamemoto, K. Tobe, et al., Troglitazone increases the number of small adipocytes without the change of white adipose tissue mass in obese Zucker rats. *J Clin Invest*, 1998: 101: p. 1354-1361 DOI: 10.1172/JCI1235.
97. Morley, T.S., J.Y. Xia, and P.E. Scherer, Selective enhancement of insulin sensitivity in the mature adipocyte is sufficient for systemic metabolic improvements. *Nat Commun*, 2015: 6: p. 7906 DOI: 10.1038/ncomms8906.

98. Mann, J.P. and D.B. Savage, What lipodystrophies teach us about the metabolic syndrome. *J Clin Invest*, 2019: 129: p. 4009-4021 DOI: 10.1172/JCI129190.
99. Jiang, Z.Y., Q.L. Zhou, K.A. Coleman, et al., Insulin signaling through Akt/protein kinase B analyzed by small interfering RNA-mediated gene silencing. *Proc Natl Acad Sci U S A*, 2003: 100: p. 7569-7574 DOI: 10.1073/pnas.1332633100.
100. Gonzalez, E., E. Flier, D. Molle, et al., Hyperinsulinemia leads to uncoupled insulin regulation of the GLUT4 glucose transporter and the FoxO1 transcription factor. *Proc Natl Acad Sci U S A*, 2011: 108: p. 10162-10167 DOI: 10.1073/pnas.1019268108.
101. Shearin, A.L., B.R. Monks, P. Seale, et al., Lack of AKT in adipocytes causes severe lipodystrophy. *Mol Metab*, 2016: 5: p. 472-479 DOI: 10.1016/j.molmet.2016.05.006.
102. Abel, E.D., O. Peroni, J.K. Kim, et al., Adipose-selective targeting of the GLUT4 gene impairs insulin action in muscle and liver. *Nature*, 2001: 409: p. 729-733 DOI: 10.1038/35055575.
103. Paglialunga, S., A. Ludzki, J. Root-McCaig, et al., In adipose tissue, increased mitochondrial emission of reactive oxygen species is important for short-term high-fat diet-induced insulin resistance in mice. *Diabetologia*, 2015: 58: p. 1071-1080 DOI: 10.1007/s00125-015-3531-x.
104. Yin, C., W.H. Liu, Y. Liu, et al., PID1 alters the antilipolytic action of insulin and increases lipolysis via inhibition of AKT/PKA pathway activation. *PLoS One*, 2019: 14: p. e0214606 DOI: 10.1371/journal.pone.0214606.
105. Lee, E.Y., K. Sakurai, X. Zhang, et al., Unsuppressed lipolysis in adipocytes is linked with enhanced gluconeogenesis and altered bile acid physiology in *Insr*(P1195L/+) mice fed high-fat-diet. *Sci Rep*, 2015: 5: p. 17565 DOI: 10.1038/srep17565.
106. Gaidhu, M.P., N.M. Anthony, P. Patel, et al., Dysregulation of lipolysis and lipid metabolism in visceral and subcutaneous adipocytes by high-fat diet: role of ATGL, HSL, and AMPK. *Am J Physiol Cell Physiol*, 2010: 298: p. C961-971 DOI: 10.1152/ajpcell.00547.2009.
107. Chen, Y.D., A. Golay, A.L. Swislocki, et al., Resistance to insulin suppression of plasma free fatty acid concentrations and insulin stimulation of glucose uptake in noninsulin-dependent diabetes mellitus. *J Clin Endocrinol Metab*, 1987: 64: p. 17-21 DOI: 10.1210/jcem-64-1-17.
108. Frazee, E., C.C. Donner, A.L. Swislocki, et al., Ambient plasma free fatty acid concentrations in noninsulin-dependent diabetes mellitus: evidence for insulin resistance. *J Clin Endocrinol Metab*, 1985: 61: p. 807-811 DOI: 10.1210/jcem-61-5-807.
109. Li, X., D. Zhang, D.F. Vatner, et al., Mechanisms by which adiponectin reverses high fat diet-induced insulin resistance in mice. *Proc Natl Acad Sci U S A*, 2020: 117: p. 32584-32593 DOI: 10.1073/pnas.1922169117.
110. Yamauchi, T., J. Kamon, H. Waki, et al., The fat-derived hormone adiponectin reverses insulin resistance associated with both lipoatrophy and obesity. *Nat Med*, 2001: 7: p. 941-946 DOI: 10.1038/90984.
111. Friedman, J.M. and J.L. Halaas, Leptin and the regulation of body weight in mammals. *Nature*, 1998: 395: p. 763-770 DOI: 10.1038/27376.
112. Maffei, M., J. Halaas, E. Ravussin, et al., Leptin levels in human and rodent: measurement of plasma leptin and ob RNA in obese and weight-reduced subjects. *Nat Med*, 1995: 1: p. 1155-1161 DOI: 10.1038/nm1195-1155.

113. Hummel, K.P., M.M. Dickie, and D.L. Coleman, Diabetes, a new mutation in the mouse. *Science*, 1966: 153: p. 1127-1128 DOI: 10.1126/science.153.3740.1127.
114. Ingalls, A.M., M.M. Dickie, and G.D. Snell, Obese, a new mutation in the house mouse. *J Hered*, 1950: 41: p. 317-318 DOI: 10.1093/oxfordjournals.jhered.a106073.
115. Zhang, Y., R. Proenca, M. Maffei, et al., Positional cloning of the mouse obese gene and its human homologue. *Nature*, 1994: 372: p. 425-432 DOI: 10.1038/372425a0.
116. Ghaben, A.L. and P.E. Scherer, Adipogenesis and metabolic health. *Nat Rev Mol Cell Biol*, 2019 DOI: 10.1038/s41580-018-0093-z.
117. Stern, J.H., J.M. Rutkowski, and P.E. Scherer, Adiponectin, Leptin, and Fatty Acids in the Maintenance of Metabolic Homeostasis through Adipose Tissue Crosstalk. *Cell Metab*, 2016: 23: p. 770-784 DOI: 10.1016/j.cmet.2016.04.011.
118. Brown, M.S. and J.L. Goldstein, Selective versus total insulin resistance: a pathogenic paradox. *Cell Metab*, 2008: 7: p. 95-96 DOI: 10.1016/j.cmet.2007.12.009.
119. Shimomura, I., M. Matsuda, R.E. Hammer, et al., Decreased IRS-2 and increased SREBP-1c lead to mixed insulin resistance and sensitivity in livers of lipodystrophic and ob/ob mice. *Mol Cell*, 2000: 6: p. 77-86.
120. Kubota, N., T. Kubota, E. Kajiwara, et al., Differential hepatic distribution of insulin receptor substrates causes selective insulin resistance in diabetes and obesity. *Nat Commun*, 2016: 7: p. 12977 DOI: 10.1038/ncomms12977.
121. Kerouz, N.J., D. Horsch, S. Pons, et al., Differential regulation of insulin receptor substrates-1 and -2 (IRS-1 and IRS-2) and phosphatidylinositol 3-kinase isoforms in liver and muscle of the obese diabetic (ob/ob) mouse. *J Clin Invest*, 1997: 100: p. 3164-3172 DOI: 10.1172/JCI119872.
122. Anai, M., M. Funaki, T. Ogihara, et al., Altered expression levels and impaired steps in the pathway to phosphatidylinositol 3-kinase activation via insulin receptor substrates 1 and 2 in Zucker fatty rats. *Diabetes*, 1998: 47: p. 13-23 DOI: 10.2337/diab.47.1.13.
123. Honma, M., S. Sawada, Y. Ueno, et al., Selective insulin resistance with differential expressions of IRS-1 and IRS-2 in human NAFLD livers. *Int J Obes (Lond)*, 2018: 42: p. 1544-1555 DOI: 10.1038/s41366-018-0062-9.
124. Smith, G.I., M. Shankaran, M. Yoshino, et al., Insulin resistance drives hepatic de novo lipogenesis in nonalcoholic fatty liver disease. *J Clin Invest*, 2020: 130: p. 1453-1460 DOI: 10.1172/JCI134165.
125. Gross, D.N., M. Wan, and M.J. Birnbaum, The role of FOXO in the regulation of metabolism. *Curr Diab Rep*, 2009: 9: p. 208-214 DOI: 10.1007/s11892-009-0034-5.
126. Basu, R., V. Chandramouli, B. Dicke, et al., Obesity and type 2 diabetes impair insulin-induced suppression of glycogenolysis as well as gluconeogenesis. *Diabetes*, 2005: 54: p. 1942-1948 DOI: 10.2337/diabetes.54.7.1942.
127. Boden, G., X. Chen, and T.P. Stein, Gluconeogenesis in moderately and severely hyperglycemic patients with type 2 diabetes mellitus. *Am J Physiol Endocrinol Metab*, 2001: 280: p. E23-30 DOI: 10.1152/ajpendo.2001.280.1.E23.
128. Cho, H., J. Mu, J.K. Kim, et al., Insulin resistance and a diabetes mellitus-like syndrome in mice lacking the protein kinase Akt2 (PKB beta). *Science*, 2001: 292: p. 1728-1731 DOI: 10.1126/science.292.5522.1728.
129. Choi, S.H. and H.N. Ginsberg, Increased very low density lipoprotein (VLDL) secretion, hepatic steatosis, and insulin resistance. *Trends Endocrinol Metab*, 2011: 22: p. 353-363 DOI: 10.1016/j.tem.2011.04.007.

130. Al-Mrabeh, A., S.V. Zhyzhneuskaya, C. Peters, et al., Hepatic Lipoprotein Export and Remission of Human Type 2 Diabetes after Weight Loss. *Cell Metab*, 2020: 31: p. 233-249 e234 DOI: 10.1016/j.cmet.2019.11.018.
131. Sparks, J.D. and C.E. Sparks, Obese Zucker (fa/fa) rats are resistant to insulin's inhibitory effect on hepatic apo B secretion. *Biochem Biophys Res Commun*, 1994: 205: p. 417-422 DOI: 10.1006/bbrc.1994.2681.
132. Wiegman, C.H., R.H. Bandsma, M. Ouwens, et al., Hepatic VLDL production in ob/ob mice is not stimulated by massive de novo lipogenesis but is less sensitive to the suppressive effects of insulin. *Diabetes*, 2003: 52: p. 1081-1089 DOI: 10.2337/diabetes.52.5.1081.
133. Kamagate, A., S. Qu, G. Perdomo, et al., FoxO1 mediates insulin-dependent regulation of hepatic VLDL production in mice. *J Clin Invest*, 2008: 118: p. 2347-2364 DOI: 10.1172/JCI32914.
134. Qu, S., J. Altomonte, G. Perdomo, et al., Aberrant Forkhead box O1 function is associated with impaired hepatic metabolism. *Endocrinology*, 2006: 147: p. 5641-5652 DOI: 10.1210/en.2006-0541.
135. Araki, E., M.A. Lipes, M.E. Patti, et al., Alternative pathway of insulin signalling in mice with targeted disruption of the IRS-1 gene. *Nature*, 1994: 372: p. 186-190 DOI: 10.1038/372186a0.
136. Surwit, R.S., C.M. Kuhn, C. Cochrane, et al., Diet-induced type II diabetes in C57BL/6J mice. *Diabetes*, 1988: 37: p. 1163-1167 DOI: 10.2337/diab.37.9.1163.
137. Lee, Y.S., P. Li, J.Y. Huh, et al., Inflammation is necessary for long-term but not short-term high-fat diet-induced insulin resistance. *Diabetes*, 2011: 60: p. 2474-2483 DOI: 10.2337/db11-0194.
138. Park, S.Y., Y.R. Cho, H.J. Kim, et al., Unraveling the temporal pattern of diet-induced insulin resistance in individual organs and cardiac dysfunction in C57BL/6 mice. *Diabetes*, 2005: 54: p. 3530-3540 DOI: 10.2337/diabetes.54.12.3530.
139. Miura, T., W. Suzuki, E. Ishihara, et al., Impairment of insulin-stimulated GLUT4 translocation in skeletal muscle and adipose tissue in the Tsumura Suzuki obese diabetic mouse: a new genetic animal model of type 2 diabetes. *Eur J Endocrinol*, 2001: 145: p. 785-790 DOI: 10.1530/eje.0.1450785.
140. Tremblay, F., C. Lavigne, H. Jacques, et al., Defective insulin-induced GLUT4 translocation in skeletal muscle of high fat-fed rats is associated with alterations in both Akt/protein kinase B and atypical protein kinase C (zeta/lambda) activities. *Diabetes*, 2001: 50: p. 1901-1910 DOI: 10.2337/diabetes.50.8.1901.
141. Hansen, P.A., D.H. Han, B.A. Marshall, et al., A high fat diet impairs stimulation of glucose transport in muscle. Functional evaluation of potential mechanisms. *J Biol Chem*, 1998: 273: p. 26157-26163 DOI: 10.1074/jbc.273.40.26157.
142. Garvey, W.T., L. Maianu, J.H. Zhu, et al., Evidence for defects in the trafficking and translocation of GLUT4 glucose transporters in skeletal muscle as a cause of human insulin resistance. *J Clin Invest*, 1998: 101: p. 2377-2386 DOI: 10.1172/JCI1557.
143. Hegarty, B.D., S.M. Furler, J. Ye, et al., The role of intramuscular lipid in insulin resistance. *Acta Physiol Scand*, 2003: 178: p. 373-383 DOI: 10.1046/j.1365-201X.2003.01162.x.

144. Stone, J.A., R.L. Houlden, P. Lin, et al., Cardiovascular Protection in People With Diabetes. *Can J Diabetes*, 2018: 42 Suppl 1: p. S162-S169 DOI: 10.1016/j.jcjd.2017.10.024.
145. Altomare, F., A. Kherani, and J. Lovshin, Retinopathy. *Can J Diabetes*, 2018: 42 Suppl 1: p. S210-S216 DOI: 10.1016/j.jcjd.2017.10.027.
146. McFarlane, P., D. Cherney, R.E. Gilbert, et al., Chronic Kidney Disease in Diabetes. *Can J Diabetes*, 2018: 42 Suppl 1: p. S201-S209 DOI: 10.1016/j.jcjd.2017.11.004.
147. Bril, V., A. Breiner, B.A. Perkins, et al., Neuropathy. *Can J Diabetes*, 2018: 42 Suppl 1: p. S217-S221 DOI: 10.1016/j.jcjd.2017.10.028.
148. Embil, J.M., Z. Albalawi, K. Bowering, et al., Foot Care. *Can J Diabetes*, 2018: 42 Suppl 1: p. S222-S227 DOI: 10.1016/j.jcjd.2017.10.020.
149. Buzzetti, E., M. Pinzani, and E.A. Tsochatzis, The multiple-hit pathogenesis of non-alcoholic fatty liver disease (NAFLD). *Metabolism*, 2016: 65: p. 1038-1048 DOI: 10.1016/j.metabol.2015.12.012.
150. Tilg, H., T.E. Adolph, and A.R. Moschen, Multiple Parallel Hits Hypothesis in Nonalcoholic Fatty Liver Disease: Revisited After a Decade. *Hepatology*, 2021: 73: p. 833-842 DOI: 10.1002/hep.31518.
151. Shum, M., J. Ngo, O.S. Shirihai, et al., Mitochondrial oxidative function in NAFLD: Friend or foe? *Mol Metab*, 2021: 50: p. 101134 DOI: 10.1016/j.molmet.2020.101134.
152. Miquilena-Colina, M.E., E. Lima-Cabello, S. Sanchez-Campos, et al., Hepatic fatty acid translocase CD36 upregulation is associated with insulin resistance, hyperinsulinaemia and increased steatosis in non-alcoholic steatohepatitis and chronic hepatitis C. *Gut*, 2011: 60: p. 1394-1402 DOI: 10.1136/gut.2010.222844.
153. Puri, P., F. Mirshahi, O. Cheung, et al., Activation and dysregulation of the unfolded protein response in nonalcoholic fatty liver disease. *Gastroenterology*, 2008: 134: p. 568-576 DOI: 10.1053/j.gastro.2007.10.039.
154. Younossi, Z.M., D. Blissett, R. Blissett, et al., The economic and clinical burden of nonalcoholic fatty liver disease in the United States and Europe. *Hepatology*, 2016: 64: p. 1577-1586 DOI: 10.1002/hep.28785.
155. Younossi, Z., M. Stepanova, J.P. Ong, et al., Nonalcoholic Steatohepatitis Is the Fastest Growing Cause of Hepatocellular Carcinoma in Liver Transplant Candidates. *Clin Gastroenterol Hepatol*, 2019: 17: p. 748-755 e743 DOI: 10.1016/j.cgh.2018.05.057.
156. About Natural Health Products. Natural and Non-prescription Health Products Directorate (NNHPD) 2016; Available from: <https://www.canada.ca/en/health-canada/services/drugs-health-products/natural-non-prescription/regulation/about-products.html>.
157. Ryan, E.A., M.E. Pick, and C. Marceau, Use of alternative medicines in diabetes mellitus. *Diabet Med*, 2001: 18: p. 242-245 DOI: 10.1046/j.1464-5491.2001.00450.x.
158. Diabetes Canada Clinical Practice Guidelines Expert, C., L.D. Grossman, R. Roscoe, et al., Complementary and Alternative Medicine for Diabetes. *Can J Diabetes*, 2018: 42 Suppl 1: p. S154-S161 DOI: 10.1016/j.jcjd.2017.10.023.
159. Natural health products. Government of Canada- Non-prescription Health Products Directorate (NNHPD) 2004; Available from: <https://www.canada.ca/en/health-canada/services/drugs-health-products/natural-non-prescription.html>.

160. Nutraceuticals/Functional Foods and Health Claims On Foods. 2002; Available from: <https://www.canada.ca/en/health-canada/services/food-nutrition/food-labelling/health-claims/nutraceuticals-functional-foods-health-claims-foods-policy-paper.html>.
161. Jia, L., L. Wang, C. Liu, et al., Bioactive peptides from foods: production, function, and application. *Food Funct*, 2021: 12: p. 7108-7125 DOI: 10.1039/d1fo01265g.
162. Meisel, H., Biochemical properties of regulatory peptides derived from milk proteins. *Biopolymers*, 1997: 43: p. 119-128 DOI: 10.1002/(SICI)1097-0282(1997)43:2<119::AID-BIP4>3.0.CO;2-Y.
163. Cao, X., W. Liao, and S. Wang, Food protein-derived bioactive peptides for the management of nutrition related chronic diseases. *Adv Food Nutr Res*, 2022: 101: p. 277-307 DOI: 10.1016/bs.afnr.2022.04.004.
164. Aluko, R.E., Antihypertensive peptides from food proteins. *Annu Rev Food Sci Technol*, 2015: 6: p. 235-262 DOI: 10.1146/annurev-food-022814-015520.
165. de Campos Zani, S.C., J. Wu, and C.B. Chan, Egg and soy-derived peptides and hydrolysates: a review of their physiological actions against diabetes and obesity. *Nutrients*, 2018: 10 DOI: 10.3390/nu10050549.
166. Li, S., L. Liu, G. He, et al., Molecular targets and mechanisms of bioactive peptides against metabolic syndromes. *Food Funct*, 2018: 9: p. 42-52 DOI: 10.1039/c7fo01323j.
167. Qiao, Q., L. Chen, X. Li, et al., Roles of Dietary Bioactive Peptides in Redox Balance and Metabolic Disorders. *Oxid Med Cell Longev*, 2021: 2021: p. 5582245 DOI: 10.1155/2021/5582245.
168. Geerts, B.F., M.G. van Dongen, B. Flameling, et al., Hydrolyzed casein decreases postprandial glucose concentrations in T2DM patients irrespective of leucine content. *J Diet Suppl*, 2011: 8: p. 280-292 DOI: 10.3109/19390211.2011.593617.
169. Kwak, J.H., C.W. Ahn, S.H. Park, et al., Weight reduction effects of a black soy peptide supplement in overweight and obese subjects: double blind, randomized, controlled study. *Food Funct*, 2012: 3: p. 1019-1024 DOI: 10.1039/c2fo10244g.
170. Kwak, J.H., J.H. Lee, C.W. Ahn, et al., Black soy peptide supplementation improves glucose control in subjects with prediabetes and newly diagnosed type 2 diabetes mellitus. *J Med Food*, 2010: 13: p. 1307-1312 DOI: 10.1089/jmf.2010.1075.
171. Manders, R.J., S.F. Praet, R.C. Meex, et al., Protein hydrolysate/leucine co-ingestion reduces the prevalence of hyperglycemia in type 2 diabetic patients. *Diabetes Care*, 2006: 29: p. 2721-2722 DOI: 10.2337/dc06-1424.
172. Plat, J., N. Severins, S. Morrison, et al., Effects of NWT-03, an egg-protein hydrolysate, on blood pressure in normotensive, high-normotensive and mild-hypertensive men and women: a dose-finding study. *Br J Nutr*, 2017: 117: p. 942-950 DOI: 10.1017/S0007114517000836.
173. Gravesteijn, E., J.J. Adam, R.P. Mensink, et al., Effects of the egg protein hydrolysate NWT-03 on cognitive function in men and women with the metabolic syndrome: a randomized, double-blind, placebo-controlled study. *Nutr Neurosci*, 2022: p. 1-10 DOI: 10.1080/1028415X.2022.2144204.
174. Lucey, A.J., C. Heneghan, E. Manning, et al., Effect of an egg ovalbumin-derived protein hydrolysate on blood pressure and cardiovascular risk in adults with a mildly elevated blood pressure: a randomized placebo-controlled crossover trial. *Eur J Nutr*, 2019: 58: p. 2823-2833 DOI: 10.1007/s00394-018-1832-9.

175. Garces-Rimon, M., C. Gonzalez, G. Vera, et al., Pepsin egg white hydrolysate improves glucose metabolism complications related to metabolic syndrome in Zucker fatty rats. *Nutrients*, 2018: 10 DOI: 10.3390/nu10040441.
176. Moreno-Fernandez, S., M. Garces-Rimon, C. Gonzalez, et al., Pepsin egg white hydrolysate ameliorates metabolic syndrome in high-fat/high-dextrose fed rats. *Food Funct*, 2018: 9: p. 78-86 DOI: 10.1039/c7fo01280b.
177. Moreno-Fernandez, S., M. Garces-Rimon, J.A. Uranga, et al., Expression enhancement in brown adipose tissue of genes related to thermogenesis and mitochondrial dynamics after administration of pepsin egg white hydrolysate. *Food Funct*, 2018: 9: p. 6599-6607 DOI: 10.1039/c8fo01754a.
178. Ochiai, M., T. Kuroda, and T. Matsuo, Increased muscular triglyceride content and hyperglycemia in Goto-Kakizaki rat are decreased by egg white hydrolysate. *Int J Food Sci Nutr*, 2014: 65: p. 495-501 DOI: 10.3109/09637486.2013.879288.
179. Ochiai, M. and Y. Azuma, Egg white hydrolysate improves glucose tolerance in type-2 diabetic NSY mice. *J Nutr Sci Vitaminol (Tokyo)*, 2017: 63: p. 422-429 DOI: 10.3177/jnsv.63.422.
180. Liu, Z., S. Ding, H. Jiang, et al., Egg Protein Transferrin-Derived Peptides Irw (Lle-Arg-Trp) and Iqw (Lle-Gln-Trp) Prevent Obesity Mouse Model Induced by a High-Fat Diet via Reducing Lipid Deposition and Reprogramming Gut Microbiota. *Int J Mol Sci*, 2022: 23 DOI: 10.3390/ijms231911227.
181. Garces-Rimon, M., C. Gonzalez, J.A. Uranga, et al., Pepsin egg white hydrolysate ameliorates obesity-related oxidative stress, inflammation and steatosis in Zucker fatty rats. *PLoS One*, 2016a: 11: p. e0151193 DOI: 10.1371/journal.pone.0151193.
182. Ochiai, M., K. Misaki, T. Takeuchi, et al., Egg White Hydrolysate Can Be a Low-Allergenic Food Material to Suppress Ectopic Fat Accumulation in Rats Fed an Equicaloric Diet. *J Nutr Sci Vitaminol (Tokyo)*, 2017: 63: p. 111-119.
183. Ochiai, M. and T. Matsuo, Effect of egg white and its hydrolysate on stearyl-CoA desaturase index and fat accumulation in rat tissues. *Int J Food Sci Nutr*, 2014: 65: p. 948-952 DOI: 10.3109/09637486.2014.937800.
184. Jiang, Z., Y. Kimura, B. Shirouchi, et al., Dietary egg white protein hydrolysate improves orotic acid-induced fatty liver in rats by promoting hepatic phospholipid synthesis and microsomal triglyceride transfer protein expression. *J Nutr Biochem*, 2021: 98: p. 108820 DOI: 10.1016/j.jnutbio.2021.108820.
185. Majumder, K. and J. Wu, Purification and characterisation of angiotensin I converting enzyme (ACE) inhibitory peptides derived from enzymatic hydrolysate of ovotransferrin. *Food Chem*, 2011: 126: p. 1614-1619 DOI: 10.1016/j.foodchem.2010.12.039.
186. Jahandideh, F., S. Chakrabarti, K. Majumder, et al., Egg white protein hydrolysate reduces blood pressure, improves vascular relaxation and modifies aortic angiotensin II receptors expression in spontaneously hypertensive rats. *J Funct Foods*, 2016: 27: p. 667-673 DOI: 10.1016/j.jff.2016.10.019.
187. Majumder, K., S. Chakrabarti, J.S. Morton, et al., Egg-derived tri-peptide IRW exerts antihypertensive effects in spontaneously hypertensive rats. *PLoS One*, 2013: 8: p. e82829 DOI: 10.1371/journal.pone.0082829.
188. Majumder, K., S. Chakrabarti, S.T. Davidge, et al., Structure and activity study of egg protein ovotransferrin derived peptides (IRW and IQW) on endothelial inflammatory

- response and oxidative stress. *J Agric Food Chem*, 2013: 61: p. 2120-2129 DOI: 10.1021/jf3046076.
189. Liao, W., S. Chakrabarti, S.T. Davidge, et al., Modulatory Effects of Egg White Ovotransferrin-Derived Tripeptide IRW (Ile-Arg-Trp) on Vascular Smooth Muscle Cells against Angiotensin II Stimulation. *J Agric Food Chem*, 2016: 64: p. 7342-7347 DOI: 10.1021/acs.jafc.6b03513.
  190. Huang, W., S. Chakrabarti, K. Majumder, et al., Egg-derived peptide IRW inhibits TNF- $\alpha$ -induced inflammatory response and oxidative stress in endothelial cells. *J Agric Food Chem*, 2010: 58: p. 10840-10846 DOI: 10.1021/jf102120c.
  191. Son, M., C.B. Chan, and J. Wu, Egg white ovotransferrin-derived ACE inhibitory peptide ameliorates angiotensin II-stimulated insulin resistance in skeletal muscle cells. *Mol Nutr Food Res*, 2018: 62 DOI: 10.1002/mnfr.201700602.
  192. Son, M. and J. Wu, Egg white hydrolysate and peptide reverse insulin resistance associated with tumor necrosis factor- $\alpha$  (TNF- $\alpha$ ) stimulated mitogen-activated protein kinase (MAPK) pathway in skeletal muscle cells. *Eur J Nutr*, 2019: 58: p. 1961-1969 DOI: 10.1007/s00394-018-1753-7.
  193. Bhullar, K.S., M. Son, E. Kerek, et al., Tripeptide IRW Upregulates NAMPT Protein Levels in Cells and Obese C57BL/6J Mice. *J Agric Food Chem*, 2021: 69: p. 1555-1566 DOI: 10.1021/acs.jafc.0c07831.
  194. Pfluger, P.T., D. Herranz, S. Velasco-Miguel, et al., Sirt1 protects against high-fat diet-induced metabolic damage. *Proc Natl Acad Sci U S A*, 2008: 105: p. 9793-9798 DOI: 10.1073/pnas.0802917105.
  195. Deng, X.Q., L.L. Chen, and N.X. Li, The expression of SIRT1 in nonalcoholic fatty liver disease induced by high-fat diet in rats. *Liver Int*, 2007: 27: p. 708-715 DOI: 10.1111/j.1478-3231.2007.01497.x.
  196. Jahandideh, F., S. Chakrabarti, S.T. Davidge, et al., Egg white hydrolysate shows insulin mimetic and sensitizing effects in 3T3-F442A pre-adipocytes. *PLoS One*, 2017: 12: p. e0185653 DOI: 10.1371/journal.pone.0185653.
  197. Jahandideh, F., S.C.C. Zani, M. Son, et al., Egg white hydrolysate enhances insulin sensitivity in high-fat diet-induced insulin-resistant rats via Akt activation. *Br J Nutr*, 2019: 122: p. 14-24 DOI: 10.1017/S0007114519000837.
  198. Jahandideh, F., P. Liu, and J. Wu, Purification and identification of adipogenic-differentiating peptides from egg white hydrolysate. *Food Chem*, 2018: 259: p. 25-30 DOI: 10.1016/j.foodchem.2018.03.099.
  199. de Campos Zani, S.C., R. Wang, H. Veida-Silva, et al., An egg white-derived peptide enhances systemic insulin sensitivity and modulates markers of non-alcoholic fatty liver disease in obese, insulin resistant mice. *Metabolites*, 2023: 13 DOI: 10.3390/metabo13020174.
  200. Younossi, Z.M., Non-alcoholic fatty liver disease - A global public health perspective. *J Hepatol*, 2019: 70: p. 531-544 DOI: 10.1016/j.jhep.2018.10.033.
  201. Friedman, S.L., B.A. Neuschwander-Tetri, M. Rinella, et al., Mechanisms of NAFLD development and therapeutic strategies. *Nat Med*, 2018: 24: p. 908-922 DOI: 10.1038/s41591-018-0104-9.
  202. Softic, S., D.E. Cohen, and C.R. Kahn, Role of Dietary Fructose and Hepatic De Novo Lipogenesis in Fatty Liver Disease. *Dig Dis Sci*, 2016: 61: p. 1282-1293 DOI: 10.1007/s10620-016-4054-0.

203. Colca, J.R. and P.E. Scherer, The metabolic syndrome, thiazolidinediones, and implications for intersection of chronic and inflammatory disease. *Mol Metab*, 2022: 55: p. 101409 DOI: 10.1016/j.molmet.2021.101409.
204. Boettcher, E., G. Csako, F. Pucino, et al., Meta-analysis: pioglitazone improves liver histology and fibrosis in patients with non-alcoholic steatohepatitis. *Aliment Pharmacol Ther*, 2012: 35: p. 66-75 DOI: 10.1111/j.1365-2036.2011.04912.x.
205. Musso, G., M. Cassader, E. Paschetta, et al., Thiazolidinediones and Advanced Liver Fibrosis in Nonalcoholic Steatohepatitis: A Meta-analysis. *JAMA Intern Med*, 2017: 177: p. 633-640 DOI: 10.1001/jamainternmed.2016.9607.
206. FUFOSE, Scientific concepts of functional foods in Europe-consensus document. *Br J Nutr*, 1999: 81: p. S1-S27 DOI: 10.1017/S0007114599000471.
207. de Campos Zani, S.C., M. Son, K.S. Bhullar, et al., IRW (Isoleucine-Arginine-Tryptophan) Improves Glucose Tolerance in High Fat Diet Fed C57BL/6 Mice via Activation of Insulin Signaling and AMPK Pathways in Skeletal Muscle. *Biomedicines*, 2022: 10 DOI: 10.3390/biomedicines10061235.
208. Rocha, A.L., T.I. de Lima, G.P. de Souza, et al., Enoxacin induces oxidative metabolism and mitigates obesity by regulating adipose tissue miRNA expression. *Sci Adv*, 2020: 6 DOI: 10.1126/sciadv.abc6250.
209. Mighiu, P.I., J.T. Yue, B.M. Filippi, et al., Hypothalamic glucagon signaling inhibits hepatic glucose production. *Nat Med*, 2013: 19: p. 766-772 DOI: 10.1038/nm.3115.
210. Yue, J.T., M.A. Abraham, P.V. Bauer, et al., Inhibition of glycine transporter-1 in the dorsal vagal complex improves metabolic homeostasis in diabetes and obesity. *Nat Commun*, 2016: 7: p. 13501 DOI: 10.1038/ncomms13501.
211. Folch, J., M. Lees, and G.H. Sloane Stanley, A simple method for the isolation and purification of total lipides from animal tissues. *J Biol Chem*, 1957: 226: p. 497-509.
212. Ferri, F., S. Carotti, G. Carpino, et al., The Propensity of the Human Liver to Form Large Lipid Droplets Is Associated with PNPLA3 Polymorphism, Reduced INSIG1 and NPC1L1 Expression and Increased Fibrogenetic Capacity. *Int J Mol Sci*, 2021: 22 DOI: 10.3390/ijms22116100.
213. Yersiz, H., C. Lee, F.M. Kaldas, et al., Assessment of hepatic steatosis by transplant surgeon and expert pathologist: a prospective, double-blind evaluation of 201 donor livers. *Liver Transpl*, 2013: 19: p. 437-449 DOI: 10.1002/lt.23615.
214. Brunt, E.M., Pathology of fatty liver disease. *Mod Pathol*, 2007: 20 Suppl 1: p. S40-48 DOI: 10.1038/modpathol.3800680.
215. Ferdouse, A., R.R. Agrawal, M.A. Gao, et al., Alcohol induced hepatic retinoid depletion is associated with the induction of multiple retinoid catabolizing cytochrome P450 enzymes. *PLoS One*, 2022: 17: p. e0261675 DOI: 10.1371/journal.pone.0261675.
216. Sakurai, Y., N. Kubota, T. Yamauchi, et al., Role of Insulin Resistance in MAFLD. *Int J Mol Sci*, 2021: 22 DOI: 10.3390/ijms22084156.
217. Gao, M., Y. Ma, M. Alsaggar, et al., Dual Outcomes of Rosiglitazone Treatment on Fatty Liver. *AAPS J*, 2016: 18: p. 1023-1031 DOI: 10.1208/s12248-016-9919-9.
218. Lee, S.M., J. Muratalla, A. Diaz-Ruiz, et al., Rosiglitazone Requires Hepatocyte PPARgamma Expression to Promote Steatosis in Male Mice With Diet-Induced Obesity. *Endocrinology*, 2021: 162 DOI: 10.1210/endo/bqab175.

219. Vidal-Puig, A., M. Jimenez-Linan, B.B. Lowell, et al., Regulation of PPAR gamma gene expression by nutrition and obesity in rodents. *J Clin Invest*, 1996: 97: p. 2553-2561 DOI: 10.1172/JCI118703.
220. Rosenstengel, S., S. Stoeppeler, R. Bahde, et al., Type of steatosis influences microcirculation and fibrogenesis in different rat strains. *J Invest Surg*, 2011: 24: p. 273-282 DOI: 10.3109/08941939.2011.586094.
221. Najt, C.P., S. Senthivinayagam, M.B. Aljazi, et al., Liver-specific loss of Perilipin 2 alleviates diet-induced hepatic steatosis, inflammation, and fibrosis. *Am J Physiol Gastrointest Liver Physiol*, 2016: 310: p. G726-738 DOI: 10.1152/ajpgi.00436.2015.
222. Lemus-Conejo, A., E. Grao-Cruces, R. Toscano, et al., A lupine (*Lupinus angustifolius* L.) peptide prevents non-alcoholic fatty liver disease in high-fat-diet-induced obese mice. *Food Funct*, 2020: 11: p. 2943-2952 DOI: 10.1039/d0fo00206b.
223. Dumeus, S., M.A. Shibu, W.T. Lin, et al., Bioactive Peptide Improves Diet-Induced Hepatic Fat Deposition and Hepatocyte Proinflammatory Response in SAMP8 Ageing Mice. *Cell Physiol Biochem*, 2018: 48: p. 1942-1952 DOI: 10.1159/000492518.
224. Song, C., W. Lv, Y. Li, et al., Alleviating the effect of quinoa and the underlying mechanism on hepatic steatosis in high-fat diet-fed rats. *Nutr Metab (Lond)*, 2021: 18: p. 106 DOI: 10.1186/s12986-021-00631-7.
225. Steckelings, U.M., R.E. Widdop, E.D. Sturrock, et al., The Angiotensin AT(2) Receptor: From a Binding Site to a Novel Therapeutic Target. *Pharmacol Rev*, 2022: 74: p. 1051-1135 DOI: 10.1124/pharmrev.120.000281.
226. Goh, G.B., M.R. Pagadala, J. Dasarathy, et al., Renin-angiotensin system and fibrosis in non-alcoholic fatty liver disease. *Liver Int*, 2015: 35: p. 979-985 DOI: 10.1111/liv.12611.
227. Zhang, W., J. Miao, P. Li, et al., Up-regulation of components of the renin-angiotensin system in liver fibrosis in the rat induced by CCL(4). *Res Vet Sci*, 2013: 95: p. 54-58 DOI: 10.1016/j.rvsc.2013.01.028.
228. Nabeshima, Y., S. Tazuma, K. Kanno, et al., Anti-fibrogenic function of angiotensin II type 2 receptor in CCl4-induced liver fibrosis. *Biochem Biophys Res Commun*, 2006: 346: p. 658-664 DOI: 10.1016/j.bbrc.2006.05.183.
229. Chai, W., W. Wang, Z. Dong, et al., Angiotensin II receptors modulate muscle microvascular and metabolic responses to insulin in vivo. *Diabetes*, 2011: 60: p. 2939-2946 DOI: 10.2337/db10-1691.
230. Henrion, D., N. Kubis, and B.I. Levy, Physiological and pathophysiological functions of the AT(2) subtype receptor of angiotensin II: from large arteries to the microcirculation. *Hypertension*, 2001: 38: p. 1150-1157 DOI: 10.1161/hy1101.096109.
231. Ito, M., J. Suzuki, S. Tsujioka, et al., Longitudinal analysis of murine steatohepatitis model induced by chronic exposure to high-fat diet. *Hepatol Res*, 2007: 37: p. 50-57 DOI: 10.1111/j.1872-034X.2007.00008.x.
232. Kristiansen, M.N.B., S.S. Veidal, C. Christoffersen, et al., Molecular Characterization of Microvesicular and Macrovesicular Steatosis Shows Widespread Differences in Metabolic Pathways. *Lipids*, 2019: 54: p. 109-115 DOI: 10.1002/lipd.12121.
233. Hayashi, Y., E. Suemitsu, K. Kajimoto, et al., Hepatic Monoacylglycerol O-acyltransferase 1 as a Promising Therapeutic Target for Steatosis, Obesity, and Type 2 Diabetes. *Mol Ther Nucleic Acids*, 2014: 3: p. e154 DOI: 10.1038/mtna.2014.4.
234. Lee, Y.J., E.H. Ko, J.E. Kim, et al., Nuclear receptor PPARgamma-regulated monoacylglycerol O-acyltransferase 1 (MGAT1) expression is responsible for the lipid

- accumulation in diet-induced hepatic steatosis. *Proc Natl Acad Sci U S A*, 2012: 109: p. 13656-13661 DOI: 10.1073/pnas.1203218109.
235. Lutkewitte, A.J., J.M. Singer, T.M. Shew, et al., Multiple antisense oligonucleotides targeted against monoacylglycerol acyltransferase 1 (Mogat1) improve glucose metabolism independently of Mogat1. *Mol Metab*, 2021: 49: p. 101204 DOI: 10.1016/j.molmet.2021.101204.
  236. Lutkewitte, A.J., K.S. McCommis, G.G. Schweitzer, et al., Hepatic monoacylglycerol acyltransferase 1 is induced by prolonged food deprivation to modulate the hepatic fasting response. *J Lipid Res*, 2019: 60: p. 528-538 DOI: 10.1194/jlr.M089722.
  237. Carreres, L., Z.M. Jilkova, G. Vial, et al., Modeling Diet-Induced NAFLD and NASH in Rats: A Comprehensive Review. *Biomedicines*, 2021: 9 DOI: 10.3390/biomedicines9040378.
  238. Charlton, M., A. Krishnan, K. Viker, et al., Fast food diet mouse: novel small animal model of NASH with ballooning, progressive fibrosis, and high physiological fidelity to the human condition. *Am J Physiol Gastrointest Liver Physiol*, 2011: 301: p. G825-834 DOI: 10.1152/ajpgi.00145.2011.
  239. Zhu, Y., F. Lao, X. Pan, et al., Food Protein-Derived Antioxidant Peptides: Molecular Mechanism, Stability and Bioavailability. *Biomolecules*, 2022: 12 DOI: 10.3390/biom12111622.
  240. McCracken, E., M. Monaghan, and S. Sreenivasan, Pathophysiology of the metabolic syndrome. *Clin Dermatol*, 2018: 36: p. 14-20 DOI: 10.1016/j.clindermatol.2017.09.004.
  241. Putnam, K., R. Shoemaker, F. Yiannikouris, et al., The renin-angiotensin system: a target of and contributor to dyslipidemias, altered glucose homeostasis, and hypertension of the metabolic syndrome. *Am J Physiol Heart Circ Physiol*, 2012: 302: p. H1219-1230 DOI: 10.1152/ajpheart.00796.2011.
  242. Agoudemos, M.M. and A.S. Greene, Localization of the renin-angiotensin system components to the skeletal muscle microcirculation. *Microcirculation*, 2005: 12: p. 627-636 DOI: 10.1080/10739680500301664.
  243. Frantz, E.D., C. Crespo-Mascarenhas, A.R. Barreto-Vianna, et al., Renin-angiotensin system blockers protect pancreatic islets against diet-induced obesity and insulin resistance in mice. *PLoS One*, 2013: 8: p. e67192 DOI: 10.1371/journal.pone.0067192.
  244. van der Zijl, N.J., C.C. Moors, G.H. Goossens, et al., Valsartan improves  $\beta$ -cell function and insulin sensitivity in subjects with impaired glucose metabolism: a randomized controlled trial. *Diabetes Care*, 2011: 34: p. 845-851 DOI: 10.2337/dc10-2224.
  245. Wang, Y., R.B. Wei, Y. Yang, et al., Valsartan Alleviates Insulin Resistance in Skeletal Muscle of Chronic Renal Failure Rats. *Med Sci Monit*, 2018: 24: p. 2413-2419 DOI: 10.12659/msm.909910.
  246. Mitsuishi, M., K. Miyashita, A. Muraki, et al., Angiotensin II reduces mitochondrial content in skeletal muscle and affects glycemic control. *Diabetes*, 2009: 58: p. 710-717 DOI: 10.2337/db08-0949.
  247. Scientific concepts of functional foods in Europe-consensus document. *Br J Nutr*, 1999: 81: p. S1-S27.
  248. Shang, N., K.S. Bhullar, B.P. Hubbard, et al., Tripeptide IRW initiates differentiation in osteoblasts differentiation via the RUNX2 pathway. *Biochimica Et Biophysica Acta-General Subjects*, 2019: 1863: p. 1138-1146 DOI: 10.1016/j.bbagen.2019.04.007.

249. Martin, M. and A. Deussen, Effects of natural peptides from food proteins on angiotensin converting enzyme activity and hypertension. *Crit Rev Food Sci Nutr*, 2019: 59: p. 1264-1283 DOI: 10.1080/10408398.2017.1402750.
250. Liao, W., H. Fan, S.T. Davidge, et al., Egg White-Derived Antihypertensive Peptide IRW (Ile-Arg-Trp) Reduces Blood Pressure in Spontaneously Hypertensive Rats via the ACE2/Ang (1-7)/Mas Receptor Axis. *Mol Nutr Food Res*, 2019: 63: p. e1900063 DOI: 10.1002/mnfr.201900063.
251. Williams, L.M., F.M. Campbell, J.E. Drew, et al., The development of diet-induced obesity and glucose intolerance in C57BL/6 mice on a high-fat diet consists of distinct phases. *PLoS One*, 2014: 9: p. e106159 DOI: 10.1371/journal.pone.0106159.
252. Heikkinen, S., C.A. Argmann, M.F. Champy, et al., Evaluation of glucose homeostasis. *Curr Protoc Mol Biol*, 2007: Chapter 29: p. Unit 29B 23 DOI: 10.1002/0471142727.mb29b03s77.
253. Bustin, S.A., V. Benes, J.A. Garson, et al., The MIQE guidelines: minimum information for publication of quantitative real-time PCR experiments. *Clin Chem*, 2009: 55: p. 611-622 DOI: 10.1373/clinchem.2008.112797.
254. (NNHPD), N.-p.H.P.D., What are natural health products, H. Canada, Editor. 2004, Government of Canada: Ottawa.
255. Rivero-Pino, F., F.J. Espejo-Carpio, and E.M. Guadix, Antidiabetic Food-Derived Peptides for Functional Feeding: Production, Functionality and In Vivo Evidences. *Foods*, 2020: 9 DOI: 10.3390/foods9080983.
256. Grootaert, C., G. Jacobs, B. Matthijs, et al., Quantification of egg ovalbumin hydrolysate-derived anti-hypertensive peptides in an in vitro model combining luminal digestion with intestinal Caco-2 cell transport. *Food Res Int*, 2017a: 99: p. 531-541 DOI: 10.1016/j.foodres.2017.06.002.
257. Okada-Iwabu, M., T. Yamauchi, M. Iwabu, et al., A small-molecule AdipoR agonist for type 2 diabetes and short life in obesity. *Nature*, 2013: 503: p. 493-499 DOI: 10.1038/nature12656.
258. Jain, S.K., J. Rains, J. Croad, et al., Curcumin supplementation lowers TNF-alpha, IL-6, IL-8, and MCP-1 secretion in high glucose-treated cultured monocytes and blood levels of TNF-alpha, IL-6, MCP-1, glucose, and glycosylated hemoglobin in diabetic rats. *Antioxid Redox Signal*, 2009: 11: p. 241-249 DOI: 10.1089/ars.2008.2140.
259. Kawabeta, K., S. Hase-Tamaru, M. Yuasa, et al., Dietary beta-Conglycinin Modulates Insulin Sensitivity, Body Fat Mass, and Lipid Metabolism in Obese Otsuka Long-Evans Tokushima Fatty (OLETF) Rats. *J Oleo Sci*, 2019: 68: p. 339-350 DOI: 10.5650/jos.ess18232.
260. Matsui, T., M. Sato, M. Tanaka, et al., Vasodilating dipeptide Trp-His can prevent atherosclerosis in apo E-deficient mice. *Br J Nutr*, 2010: 103: p. 309-313 DOI: 10.1017/S0007114509991814.
261. Tanaka, M., S.M. Hong, S. Akiyama, et al., Visualized absorption of anti-atherosclerotic dipeptide, Trp-His, in Sprague-Dawley rats by LC-MS and MALDI-MS imaging analyses. *Mol Nutr Food Res*, 2015: 59: p. 1541-1549 DOI: 10.1002/mnfr.201500075.
262. Al Za'abi, M., B.H. Ali, Y. Al Suleimani, et al., The Effect of Metformin in Diabetic and Non-Diabetic Rats with Experimentally-Induced Chronic Kidney Disease. *Biomolecules*, 2021: 11 DOI: 10.3390/biom11060814.

263. Zhang, Z.M., Z.H. Liu, Q. Nie, et al., Metformin improves high-fat diet-induced insulin resistance in mice by downregulating the expression of long noncoding RNA NONMMUT031874.2. *Exp Ther Med*, 2022: 23: p. 332 DOI: 10.3892/etm.2022.11261.
264. Kurth-Kraczek, E.J., M.F. Hirshman, L.J. Goodyear, et al., 5' AMP-activated protein kinase activation causes GLUT4 translocation in skeletal muscle. *Diabetes*, 1999: 48: p. 1667-1671 DOI: 10.2337/diabetes.48.8.1667.
265. Bergeron, R., R.R. Russell, 3rd, L.H. Young, et al., Effect of AMPK activation on muscle glucose metabolism in conscious rats. *Am J Physiol*, 1999: 276: p. E938-944 DOI: 10.1152/ajpendo.1999.276.5.E938.
266. Liao, W., K.S. Bhullar, S. Chakrabarti, et al., Egg White-Derived Tripeptide IRW (Ile-Arg-Trp) Is an Activator of Angiotensin Converting Enzyme 2. *J Agric Food Chem*, 2018: 66: p. 11330-11336 DOI: 10.1021/acs.jafc.8b03501.
267. Gheblawi, M., K. Wang, A. Viveiros, et al., Angiotensin-Converting Enzyme 2: SARS-CoV-2 Receptor and Regulator of the Renin-Angiotensin System: Celebrating the 20th Anniversary of the Discovery of ACE2. *Circ Res*, 2020: 126: p. 1456-1474 DOI: 10.1161/CIRCRESAHA.120.317015.
268. Chai, W., W. Wang, J. Liu, et al., Angiotensin II type 1 and type 2 receptors regulate basal skeletal muscle microvascular volume and glucose use. *Hypertension*, 2010: 55: p. 523-530 DOI: 10.1161/HYPERTENSIONAHA.109.145409.
269. Huang, Y., Y. Li, Q. Liu, et al., Telmisartan attenuates obesity-induced insulin resistance via suppression of AMPK mediated ER stress. *Biochem Biophys Res Commun*, 2020: 523: p. 787-794 DOI: 10.1016/j.bbrc.2019.12.111.
270. Shinshi, Y., K. Higashiura, D. Yoshida, et al., Angiotensin II inhibits glucose uptake of skeletal muscle via the adenosine monophosphate-activated protein kinase pathway. *J Am Soc Hypertens*, 2007: 1: p. 251-255 DOI: 10.1016/j.jash.2007.04.007.
271. Ohshima, K., M. Mogi, F. Jing, et al., Direct angiotensin II type 2 receptor stimulation ameliorates insulin resistance in type 2 diabetes mice with PPARgamma activation. *PLoS One*, 2012: 7: p. e48387 DOI: 10.1371/journal.pone.0048387.
272. Olefsky, J.M., Treatment of insulin resistance with peroxisome proliferator-activated receptor gamma agonists. *J Clin Invest*, 2000: 106: p. 467-472 DOI: 10.1172/JCI10843.
273. Jiang, G., Q. Dallas-Yang, Z. Li, et al., Potentiation of insulin signaling in tissues of Zucker obese rats after acute and long-term treatment with PPARgamma agonists. *Diabetes*, 2002: 51: p. 2412-2419 DOI: 10.2337/diabetes.51.8.2412.
274. Hevener, A.L., W. He, Y. Barak, et al., Muscle-specific Pparg deletion causes insulin resistance. *Nat Med*, 2003: 9: p. 1491-1497 DOI: 10.1038/nm956.
275. Li, G.S., X.H. Liu, H. Zhu, et al., Skeletal muscle insulin resistance in hamsters with diabetes developed from obesity is involved in abnormal skeletal muscle LXR, PPAR and SREBP expression. *Exp Ther Med*, 2016: 11: p. 2259-2269 DOI: 10.3892/etm.2016.3209.
276. Amankwaah, A.F., J.L. Hudson, J.E. Kim, et al., Reductions in whole-body fat mass but not increases in lean mass predict changes in cardiometabolic health indices with exercise training among weight-stable adults. *Nutr Res*, 2019: 63: p. 63-69 DOI: 10.1016/j.nutres.2018.11.004.
277. Kim, G.H., J.Y. Ju, K.S. Chung, et al., Rice Hull Extract (RHE) Suppresses Adiposity in High-Fat Diet-Induced Obese Mice and Inhibits Differentiation of 3T3-L1 Preadipocytes. *Nutrients*, 2019: 11 DOI: 10.3390/nu11051162.

278. Quiroga, D.T., M.C. Munoz, C. Gil, et al., Chronic administration of the angiotensin type 2 receptor agonist C21 improves insulin sensitivity in C57BL/6 mice. *Physiol Rep*, 2018: 6: p. e13824 DOI: 10.14814/phy2.13824.
279. Nag, S., S. Patel, S. Mani, et al., Role of angiotensin type 2 receptor in improving lipid metabolism and preventing adiposity. *Mol Cell Biochem*, 2019: 461: p. 195-204 DOI: 10.1007/s11010-019-03602-y.
280. Fromme, T. and M. Klingenspor, Uncoupling protein 1 expression and high-fat diets. *Am J Physiol Regul Integr Comp Physiol*, 2011: 300: p. R1-8 DOI: 10.1152/ajpregu.00411.2010.
281. Seale, P., H.M. Conroe, J. Estall, et al., Prdm16 determines the thermogenic program of subcutaneous white adipose tissue in mice. *J Clin Invest*, 2011: 121: p. 96-105 DOI: 10.1172/JCI44271.
282. Cohen, P., J.D. Levy, Y. Zhang, et al., Ablation of PRDM16 and beige adipose causes metabolic dysfunction and a subcutaneous to visceral fat switch. *Cell*, 2014: 156: p. 304-316 DOI: 10.1016/j.cell.2013.12.021.
283. Rubio-Ruiz, M.E., V. Guarner-Lans, I. Perez-Torres, et al., Mechanisms Underlying Metabolic Syndrome-Related Sarcopenia and Possible Therapeutic Measures. *Int J Mol Sci*, 2019: 20 DOI: 10.3390/ijms20030647.
284. Albert, V. and M.N. Hall, mTOR signaling in cellular and organismal energetics. *Curr Opin Cell Biol*, 2015: 33: p. 55-66 DOI: 10.1016/j.ceb.2014.12.001.
285. Younossi, Z., Q.M. Anstee, M. Marietti, et al., Global burden of NAFLD and NASH: trends, predictions, risk factors and prevention. *Nat Rev Gastroenterol Hepatol*, 2018: 15: p. 11-20 DOI: 10.1038/nrgastro.2017.109.
286. Wiering, L. and F. Tacke, Treating inflammation to combat non-alcoholic fatty liver disease. *J Endocrinol*, 2023: 256 DOI: 10.1530/JOE-22-0194.
287. Prasun, P., I. Ginevic, and K. Oishi, Mitochondrial dysfunction in nonalcoholic fatty liver disease and alcohol related liver disease. *Transl Gastroenterol Hepatol*, 2021: 6: p. 4 DOI: 10.21037/tgh-20-125.
288. Ratziu, V., S.A. Harrison, S. Francque, et al., Elafibranor, an Agonist of the Peroxisome Proliferator-Activated Receptor-alpha and -delta, Induces Resolution of Nonalcoholic Steatohepatitis Without Fibrosis Worsening. *Gastroenterology*, 2016: 150: p. 1147-1159 e1145 DOI: 10.1053/j.gastro.2016.01.038.
289. Harrison, S.A., M.F. Abdelmalek, G. Neff, et al., Aldafermin in patients with non-alcoholic steatohepatitis (ALPINE 2/3): a randomised, double-blind, placebo-controlled, phase 2b trial. *Lancet Gastroenterol Hepatol*, 2022: 7: p. 603-616 DOI: 10.1016/S2468-1253(22)00017-6.
290. Garcia-Tsao, G., J. Bosch, Z. Kayali, et al., Randomized placebo-controlled trial of emricasan for non-alcoholic steatohepatitis-related cirrhosis with severe portal hypertension. *J Hepatol*, 2020: 72: p. 885-895 DOI: 10.1016/j.jhep.2019.12.010.
291. Nesto, R.W., D. Bell, R.O. Bonow, et al., Thiazolidinedione use, fluid retention, and congestive heart failure: a consensus statement from the American Heart Association and American Diabetes Association. *Diabetes Care*, 2004: 27: p. 256-263 DOI: 10.2337/diacare.27.1.256.
292. Stafylas, P.C., P.A. Sarafidis, and A.N. Lasaridis, The controversial effects of thiazolidinediones on cardiovascular morbidity and mortality. *Int J Cardiol*, 2009: 131: p. 298-304 DOI: 10.1016/j.ijcard.2008.06.005.

293. Singh, B.P., R.E. Aluko, S. Hati, et al., Bioactive peptides in the management of lifestyle-related diseases: Current trends and future perspectives. *Crit Rev Food Sci Nutr*, 2022: 62: p. 4593-4606 DOI: 10.1080/10408398.2021.1877109.
294. Evans, R.M., G.D. Barish, and Y.X. Wang, PPARs and the complex journey to obesity. *Nat Med*, 2004: 10: p. 355-361 DOI: 10.1038/nm1025.
295. Kahn, C.R., G. Wang, and K.Y. Lee, Altered adipose tissue and adipocyte function in the pathogenesis of metabolic syndrome. *J Clin Invest*, 2019: 129: p. 3990-4000 DOI: 10.1172/JCI129187.
296. Xu, H., Q. Zhao, N. Song, et al., AdipoR1/AdipoR2 dual agonist recovers nonalcoholic steatohepatitis and related fibrosis via endoplasmic reticulum-mitochondria axis. *Nat Commun*, 2020: 11: p. 5807 DOI: 10.1038/s41467-020-19668-y.
297. Bugianesi, E., U. Pagotto, R. Manini, et al., Plasma adiponectin in nonalcoholic fatty liver is related to hepatic insulin resistance and hepatic fat content, not to liver disease severity. *J Clin Endocrinol Metab*, 2005: 90: p. 3498-3504 DOI: 10.1210/jc.2004-2240.
298. Fullerton, M.D., S. Galic, K. Marcinko, et al., Single phosphorylation sites in Acc1 and Acc2 regulate lipid homeostasis and the insulin-sensitizing effects of metformin. *Nat Med*, 2013: 19: p. 1649-1654 DOI: 10.1038/nm.3372.
299. Steinberg, G.R., S.L. Macaulay, M.A. Febbraio, et al., AMP-activated protein kinase--the fat controller of the energy railroad. *Can J Physiol Pharmacol*, 2006: 84: p. 655-665 DOI: 10.1139/y06-005.
300. Vila, L., I. Elias, C. Roca, et al., AAV8-mediated Sirt1 gene transfer to the liver prevents high carbohydrate diet-induced nonalcoholic fatty liver disease. *Mol Ther Methods Clin Dev*, 2014: 1: p. 14039 DOI: 10.1038/mtm.2014.39.
301. Wang, L.F., X.N. Wang, C.C. Huang, et al., Inhibition of NAMPT aggravates high fat diet-induced hepatic steatosis in mice through regulating Sirt1/AMPKalpha/SREBP1 signaling pathway. *Lipids Health Dis*, 2017: 16: p. 82 DOI: 10.1186/s12944-017-0464-z.
302. Zhou, C.C., X. Yang, X. Hua, et al., Hepatic NAD(+) deficiency as a therapeutic target for non-alcoholic fatty liver disease in ageing. *Br J Pharmacol*, 2016: 173: p. 2352-2368 DOI: 10.1111/bph.13513.
303. Canto, C. and J. Auwerx, PGC-1alpha, SIRT1 and AMPK, an energy sensing network that controls energy expenditure. *Curr Opin Lipidol*, 2009: 20: p. 98-105 DOI: 10.1097/MOL.0b013e328328d0a4.
304. Morris, E.M., R.S. Rector, J.P. Thyfault, et al., Mitochondria and redox signaling in steatohepatitis. *Antioxid Redox Signal*, 2011: 15: p. 485-504 DOI: 10.1089/ars.2010.3795.
305. Garcia-Ruiz, I., P. Solis-Munoz, D. Fernandez-Moreira, et al., High-fat diet decreases activity of the oxidative phosphorylation complexes and causes nonalcoholic steatohepatitis in mice. *Dis Model Mech*, 2014: 7: p. 1287-1296 DOI: 10.1242/dmm.016766.
306. Garcia-Ruiz, I., P. Solis-Munoz, D. Fernandez-Moreira, et al., NADPH oxidase is implicated in the pathogenesis of oxidative phosphorylation dysfunction in mice fed a high-fat diet. *Sci Rep*, 2016: 6: p. 23664 DOI: 10.1038/srep23664.
307. Morris, E.M., G.M. Meers, F.W. Booth, et al., PGC-1alpha overexpression results in increased hepatic fatty acid oxidation with reduced triacylglycerol accumulation and secretion. *Am J Physiol Gastrointest Liver Physiol*, 2012: 303: p. G979-992 DOI: 10.1152/ajpgi.00169.2012.

308. Fromenty, B. and M. Roden, Mitochondrial alterations in fatty liver diseases. *J Hepatol*, 2023: 78: p. 415-429 DOI: 10.1016/j.jhep.2022.09.020.
309. Joaquim, M. and M. Escobar-Henriques, Role of Mitofusins and Mitophagy in Life or Death Decisions. *Front Cell Dev Biol*, 2020: 8: p. 572182 DOI: 10.3389/fcell.2020.572182.
310. Caldwell, S.H., R.H. Swerdlow, E.M. Khan, et al., Mitochondrial abnormalities in non-alcoholic steatohepatitis. *J Hepatol*, 1999: 31: p. 430-434 DOI: 10.1016/s0168-8278(99)80033-6.
311. Lotowska, J.M., M.E. Sobaniec-Lotowska, S.B. Bockowska, et al., Pediatric non-alcoholic steatohepatitis: the first report on the ultrastructure of hepatocyte mitochondria. *World J Gastroenterol*, 2014: 20: p. 4335-4340 DOI: 10.3748/wjg.v20.i15.4335.
312. Yamada, T., D. Murata, Y. Adachi, et al., Mitochondrial Stasis Reveals p62-Mediated Ubiquitination in Parkin-Independent Mitophagy and Mitigates Nonalcoholic Fatty Liver Disease. *Cell Metab*, 2018: 28: p. 588-604 e585 DOI: 10.1016/j.cmet.2018.06.014.
313. Gong, F., L. Gao, and T. Ding, IDH2 protects against nonalcoholic steatohepatitis by alleviating dyslipidemia regulated by oxidative stress. *Biochem Biophys Res Commun*, 2019: 514: p. 593-600 DOI: 10.1016/j.bbrc.2019.04.069.
314. Hernandez-Alvarez, M.I., D. Sebastian, S. Vives, et al., Deficient Endoplasmic Reticulum-Mitochondrial Phosphatidylserine Transfer Causes Liver Disease. *Cell*, 2019: 177: p. 881-895 e817 DOI: 10.1016/j.cell.2019.04.010.
315. Hu, H., L. Guo, J. Overholser, et al., Mitochondrial VDAC1: A Potential Therapeutic Target of Inflammation-Related Diseases and Clinical Opportunities. *Cells*, 2022: 11 DOI: 10.3390/cells11193174.
316. Hallberg, M., D.L. Morganstein, E. Kiskinis, et al., A functional interaction between RIP140 and PGC-1alpha regulates the expression of the lipid droplet protein CIDEA. *Mol Cell Biol*, 2008: 28: p. 6785-6795 DOI: 10.1128/MCB.00504-08.
317. Sans, A., S. Bonnafous, D. Rousseau, et al., The Differential Expression of Cide Family Members is Associated with Nafld Progression from Steatosis to Steatohepatitis. *Sci Rep*, 2019: 9: p. 7501 DOI: 10.1038/s41598-019-43928-7.
318. Viswakarma, N., S. Yu, S. Naik, et al., Transcriptional regulation of Cidea, mitochondrial cell death-inducing DNA fragmentation factor alpha-like effector A, in mouse liver by peroxisome proliferator-activated receptor alpha and gamma. *J Biol Chem*, 2007: 282: p. 18613-18624 DOI: 10.1074/jbc.M701983200.
319. Murakami, K., Y. Sasaki, M. Asahiyama, et al., Selective PPARalpha Modulator Pemafibrate and Sodium-Glucose Cotransporter 2 Inhibitor Tofogliflozin Combination Treatment Improved Histopathology in Experimental Mice Model of Non-Alcoholic Steatohepatitis. *Cells*, 2022: 11 DOI: 10.3390/cells11040720.
320. Tang, S., F. Wu, X. Lin, et al., The Effects of New Selective PPARalpha Agonist CP775146 on Systematic Lipid Metabolism in Obese Mice and Its Potential Mechanism. *J Diabetes Res*, 2020: 2020: p. 4179852 DOI: 10.1155/2020/4179852.
321. Akazawa, S., F. Sun, M. Ito, et al., Efficacy of troglitazone on body fat distribution in type 2 diabetes. *Diabetes Care*, 2000: 23: p. 1067-1071 DOI: 10.2337/diacare.23.8.1067.
322. Patel, J., R.J. Anderson, and E.B. Rappaport, Rosiglitazone monotherapy improves glycaemic control in patients with type 2 diabetes: a twelve-week, randomized, placebo-controlled study. *Diabetes Obes Metab*, 1999: 1: p. 165-172 DOI: 10.1046/j.1463-1326.1999.00020.x.

323. Bastien, M., P. Poirier, P. Brassard, et al., Effect of PPARgamma agonist on aerobic exercise capacity in relation to body fat distribution in men with type 2 diabetes mellitus and coronary artery disease: a 1-yr randomized study. *Am J Physiol Endocrinol Metab*, 2019: 317: p. E65-E73 DOI: 10.1152/ajpendo.00505.2018.
324. Hiradate, R., I.A. Khalil, A. Matsuda, et al., A novel dual-targeted rosiglitazone-loaded nanoparticle for the prevention of diet-induced obesity via the browning of white adipose tissue. *J Control Release*, 2021: 329: p. 665-675 DOI: 10.1016/j.jconrel.2020.10.002.
325. Chen, M.T., J.S. Huang, D.D. Gao, et al., Combined treatment with FABP4 inhibitor ameliorates rosiglitazone-induced liver steatosis in obese diabetic db/db mice. *Basic Clin Pharmacol Toxicol*, 2021: 129: p. 173-182 DOI: 10.1111/bcpt.13621.
326. Qu, P., O. Rom, K. Li, et al., DT-109 ameliorates nonalcoholic steatohepatitis in nonhuman primates. *Cell Metab*, 2023: 35: p. 742-757 e710 DOI: 10.1016/j.cmet.2023.03.013.
327. Hall, J.E., J.P. Granger, J.M. do Carmo, et al., Hypertension: physiology and pathophysiology. *Compr Physiol*, 2012: 2: p. 2393-2442 DOI: 10.1002/cphy.c110058.
328. Yao, J., S. Fan, X. Shi, et al., Angiotensin-converting enzyme inhibitors versus angiotensin II receptor blockers on insulin sensitivity in hypertensive patients: A meta-analysis of randomized controlled trials. *PLoS One*, 2021: 16: p. e0253492 DOI: 10.1371/journal.pone.0253492.
329. Unger, T., U.M. Steckelings, and V.J. Dzau, Chapter 1 - The Angiotensin AT2 Receptor: From Enigma to Therapeutic Target, in *The Protective Arm of the Renin Angiotensin System (RAS)*, T. Unger, U.M. Steckelings, and R.A.S. dos Santos, Editors. 2015, Academic Press: Boston. p. 1-9.
330. Carey, R.M., Cardiovascular and renal regulation by the angiotensin type 2 receptor: the AT2 receptor comes of age. *Hypertension*, 2005: 45: p. 840-844 DOI: 10.1161/01.HYP.0000159192.93968.8f.
331. Patel, V.B., J.C. Zhong, M.B. Grant, et al., Role of the ACE2/Angiotensin 1-7 Axis of the Renin-Angiotensin System in Heart Failure. *Circ Res*, 2016: 118: p. 1313-1326 DOI: 10.1161/CIRCRESAHA.116.307708.
332. Olivares-Reyes, J.A., A. Arellano-Plancarte, and J.R. Castillo-Hernandez, Angiotensin II and the development of insulin resistance: implications for diabetes. *Mol Cell Endocrinol*, 2009: 302: p. 128-139 DOI: 10.1016/j.mce.2008.12.011.
333. Wang, C.H., H.M. Liu, Z.Y. Chang, et al., Losartan Prevents Hepatic Steatosis and Macrophage Polarization by Inhibiting HIF-1alpha in a Murine Model of NAFLD. *Int J Mol Sci*, 2021: 22 DOI: 10.3390/ijms22157841.
334. Liu, H.M., C.H. Wang, Z.Y. Chang, et al., Losartan Attenuates Insulin Resistance and Regulates Browning Phenomenon of White Adipose Tissue in ob/ob Mice. *Curr Issues Mol Biol*, 2021: 43: p. 1828-1843 DOI: 10.3390/cimb43030128.
335. Loloi, J., A.J. Miller, S.S. Bingaman, et al., Angiotensin-(1-7) contributes to insulin-sensitizing effects of angiotensin-converting enzyme inhibition in obese mice. *Am J Physiol Endocrinol Metab*, 2018: 315: p. E1204-E1211 DOI: 10.1152/ajpendo.00281.2018.
336. Shiuchi, T., T.X. Cui, L. Wu, et al., ACE inhibitor improves insulin resistance in diabetic mouse via bradykinin and NO. *Hypertension*, 2002: 40: p. 329-334 DOI: 10.1161/01.hyp.0000028979.98877.0c.

337. Shum, M., S. Pinard, M.O. Guimond, et al., Angiotensin II type 2 receptor promotes adipocyte differentiation and restores adipocyte size in high-fat/high-fructose diet-induced insulin resistance in rats. *Am J Physiol Endocrinol Metab*, 2013: 304: p. E197-210 DOI: 10.1152/ajpendo.00149.2012.
338. Wu, J., A Novel Angiotensin Converting Enzyme 2 (ACE2) Activating Peptide: A Reflection of 10 Years of Research on a Small Peptide Ile-Arg-Trp (IRW). *J Agric Food Chem*, 2020: 68: p. 14402-14408 DOI: 10.1021/acs.jafc.0c05544.
339. Ashkar, F., K.S. Bhullar, X. Jiang, et al. Tripeptide IRW Improves AMPK/eNOS Signaling Pathway via Activating ACE2 in the Aorta of High-Fat-Diet-Fed C57BL/6 Mice. *Biology*, 2023. 12, DOI: 10.3390/biology12040556.
340. Yang, M., X. Ma, X. Xuan, et al., Liraglutide Attenuates Non-Alcoholic Fatty Liver Disease in Mice by Regulating the Local Renin-Angiotensin System. *Front Pharmacol*, 2020: 11: p. 432 DOI: 10.3389/fphar.2020.00432.
341. Chen, S., Z. Lu, H. Jia, et al., Hepatocyte-specific Mas activation enhances lipophagy and fatty acid oxidation to protect against acetaminophen-induced hepatotoxicity in mice. *J Hepatol*, 2023: 78: p. 543-557 DOI: 10.1016/j.jhep.2022.10.028.
342. Song, L.N., J.Y. Liu, T.T. Shi, et al., Angiotensin-(1-7), the product of ACE2 ameliorates NAFLD by acting through its receptor Mas to regulate hepatic mitochondrial function and glycolipid metabolism. *FASEB J*, 2020: 34: p. 16291-16306 DOI: 10.1096/fj.202001639R.
343. Liu, J., X. Li, Q. Lu, et al., AMPK: a balancer of the renin-angiotensin system. *Biosci Rep*, 2019: 39 DOI: 10.1042/BSR20181994.
344. Palmer, J.P., R.M. Walter, and J.W. Ensink, Arginine-stimulated acute phase of insulin and glucagon secretion. I. in normal man. *Diabetes*, 1975: 24: p. 735-740 DOI: 10.2337/diab.24.8.735.
345. Heeboll, S., J. Risikesan, S. Ringgaard, et al., Impaired Glucagon-Mediated Suppression of VLDL-Triglyceride Secretion in Individuals With Metabolic Dysfunction-Associated Fatty Liver Disease (MAFLD). *Diabetes*, 2022: 71: p. 2402-2411 DOI: 10.2337/db22-0313.
346. Galsgaard, K.D., J. Pedersen, F.K. Knop, et al., Glucagon Receptor Signaling and Lipid Metabolism. *Front Physiol*, 2019: 10: p. 413 DOI: 10.3389/fphys.2019.00413.
347. Jiang, X. and J. Wu, Structure and activity study of tripeptide IRW in TNF-alpha induced insulin resistant skeletal muscle cells. *Food Funct*, 2022: 13: p. 4061-4068 DOI: 10.1039/d1fo02893f.
348. Hauner, H., The mode of action of thiazolidinediones. *Diabetes Metab Res Rev*, 2002: 18 Suppl 2: p. S10-15 DOI: 10.1002/dmrr.249.
349. Yang, F.-j., X. Chen, M.-c. Huang, et al., Molecular characteristics and structure–activity relationships of food-derived bioactive peptides. *Journal of Integrative Agriculture*, 2021: 20: p. 2313-2332 DOI: 10.1016/S2095-3119(20)63463-3.
350. Daskaya-Dikmen, C., A. Yucetepe, F. Karbancioglu-Guler, et al., Angiotensin-I-Converting Enzyme (ACE)-Inhibitory Peptides from Plants. *Nutrients*, 2017: 9 DOI: 10.3390/nu9040316.
351. Cersosimo, E. and R.A. DeFronzo, Insulin resistance and endothelial dysfunction: the road map to cardiovascular diseases. *Diabetes Metab Res Rev*, 2006: 22: p. 423-436 DOI: 10.1002/dmrr.634.

352. Laakso, M., S.V. Edelman, G. Brechtel, et al., Decreased effect of insulin to stimulate skeletal muscle blood flow in obese man. A novel mechanism for insulin resistance. *J Clin Invest*, 1990: 85: p. 1844-1852 DOI: 10.1172/JCI114644.
353. Olefsky, J., J.W. Farquhar, and G. Reaven, Relationship between fasting plasma insulin level and resistance to insulin-mediated glucose uptake in normal and diabetic subjects. *Diabetes*, 1973: 22: p. 507-513 DOI: 10.2337/diab.22.7.507.
354. Arcaro, G., A. Cretti, S. Balzano, et al., Insulin causes endothelial dysfunction in humans: sites and mechanisms. *Circulation*, 2002: 105: p. 576-582 DOI: 10.1161/hc0502.103333.
355. Bejjani, S. and J. Wu, Transport of IRW, an ovotransferrin-derived antihypertensive peptide, in human intestinal epithelial Caco-2 cells. *J Agric Food Chem*, 2013: 61: p. 1487-1492 DOI: 10.1021/jf302904t.
356. Guo, Y., X. Huang, W. Liao, et al., Discovery and Optimization of Highly Potent and Selective AT(2)R Antagonists to Relieve Peripheral Neuropathic Pain. *ACS Omega*, 2021: 6: p. 15412-15420 DOI: 10.1021/acsomega.1c01866.
357. Munoz, M.C., V. Burghi, J.G. Miquet, et al., Chronic blockade of the AT2 receptor with PD123319 impairs insulin signaling in C57BL/6 mice. *Peptides*, 2017: 88: p. 37-45 DOI: 10.1016/j.peptides.2016.12.003.
358. Lubel, J.S., C.B. Herath, J. Tchongue, et al., Angiotensin-(1-7), an alternative metabolite of the renin-angiotensin system, is up-regulated in human liver disease and has antifibrotic activity in the bile-duct-ligated rat. *Clin Sci (Lond)*, 2009: 117: p. 375-386 DOI: 10.1042/CS20080647.
359. Ichiki, T., P.A. Labosky, C. Shiota, et al., Effects on blood pressure and exploratory behaviour of mice lacking angiotensin II type-2 receptor. *Nature*, 1995: 377: p. 748-750 DOI: 10.1038/377748a0.
360. Silva, A.R., E.C. Aguilar, J.I. Alvarez-Leite, et al., Mas receptor deficiency is associated with worsening of lipid profile and severe hepatic steatosis in ApoE-knockout mice. *Am J Physiol Regul Integr Comp Physiol*, 2013: 305: p. R1323-1330 DOI: 10.1152/ajpregu.00249.2013.
361. Xu, J., Structure and activity study of IRW on improving insulin sensitivity. Department of Agricultural, Food and Nutritional Science, 2022: Master of Science DOI: 10.7939/r3-me6g-8422.
362. Aoyama, T., K. Fukui, K. Takamatsu, et al., Soy protein isolate and its hydrolysate reduce body fat of dietary obese rats and genetically obese mice (yellow KK). *Nutrition*, 2000: 16: p. 349-354 DOI: 10.1016/s0899-9007(00)00230-6.
363. Liyanage, R., K.H. Han, S. Watanabe, et al., Potato and soy peptide diets modulate lipid metabolism in rats. *Biosci Biotechnol Biochem*, 2008: 72: p. 943-950 DOI: 10.1271/bbb.70593.
364. Zhu, G. and A.S. Lee, Role of the unfolded protein response, GRP78 and GRP94 in organ homeostasis. *J Cell Physiol*, 2015: 230: p. 1413-1420 DOI: 10.1002/jcp.24923.
365. Lee, S., S. Kim, S. Hwang, et al., Dysregulated expression of proteins associated with ER stress, autophagy and apoptosis in tissues from nonalcoholic fatty liver disease. *Oncotarget*, 2017: 8: p. 63370-63381 DOI: 10.18632/oncotarget.18812.
366. Duffuler, P., K.S. Bhullar, S.C. de Campos Zani, et al., Bioactive Peptides: From Basic Research to Clinical Trials and Commercialization. *J Agric Food Chem*, 2022: 70: p. 3585-3595 DOI: 10.1021/acs.jafc.1c06289.

## **APPENDIX 1**

PDF file for the paper published and included in this thesis in Chapter 3

# An Egg White-Derived Peptide Enhances Systemic Insulin Sensitivity and Modulates Markers of Non-Alcoholic Fatty Liver Disease in Obese, Insulin Resistant Mice

Stepheny C. de Campos Zani <sup>1,2</sup>, Ren Wang <sup>3</sup>, Hellen Veida-Silva <sup>1,2</sup>, Robin D. Clugston <sup>1</sup>, Jessica T. Y. Yue <sup>1,2,4</sup>, Marcelo A. Mori <sup>5</sup>, Jianping Wu <sup>3</sup> and Catherine B. Chan <sup>1,2,3,\*</sup>

<sup>1</sup> Department of Physiology, University of Alberta, Edmonton, AB T6G 2H7, Canada

<sup>2</sup> Alberta Diabetes Institute, University of Alberta, Edmonton, AB T6G 2E1, Canada

<sup>3</sup> Department of Agricultural Food & Nutritional Science, University of Alberta, Edmonton, AB T6G 1C9, Canada

<sup>4</sup> Molecular and Cell Biology of Lipids Group, University of Alberta, Edmonton, AB T6G 2H7, Canada

<sup>5</sup> Department of Biochemistry and Tissue biology, University of Campinas, Campinas P.O. Box 6109, Brazil

\* Correspondence: cbchan@ualberta.ca; Tel.: +1-780-492-9964

**Citation:** de Campos Zani, S.C.; Wang, R.; Veida-Silva, H.; Clugston, R.D.; Yue, J.T.Y.; Mori, M.A.; Chan, C. An Egg White-Derived Peptide Enhances Systemic Insulin Sensitivity and Modulates Markers of Non-Alcoholic Fatty Liver Disease in Obese, Insulin Resistant Mice. *Metabolites* **2023**, *13*, 174. <https://doi.org/10.3390/metabo13020174>

Academic Editors: Kamila Kasprzak-Drozd, Przemysław Niziński and Anna Oniszczuk

Received: 5 January 2023

Revised: 16 January 2023

Accepted: 20 January 2023

Published: 24 January 2023



**Copyright:** © 2023 by the authors. Licensee MDPI, Basel, Switzerland. This article is an open access article distributed under the terms and conditions of the Creative Commons Attribution (CC BY) license (<https://creativecommons.org/licenses/by/4.0/>).

**Abstract:** Non-alcoholic fatty liver disease (NAFLD), the hepatic manifestation of the metabolic syndrome, is a global health problem. Currently, no pharmacological treatment is approved for NAFLD. Natural health products, including bioactive peptides, are potential candidates to aid in the management of metabolic syndrome-related conditions, including insulin resistance and obesity. In this study, we hypothesized that an egg-white-derived bioactive peptide QAMPFRVTEQE (Peptide 2) would improve systemic and local white adipose tissue insulin sensitivity, thereby preventing high-fat diet-induced exacerbation of pathological features associated with NAFLD, such as lipid droplet size and number, inflammation, and hepatocyte hypertrophy in high-fat diet-fed mice. Similar to rosiglitazone, Peptide 2 supplementation improved systemic insulin resistance during the hyperinsulinemic-euglycemic clamp and enhanced insulin signalling in white adipose tissue, modulating ex vivo lipolysis. In the liver, compared with high-fat diet fed animals, Peptide 2 supplemented animals presented decreased hepatic cholesterol accumulation ( $p < 0.05$ ) and area of individual hepatic lipid droplet by around 50% ( $p = 0.09$ ) and reduced hepatic inflammatory infiltration ( $p < 0.05$ ) whereas rosiglitazone exacerbated steatosis. In conclusion, Peptide 2 supplementation improved insulin sensitivity and decreased hepatic steatosis, unlike the insulin-sensitizing drug rosiglitazone.

**Keywords:** Bioactive peptides; egg; metabolic syndrome; non-alcoholic fatty liver disease; type 2 diabetes

## 1. Introduction

Metabolic syndrome pathophysiology exemplifies a clear crosstalk between major metabolic organs, including the liver and white adipose tissue (WAT). Non-alcoholic fatty liver disease (NAFLD) affects 25% of the global population and is strongly associated with obesity, type 2 diabetes (T2D)/insulin resistance (IR), and dyslipidemia. All of these conditions are a public health concern and beget socioeconomic problems [1]. Hepatic steatosis in NAFLD results from an imbalance between substrate availability (fatty acids and carbohydrates) and the hepatic capacity to dispose of fats properly. In humans, the two main sources of non-esterified fatty acids (NEFA) in the liver are WAT lipolysis and de novo lipogenesis (DNL) [2]. DNL produces fatty acids from non-lipid precursors such as glucose or fructose and is increased in IR states [3], and plays an important role in NAFLD [4]. NAFLD may progress to non-alcoholic steatohepatitis (NASH) in which

inflammation, fibrosis and cellular damage are present, then to cirrhosis and further to hepatic cancer, increasing the need for liver transplantation [2] and seriously impacting quality of life.

Lifestyle interventions (diet and physical activity) improve NAFLD, but currently no pharmacological treatment is approved for NAFLD. Several drugs, including thiazolidinediones (peroxisome proliferator-activated receptor gamma (PPAR $\gamma$ ) agonists that are insulin sensitizers) are being investigated as therapies to reduce hepatic steatosis, inflammation, and fibrosis [5,6]. However, findings are controversial [7,8]. Natural health products and functional foods include potential candidates to aid in the management of metabolic conditions. Food-derived bioactive peptides have effects beyond their nutritive value and can modulate physiological processes promoting health benefits [9]. There are many food sources of bioactive peptides, including the egg, a universally available and consumed source of protein.

Previously, our group showed that an egg white hydrolysate (EWH) alleviates hypertension [10] and IR in rat models [11], and mimics insulin action in preadipocytes [12]. In addition, IRW, a specific peptide found in the EWH improves hypertension [13] and IR in rodents [14]. Another peptide identified in the EWH is QAMPFRVTEQE (aka Peptide 2), which mimics insulin actions to enhance PPAR $\gamma$  protein abundance and other markers of adipogenesis in preadipocyte cell culture [15] but its *in vivo* efficacy is not established. Considering the need of new therapies for NAFLD and the crosstalk between insulin signaling, WAT and the liver, we aimed to identify specific effects of Peptide 2 diet supplementation on manifestations of the metabolic syndrome including systemic IR, WAT response to insulin and NAFLD markers, compared with the thiazolidinedione rosiglitazone. We hypothesized that Peptide 2 supplementation improves systemic and local insulin sensitivity, which in turn alleviates pathological cellular features associated with NAFLD, therefore modulating both glucose and lipid metabolism.

## 2. Materials and Methods

### 2.1. Animals and Diet

Protocol 1: This protocol and some results of a previous intervention trial were previously published by our group [11]. Briefly, male Sprague Dawley (SD) rats ( $n = 48$ ) were fed with high fat diet (HFD) for 6 wks. Then, half of the animals received HFD+4% EWH with the remainder serving as HFD controls for another 6 wks. At the end of week 12, half of the animals received an intraperitoneal injection of insulin (2 IU/kg of body weight (BW)) to stimulate insulin signaling prior to euthanization using CO<sub>2</sub>. Diet composition was published elsewhere [11] and was matched for macronutrient and energy content. Herein, we report lipolysis pathway data from WAT tissues; a full description of the rat phenotype after EWH treatment is published elsewhere [11].

Protocol 2: Male C57BL/6 mice (5 wks old) purchased from Charles River Canada were housed 4/cage with *ad libitum* access to food and water, exposed to 12:12 h light:dark in a humidity- and temperature-controlled environment (60% humidity, 23 °C). Mice received a low fat diet (LFD, 10% kcal fat) or a high fat diet (HFD, 45% kcal fat) for 6 wks. After that, the HFD animals were divided into 3 groups: HFD only, HFD + Peptide 2 (PEP2) and HFD + rosiglitazone (ROSI) and continued receiving their respective diets for another 8 wks. LFD animals continued receiving LFD for another 8 wks. After a total of 14 wks, mice either received an intraperitoneal injection of insulin (1.5 IU/kg BW) prior to euthanasia or were directly euthanized using CO<sub>2</sub>, while some mice underwent hyperinsulinemic-euglycemic clamp prior to euthanasia by ketamine. Diet composition is shown in Table S1. Peptide 2 was administered at 45 mg/Kg BW/day daily mixed in the diet. The characteristics of Peptide 2 are reported in Table 1 [15]; it was synthesized by Genscript (Piscataway, NJ, USA) with 97.9% compound purity and no terminus modifications. Peptide 2 is soluble in water, dimethyl sulfoxide and phosphate buffered saline at a concentration  $\leq 10$  mg/mL. High performance liquid chromatography chromatogram and the

mass spectra of the peptide provided by Genscript are shown in Figure S1. Rosiglitazone (Sigma-Aldrich, ST. Louis, MA, USA) was administered at 2.5  $\mu\text{mol/kg}$  BW/day in the drinking water.

**Table 1.** Peptide 2 specifications.

	<b>Peptide 2</b>
Amino acid sequence	QAMPFRVTEQE
Number of amino acids	11
Theoretical molecular weight (g/mol) *	1335.50
Observed molecular weight (g/mol)	1335.8
Theoretical isoelectric point *	4.53
Grand average of hydropathicity (GRAVY) *	-0.918
Hydrophobicity *	22
Terminus modifications	None
Net charge at pH 7.0 *	-1

\* Parameters calculated using online tools: ProtParam (Expasy); Bachem peptide calculator and Thermofischer Peptide analyzing tool. Observed molecular weight provided by Genscript.

## 2.2. Body Weight, Body Composition and Sample Collection

Mice were weighed weekly. Body composition was measured at week 14 in fasted conditions using an ECHO magnetic resonance imaging (ECHO MRI) as per manufacturer's instructions. Blood was collected by cardiac puncture into EDTA tubes and plasma was stored at  $-80\text{ }^{\circ}\text{C}$  until further analysis. Liver and WAT (retroperitoneal (rWAT), epididymal (eWAT) and inguinal (iWAT)) were collected, weighed and snap frozen in liquid nitrogen. A sample of each tissue was fixed in formalin, dehydrated and preserved in paraffin blocks for histological analysis.

## 2.3. Adipose Tissue Organ Culture

During tissue collection, a piece of approx. 100 mg each and of each fat pad (iWAT, eWAT and rWAT) were collected and washed with cold phosphate-buffered saline + 1% penicillin/streptomycin (Gibco, Waltham, MA, USA) and kept in M199 media (Sigma-Aldrich, St. Louis, MA, USA) supplemented with 50  $\mu\text{U}$  insulin (Sigma-Aldrich, St. Louis, MA, USA), 2.5 nM dexamethasone (Sigma-Aldrich, St. Louis, MA, USA) and 1% penicillin/streptomycin in a cell incubator at  $37\text{ }^{\circ}\text{C}$  for 24 h. After that, the media was replaced with fresh M199 supplemented only with 2.5% fatty acid-free bovine serum albumin (MP Biomedicals, St Ana, CA, USA). Each piece received one of the following treatments: sterile  $\text{H}_2\text{O}$  or norepinephrine (1  $\mu\text{M}$ , Sigma-Aldrich, St. Louis, MA, USA) or norepinephrine (1  $\mu\text{M}$ ) + insulin (1 IU/mL) for 2 h. An aliquot of the media was collected after 2 h and kept at  $-80\text{ }^{\circ}\text{C}$  for future glycerol analysis.

## 2.4. Preadipocyte Cell Culture

Preadipocytes derived from mouse inguinal WAT (9 W) and from brown adipose tissue (9 B) were cultured and differentiated as previously described [16]. Briefly, cells were cultured in Dulbecco's modified Eagle's medium (DMEM) containing 10% of fetal bovine serum and 1% penicillin/streptomycin until confluence was reached. After that, cells were differentiated in DMEM containing 20 nM insulin, 1 nM triiodothyronine, 0.5 mM isobutyl methylxanthine, 1  $\mu\text{M}$  dexamethasone, 0.125 mM indomethacin, and 2.8  $\mu\text{M}$  of rosiglitazone. Because we wanted to compare the effect of Peptide 2 with rosiglitazone during preadipocyte differentiation, we modified the above differentiation cocktail as follows: the control (C) received the cocktail described above, the C+PEP2 was treated with the above cocktail supplemented with 100  $\mu\text{M}$  of Peptide 2, the negative control (Rosi neg) received the above cocktail without rosiglitazone and the Rosi neg+PEP2 received the above cocktail without rosiglitazone but supplemented with Peptide 2 (100  $\mu\text{M}$ ).

### 2.5. Hyperinsulinemic-Euglycemic Clamp

The euglycemic clamp was performed as previously described [17,18] with the following modifications: briefly, mice were anaesthetized using ketamine (90 mg/kg BW) and xylazine (10 mg/kg BW) and underwent aseptic right jugular vein catheterization for intravenous infusions. Post-surgical body weight and food intake were monitored daily. After 3–4 days (to re-establish a minimum of 90% of pre-surgical BW), the mice were fasted for 5 h and underwent a hyperinsulinemic-euglycemic clamp, in which a primed, continuous infusion of tritiated glucose (1  $\mu$ Ci bolus + 0.1  $\mu$ Ci infusion; Perkin Elmer, Waltham, MA, USA) was maintained for the duration of the experiment to assess glucose kinetics. After a basal period, the hyperinsulinemic-euglycemic clamp was initiated with a primed, continuous infusion of insulin (3.0 mU/kg/min) for 120 min, and plasma glucose levels were maintained at a similar euglycemic level to the basal period using a variable infusion of 10% glucose solution. Plasma samples were obtained every 10 min for the measurement of glucose concentration (Analox Glucose Analyzer, Huntington beach, CA, USA) and [3-<sup>3</sup>H]-glucose specific activity. At conclusion of the clamp period, mice were euthanized using an infusion of 0.02 mL ketamine via the jugular vein, followed by decapitation.

### 2.6. Oral Glucose Tolerance Test (OGTT)

OGTT were performed at week 13. Briefly, after overnight fasting a bolus of glucose (1 g/kg BW) was orally gavaged to mice and blood glucose was measured after 0, 15, 30, 60, 90, and 120 min from the tail vein using a glucometer (Contour<sup>®</sup>Next, Mississauga, ON, CA). OGTT were performed at week 14. After 4 hr fasting, mice received an intraperitoneal injection with insulin (0.75 U/Kg BW) and glucose was measured after 0, 15, 30, 60, 90, and 120 min as cited above.

### 2.7. Liver Triglyceride and Cholesterol Content

Liver triglyceride (TG) and cholesterol were extracted using approximately 100 mg of tissue and as previously described [19]. Briefly, tissue was homogenized in 1 mL of NaCl solution. A total of 500  $\mu$ L of the extract was mixed with 2 mL of Folch solution (chloroform:methanol (2:1)), centrifuged at 3000 $\times$  g rpm for 10 min and the lower phase collected. Samples were dried under nitrogen and resuspended with 1 mL of 2% TritonX-100 solution in chloroform and dried under nitrogen. The dried sample was then resuspended in ddH<sub>2</sub>O and kept at -20 °C until further use. Triglyceride and cholesterol content was measured using a commercial kit (Infinity<sup>™</sup>, Thermo Scientific, Waltham, MA, USA).

### 2.8. PPAR $\gamma$ DNA Binding Activity

Nuclear protein extraction was performed using a commercial kit (Active Motif Inc., Carlsbad, CA, USA) following the manufacturer's instructions for frozen tissue and using 100 mg of tissue for each extraction. PPAR- $\gamma$  DNA binding activity was assessed by a TransAM<sup>™</sup> PPAR- $\gamma$  kit (Active Motif Inc., Carlsbad, CA, USA) using 10  $\mu$ g/10 $\mu$ L of nuclear protein extract following the manufacturer's instructions.

### 2.9. Plasma Biochemical Analysis

All biochemical parameters were assessed after overnight fasting (14–16 h) and using the following commercial kits or reagents as per manufacturer's instructions: mouse insulin ELISA (ALPCO, Salem, NH, USA); NEFA and liver L-type triglyceride M colorimetric assay (Wako Pure Chemical Industries Ltd., Richmond, VA, USA); adiponectin and resistin (Mesoscale Discovery); non-esterified fatty acids using glycerol free reagent as standard (Sigma-Aldrich, St. Louis, MA, USA); alanine transaminase (ALT) (Abcam, Cambridge, UK). Homeostatic model assessment of insulin resistance (HOMA-IR) was calculated using the formula: [fasting glucose (mmol/L)]  $\times$  [fasting insulin ( $\mu$ U/L)]/22.5].

### 2.10. Protein Extraction and Western Blot

All reagents were purchased from Sigma-Aldrich (Sigma-Aldrich, St. Louis, MA, USA) unless otherwise specified. Liver tissue was homogenized using a tissue homogenizer in RIPA buffer (50 mM Tris HCL pH:8.0, 150 mM NaCl, 0.1% Triton X-100, 0.5% sodium deoxycholate, 0.1% SDS) supplemented with 2 µg/mL aprotinin (Calbiochem), 5 mM sodium fluoride, 5 mM sodium orthovanadate, and protease inhibitor cocktail (FastPrep®-24, MP Biomedicals). Adipose tissue protein was extracted using an extraction kit (AT-022, Invent biotechnologies, Plymouth, MN, USA). Lysates were stored at −80 °C for future analysis. Protein extracts were separated by SDS-PAGE 12% polyacrylamide gels as previously reported [11] and probed for p-AKT (Cell Signaling Technology (CS-4060S), AKT (CS-9272), PPAR $\gamma$  (Santa Cruz Biotechnology-7196), AT2R (abcam92445), p-HSL (CS-41265), HSL (abcam45422), p-PKA (CS-5661S or PKA (CS-58425) overnight before incubation with fluorescent secondary antibodies (Li-cor Biosciences) for 1 h at RT. Images were analyzed using Image Studio Lite software (Li-cor Biosciences, Lincoln, NE, USA). All the phosphorylated proteins bands were normalized to their corresponding total protein. Total proteins were normalized to  $\beta$ -actin (Sigma-Aldrich A5441).

### 2.11. Histology

Paraffin blocks of liver or WAT were cut into 5 µm sections and affixed to glass slides. Hematoxylin and eosin (H&E) staining was performed as previously reported [11]. Fibrosis was assessed using Masson's trichrome staining kit (Sigma-Aldrich, St. Louis, MA, USA). Adipocyte size: 10 random photomicroscopic images of each slide (1 slide per animal) were captured using the microscope 20 $\times$  objective lens and Axion Vision 4.8 software. ImageJ software "freehand selections" tool was used to measure adipocyte area (mm<sup>2</sup>) of 300 cells or 10 images per sample, whichever was reached first. Liver morphological characterization: Random photomicroscopic images (20 $\times$ , Axio Vision 4.8 software, n = 3 per mouse) were taken and a researcher blinded to group assignment used ImageJ software "freehand selections" tool to quantify lipid droplet (LD) area, cell number and inflammatory foci (a cluster with >5 immune cells). Each image was divided into four equal areas and the top left quadrant (standard area: 88,884.66 µm<sup>2</sup>) was analyzed as a representation of the total image. In terms of LD size, there is not a defined numerical threshold for small or large LD categories. However, based on the literature, hepatic lipid accumulation was divided into three categories, macrovesicular with one large LD displacing the nucleus to the side, macrovesicular with one single small LD not displacing the nucleus and true microvesicular steatosis where several small LD occupy a hepatocyte, giving it a foamy appearance [20–22].

### 2.12. Quantitative PCR (qPCR)

Primer sequences are provided in Table S2. Liver RNA was extracted using the QIAGEN RNeasy min plus kit following the manufacturer's instructions and as previously described [23] with the following modifications: frozen tissue (50–100 mg) was lysed and homogenized using 1 mL of TRIzol. After 5 min at RT, 0.2 mL of chloroform per mL of TRIzol was added. Samples were shaken vigorously and incubated at RT for 3 min, followed by centrifugation at 12,000 $\times$  g for 10 min at 2–8 °C. The supernatant was collected, and the manufacturer's instructions were followed for the remaining steps until RNA was obtained. RNA concentration and purity were measured using a Nanodrop (Thermo Fisher, Waltham, MA, USA) and cDNA synthesis was performed using the high-capacity cDNA RT kit (Applied Biosystems, Waltham, MA, USA) using 2 µg RNA per reaction in a ProFlex PCR system thermo cycler (Applied Biosystems, Waltham, MA, USA). qPCR was performed using PerfeCTa SYBR Green SuperMix ROX (Quantabio, Beverly, MA, USA) in a QuantStudio3 machine (Applied Biosystems, Waltham, MA, USA) using beta actin as the reference gene.

### 2.13. Statistical Analysis

All data presented are expressed as means  $\pm$  SEM of 'n' mice as indicated in each figure description. Statistical analysis was performed using GraphPad Prism software 7.0 (GraphPad Software Inc., San Diego, CA, USA). Data were checked for normal distribution by the Shapiro–Wilk test and any identified outliers were removed. T-test was used to compare LFD to HFD (to establish IR-related differences), while one-way ANOVA was used to compare HFD groups (i.e., HFD, PEP2 and ROSI) to identify treatment effects. Two-way ANOVA was used to compare insulin regulation of AKT, PKA and HSL. Bonferroni's or Dunn's post-hoc tests were performed to assess differences between groups when a significant main effect was observed. A  $p$ -value  $\leq 0.05$  was considered statistically significant.

## 3. Results

### 3.1. EHW Effects on WAT Lipolytic Pathway from Obese, Insulin Resistant Rats

Previously we showed that 4% EWH improved glucose tolerance and insulin sensitivity, reduced adipocyte size and enhanced PPAR $\gamma$  abundance in WAT in rats [11]; thus, its effects on lipolytic enzymes in WAT was investigated here. PPAR $\gamma$  DNA binding activity was reduced by 4% EWH in eWAT ( $p < 0.01$ ), but significantly increased in rWAT ( $p < 0.01$ ) (Figure 1A,B). The investigation of key enzymes involved in lipolysis by two-way ANOVA showed a significant overall diet effect ( $p < 0.05$ ) in rWAT p-PKA/PKA ratio and an overall insulin effect ( $p < 0.05$ ) in p-HSL/HSL. The post-hoc analysis revealed that 4% EHW treated animals had reduced p-HSL in rWAT after intraperitoneal injection of insulin ( $p < 0.05$ ) despite no change in phosphorylation on PKA (Figure 1C,D). No changes in total PKA or HSL protein abundance were seen in rWAT (Figure S2). In eWAT, two-way ANOVA revealed a significant overall diet effect ( $p < 0.05$ ) on p-PKA/PKA, while no overall effect was seen in p-HSL/HSL. No changes in p-HSL or p-PKA (Figure 1E,F) or total HSL (Figure S2) were seen. However, total PKA abundance was reduced by 4% EWH treatment (Figure S2). Plasma and WAT adiponectin and resistin concentrations were not different between groups (Table 2).

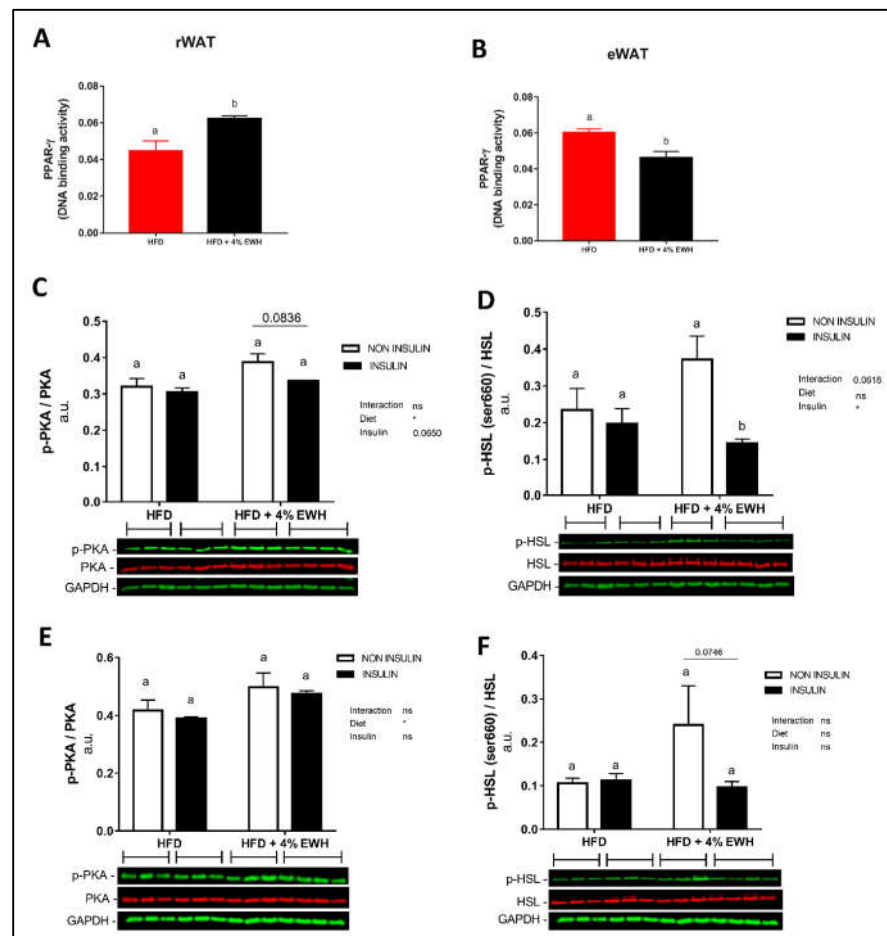


**Figure 1.** EWH effects in WAT of Sprague Dawley rats fed EWH for 6 weeks (Protocol 1). PPAR $\gamma$  DNA binding activity in rWAT (A) and eWAT (B). Data expressed as mean  $\pm$  SEM and analyzed by two-tailed t-test ( $n = 6-7$ ). PKA, p-PKA, HSL and p-HSL protein abundance in rWAT (C,D) and eWAT (E,F). Data expressed as mean  $\pm$  SEM and analyzed by two-way ANOVA ( $n = 3-4$ ). Bars with different letters indicate  $p \leq 0.05$ . EWH, egg white hydrolysate; PKA, protein kinase A; PPAR $\gamma$ , Peroxisome proliferator-activated receptor gamma; HSL, hormone sensitive lipase; WAT, white adipose tissue; rWAT, retroperitoneal WAT; eWAT, epididymal WAT.

Based on these indications that 4% EWH had the potential to improve insulin-mediated suppression of lipolysis and activate PPAR $\gamma$ , a trial of 4 EWH-derived, purified peptides (Peptides 1–4) that elicited increased PPAR $\gamma$  in vitro [15] was initiated. From preliminary data ( $n = 12$  mice/group), insulin tolerance was improved by Peptide 2 ( $p < 0.05$ ) together with lower iWAT and rWAT weights compared to HFD (Figure S3), whereas Peptides 1, 3 and 4 did not affect any WAT depot weight. Notably, Peptide 2 had the lowest and ROSI the highest liver weight. Therefore, additional experiments were performed, focusing on the effects of Peptide 2 on the IR phenotype and iWAT/rWAT lipid metabolism.

**Table 2.** Resistin and adiponectin concentration in plasma, epididymal and retroperitoneal adipose tissue in Sprague Dawley rats treated with HFD+4% EWH for 6 weeks (Protocol 1). Data expressed as mean  $\pm$  SEM and analyzed by two-tailed t-test ( $n = 6-7$ ).

	HFD	HFD+4% EWH
Plasma (fasting)		
Resistin (pg/mL)	1047 $\pm$ 84.55	1011 $\pm$ 82.99
Adiponectin (ng/mL)	55,853 $\pm$ 2832	60,270 $\pm$ 7367
eWAT		
Resistin (pg/mL)	175.1 $\pm$ 15.67	166.5 $\pm$ 11.14

Adiponectin (ng/mL)	1002 ± 28.44	1044 ± 19.54
rWAT		
Resistin (pg/mL)	172.3 ± 20.14	175.1 ± 15.67
Adiponectin (ng/mL)	1033 ± 25	1026 ± 28.73

Abbreviations: HFD, high fat diet; EWH, egg white hydrolysate; eWAT, epididymal adipose tissue; rWAT, retroperitoneal adipose tissue.

### 3.2. Peptide 2 and Rosiglitazone Effects in HFD Induced Obese and Insulin Resistant Mice

#### 3.2.1. Food Intake, Body Composition and Tissue Weight

Food and water intake were not different between any of the groups compared to HFD animals (Figure S4A–D). As expected, after 6 wks of HFD feeding, the HFD group presented higher BW than LFD animals (Table 3) and were glucose intolerant (Figure S5). At the end of the trial, HFD group maintained higher BW and BW gain than LFD. Initial BW was not different between all the HFD groups; however, the ROSI group had reduced rate of BW gain than HFD group after 3 weeks of treatment leading to a reduced final BW. Peptide 2 supplementation did not influence final BW or BW gain in comparison to HFD. Body composition analysis revealed that only the LFD animals had a lower fat mass % and higher lean mass % than HFD (Table 3).

**Table 3.** Body weight, body composition and plasma profile of C57BL/6 mice at the end of the Peptide 2 feeding trial (Protocol 2). Data expressed as mean + SEM and analyzed by two-tailed t-test (LFD × HFD) and by one-way ANOVA or Kruskal-Wallis (HFD groups). Different letters on the same row indicates  $p < 0.05$  for HFD groups. # Indicates  $p \leq 0.05$  and ^ indicates  $p < 0.1$  compared to HFD.

	LFD	HFD	HFD+PEP2	HFD+ROSI
Body composition (not fasted)				
Initial BW (g) (week 6)	29.1 ± 0.6 #	33.9 ± 0.7 a	32.9 ± 0.6 a	33.5 ± 0.7 a
Final BW (g)	33.4 ± 0.7 #	42.5 ± 0.7 a	41.4 ± 0.5 a,b	39.4 ± 0.8 b
BW gain (%) (week 6–13)	15.4 ± 1.0 #	25.0 ± 1.3 a	26.2 ± 1.2 a	17.7 ± 1.5 b
Final fat mass (% BW)	25.6 ± 1.3 #	38.5 ± 1.1 a	38.6 ± 0.6 a	36.1 ± 1.1 a
Final lean mass(% BW)	65.9 ± 1.2 #	54.2 ± 1.0 a	54.3 ± 0.6 a	56.5 ± 1.0 a
Tissue weight (g/BW)				
eWAT	0.039 ± 0.0029 #	0.059 ± 0.0029 a	0.061 ± 0.0014 a	0.057 ± 0.0025 a
rWAT	0.017 ± 0.00079 #	0.028 ± 0.00084 a	0.025 ± 0.00096 a,b	0.022 ± 0.0014 b
iWAT	0.046 ± 0.0070 #	0.073 ± 0.0049 a	0.065 ± 0.0027 a	0.062 ± 0.0040 a
Liver	0.036 ± 0.0019	0.033 ± 0.0015 a	0.032 ± 0.0007 a	0.044 ± 0.0015 b
Plasma (fasting)				
Glucose (mmo/L)	4.5 ± 0.3 #	5.9 ± 0.3 a	5.3 ± 0.3 a	5.6 ± 0.2 a
Insulin (ng/mL)	0.5 ± 0.1 ^	1.0 ± 0.1 a	0.9 ± 0.1 a	0.6 ± 0.1 a
HOMA-IR	0.8 ± 0.2 #	2.4 ± 0.6 a	1.8 ± 0.3 a	1.9 ± 0.3 a
NEFA (mEq/L)	0.4 ± 0.02	0.4 ± 0.02 a	0.5 ± 0.03 a	0.5 ± 0.04 a
TG (mg/dL)	39.4 ± 5.6	52.6 ± 5.8 a	43.2 ± 4.2 a	41.9 ± 4.6 a
Plasma ALT (mU/mL)	8.4 ± 4.0 #	28.4 ± 27.1 a	24.9 ± 15.1 a	20.9 ± 13.5 a
Liver content (mg/g tissue)				
TG	46.8 ± 2.3 #	71.5 ± 11.0 a	57.6 ± 6.7 a	132.7 ± 12.1 b
Cholesterol	2.4 ± 0.2	2.1 ± 0.2 a	1.3 ± 0.1 b	1.8 ± 0.1 a

Abbreviations: ALT, alanine aminotransferase; BW, body weight; eWAT, epididymal white adipose tissue (WAT); HFD, high fat diet; HOMA-IR, homeostatic model assessment of insulin resistance; iWAT, inguinal WAT; LFD, low fat diet; NEFA, non-esterified fatty acids; rWAT, retroperitoneal WAT; TG, triglycerides.

Compared to HFD, LFD animals had decreased mass of all three fat pads. ROSI group presented lower rWAT mass compared to HFD, while PEP2 animals had an

intermediate rWAT mass, between ROSI and HFD groups. eWAT and iWAT did not change between all the HFD groups. Liver weight of LFD and HFD groups was not different. ROSI animals had a heavier liver than all the other HFD groups (Table 3).

### 3.2.2. Plasma Biochemical Parameters

Fasted LFD animals had lower blood glucose concentration than HFD, while no statistical difference was seen between the HFD groups. No statistical difference was seen in fasting plasma insulin concentration between any of the groups, despite a considerable reduction in LFD ( $p < 0.1$ ) and ROSI groups compared to HFD. This was accompanied by a lower HOMA-IR in LFD animals compared to HFD but no differences between HFD groups. No changes were seen regarding plasma lipid profile (NEFA and TG) between any of the groups (Table 3).

### 3.2.3. Glucose Homeostasis and Systemic Insulin Sensitivity

In vivo tests confirmed that at week 14 HFD animals were glucose intolerant compared to LFD animals (Figure 2A,C), and that the ROSI group had improved glucose tolerance compared to HFD group (Figure 2B,C, right). Two-way ANOVA analysis show a significant treatment  $\times$  time interaction ( $p < 0.0001$ ) and a significant effect of diet ( $p = 0.0437$ ) among the HFD groups. However, despite changes in the OGTT curve and AUC, the incremental AUC was not different between groups (Figure 2D). This is likely because fasting glucose concentration in the OGTT was significantly lower in the LFD group compared to HFD (Figure 2E, left). During the hyperinsulinemic-euglycemic clamp LFD, ROSI and PEP2 groups had improved insulin sensitivity compared to HFD (Figure 2F–I and Figure S6). Plasma glucose during the hyperinsulinemic-euglycemic clamp was not different among the groups (Figure 2F). Similarly, there was no difference in plasma insulin during the clamp procedure (Figure 2G), both validating the clamp technique. IR of the HFD group was indicated by the lower glucose infusion rate (GIR) (Figure 2H, left) and higher glucose production during the clamp than LFD (Figure 2I, left). Moreover, GIR was higher in PEP2 and ROSI compared to HFD (Figure 2H, right). In addition, glucose production was reduced in the PEP2 group compared to HFD, while ROSI showed an intermediate effect (Figure 2I, right). When comparing basal vs. clamp glucose production within group, glucose production was only suppressed in the PEP2 group, with a similar pattern in the LFD group (Figure S6A). Insulin-stimulated glucose disposal was higher in the LFD and ROSI groups compared to HFD and although it was also numerically higher in the PEP2 group, no significance was seen (Figure S6B). Improvement in insulin sensitivity after PEP2 and ROSI treatment was confirmed during the insulin tolerance test (Figure S6C–I).

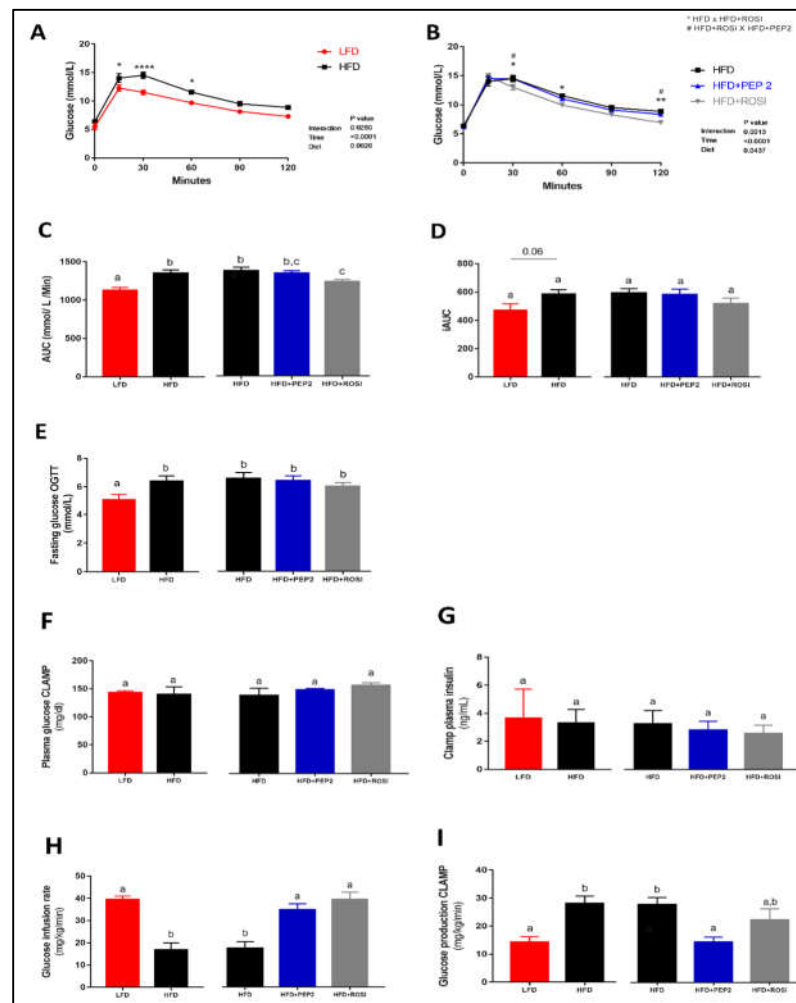


**Figure 2.** Glucose tolerance test and hyperinsulinemic-euglycemic clamp in mice treated with Peptide 2 (Protocol 2). (A,B) Glucose tolerance test (OGTT), (C) OGTT area under the curve (AUC), (D) OGTT incremental AUC, (E) overnight fasting glucose on OGTT day ( $n = 11\text{--}12$ ). Data expressed as mean  $\pm$  SEM and analyzed by two-tailed t-test (LFD vs. HFD) and by one-way ANOVA or Kruskal-Wallis (HFD groups) or two-way ANOVA. In the hyperinsulinemic-euglycemic clamp: (F) plasma glucose concentration; (G) plasma insulin; (H) glucose infusion rate and (I) glucose production. Data expressed as mean  $\pm$  SEM of  $n = 4\text{--}7$  and analyzed by two-tailed t-test (LFD vs. HFD) or by one-way ANOVA (HFD groups). Bars with different letters indicate  $p \leq 0.05$ . \* and # indicate  $p \leq 0.05$ ; \*\* indicates  $p \leq 0.01$ ; \*\*\*\* indicates  $p \leq 0.0001$ .

### 3.2.4. WAT Regulation by Insulin: Lipolysis and AKT

Tissue collected from fasted HFD animals had impaired norepinephrine-stimulated lipolysis ex vivo in eWAT and iWAT (Figure 3A,B), while in rWAT lipolysis stimulation occurred in all the groups, despite HFD having a lower magnitude of stimulation (Figure 3C). Two-way ANOVA diet overall effect was significant in rWAT and iWAT ( $p < 0.05$ ), but not in eWAT. The overall stimulatory effect was significant in all three fat pads ( $p < 0.05$ ). Interestingly, none of the groups showed suppression of lipolysis by insulin in the eWAT (Figure 3A), but the lack of suppression of lipolysis by insulin in HFD was rescued by Peptide 2 in both iWAT (Figure 3B) and rWAT (Figure 3C). ROSI normalized lipolysis suppression in iWAT (Figure 3B) but not in rWAT (Figure 3C). Because only rWAT and iWAT demonstrated rescued suppression of lipolysis we investigated insulin regulation of the lipolytic pathway only in these two fat pads. rWAT and iWAT exhibited enhanced AKT phosphorylation after insulin stimulation in LFD, PEP2 and ROSI but not in HFD groups, with an overall effect of insulin in both fat pads, but a dietary overall effect only in iWAT (Figures 3D,E and S7).

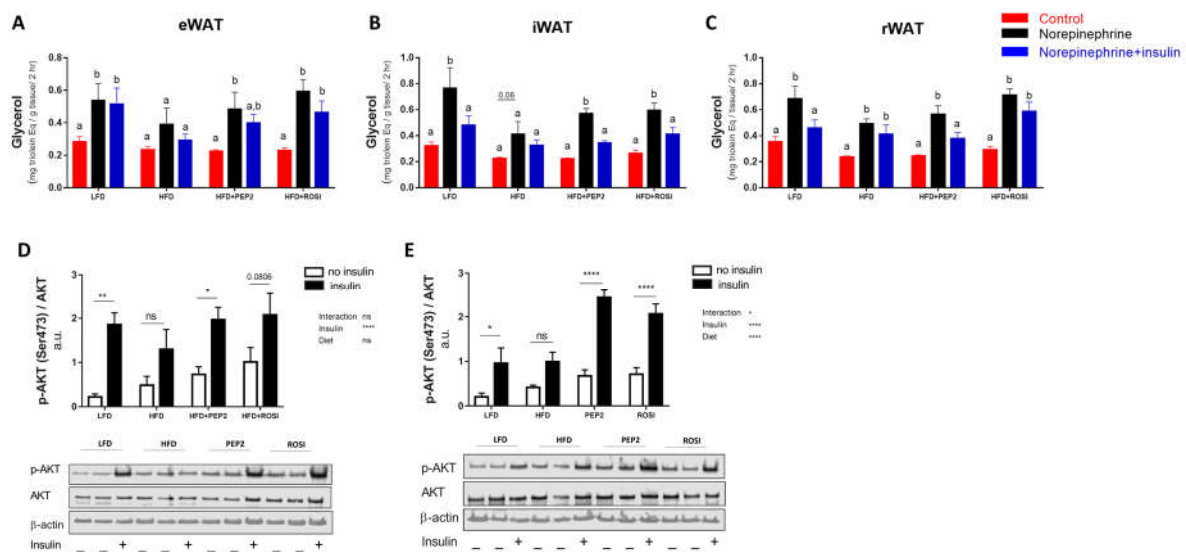


**Figure 3.** White adipose tissue (WAT) ex vivo lipolysis and protein kinase B (AKT) activation in tissues harvested from mice treated with Peptide 2 (Protocol 2). Lipolysis ex-vivo in (A) eWAT (n = 5–6), (B) iWAT (n = 5–6) and (C) rWAT (n = 4–6). (D) rWAT p-AKT/AKT (n = 6) and (E) iWAT p-AKT/AKT (n = 6). Data expressed as mean  $\pm$  SEM and analyzed by two-way ANOVA (D,E). Bars with different letters and \* indicate  $p \leq 0.05$ ; \*\*  $p < 0.01$  and \*\*\*\*  $p < 0.0001$ . HFD, high fat diet; rWAT, retroperitoneal WAT; eWAT, epididymal WAT, iWAT inguinal WAT; LFD, low fat diet; ROSI, rosiglitazone.

### 3.2.5. PPAR $\gamma$ Activation, Adipocyte Size and Adipogenesis Markers

Despite being increased 40–50% in PEP2 and ROSI groups, PPAR $\gamma$  protein abundance in rWAT did not reach statistical significance (Figure 4A). However, PPAR $\gamma$  activation was increased in LFD and ROSI groups compared to HFD, but not in PEP2 (Figure 4B). Image analysis revealed no differences in average adipocyte size or distribution in the rWAT (Figures 4C and S8, respectively) in any diet group. In iWAT, total PPAR $\gamma$  protein abundance was similar between groups (Figure 4E) and PPAR $\gamma$  activation was not different between groups (Figure 4F). Average adipocyte size in LFD group was smaller than HFD (Figure 4, left). However, no changes were seen among the HFD groups (Figure 4G, right). The distribution curve showed reduced percentage of larger adipocytes (>0.017 mm<sup>2</sup>) in the LFD compared to HFD (Figure S8). Protein abundance of adipogenesis markers of adipogenesis, including adiponectin, perilipin-1, fatty-acid binding protein 4 and fatty acid synthase were similar between HFD groups in both rWAT and iWAT (Figure S8). In addition, we tested the effect of Peptide 2 during the differentiation of pre-adipocytes derived from both subcutaneous (9 W) and brown (9 B) adipose tissue pads from mice. However, no major effects were observed in terms of adipogenesis, lipolysis, lipogenesis and WAT browning (Figures S9 and S10).

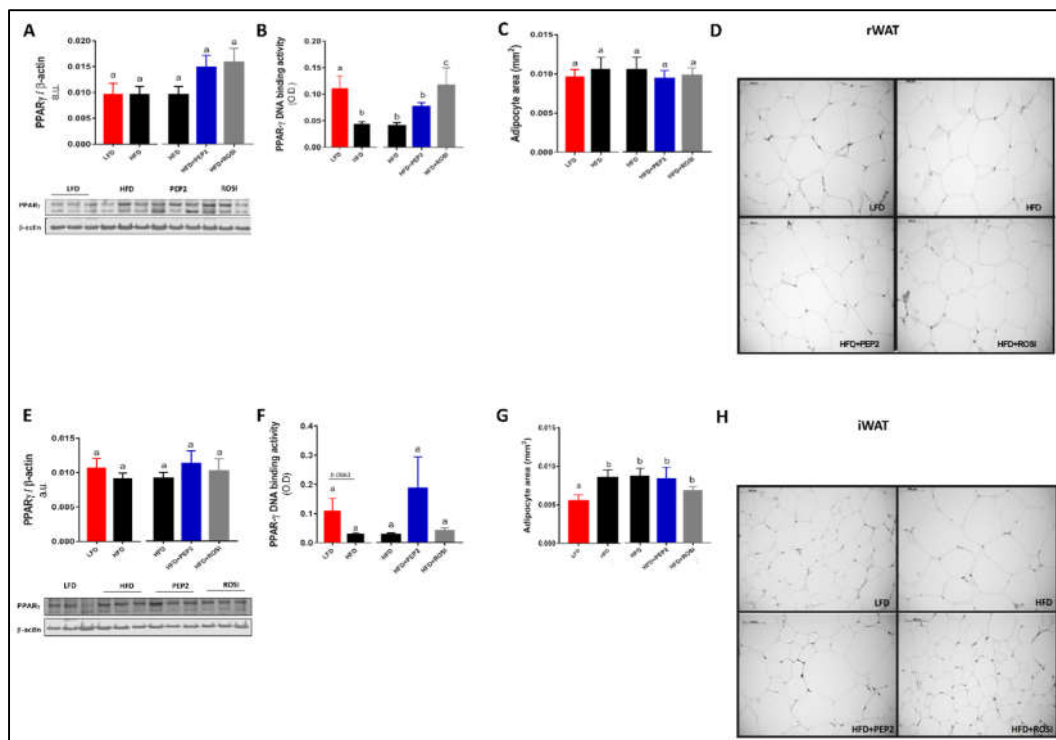


**Figure 4.** Retroperitoneal white adipose tissue (rWAT) and inguinal white adipose tissue (iWAT) adipogenesis markers in tissues harvested from mice treated with Peptide 2 (Protocol 2). (A) PPAR $\gamma$  protein abundance in rWAT; (B) PPAR $\gamma$  DNA binding activity in rWAT ( $n = 5-6$ ); (C) adipocytes mean area in rWAT ( $n = 4$ ); (D) representative image in rWAT; (E) PPAR $\gamma$  protein abundance in iWAT; (F) PPAR $\gamma$  DNA binding activity in iWAT ( $n = 5-6$ ); (G) adipocytes mean area in iWAT ( $n = 4$ ); (H) representative image in iWAT. Data expressed as mean  $\pm$  SEM and analyzed by two tailed t-test (LFD vs. HFD) and by one-way ANOVA or Kruskal–Wallis (HFD groups). Bars with different letters indicates  $p \leq 0.05$ . HFD, high fat diet; LFD, low fat diet; rWAT, retroperitoneal WAT; eWAT, epididymal WAT; iWAT, inguinal WAT; PPAR $\gamma$ , peroxisome proliferator activated receptor gamma; ROSI, rosiglitazone.

### 3.2.6. Liver Characterization

Morphological characterization of LD showed no differences between LFD and HFD groups in terms of total LD number (Figure 5A, left) and total LD area (Figure 5C, left), but LFD had 30–40% smaller individual LD area ( $p = 0.09$ ) (Figure 5B, left). Among HFD groups, despite a similar number of LD in all the groups (Figure 5A, right), ROSI had a similar individual LD area to HFD and an increased total LD area (Figure 5B,C, right, respectively). PEP2 had smaller individual LD area compared to ROSI, and around 50% smaller area compared to HFD ( $p = 0.09$ ) (Figure 5B, right). In addition, PEP2 had 40–50% smaller total LD area compared to HFD, but while the ANOVA showed a  $p = 0.0001$  suggesting an overall treatment effect, no statistical difference was observed between these groups (Figure 5C, right,  $p = 0.2$ ). Albeit not statistically significant, the qualitative analysis of the images reveals that the majority of the animals had visibly less liver fat (first, second and fourth panel on Figure 5G) while the minority did not (third panel Figure 5G). These differences are also reflected by the distribution curve (Figure 5D), which emphasizes the right-shift in LD area as well as more abundant LD  $> 50 \mu\text{m}^2$  in area in the ROSI livers. Regarding hepatocyte size, no difference between LFD and HFD was observed, but PEP2 had a higher number of cells per area than ROSI, indicative of less hypertrophy (Figure 5E, right). Moreover, PEP2 and LFD exhibited fewer inflammatory foci compared to HFD, while ROSI had an intermediate effect (Figure 5F, right). The differences seen in hepatic TG content (Table 3) and LD characterization are supported by the representative images, where we observed smaller LD, less area covered in LD and reduced inflammatory foci presence in LFD and PEP2 groups, while ROSI exhibited most of the image covered in LD

(Figure 5G). Hepatic cholesterol content was lower in the PEP2 group compared to HFD and ROSI groups, but not different between LFD and HFD (Table 3). Plasma ALT was not different among the HFD groups, but LFD had lower plasma ALT concentration than HFD animals (Table 3). Collagen staining to identify fibrosis revealed no presence of collagen within the hepatic parenchyma in almost all of the samples. However, all the samples from ROSI group had at least 1 image out of 19 with presence of weak collagen staining. One sample in the LFD group exhibited marked collagen staining, which was attributed to a random finding of fibrosis (Table S3).

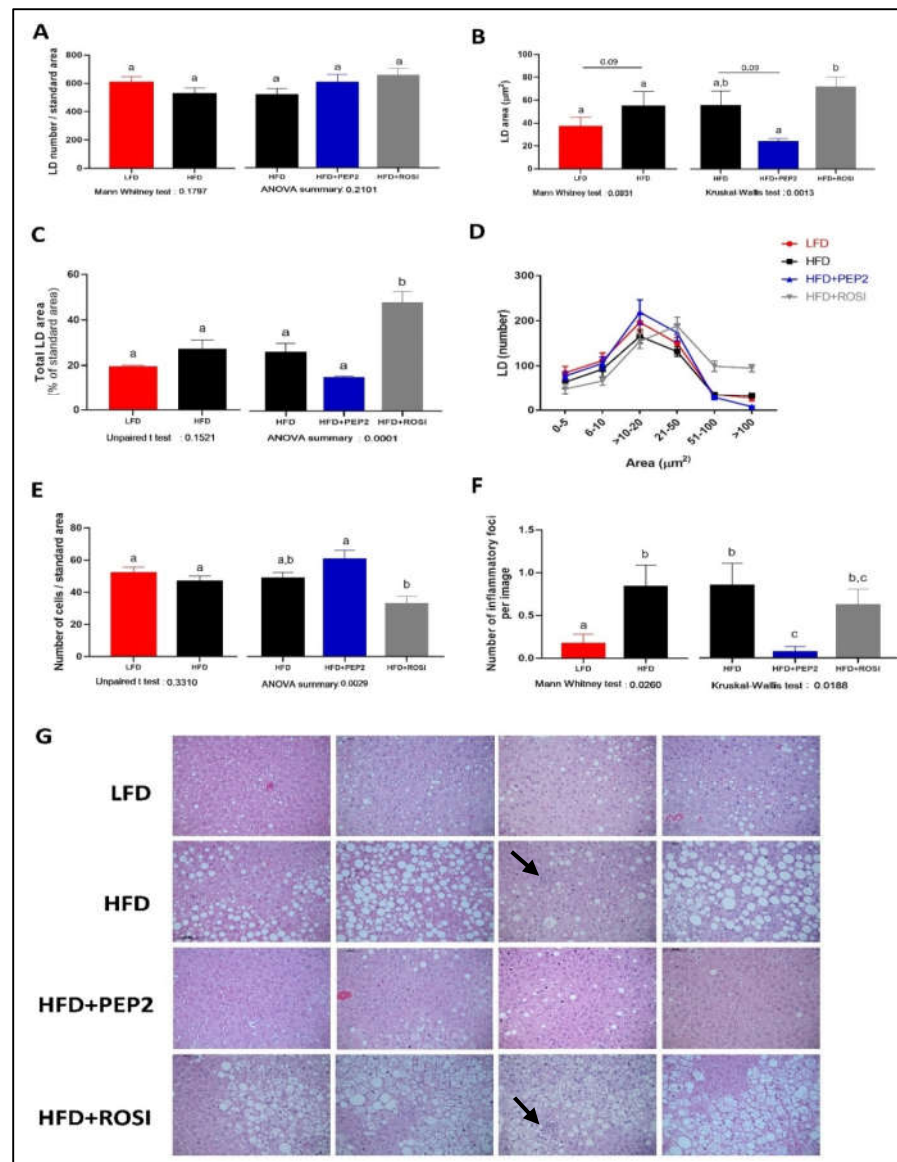


**Figure 5.** Liver characterization in tissues harvested from mice treated with Peptide 2 (Protocol 2). (A) total LD number (n = 6); (B) average individual LD area (n = 6); (C) average area covered by LD (n = 6); (D) LD distribution by size (n = 6); (E) number of cells per liver area analyzed (n = 6); (F) average inflammatory foci per image (n = 5–6); (G) liver representative images. Data expressed as mean ± SEM and analyzed by two tailed t-test (LFD vs. HFD) and by one-way ANOVA or Kruskal–Wallis (HFD groups). Arrows indicate inflammatory foci. Bars/lines with different letters indicates  $p \leq 0.05$ . LD, lipid droplet; HFD, high fat diet; LFD, low fat diet; ROSI, rosiglitazone.

### 3.2.7. Liver PPAR $\gamma$ and AT2R and Insulin Signaling

Hepatic PPAR $\gamma$  abundance was similar between all groups (Figure 6A). Interestingly, angiotensin II-type 2 receptor (AT2R) protein abundance was enhanced 2-fold ( $p < 0.05$ ) in the PEP2 group compared to HFD (Figure 6B, right).

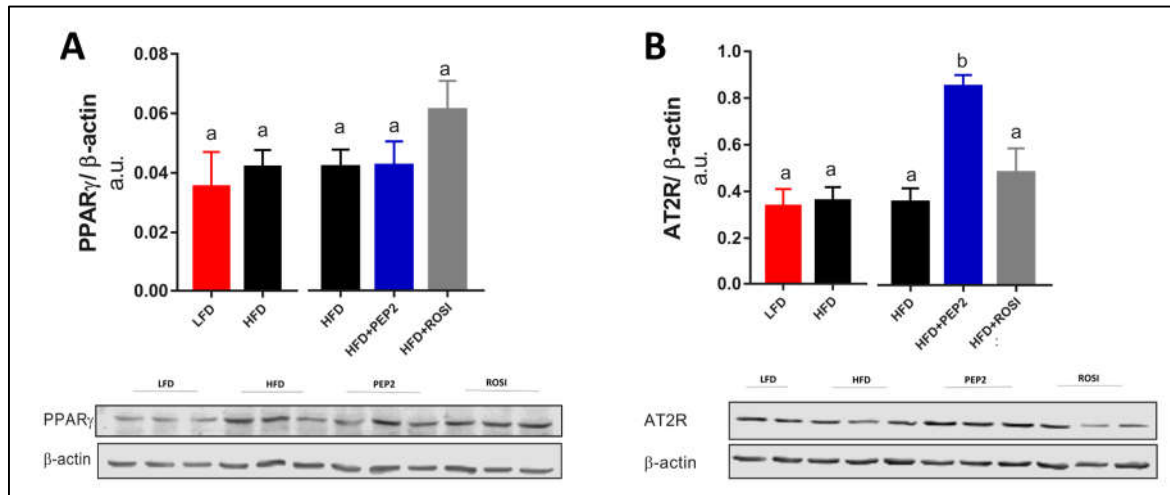


**Figure 6.** Liver protein abundance in tissues harvested from mice treated with Peptide 2 (Protocol 2). (A) PPAR $\gamma$  protein abundance and (B) AT2R. Data expressed as mean  $\pm$  SEM of  $n = 5$ – $6$  mice. Data analyzed by two-tailed t-test (LFD vs. HFD) and by one-way ANOVA or Kruskal-Wallis (HFD groups). Bars with different letters indicates  $p \leq 0.05$ . PPAR $\gamma$ , peroxisome proliferator-activated receptor gamma; AT2R, angiotensin II type 2 receptor.

### 3.2.8. Lipid Metabolism, Inflammation, and Fibrosis Genes

mRNA expression of PPAR alpha (*Ppara*), gamma (*Pparg*) and gamma2 (*Pparg2*) was not different among the HFD groups (Figure 7A). Although pro-inflammatory gene *Tnfa* was not different among the HFD groups, a trend of reduced *Col1a1* ( $p = 0.055$ ), a marker of fibrosis, was observed in PEP2 compared with ROSI (Figure 7B). Among the several genes involved in lipid metabolism analyzed, only *Mogat1* showed a significant difference, with a 3-fold increase in the PEP2 group compared to HFD, and an approximately 1.5-fold increase compared to ROSI (Figure 7C). No changes were seen in selected genes that encode LD-associated proteins or that are involved in lipolysis (Figure 7D). No difference in any of the analyzed genes was observed between LFD and HFD (Figure S11).

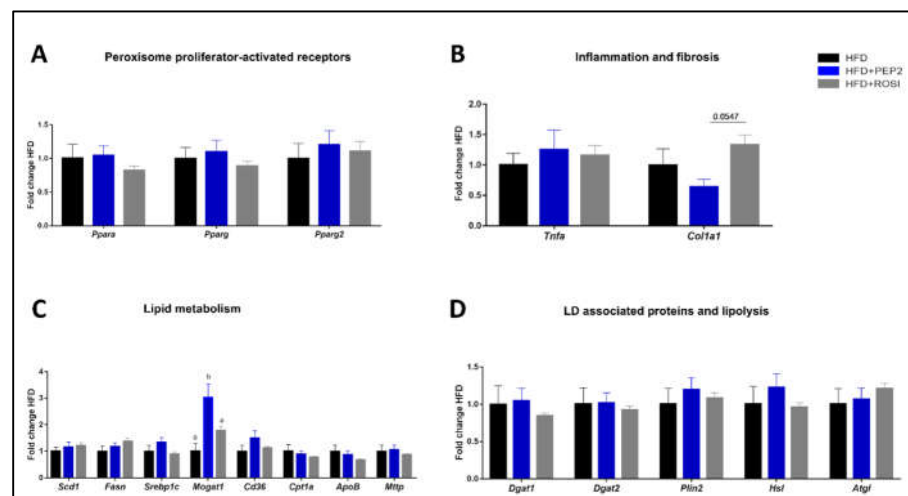


**Figure 7.** Liver gene expression in tissues harvested from mice treated with Peptide 2 (Protocol 2). (A) Peroxisome proliferator-activated receptors; (B) inflammation and fibrosis related genes; (C)

lipid metabolism related genes and (D) LD associated proteins and lipolysis related genes. Data expressed as mean  $\pm$  SEM of fold change of HFD control (n = 7–8) and analyzed by one-way ANOVA or Kruskal–Wallis test. Data normalized to  $\beta$ -actin gene expression. Bars with different letters indicates  $p \leq 0.05$ . LD, lipid droplet.

#### 4. Discussion

The prevalences of NAFLD, obesity and T2D are increasing in parallel. In fact, because of the relationship between hepatic steatosis and metabolic diseases, there is a movement to change the parameters used for diagnosis of NAFLD and a name change to metabolic-associated fatty liver disease (MAFLD) is also proposed [24]; however, we have used NAFLD as the chosen abbreviation. Bioactive peptides have potential to aid in the management of metabolic diseases because they can modulate physiological processes [9] either in conjunction with pharmacological treatments or as novel, stand-alone approaches for conditions without approved pharmacotherapy, such as NAFLD. In this study, we hypothesized that diet supplementation with Peptide 2 would improve systemic and local IR and as a consequence, modulate features of NAFLD in HFD-induced obese-IR mice. We found that Peptide 2 supplementation: (1) improved systemic IR during the hyperinsulinemic-euglycemic clamp; (2) rescued insulin-regulated lipolysis in rWAT and iWAT, despite no change in adipocyte size or BW; (3) reduced hepatic lipid accumulation while increasing monoacylglycerol O-acyltransferase 1 (*Mogat1*) gene expression in the liver; and (4) reduced hepatic inflammatory infiltration.

EWH is a mixture of bioactive peptides shown before to improve IR and reduce adipocyte size in rodents [11]. Herein, we showed that PPAR $\gamma$  activation is enhanced in rWAT of EWH supplemented animals, which was accompanied by a better response to insulin in terms of suppression of enzymes involved in lipolysis in rWAT as well as increased p-AKT [11]. Another possibility is that HFD reduced baseline p-HSL/HSL ratio, which was restored by EWH leading to the insulin suppression of p-HSL observed. Nevertheless, these findings led us to hypothesize that the metabolic improvements seen in vivo were due to modulation of PPAR $\gamma$  in WAT, similar to the action of thiazolidinediones, which would induce adipogenesis and promote the appearance of more insulin sensitive adipocytes [25] improving systemic insulin sensitivity. We then asked if there were specific peptides from the EWH mixture that could modulate PPAR $\gamma$  abundance and an in vitro screening revealed that a few peptides were able to mimic insulin effect of enhancing PPAR $\gamma$  in preadipocytes [15], which led us to investigate their effects in vivo. The peptide with greater potential based on our screening (Figure S3) was Peptide 2 and we further evaluated its effects in obese and IR mice focusing on WAT and the liver.

IR is a key feature of T2D, and it plays a significant, multi-factorial role in the development of NAFLD [26]. IR in WAT leads to impaired suppression of lipolysis, which increases NEFA delivered to the liver whereas hepatic IR impairs the suppression of gluconeogenesis [26]. Egg-derived peptides and hydrolysates were shown before to improve insulin sensitivity in rodents [11,14,27] but relative contributions of hepatic versus non-hepatic tissues were not evaluated. Therefore, we first investigated the potential of Peptide 2 supplementation to reduce IR using a hyperinsulinemic-euglycemic clamp, the gold standard technique for this outcome measurement. We observed that LFD, PEP2 and ROSI groups had lower IR compared to HFD group. Although rosiglitazone, a known insulin sensitizer, was expected to reduce IR, this is the first study showing that dietary supplementation with Peptide 2 improves IR, despite no changes in glucose tolerance or BW. Moreover, suppression of endogenous glucose production during clamp was stronger in the PEP2 and LFD groups compared to HFD, consistent with better hepatic insulin sensitivity. This improvement in IR is supported by a reduced HOMA-IR in the LFD group, but despite a decrease in PEP2 group HOMA-IR, it was not statistically significant. Not only was systemic insulin sensitivity was improved by Peptide 2 supplementation but WAT insulin signaling was also rescued. The normalized regulation of lipolysis by insulin would be predicted to reduce NEFA delivery to the liver. Taken together, these

results suggests that the improvement in systemic insulin sensitivity in the PEP2 group could be in part because of a decreased spillover of lipids from WAT to non-adipose tissues due to a better hormonal regulation of lipolysis.

We then asked if the improvement in WAT insulin signaling was associated with PPAR $\gamma$  activation. PPAR $\gamma$  regulates adipogenesis and has an important role in glucose and lipid metabolism. We previously showed that Peptide 2 increased PPAR $\gamma$  protein in adipocyte cell culture [15]. However, we did not see higher PPAR $\gamma$  activation in any of the fat pads tested. This is accompanied by no overall changes in WAT adipocyte size or adipogenesis markers among HFD group, substantiated by no effect in adipogenesis markers during preadipocyte differentiation of mouse-derived cells in culture. On the other hand, we observed increased activation of PPAR $\gamma$  in rWAT of ROSI animals. Therefore, the effects of Peptide 2 are different from rosiglitazone, supporting a PPAR $\gamma$  independent mechanism of action. We conclude at this point that Peptide 2 acting to improve insulin signaling independently of PPAR $\gamma$ , at least in the models used in this study; therefore, other mechanisms need to be investigated.

Ongoing efforts seek to validate the use of insulin sensitizers, such as thiazolidinediones for the treatment of NAFLD. However, findings are controversial, with most of the benefits seen with pioglitazone rather than rosiglitazone [7,8]. In rodents, rosiglitazone plays a dual role depending on the level of hepatic PPAR $\gamma$  expression [28]. For example, in mice with low hepatic expression of PPAR $\gamma$ , rosiglitazone protects against lipid accumulation while in obese mice with elevated PPAR $\gamma$ , rosiglitazone exacerbates hepatic steatosis [28]. In fact, PPAR $\gamma$  is a key up-regulator of hepatic steatosis in HFD-induced obese mice treated with rosiglitazone [29]. Similarly, in this study we show that the ROSI group, although more insulin-sensitive, exhibits higher liver weight and TG content compared to HFD, whereas PEP2 does not worsen HFD-induced hepatic steatosis. PPAR $\gamma$  is mainly expressed in adipose tissue, but it is also expressed in the liver [30] and its expression is enhanced in the liver of HFD fed animals [28,29]. Similarly to the literature, in our study HFD feeding tended to increase hepatic *Pparg2* gene expression and protein compared to the LFD group, but neither PEP2 nor ROSI groups affected *Pparg* or *Pparg2* mRNA. However, albeit not significant, we saw a trend to increased hepatic PPAR $\gamma$  protein abundance in the ROSI group compared to HFD control. Peptide 2 supplementation did not increase PPAR $\gamma$  protein abundance above the HFD-induced effect. Although we did not measure hepatic PPAR $\gamma$  DNA binding activity, the results suggest that Peptide 2 may not be directly activating hepatic PPAR $\gamma$ , suggesting a difference in mechanism from rosiglitazone.

In NAFLD, progression to NASH is characterized by increased LD size, hepatocyte hypertrophy and inflammation [2,5]. Surprisingly, the ROSI group exhibited a true microvesicular steatosis mixed with macrovesicular steatosis, while PEP2 and HFD groups appeared to have macrovesicular steatosis, which is considered more pathological [20–22]. However, PEP2 tended to decrease LD area compared to HFD. Therefore, PEP2 group presented a macrovesicular steatosis with small LD vs. macrovesicular steatosis with large LD in the HFD group. The importance of LD size is highlighted by findings showing that macrovesicular steatosis is linked to fibrosis and microcirculation impairment in rodents [31,32] and fibrogenesis in humans [20]. Moreover, the extent of macrovesicular steatosis can impact liver transplantation and graft survival in humans [21]. Other food-derived peptides reduce LD size, for example pepsin-generated EWH supplementation reduces the number and size of LD in rats, accompanied by a decrease in plasma inflammatory and oxidative stress markers [33]. In addition, supplementation with a peptide derived from sweet lupine (GPETAFLR) improves hepatic steatosis and reduces TG content. The mechanism of action suggested was through PPAR $\alpha$  and uncoupling protein 1 (UCP1) activation and reduced hepatic expression of fatty-acid synthase gene (*Fasn*) and inflammatory markers, but only mRNA levels were measured, not their activity [34]. In another study, the improvement in NAFLD seen after potato-derived peptide (DIKTNKPVIF) supplementation is accredited to adenosine monophosphate-activated protein kinase (AMPK) activation and decreased inflammatory markers [35]. We find no changes in gene

expression of *Ppara* or *Fasn* after Peptide 2 supplementation. Therefore, the mechanism behind the effect of PEP2 supplementation to modulate hepatic LD size is unclear. Decrease in BW is associated with improvements in NAFLD; being an important confounding factor when evaluating an interventional study. However, we observed modulation of LD size by Peptide 2 independently of changes in BW. In the studies mentioned above one of them reported similar final BW but a lower eWAT mass [33], while the other reported decreased BW [34] and one did not report BW measurements [35]. It is worth noting that several peptides reduce hepatic lipid accumulation; however, whether it is a protein (amino-acid)-related or a peptide-specific effect still remains to be determined.

The observed improvement in liver morphology was independent of hepatic TG content, which was not significantly different between PEP2 and HFD groups, but a decrease in cholesterol content was seen between HFD and PEP2 groups, similar to Song et al. [36], who reports a reduction of the hepatic total cholesterol content after quinoa supplementation but no difference between HFD and quinoa supplemented groups in terms of hepatic TG [36] and attributes the improvement in NAFLD in part to changes in hepatic phospholipids, such as increased lysophosphatidylcholine and pantothenic acid, and decreased phosphatidylcholine and dioleoylphosphatidylcholine [36]. Indeed, impairment of cholesterol metabolism may be the key driver to large LD formation, rather than TG metabolism [20]. Despite higher hepatic TG content in the ROSI group, lack of change in plasma ALT indicates no further liver damage on top of that induced by HFD. Therefore, rather than only LD size or amount, its lipid composition also plays a key role in causing hepatic damage.

Inflammation and fibrosis are important markers to evaluate NAFLD progression to NASH. Peptide 2 supplementation attenuated the density of hepatic inflammatory foci consistent with the parent EWH hydrolysate decreasing plasma inflammatory markers. In the same study, an increase in AT2R was seen in WAT and liver [11]. Moreover, the hydrolysate reduced blood pressure in rats by modulating the renin-angiotensin system (RAS), including reduction of angiotensin II-type 1 receptor and induction of AT2R abundance in the aorta of rats [10]. AT2R is not only involved in the modulation of blood pressure by opposing angiotensin II-type 1 receptor activity, but its stimulation is associated with reno- and cardio-protective effects, anti-inflammatory and antifibrotic action, among others as extensively reviewed elsewhere [37]. In fact, RAS modulation is linked to hepatic fibrosis in rodents and humans with NAFLD [38,39]. In addition, AT2R has antifibrotic action in the liver of mice [40] and plays a role in blood flow regulation [41,42]. When we evaluated the presence of collagen staining as an indication of fibrosis, we found no presence of collagen in most of the samples. This may be because 14 wk of 45% HFD is insufficient to induce marked inflammation and fibrosis. Although *Col1a1* mRNA was increased after 19 wk of 60% HFD, only at 50 wk of dietary intervention was fibrosis seen in histological analysis [43]. Considering that macrovesicular steatosis with large LD impairs hepatic blood flow [31] and our finding that PEP2 had the highest hepatic AT2R and lowest mRNA expression of type 1 collagen, we speculate that AT2R up-regulation may be a mechanism by which PEP2 decreases inflammation and fibrosis over a longer-term of NAFLD but further research is needed to confirm this speculation. Conversely, ROSI did not induce AT2R or suppress collagen gene expression, differentiating its hepatic effects from PEP2.

Many pathways underlie hepatic lipid accumulation including increased delivery of NEFA to the liver following WAT lipolysis, decreased fatty acid oxidation, increased DNL or decreased VLDL secretion [2]. Although differences in gene expression involved in glucose and lipid metabolism occur between hepatocytes displaying large and small LD in the liver [44], surprisingly the mRNA expression patterns are similar between ROSI and HFD groups. This does not exclude the role of ROSI in modulating lipid metabolism pathways since we did not measure the activity of the related enzymes. The only difference observed between PEP2 and HFD group was higher *Mogat1* gene expression in the PEP2 group. *Mogat1* encodes the mannosylglycoprotein N-acetyl-glucosaminyl transferase 1

(MGAT1), which catalyzes TG synthesis via the monoacylglycerol O-acyltransferase pathway. The role of MGAT1 in liver steatosis is controversial, with some studies showing that silencing of hepatic MGAT1 improves steatosis and blood glucose levels [45,46]. Conversely, others demonstrate that MGAT1 knockout in liver does not improve hepatic steatosis, liver TG content, insulin sensitivity or glucose tolerance in HFD-fed mice [47]. Moreover, hepatic overexpression of MGAT1 does not increase liver TG content in HFD mice, but does in LFD animals [47]. In our study using fasted animals, we found reduced LD size concomitant with higher *Mogat1* gene expression, but no other direct target of PPAR $\gamma$  had increased expression. Intriguingly, increased hepatic *Mogat1* expression and MGAT activity occur after prolonged fasting with higher fat oxidation, and are both dependent and independent of *Ppara* expression, suggesting that MGAT1 regulates the hepatic fasting response [48]. This is consistent with the reduced LD size found in our study. We did not see altered *Ppara* gene expression, and we did not measure its activity directly, therefore, further investigation is needed to elucidate the role of Peptide 2 in hepatic lipid metabolism and its relationship to MGAT1.

Because our intended use of rosiglitazone was as a positive control for insulin sensitization and PPAR $\gamma$  agonism, differences in the hepatic phenotype versus PEP2 were unexpected. Our results suggest that, in contrast to rosiglitazone, Peptide 2 does not activate PPAR $\gamma$  and, in conditions of HFD-induced obesity and IR, Peptide 2 does not worsen HFD-induced hepatic steatosis. Rather, Peptide 2 supplementation improves IR and rescues insulin-regulated lipolysis in WAT while tending to reduce LD area, decreasing inflammation, and possibly preventing fibrosis, crucial processes to prevent NAFLD progression to NASH.

We note that an HFD containing 45% kcal fat is not commonly used to generate NASH animal models, with most of the diet-induced models receiving a high fat/high sugar diet. Thus, less hepatic inflammation and fibrosis in our model was observed compared with the available literature [49,50]. The peptide was administered mixed in the animals' diet, which does not allow for precise specification of the dose of peptide received by each animal. On the other hand, this dietary intervention has advantages over daily gavage for chronic studies in terms of reducing stress in the animals, which worsens IR, our main outcome. It is important to note that oxidative stress can also be involved in hepatic steatosis progression to NASH and that several food-derived peptides exert antioxidant activity as recently reviewed [51]. In future research, it would be worth exploring the antioxidant activity of Peptide 2 as a possible mechanism of preventing disease progression. In addition, it would be relevant to test Peptide 2 bioavailability and absorption pathways, including ability to modulate cell junction proteins. Lastly, all of our data reflect the overnight fasting state which, compared to fed state, may yield a different gene expression pattern and less pronounced effects in some of the outcomes reported.

In conclusion, this study shows for the first time that Peptide 2 diet supplementation improves IR in HFD-induced obese and IR mice, while at the same time preventing further exacerbation of HFD-induced NAFLD features independently of BW. On the other hand, rosiglitazone-treated mice, despite having improved IR, exhibited worse hepatic steatosis if administered together with HFD. Therefore, compared to rosiglitazone, Peptide 2 promotes more beneficial effects on the combined outcomes of insulin resistance, WAT dysfunction and hepatic steatosis.

**Supplementary Materials:** The following supporting information can be downloaded at: <https://www.mdpi.com/article/10.3390/metabo13020174/s1>, Table S1: diet composition; Table S2: primers sequence; Table S3: fibrosis assessment; Figure S1: high performance liquid chromatography and mass spectrometry of Peptide 2; Figure S2: EWH effects in WAT of Sprague Dawley; Figure S3: ITT and tissues weight for the in vivo peptide screening; Figure S4: Food and water intake; Figure S5: OGTT before peptide treatment; Figure S6: hyperinsulinemic-euglycemic clamp and ITT; Figure S7: adipose tissue total AKT and p-AKT; Figure S8: adipogenesis markers; Figure S9: Effect of PEP2 on 9 W pre-adipocyte differentiation; Figure S10: Effect of PEP2 on 9 B pre-adipocyte differentiation; Figure S11: lipid metabolism gene expression in LFD and HFD groups.

**Author Contributions:** S.C.d.C.Z. Conceptualization; formal analysis; investigation; methodology; visualization; writing—original draft; writing—review and editing. R.W. Investigation; writing—review and editing. J.T.Y.Y. Investigation; methodology; writing—review and editing. R.D.C. Methodology; writing—review and editing. J.W. Conceptualization; funding acquisition; methodology; writing—review and editing. H.V.-S. Investigation. C.B.C. Conceptualization; funding acquisition; methodology; supervision; writing—review and editing. M.A.M. Methodology; formal analysis; writing—review and editing. All authors have read and agreed to the published version of the manuscript.

**Funding:** S.C.d.C.Z was or is being funded by Alberta Diabetes Institute (ADI), University of Alberta and the Canadian Institute of Health Research (CIHR). J.T. is supported by the Canadian Institutes for Health Research (CIHR; PJT-378765), Natural Sciences and Engineering Research Council of Canada (NSERC; RGPIN-2016-06657), Canada Foundation for Innovation John R. Evans Leaders Fund (37267), and is a Tier 2 Canada Research Chair in Brain Regulation of Metabolism at the University of Alberta. J.W. is supported by the Natural Sciences and Engineering Research Council of Canada (RGPIN- 2018-04680 and NSERC CRDPJ 532150-18), and Egg Farmers of Canada. RDC is supported by CIHR (PJT 156226 and 169060) and NSERC (RGPIN-2017-04710). Grant funding was from Alberta Health Services. M.A.M. was funded by Conselho Nacional de Desenvolvimento Científico e Tecnológico (CNPq) (310287/2018-9) and Fundação de Amparo à Pesquisa do Estado de São Paulo (FAPESP) (2021/08354-2 and 2017/01184-9).

**Institutional Review Board Statement:** The animal study protocol was approved by the Animal Care and Use Committee of the University of Alberta (Protocol# 1472) in accordance with guidelines issued by the Canadian Council on Animal Care.

**Informed Consent Statement:** Not applicable.

**Data Availability Statement:** Data are contained within the article or Supplementary Materials.

**Acknowledgments:** We would like to thank Bryan Lum, Samantha Kinney, and Henver Brunetta for their skilled assistance during the clamp experiments, qPCR and cell culture experiments, respectively.

**Conflicts of Interest:** The authors declare no conflicts of interest.

## References

1. Younossi, Z.M. Non-alcoholic fatty liver disease—A global public health perspective. *J. Hepatol.* **2019**, *70*, 531–544. <https://doi.org/10.1016/j.jhep.2018.10.033>.
2. Friedman, S.L.; Neuschwander-Tetri, B.A.; Rinella, M.; Sanyal, A.J. Mechanisms of NAFLD development and therapeutic strategies. *Nat. Med.* **2018**, *24*, 908–922. <https://doi.org/10.1038/s41591-018-0104-9>.
3. Smith, G.I.; Shankaran, M.; Yoshino, M.; Schweitzer, G.G.; Chondronikola, M.; Beals, J.W.; Okunade, A.L.; Patterson, B.W.; Nyangau, E.; Field, T.; et al. Insulin resistance drives hepatic de novo lipogenesis in nonalcoholic fatty liver disease. *J. Clin. Investig.* **2020**, *130*, 1453–1460. <https://doi.org/10.1172/JCI134165>.
4. Softic, S.; Cohen, D.E.; Kahn, C.R. Role of Dietary Fructose and Hepatic De Novo Lipogenesis in Fatty Liver Disease. *Dig. Dis. Sci.* **2016**, *61*, 1282–1293. <https://doi.org/10.1007/s10620-016-4054-0>.
5. Godoy-Matos, A.F.; Silva Junior, W.S.; Valerio, C.M. NAFLD as a continuum: From obesity to metabolic syndrome and diabetes. *Diabetol. Metab. Syndr.* **2020**, *12*, 60. <https://doi.org/10.1186/s13098-020-00570-y>.
6. Colca, J.R.; Scherer, P.E. The metabolic syndrome, thiazolidinediones, and implications for intersection of chronic and inflammatory disease. *Mol. Metab.* **2022**, *55*, 101409. <https://doi.org/10.1016/j.molmet.2021.101409>.
7. Boettcher, E.; Csako, G.; Pucino, F.; Wesley, R.; Loomba, R. Meta-analysis: Pioglitazone improves liver histology and fibrosis in patients with non-alcoholic steatohepatitis. *Aliment. Pharmacol. Ther.* **2012**, *35*, 66–75. <https://doi.org/10.1111/j.1365-2036.2011.04912.x>.
8. Musso, G.; Cassader, M.; Paschetta, E.; Gambino, R. Thiazolidinediones and Advanced Liver Fibrosis in Nonalcoholic Steatohepatitis: A Meta-analysis. *JAMA Intern. Med.* **2017**, *177*, 633–640. <https://doi.org/10.1001/jamainternmed.2016.9607>.
9. FUFOSE. Scientific concepts of functional foods in Europe-consensus document. *Br. J. Nutr.* **1999**, *81*, S1–S27. <https://doi.org/10.1017/S0007114599000471>.
10. Jahandideh, F.; Chakrabarti, S.; Majumder, K.; Li, Q.; Panahi, S.; Morton, J.S.; Davidge, S.T.; Wu, J. Egg white protein hydrolysate reduces blood pressure, improves vascular relaxation and modifies aortic angiotensin II receptors expression in spontaneously hypertensive rats. *J. Funct. Foods* **2016**, *27*, 667–673. <https://doi.org/10.1016/j.jff.2016.10.019>.
11. Jahandideh, F.; Zani, S.C.C.; Son, M.; Proctor, S.D.; Davidge, S.T.; Chan, C.B.; Wu, J. Egg white hydrolysate enhances insulin sensitivity in high-fat diet-induced insulin-resistant rats via Akt activation. *Br. J. Nutr.* **2019**, *122*, 14–24. <https://doi.org/10.1017/S0007114519000837>.

12. Jahandideh, F.; Chakrabarti, S.; Davidge, S.T.; Wu, J. Egg white hydrolysate shows insulin mimetic and sensitizing effects in 3T3-F442A pre-adipocytes. *PLoS ONE* **2017**, *12*, e0185653. <https://doi.org/10.1371/journal.pone.0185653>.
13. Majumder, K.; Chakrabarti, S.; Morton, J.S.; Panahi, S.; Kaufman, S.; Davidge, S.T.; Wu, J. Egg-derived tri-peptide IRW exerts anti-hypertensive effects in spontaneously hypertensive rats. *PLoS ONE* **2013**, *8*, e82829. <https://doi.org/10.1371/journal.pone.0082829>.
14. de Campos Zani, S.C.; Son, M.; Bhullar, K.S.; Chan, C.B.; Wu, J. IRW (Isoleucine-Arginine-Tryptophan) Improves Glucose Tolerance in High Fat Diet Fed C57BL/6 Mice via Activation of Insulin Signaling and AMPK Pathways in Skeletal Muscle. *Biomedicines* **2022**, *10*, 1235. <https://doi.org/10.3390/biomedicines10061235>.
15. Jahandideh, F.; Liu, P.; Wu, J. Purification and identification of adipogenic-differentiating peptides from egg white hydrolysate. *Food Chem.* **2018**, *259*, 25–30. <https://doi.org/10.1016/j.foodchem.2018.03.099>.
16. Rocha, A.L.; de Lima, T.I.; de Souza, G.P.; Correa, R.O.; Ferrucci, D.L.; Rodrigues, B.; Lopes-Ramos, C.; Nilsson, D.; Knittel, T.L.; Castro, P.R.; et al. Enoxacin induces oxidative metabolism and mitigates obesity by regulating adipose tissue miRNA expression. *Sci. Adv.* **2020**, *6*, eabc6250. <https://doi.org/10.1126/sciadv.abc6250>.
17. Mighiu, P.I.; Yue, J.T.; Filippi, B.M.; Abraham, M.A.; Chari, M.; Lam, C.K.; Yang, C.S.; Christian, N.R.; Charron, M.J.; Lam, T.K. Hypothalamic glucagon signaling inhibits hepatic glucose production. *Nat. Med.* **2013**, *19*, 766–772. <https://doi.org/10.1038/nm.3115>.
18. Yue, J.T.; Abraham, M.A.; Bauer, P.V.; LaPierre, M.P.; Wang, P.; Duca, F.A.; Filippi, B.M.; Chan, O.; Lam, T.K. Inhibition of glycine transporter-1 in the dorsal vagal complex improves metabolic homeostasis in diabetes and obesity. *Nat. Commun.* **2016**, *7*, 13501. <https://doi.org/10.1038/ncomms13501>.
19. Folch, J.; Lees, M.; Sloane Stanley, G.H. A simple method for the isolation and purification of total lipides from animal tissues. *J. Biol. Chem.* **1957**, *226*, 497–509.
20. Ferri, F.; Carotti, S.; Carpino, G.; Mischitelli, M.; Cantafora, A.; Molinaro, A.; Argenziano, M.E.; Parisse, S.; Corsi, A.; Riminucci, M.; et al. The Propensity of the Human Liver to Form Large Lipid Droplets Is Associated with PNPLA3 Polymorphism, Reduced INSIG1 and NPC1L1 Expression and Increased Fibrogenetic Capacity. *Int. J. Mol. Sci.* **2021**, *22*, 6100. <https://doi.org/10.3390/ijms22116100>.
21. Yersiz, H.; Lee, C.; Kaldas, F.M.; Hong, J.C.; Rana, A.; Schnickel, G.T.; Wertheim, J.A.; Zarrinpar, A.; Agopian, V.G.; Gornbein, J.; et al. Assessment of hepatic steatosis by transplant surgeon and expert pathologist: A prospective, double-blind evaluation of 201 donor livers. *Liver Transpl.* **2013**, *19*, 437–449. <https://doi.org/10.1002/lt.23615>.
22. Brunt, E.M. Pathology of fatty liver disease. *Mod. Pathol.* **2007**, *20* (Suppl. S1), S40–S48. <https://doi.org/10.1038/modpathol.3800680>.
23. Ferdouse, A.; Agrawal, R.R.; Gao, M.A.; Jiang, H.; Blaner, W.S.; Clugston, R.D. Alcohol induced hepatic retinoid depletion is associated with the induction of multiple retinoid catabolizing cytochrome P450 enzymes. *PLoS ONE* **2022**, *17*, e0261675. <https://doi.org/10.1371/journal.pone.0261675>.
24. Eslam, M.; Newsome, P.N.; Sarin, S.K.; Anstee, Q.M.; Targher, G.; Romero-Gomez, M.; Zelber-Sagi, S.; Wai-Sun Wong, V.; Dufour, J.F.; Schattenberg, J.M.; et al. A new definition for metabolic dysfunction-associated fatty liver disease: An international expert consensus statement. *J. Hepatol.* **2020**, *73*, 202–209. <https://doi.org/10.1016/j.jhep.2020.03.039>.
25. Ghaben, A.L.; Scherer, P.E. Adipogenesis and metabolic health. *Nat. Rev. Mol. Cell Biol.* **2019**, *20*, 242–258. <https://doi.org/10.1038/s41580-018-0093-z>.
26. Sakurai, Y.; Kubota, N.; Yamauchi, T.; Kadowaki, T. Role of Insulin Resistance in MAFLD. *Int. J. Mol. Sci.* **2021**, *22*, 4156. <https://doi.org/10.3390/ijms22084156>.
27. Garces-Rimon, M.; Gonzalez, C.; Vera, G.; Uranga, J.A.; Lopez-Fandino, R.; Lopez-Miranda, V.; Miguel, M. Pepsin egg white hydrolysate improves glucose metabolism complications related to metabolic syndrome in Zucker fatty rats. *Nutrients* **2018**, *10*, 441. <https://doi.org/10.3390/nu10040441>.
28. Gao, M.; Ma, Y.; Alsaggar, M.; Liu, D. Dual Outcomes of Rosiglitazone Treatment on Fatty Liver. *AAPS J.* **2016**, *18*, 1023–1031. <https://doi.org/10.1208/s12248-016-9919-9>.
29. Lee, S.M.; Muratalla, J.; Diaz-Ruiz, A.; Remon-Ruiz, P.; McCann, M.; Liew, C.W.; Kineman, R.D.; Cordoba-Chacon, J. Rosiglitazone Requires Hepatocyte PPARgamma Expression to Promote Steatosis in Male Mice With Diet-Induced Obesity. *Endocrinology* **2021**, *162*, bqab175. <https://doi.org/10.1210/endo/bqab175>.
30. Vidal-Puig, A.; Jimenez-Linan, M.; Lowell, B.B.; Hamann, A.; Hu, E.; Spiegelman, B.; Flier, J.S.; Moller, D.E. Regulation of PPAR gamma gene expression by nutrition and obesity in rodents. *J. Clin. Investig.* **1996**, *97*, 2553–2561. <https://doi.org/10.1172/JCI118703>.
31. Rosenstengel, S.; Stoeppler, S.; Bahde, R.; Spiegel, H.U.; Palmes, D. Type of steatosis influences microcirculation and fibrogenesis in different rat strains. *J. Investig. Surg.* **2011**, *24*, 273–282. <https://doi.org/10.3109/08941939.2011.586094>.
32. Najt, C.P.; Senthivayagam, S.; Aljazi, M.B.; Fader, K.A.; Olenic, S.D.; Brock, J.R.; Lydic, T.A.; Jones, A.D.; Atshaves, B.P. Liver-specific loss of Perilipin 2 alleviates diet-induced hepatic steatosis, inflammation, and fibrosis. *Am. J. Physiol. Gastrointest. Liver Physiol.* **2016**, *310*, G726–738. <https://doi.org/10.1152/ajpgi.00436.2015>.
33. Garces-Rimon, M.; Gonzalez, C.; Uranga, J.A.; Lopez-Miranda, V.; Lopez-Fandino, R.; Miguel, M. Pepsin egg white hydrolysate ameliorates obesity-related oxidative stress, inflammation and steatosis in Zucker fatty rats. *PLoS ONE* **2016**, *11*, e0151193. <https://doi.org/10.1371/journal.pone.0151193>.

34. Lemus-Conejo, A.; Grao-Cruces, E.; Toscano, R.; Varela, L.M.; Claro, C.; Pedroche, J.; Millan, F.; Millan-Linares, M.C.; Montserrat-de la Paz, S. A lupine (*Lupinus angustifolius* L.) peptide prevents non-alcoholic fatty liver disease in high-fat-diet-induced obese mice. *Food Funct.* **2020**, *11*, 2943–2952. <https://doi.org/10.1039/d0fo00206b>.
35. Dumeus, S.; Shibu, M.A.; Lin, W.T.; Wang, M.F.; Lai, C.H.; Shen, C.Y.; Lin, Y.M.; Viswanadha, V.P.; Kuo, W.W.; Huang, C.Y. Bioactive Peptide Improves Diet-Induced Hepatic Fat Deposition and Hepatocyte Proinflammatory Response in SAMP8 Ageing Mice. *Cell Physiol. Biochem.* **2018**, *48*, 1942–1952. <https://doi.org/10.1159/000492518>.
36. Song, C.; Lv, W.; Li, Y.; Nie, P.; Lu, J.; Geng, Y.; Heng, Z.; Song, L. Alleviating the effect of quinoa and the underlying mechanism on hepatic steatosis in high-fat diet-fed rats. *Nutr. Metab.* **2021**, *18*, 106. <https://doi.org/10.1186/s12986-021-00631-7>.
37. Steckelings, U.M.; Widdop, R.E.; Sturrock, E.D.; Lubbe, L.; Hussain, T.; Kaschina, E.; Unger, T.; Hallberg, A.; Carey, R.M.; Summers, C. The Angiotensin AT(2) Receptor: From a Binding Site to a Novel Therapeutic Target. *Pharmacol. Rev.* **2022**, *74*, 1051–1135. <https://doi.org/10.1124/pharmrev.120.000281>.
38. Goh, G.B.; Pagadala, M.R.; Dasarathy, J.; Unalp-Arida, A.; Sargent, R.; Hawkins, C.; Sourianarayanan, A.; Khiyami, A.; Yerian, L.; Pai, R.; et al. Renin-angiotensin system and fibrosis in non-alcoholic fatty liver disease. *Liver Int.* **2015**, *35*, 979–985. <https://doi.org/10.1111/liv.12611>.
39. Zhang, W.; Miao, J.; Li, P.; Wang, Y.; Zhang, Y. Up-regulation of components of the renin-angiotensin system in liver fibrosis in the rat induced by CCL(4). *Res. Vet. Sci.* **2013**, *95*, 54–58. <https://doi.org/10.1016/j.rvsc.2013.01.028>.
40. Nabeshima, Y.; Tazuma, S.; Kanno, K.; Hyogo, H.; Iwai, M.; Horiuchi, M.; Chayama, K. Anti-fibrogenic function of angiotensin II type 2 receptor in CCl4-induced liver fibrosis. *Biochem. Biophys. Res. Commun.* **2006**, *346*, 658–664. <https://doi.org/10.1016/j.bbrc.2006.05.183>.
41. Chai, W.; Wang, W.; Dong, Z.; Cao, W.; Liu, Z. Angiotensin II receptors modulate muscle microvascular and metabolic responses to insulin in vivo. *Diabetes* **2011**, *60*, 2939–2946. <https://doi.org/10.2337/db10-1691>.
42. Henrion, D.; Kubis, N.; Levy, B.I. Physiological and pathophysiological functions of the AT(2) subtype receptor of angiotensin II: From large arteries to the microcirculation. *Hypertension* **2001**, *38*, 1150–1157. <https://doi.org/10.1161/hy1101.096109>.
43. Ito, M.; Suzuki, J.; Tsujioka, S.; Sasaki, M.; Gomori, A.; Shirakura, T.; Hirose, H.; Ito, M.; Ishihara, A.; Iwaasa, H.; et al. Longitudinal analysis of murine steatohepatitis model induced by chronic exposure to high-fat diet. *Hepatol. Res.* **2007**, *37*, 50–57. <https://doi.org/10.1111/j.1872-034X.2007.00008.x>.
44. Kristiansen, M.N.B.; Veidal, S.S.; Christoffersen, C.; Jelsing, J.; Rigbolt, K.T.G. Molecular Characterization of Microvesicular and Macrovesicular Steatosis Shows Widespread Differences in Metabolic Pathways. *Lipids* **2019**, *54*, 109–115. <https://doi.org/10.1002/lipd.12121>.
45. Hayashi, Y.; Suemitsu, E.; Kajimoto, K.; Sato, Y.; Akhter, A.; Sakurai, Y.; Hatakeyama, H.; Hyodo, M.; Kaji, N.; Baba, Y.; et al. Hepatic Monoacylglycerol O-acyltransferase 1 as a Promising Therapeutic Target for Steatosis, Obesity, and Type 2 Diabetes. *Mol. Ther. Nucleic Acids* **2014**, *3*, e154. <https://doi.org/10.1038/mtna.2014.4>.
46. Lee, Y.J.; Ko, E.H.; Kim, J.E.; Kim, E.; Lee, H.; Choi, H.; Yu, J.H.; Kim, H.J.; Kim, K.S.; Seong, J.K.; Kim, K.S.; et al. Nuclear receptor PPAR-gamma-regulated monoacylglycerol O-acyltransferase 1 (MGAT1) expression is responsible for the lipid accumulation in diet-induced hepatic steatosis. *Proc. Natl. Acad. Sci. USA* **2012**, *109*, 13656–13661. <https://doi.org/10.1073/pnas.1203218109>.
47. Lutkewitte, A.J.; Singer, J.M.; Shew, T.M.; Martino, M.R.; Hall, A.M.; He, M.; Finck, B.N. Multiple antisense oligonucleotides targeted against monoacylglycerol acyltransferase 1 (Mogat1) improve glucose metabolism independently of Mogat1. *Mol. Metab.* **2021**, *49*, 101204. <https://doi.org/10.1016/j.molmet.2021.101204>.
48. Lutkewitte, A.J.; McCommis, K.S.; Schweitzer, G.G.; Chambers, K.T.; Graham, M.J.; Wang, L.; Patti, G.J.; Hall, A.M.; Finck, B.N. Hepatic monoacylglycerol acyltransferase 1 is induced by prolonged food deprivation to modulate the hepatic fasting response. *J. Lipid Res.* **2019**, *60*, 528–538. <https://doi.org/10.1194/jlr.M089722>.
49. Carreres, L.; Jilkova, Z.M.; Vial, G.; Marche, P.N.; Decaens, T.; Lerat, H. Modeling Diet-Induced NAFLD and NASH in Rats: A Comprehensive Review. *Biomedicines* **2021**, *9*, 378. <https://doi.org/10.3390/biomedicines9040378>.
50. Charlton, M.; Krishnan, A.; Viker, K.; Sanderson, S.; Cazanave, S.; McConico, A.; Masuoko, H.; Gores, G. Fast food diet mouse: Novel small animal model of NASH with ballooning, progressive fibrosis, and high physiological fidelity to the human condition. *Am. J. Physiol. Gastrointest. Liver Physiol.* **2011**, *301*, G825–834. <https://doi.org/10.1152/ajpgi.00145.2011>.
51. Zhu, Y.; Lao, F.; Pan, X.; Wu, J. Food Protein-Derived Antioxidant Peptides: Molecular Mechanism, Stability and Bioavailability. *Biomolecules* **2022**, *12*, 1622. <https://doi.org/10.3390/biom12111622>.

**Disclaimer/Publisher’s Note:** The statements, opinions and data contained in all publications are solely those of the individual author(s) and contributor(s) and not of MDPI and/or the editor(s). MDPI and/or the editor(s) disclaim responsibility for any injury to people or property resulting from any ideas, methods, instructions or products referred to in the content.

## **APPENDIX 2**

PDF file for the paper published and included in this thesis in Chapter 4



Article

# IRW (Isoleucine–Arginine–Tryptophan) Improves Glucose Tolerance in High Fat Diet Fed C57BL/6 Mice via Activation of Insulin Signaling and AMPK Pathways in Skeletal Muscle

Stepheny C. de Campos Zani <sup>1</sup>, Myoungjin Son <sup>2</sup>, Khushwant S. Bhullar <sup>2,3</sup>, Catherine B. Chan <sup>1,2</sup> and Jianping Wu <sup>2,\*</sup>

- <sup>1</sup> Department of Physiology, University of Alberta, Edmonton, AB T6G 2H7, Canada; zani@ualberta.ca (S.C.d.C.Z.); cbchan@ualberta.ca (C.B.C.)  
<sup>2</sup> Department of Agricultural Food & Nutritional Science, University of Alberta, Edmonton, AB T6G 2P5, Canada; mjson0823@gmail.com (M.S.); bhullar@ualberta.ca (K.S.B.)  
<sup>3</sup> Department of Pharmacology, University of Alberta, Edmonton, AB T6G 2H7, Canada  
\* Correspondence: jw3@ualberta.ca; Tel.: +1-780-492-6885; Fax: +1-780-492-4346



**Citation:** de Campos Zani, S.C.; Son, M.; Bhullar, K.S.; Chan, C.B.; Wu, J. IRW (Isoleucine–Arginine–Tryptophan) Improves Glucose Tolerance in High Fat Diet Fed C57BL/6 Mice via Activation of Insulin Signaling and AMPK Pathways in Skeletal Muscle. *Biomedicines* **2022**, *10*, 1235. <https://doi.org/10.3390/biomedicines10061235>

Academic Editor: Jun Lu

Received: 11 May 2022

Accepted: 25 May 2022

Published: 26 May 2022

**Publisher's Note:** MDPI stays neutral with regard to jurisdictional claims in published maps and institutional affiliations.



**Copyright:** © 2022 by the authors. Licensee MDPI, Basel, Switzerland. This article is an open access article distributed under the terms and conditions of the Creative Commons Attribution (CC BY) license (<https://creativecommons.org/licenses/by/4.0/>).

**Abstract:** IRW (Isoleucine–Arginine–Tryptophan), has antihypertensive and anti-inflammatory properties in cells and animal models and prevents angiotensin-II- and tumor necrosis factor (TNF)- $\alpha$ -induced insulin resistance (IR) in vitro. We investigated the effects of IRW on body composition, glucose homeostasis and insulin sensitivity in a high-fat diet (HFD) induced insulin resistant (IR) model. C57BL/6 mice were fed HFD for 6 weeks, after which IRW was incorporated into the diet (45 or 15 mg/kg body weight (BW)) until week 14. IRW45 (at a dose of 45 mg/kg BW) reduced BW ( $p = 0.0327$ ), fat mass gain ( $p = 0.0085$ ), and preserved lean mass of HFD mice ( $p = 0.0065$ ), concomitant with enhanced glucose tolerance and reduced fasting glucose ( $p < 0.001$ ). In skeletal muscle, IRW45 increased insulin-stimulated protein kinase B (AKT) phosphorylation ( $p = 0.0132$ ) and glucose transporter 4 (GLUT4) translocation ( $p < 0.001$ ). Angiotensin 2 receptor (AT2R) ( $p = 0.0024$ ), phosphorylated 5'-AMP-activated protein kinase (AMPK $\alpha$ ) ( $p < 0.0124$ ) and peroxisome proliferator-activated receptor gamma (PPAR $\gamma$ ) ( $p < 0.001$ ) were enhanced in skeletal muscle of IRW45-treated mice, as was the expression of genes involved in myogenesis. Plasma angiotensin converting enzyme-2 (ACE2) activity was increased ( $p = 0.0016$ ). Uncoupling protein-1 in white adipose tissue (WAT) was partially restored after IRW supplementation. IRW improves glucose tolerance and body composition in HFD-fed mice and promotes glucose uptake in skeletal muscle via multiple signaling pathways, independent of angiotensin converting enzyme (ACE) inhibition.

**Keywords:** ACE; bioactive peptides; IRW; insulin resistance; obesity

## 1. Introduction

The pathophysiology of Metabolic syndrome (MetS) is complex involving obesity, IR, dyslipidemia, and hypertension, but oxidative stress and inflammation also contribute to its progression [1]. MetS also involves overactivation of the renin angiotensin system (RAS), which is linked to obesity and IR [2]. Besides the systemic RAS, an independent local RAS in skeletal muscle [3] influences insulin responsiveness [4]. ACE inhibitors or angiotensin II type 1 receptor (AT1R) blockers reduce IR in animal models and also improve insulin sensitivity in humans [5–7], supporting the link between RAS and IR. Also, RAS blockade reverses the deleterious effect of exogenous angiotensin II on skeletal muscle mitochondria and improves glycemic control in mice [8].

Food-derived bioactive peptides exert effects beyond their nutritional value and modulate physiological parameters in different tissues [9]. Previous research demonstrated the beneficial effects of egg-derived peptides and hydrolysates on glucose tolerance [10], adipogenic capacity [11], and osteoblast differentiation [12]. Some egg-derived bioactive

peptides are ACE inhibitors [13] and ameliorate IR and glucose intolerance [14]. Of particular interest is the ovotransferrin-derived, ACE inhibitory peptide [15] tripeptide IRW (Isoleucine–Arginine–Tryptophan), which exhibits anti-inflammatory and antioxidant effects in endothelial cells [16,17], reduces blood pressure in rodents [18,19], and improves angiotensin II- or TNF- $\alpha$ -induced IR in a skeletal muscle cell line [20,21]. However, whether IRW has glucoregulatory properties in vivo is unknown.

In this study, we investigated the insulin sensitizing effects of IRW in vivo using a high fat diet (HFD)-induced obese-IR mouse model. Because of the intimate crosstalk between obesity, hypertension, and IR, we hypothesized that IRW supplementation improves glucose intolerance by inhibiting RAS locally in skeletal muscle to improve insulin signaling.

## 2. Materials and Methods

### 2.1. Animals, Diet, and Body Weight (BW) Measurements

The animal experimental protocol was approved by the Animal Care and Use Committee of the University of Alberta (Protocol# 1402) in accordance with guidelines issued by the Canadian Council on Animal Care and followed the ARRIVE guidelines. Thirty-two male 4-week-old C57BL/6 mice were purchased from Charles River Canada (St. Constant, QC, Canada) and housed 2 per cage with *ad libitum* access to standard food and water, a 12:12-h cycle of light:dark with 60% humidity and 23 °C temperature. Eight mice were fed with low fat diet (LFD, 10% kcal from fat, Envigo, Indianapolis, IN, USA, TD06415) and the remainder with HFD (45% kcal from fat, Envigo TD110675) for 6 weeks. Diet composition is shown in Table 1. The initial 6 weeks of HFD were used to induce obesity, confirmed by at least a 20% increase in BW and significantly higher fat mass and lower lean mass compared to low fat diet (LFD) fed animals (Supplementary Table S1). Animals were then divided into 4 groups: LFD control, HFD control, high dose IRW + HFD (IRW45; at a dose of 45 mg/kg BW), low dose IRW + HFD (IRW15; at a dose of 15 mg/kg BW) (n = 8/group). These diets continued for another 8 weeks with *ad libitum* access to food and water. In total, mice consumed HFD for 14 weeks to induce obesity and glucose intolerance [22]. Food consumption was measured once every 3 days and BW twice weekly. Body composition was evaluated using magnetic resonance imaging (MRI), Echo MRI<sup>TM</sup> (Echo Medical Systems LLC, Houston, TX, USA) at week 6 and week 14.

**Table 1.** Diet composition.

	LFD	HFD	IRW15	IRW45
Casein (g/kg)	210.0	245.0	245.0	245.0
L-Cystine (g/kg)	3.0	3.5	3.5	3.5
Corn Starch (g/kg)	445.0	85.0	85.0	85.0
Maltodextrin (g/kg)	50.0	115.0	115.0	115.0
Sucrose (g/kg)	160.0	200.0	200.0	200.0
Lard (g/kg)	20.0	195.0	195.0	195.0
Soybean Oil (g/kg)	20.0	30.0	30.0	30.0
Cellulose (g/kg)	37.15	58.0	58.0	58.0
Mineral Mix, AIN-93G-MX (94046) (g/kg)	35.0	43.0	43.0	43.0
Calcium Phosphate, dibasic (g/kg)	2.0	3.4	3.4	3.4
Vitamin Mix, AIN-93-VX (94047) (g/kg)	15.0	19.0	19.0	19.0
Choline Bitartrate (g/kg)	2.75	3.0	3.0	3.0
IRW (mg/kg BW)	n/a	n/a	15	45

### 2.2. IRW Dosage

The estimated doses of IRW used were 45 mg/kg BW and 15 mg/kg BW. The dosages were selected based on previous studies done by our group in spontaneous hypertensive rats [18,19] and cell line studies [15,16]. The peptide was administered mixed in the animal's diet starting at week 7 of the 14-week trial, and the animals had *ad libitum* access to food and water. IRW was synthesized by Genscript (Piscataway, NJ, USA) with  $\geq 98\%$  purity.

### 2.3. Oral Glucose Tolerance and Insulin Tolerance Tests

At weeks 12 and 13, respectively, ITT and OGTT were performed [23] with the following modifications: For ITT, 1.5 IU/kg BW insulin was injected intraperitoneally. For OGTT, 70% glucose solution was used, and 1 g of glucose/kg BW was given via oral gavage. In both cases, blood glucose was measured for up to 2 h. Blood glucose was measured from the tail vein using a Contour<sup>®</sup>Next glucometer (Mississauga, ON, Canada). Fasting glucose and fasting insulin were used to calculate homeostatic model assessment insulin resistance (HOMA-IR) using the formula: (fasting glucose (mmol/L)) × (fasting insulin (μU/mL))/22.5). OGTT was the primary outcome assessed in this study.

### 2.4. Tissue Collection

At week 14, all animals were fasted for 16 h and injected with insulin (2 IU/kg BW) intraperitoneally to stimulate insulin signaling 10 min prior to euthanasia. Animals were euthanized using CO<sub>2</sub> and blood was collected via cardiac puncture. Plasma, gastrocnemius skeletal muscle and WAT from retroperitoneal and epididymal depots were collected, snap frozen, and stored at −80 °C until further analysis.

### 2.5. Protein Extraction and Western Blotting

Total protein from skeletal muscle was extracted using a lysis buffer containing phosphatase and protease inhibitors. WAT total protein extraction was performed using a commercial kit (Invent Biotechnologies Inc., Plymouth, MA, USA). Plasma membrane protein was extracted using a commercial kit (Thermo Fisher Scientific, Waltham, MA, USA) [20]. Total protein content was measured using the bicinchoninic acid assay. Western blotting was performed as previously [10] with the following modifications: a 9% sodium dodecyl sulfate polyacrylamide gel electrophoresis was run and protein was transferred to a nitrocellulose membrane, which was incubated overnight with antibodies against p-AKT (Cell Signaling Technology, Beverly, MA, USA), AKT (Santa Cruz Biotechnologies Inc., Dallas, TX, USA), GLUT4 (Abcam, Toronto, ON, Canada), ACE, ACE2, AT1R, AT2R, Mas receptor, PPAR-γ, mammalian target of rapamycin (mTOR), p-mTOR, AMPKα, p-AMPKα (Thr172), P70 S6 kinase (S6K), p-P70 S6K (Thr389), uncoupling protein (UCP)-1 (Sigma, St. Louis, MO, USA), β-actin (Sigma) and glyceraldehyde-3-phosphate dehydrogenase (GAPDH). After incubating with appropriate fluorescent-conjugated secondary antibodies (Li-cor Biosciences, Lincoln, NE, USA) for 1 h at room temperature, protein bands were quantified by densitometry using Image Studio Lite 5.2 (Li-Cor Biosciences).

### 2.6. Plasma RAS Components and Insulin

Plasma concentrations of RAS components were quantified by mouse specific commercial ELISAs: ACE (Aviva System, San Diego, CA, USA), ACE2 (Abcam), angiotensin II (Enzo Life Sciences, Burlington, ON, Canada), angiotensin (1–7) (Aviva System). Insulin was measured using an ELISA from (Abcam, Toronto, ON, Canada).

### 2.7. RNA Sequencing and Quantitative RT-PCR (qPCR)

Total RNA was extracted from skeletal muscle using TRIzol reagent (Invitrogen, Life Technologies Inc., Burlington, ON, Canada) and quantified by measuring the absorbance at 260 nm and purity assessed by the A<sub>260</sub>/280 ratio. Total RNA (500 ng, with RNA integrity number > 8 for all samples) was used for the preparation of RNAseq libraries with the NEBNext Ultra II Directional RNA Library Prep Kit from Illumina (NEB, Mississauga, ON, Canada). Enriched mRNA was reverse-transcribed and second-strand cDNA synthesis was performed. Double-stranded cDNAs were A-tailed to enable adapter ligation and, finally, libraries were indexed by 15 PCR cycles. Libraries were sequenced on a NextSeq 500 instrument (Illumina), following a paired-end 150 cycle protocol. Deregulated transcripts were annotated using the BioMart database from Ensembl (EMBL-EBI Hinxton, Cambridgeshire, UK).

For qPCR, cDNA was synthesized from 1 µg total RNA using the High-Capacity cDNA Reverse Transcription Kit (Thermo Fisher Scientific, Waltham, MA, USA). mRNA expression of target genes was determined by real-time qPCR using GAPDH as the endogenous control. All of the qPCR experiments and analyses were conducted using the MIQE guidelines [24]. The primers were designed based on the genomic sequence deposited in GenBank are described in Table S2.

### 2.8. Statistics and Sample Size

All data presented were expressed as mean ± SEM of 5–8 mice from each treatment group as indicated in the figure and table legends. Statistical analysis was performed using GraphPad Prism 7.0 (San Diego, CA, USA). Outliers indicated by the statistical software were removed prior to data evaluation. Data were evaluated by one-way ANOVA, Kruskal–Wallis’ test, or two-way ANOVA when appropriate. HFD group was set as the control group for all the analysis because our intention was to evaluate the impact of a HFD supplemented with peptide compared to HFD alone. For RNA sequencing, transcripts were considered differentially expressed when they had a corrected *p*-value < 0.05. Post hoc analysis was done using Bonferroni’s or Dunn’s test. *p*-value was considered significant if < 0.05.

## 3. Results

### 3.1. Food Intake and Body Composition

No sustained differences in food intake were detected between the groups (Supplementary Figure S1). At week 14 the LFD group had lower BW than the HFD group (*p* < 0.001). Of the peptide treatments, only the high dose of IRW (IRW45) reduced final BW (*p* = 0.0327) and both absolute (g) and relative (%) BW gain (*p* < 0.001). Moreover, the IRW45 group presented lower absolute (g) (*p* < 0.001) and relative (%) fat mass gain (*p* = 0.0085), and less relative (%) lean mass loss (*p* = 0.0065) compared to the HFD group (Table 2). BW and composition changes were not seen with IRW15.

**Table 2.** Body composition and metabolic profile of mice supplemented with IRW. Analysis by one-way ANOVA followed by Bonferroni’s post hoc test (lean mass change, fasting glucose initial and HOMA-IR) or Kruskal–Wallis’s test followed by Dunn’s post-hoc test. Data expressed as mean ± SEM of *n* = 7–8 mice. Values in the same row represented by different letters are statistically different (*p* ≤ 0.05) compared to HFD control.

	LFD	HFD	IRW45	IRW15
<b>Body composition</b>				
BW week 6 (g)	28.1 ± 0.8 <sup>a</sup>	31.3 ± 0.7 <sup>a</sup>	30.9 ± 0.9 <sup>a</sup>	31.7 ± 1.0 <sup>a</sup>
BW week 14 (g)	35.0 ± 0.7 <sup>a</sup>	41.6 ± 0.8 <sup>b</sup>	36.9 ± 0.5 <sup>a</sup>	40.4 ± 1.0 <sup>b</sup>
BW gain (g) (week 6–14)	7.0 ± 0.2 <sup>a</sup>	10.2 ± 0.3 <sup>b</sup>	6.0 ± 0.6 <sup>a</sup>	8.6 ± 0.6 <sup>b</sup>
BW gain (% of week 6)	25.1 ± 1.2 <sup>a</sup>	32.8 ± 1.3 <sup>b</sup>	19.9 ± 2.3 <sup>a</sup>	27.5 ± 2.2 <sup>b</sup>
Fat mass gain (g)	3.9 ± 0.5 <sup>a</sup>	7.0 ± 0.3 <sup>b</sup>	3.6 ± 0.4 <sup>a</sup>	6.1 ± 0.4 <sup>b</sup>
Fat mass gain (% BW)	8.2 ± 1.1 <sup>b</sup>	9.5 ± 0.8 <sup>b</sup>	4.8 ± 0.9 <sup>a</sup>	8.9 ± 0.9 <sup>b</sup>
Lean mass change (g)	0.8 ± 0.3 <sup>a</sup>	2.6 ± 0.1 <sup>b</sup>	2.0 ± 0.1 <sup>b</sup>	2.3 ± 0.2 <sup>b</sup>
Lean mass change (% BW)	−7.8 ± 1.0 <sup>b</sup>	−9.2 ± 0.7 <sup>b</sup>	−5.0 ± 0.9 <sup>a</sup>	−7.9 ± 0.9 <sup>b</sup>
<b>Metabolic profile</b>				
Fasting glucose week 6 (mmol/L)	4.5 ± 0.06 <sup>a</sup>	4.7 ± 0.3 <sup>a</sup>	5.0 ± 0.3 <sup>a</sup>	4.7 ± 0.2 <sup>a</sup>
Fasting glucose week 14 (mmol/L)	4.8 ± 0.1 <sup>a</sup>	6.3 ± 0.4 <sup>b</sup>	4.4 ± 0.2 <sup>a</sup>	5.7 ± 0.2 <sup>b</sup>
Fasting insulin week 14 (uU/mL)	192.4 ± 37.3 <sup>a</sup>	780.0 ± 56.4 <sup>b</sup>	383.1 ± 72.5 <sup>a</sup>	623.7 ± 112.7 <sup>b</sup>
HOMA-IR	5.7 ± 0.8 <sup>a</sup>	32.0 ± 3.2 <sup>b</sup>	11.0 ± 2.0 <sup>a</sup>	23.0 ± 4.7 <sup>b</sup>

### 3.2. Glucose Homeostasis and Plasma Insulin

The IRW45 group had lower fasting blood glucose beginning at week 9 of treatment compared to the HFD group (Figure 1A) and two-way ANOVA analysis showed significant

interaction ( $p < 0.001$ ) and diet effects ( $p < 0.001$ ). At week 14, the LFD and IRW45 groups had lower fasting plasma insulin concentration ( $p < 0.001$ ) and fasting blood glucose ( $p < 0.001$ ) compared to the HFD (Table 2). HOMA-IR was lower in LFD ( $p < 0.0001$ ) and IRW45 ( $p < 0.001$ ) groups compared to HFD. However, HOMA-IR from the IRW15 did not differ from the HFD group (Table 2). Two-way ANOVA showed a diet effect on OGTT ( $p = 0.001$ ). Both doses of IRW lowered circulating glucose at 15 and 30 min compared with HFD (Figure 1B). The area under the curve (AUC) was lower in the LFD ( $p < 0.001$ ) and IRW45 ( $p = 0.0195$ ) compared to the HFD group (Figure 1C). Despite changes in ITT when expressed as absolute glucose concentrations (Supplementary Figure S2), no significant differences between the groups were observed when data were adjusted to baseline blood glucose concentration (Figure 1D).

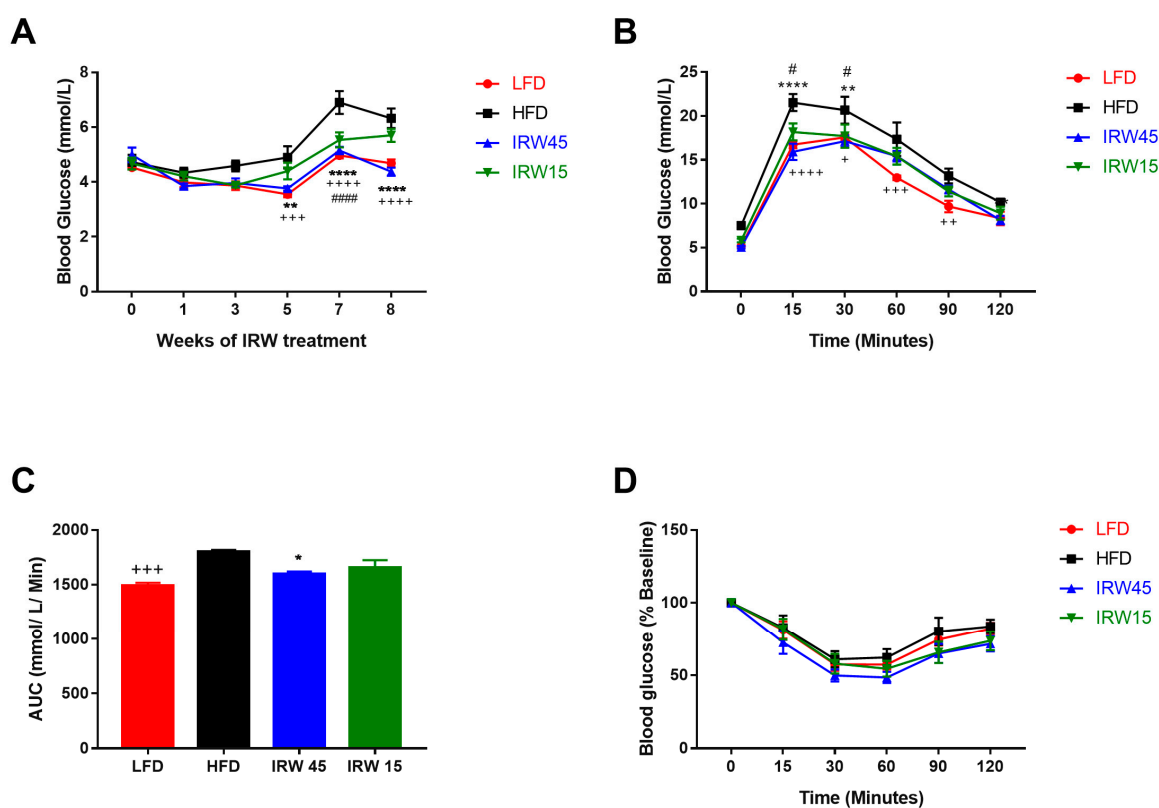


**Figure 1.** Glucose homeostasis after IRW supplementation. (A) Fasting glucose over time ( $n = 6–8$ ), (B) Oral glucose tolerance test (OGTT) ( $n = 6–8$ ). (C) Area under the curve (AUC) for OGTT ( $n = 5–8$ ). (D) Insulin tolerance test (ITT) as percentage of the baseline glucose values ( $n = 8$ ). Data expressed as mean  $\pm$  SEM and analyzed by two-way ANOVA (A,C,D) or one-way ANOVA (B) followed by Bonferroni’s post-hoc comparison test. \*  $p < 0.05$ , \*\*  $p < 0.01$  and \*\*\*\*  $p < 0.0001$  between IRW45 and HFD. #  $p < 0.05$  and #####  $p < 0.0001$  between IRW15 and HFD. +  $p < 0.05$ , ++  $p < 0.01$ , +++  $p < 0.001$  and ++++  $p < 0.0001$  between LFD and HFD.

### 3.3. Insulin Signaling and PPAR $\gamma$ Abundance

Insulin-stimulated phosphorylation of AKT (Ser473) in muscle was higher in LFD ( $p = 0.0196$ ) and IRW45 ( $p = 0.0132$ ) compared to the HFD group, whereas IRW15 was non-significantly increased (Figure 2A). Consistent with this result, GLUT 4 translocation to the plasma membrane in skeletal muscle was ~4-fold higher in the IRW45 ( $p < 0.001$ ) and 2-fold higher in IRW15 ( $p = 0.04$ ) compared to the HFD group, as shown by the ratio of membrane GLUT4/cytosol GLUT4 (Figure 2B). In addition, PPAR $\gamma$  abundance was 15–17-fold higher in LFD ( $p = 0.0013$ ) and IRW45 ( $p < 0.001$ ) compared to HFD (Figure 2C).

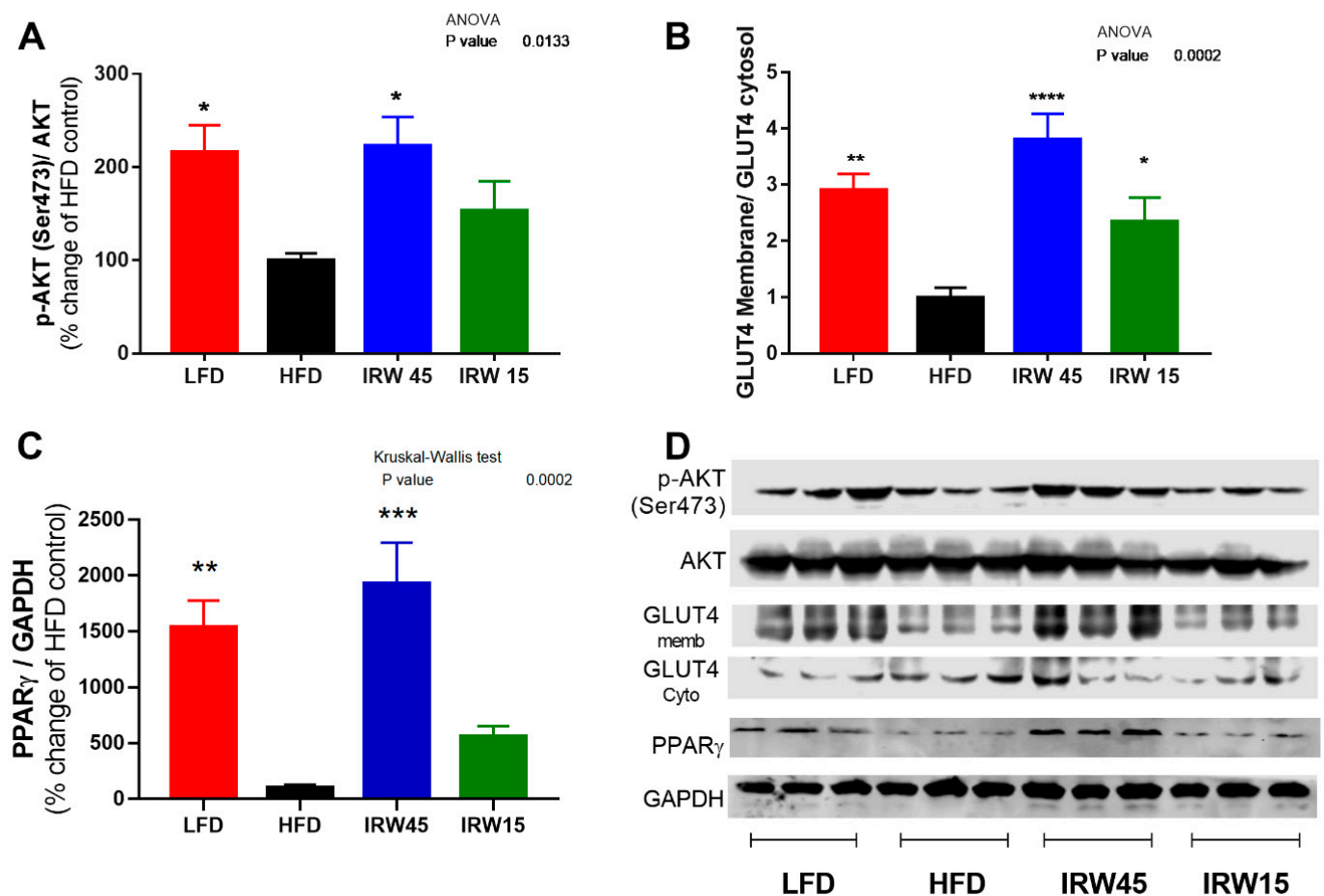


**Figure 2.** Skeletal muscle insulin signaling and PPAR<sub>γ</sub> abundance. (A) p-AKT, (B) GLUT4 membrane/cytosol, (C) PPAR<sub>γ</sub>, and (D) representative blots. p-AKT was normalized to total AKT. GLUT4 is expressed as a ratio of membrane to cytosolic GLUT4. PPAR<sub>γ</sub> was normalized to GAPDH. Data expressed as mean ± SEM of n = 6. Analysis by one-way ANOVA followed by Bonferroni's post-hoc test or Kruskal–Wallis followed by Dunn's post-hoc test. \*  $p < 0.05$ , \*\*  $p < 0.01$  \*\*\*  $p < 0.001$  and \*\*\*\*  $p < 0.0001$  versus HFD. AKT, Protein kinase B; PPAR<sub>γ</sub>, Peroxisome proliferator-activated receptor gamma; GLUT4, glucose transporter 4.

In both retroperitoneal and epididymal WAT, no changes in AKT phosphorylation or PPAR<sub>γ</sub> abundance were seen following IRW supplementation (Supplementary Figure S3A–F).

### 3.4. RAS Components

In skeletal muscle, there were no significant differences in ACE2, AT1R, and Mas receptor between the groups (Figure 3B,C,F). However, a lower ACE abundance in LFD ( $p = 0.0259$ ), IRW15 ( $p = 0.0157$ ), and IRW45 ( $p = 0.0113$ ) groups was observed compared to HFD (Figure 3A). In addition, AT2R abundance increased almost 3-fold in the IRW45 group compared to HFD ( $p = 0.0024$ ) (Figure 3D). The plasma ACE activity was similar between groups (Figure 4A). Although ANOVA analysis identified an overall effect ( $p = 0.01$ ) on plasma angiotensin II, post-hoc analysis showed no significant differences between groups (Figure 4C). Whereas ACE2 activity was highest in the IRW45 group ( $p = 0.0016$ ) (Figure 4B), while plasma Ang (1–7) plasma concentration was not increased by IRW compared to the HFD (Figure 4D).

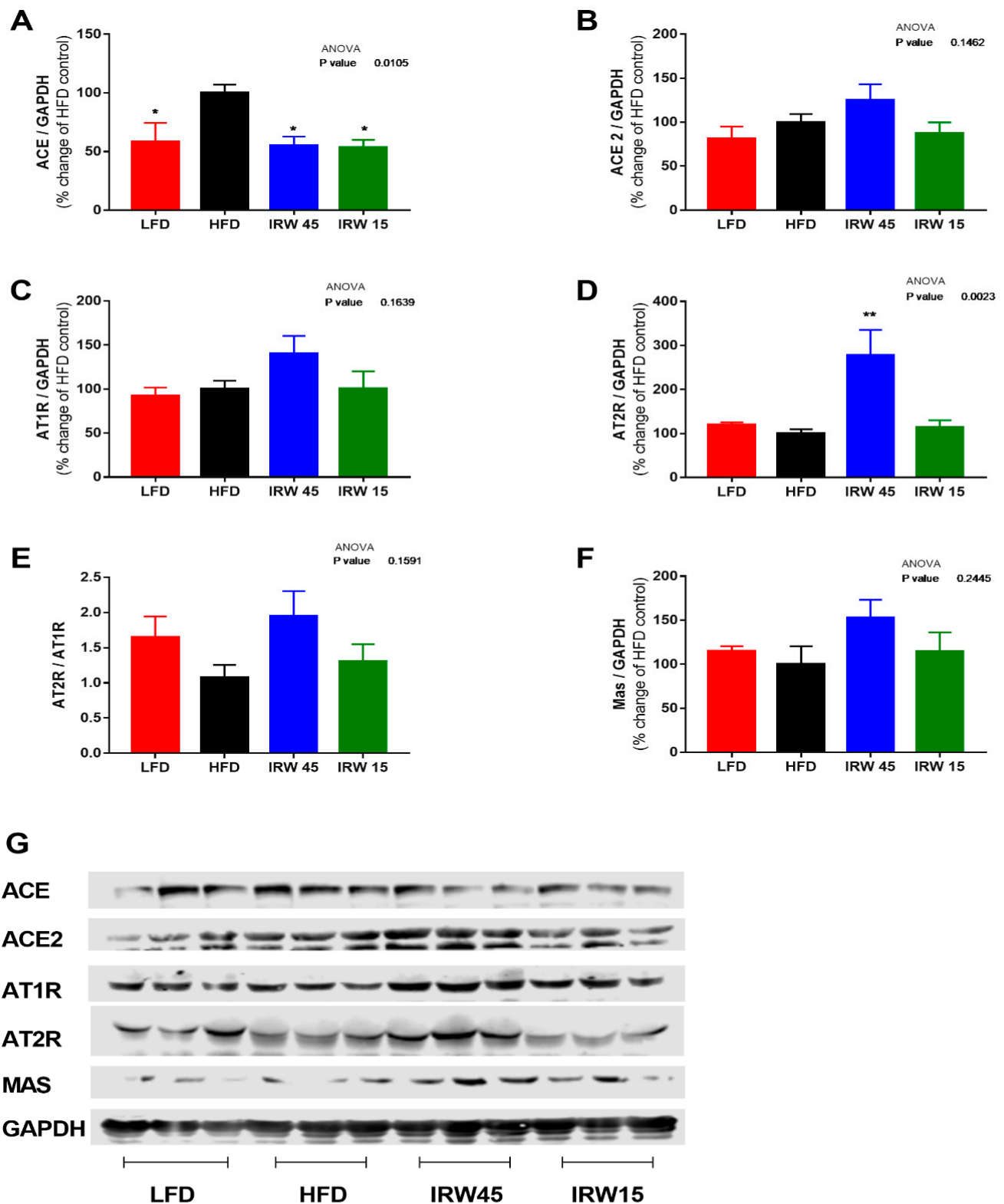


**Figure 3.** Skeletal muscle renin angiotensin system components. (A) ACE, (B) ACE2, (C) AT1R, (D) AT2R, (E) AT2R/AT1R ratio, (F) Mas receptor, and (G) representative blot. ACE, ACE2, AT1R, AT2R, and Mas were normalized to GAPDH. Data expressed as mean  $\pm$  SEM of  $n = 5-6$  mice. Analysis by one-way ANOVA followed by Bonferroni's post-hoc test. \*  $p < 0.05$  and \*\*  $p < 0.01$  versus HFD. ACE, angiotensin converting enzyme; ACE2, angiotensin converting enzyme 2; AT1R, angiotensin receptor type 1; AT2R, angiotensin receptor type 2.

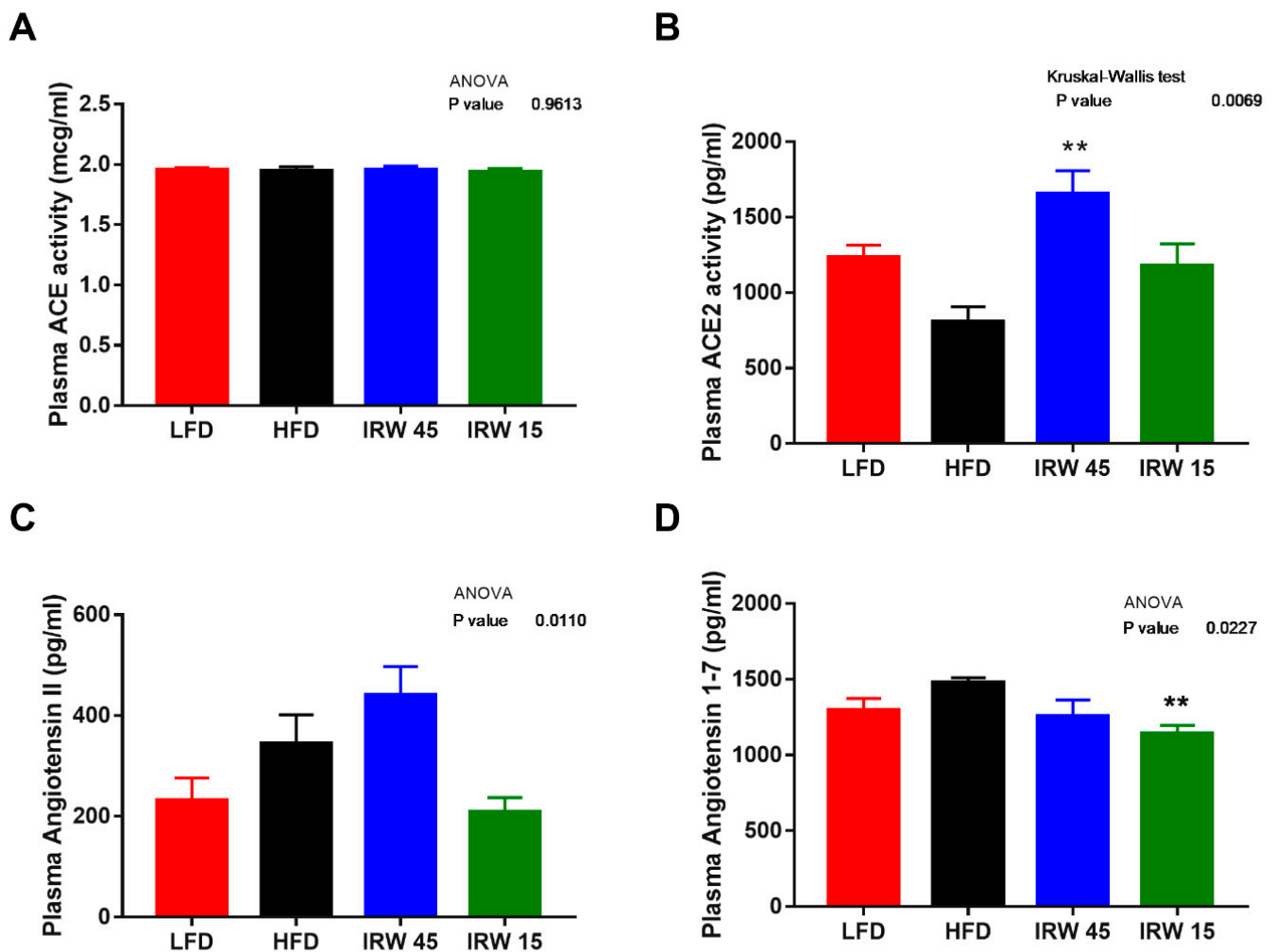


**Figure 4.** Plasma renin angiotensin system components. (A) Plasma angiotensin converting enzyme (ACE), (B) Plasma angiotensin converting enzyme 2 (ACE2), (C) Plasma angiotensin II, and (D) Plasma angiotensin (1–7). Data expressed as mean  $\pm$  SEM of  $n = 4$ –7 mice. Analysis by one-way ANOVA followed by Bonferroni’s post-hoc comparison test or Kruskal–Wallis followed by Dunn’s post hoc test when appropriate. \*\*  $p < 0.01$  versus HFD.

### 3.5. Skeletal Muscle Gene Expression

RNA sequencing of gastrocnemius muscle transcripts revealed that IRW45 elicited a generally higher abundance of transcripts related to muscle synthesis (Figure 5A). qPCR validation identified *Rbm5* ( $p = 0.0094$ ), *Mdm2* ( $p = 0.0094$ ), *Dlg1* ( $p < 0.001$ ), and *Myom1* ( $p < 0.001$ ) genes upregulated and *Aspn* ( $p < 0.001$ ) downregulated by IRW45 compared to the HFD group (Figure 5B). For PPAR $\gamma$  related genes, IRW45 significantly enhanced the expression of *Pparg* ( $p = 0.0112$ ) and *Lpl* ( $p < 0.001$ ) but not *Plin2* or *Cebpa* (Figure 5C). However, it should be noted that the expression of *Plin2* and *Cebpa* were 15 and  $\sim 50$ -fold higher in HFD and IRW45 than LFD.

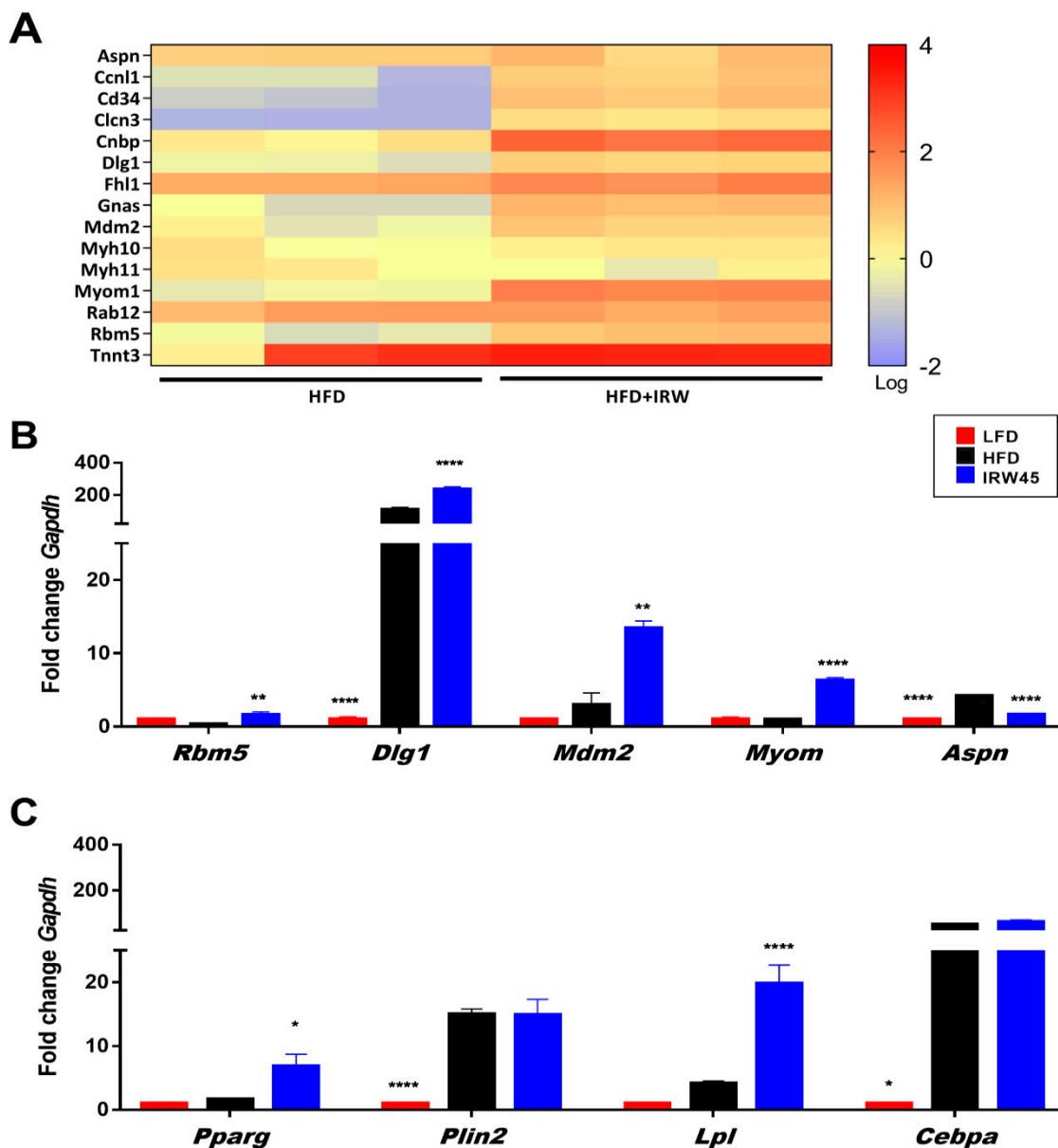


**Figure 5.** Skeletal muscle gene expression of mice fed IRW for 8 weeks. (A) Heatmap showing the abundance of major genes involved in muscle synthesis modulated by IRW45 determined by RNA sequencing. (B) *Rbm5*, *Mdm2*, *Dlg1*, *Myom1*, and *Aspn* qPCR validation of IRW in vivo using gastrocnemius skeletal muscle. Data expressed as mean  $\pm$  SEM of  $n = 5$  mice (C) *Pparg*, *Plin2*, *Cebpa* and *Lpl* qPCR validation using gastrocnemius skeletal muscle. Data expressed as mean  $\pm$  SEM of  $n = 5$  mice. Analysis by one-way ANOVA followed by Bonferroni's post-hoc comparison test or Kruskal–Wallis followed by Dunn's post hoc test when appropriate. \*  $p < 0.05$ , \*\*  $p < 0.01$ , and \*\*\*\*  $p < 0.0001$  versus HFD.

### 3.6. AMPK $\alpha$ Abundance and mTOR Signaling

IRW45 treatment elicited a ~10-fold increase in AMPK $\alpha$  phosphorylation (Thr172) relative to total AMPK $\alpha$  in skeletal muscle compared to HFD ( $p < 0.0124$ ) (Figure 6A), with no change in total AMPK $\alpha$  (Figure 6B). ANOVA indicated an overall diet effect in p-AMPK $\alpha$  over GAPDH (Figure 6C), consistent with findings in Figure 6A. No changes in total or phosphorylated AMPK $\alpha$  abundance in retroperitoneal or epididymal WAT were observed after IRW supplementation (Supplementary Figure S4 and Figure S5, respectively).

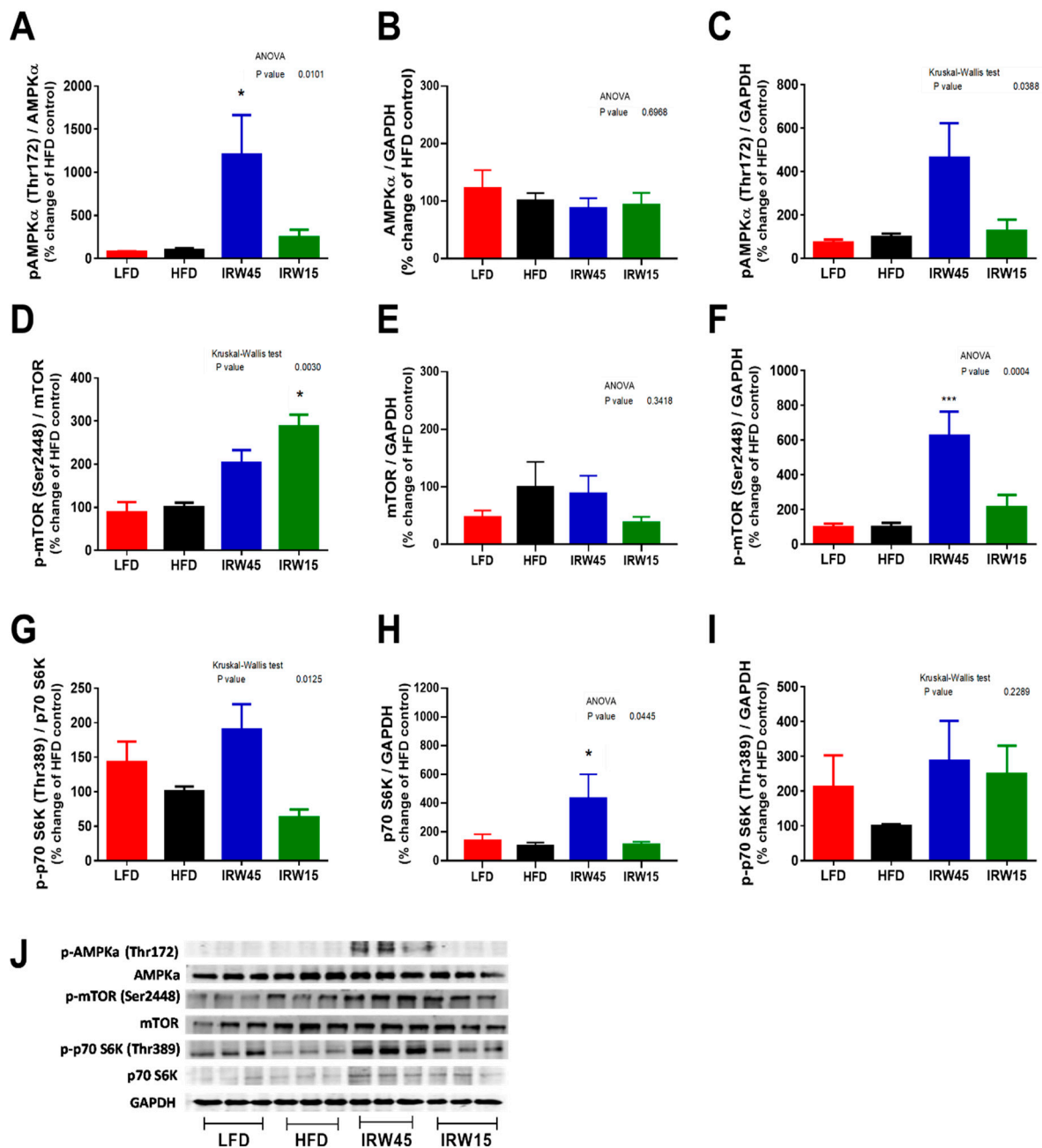


**Figure 6.** Skeletal muscle AMPK $\alpha$ , mTOR and P70 S6K protein abundance. (A) p-AMPK $\alpha$ /AMPK $\alpha$ . (B) AMPK $\alpha$ /GAPDH. (C) p-AMPK $\alpha$ /GAPDH. (D) p-mTOR/mTOR. (E) mTOR/GAPDH. (F) p-mTOR/GAPDH. (G) p-P70 S6K/P70 S6K. (H) P70 S6K/GAPDH. (I) p-P70 S6K/GAPDH and (J) representative blots. Data expressed as mean  $\pm$  SEM of  $n = 5-6$  mice. Analysis by one-way ANOVA followed by Bonferroni's post-hoc comparison test or Kruskal–Wallis followed by Dunn's post hoc test when appropriate. \*  $p < 0.05$  and \*\*\*  $p < 0.001$  versus HFD. AMPK, 5' AMP-activated protein kinase; mTOR, mammalian target of rapamycin; P70 S6K, Ribosomal protein S6 kinase beta-1.

Phosphorylated (Ser2448) mTOR relative to total mTOR had an overall significant increase ( $p = 0.003$ ) in skeletal muscle, but the post-hoc analysis revealed no statistical significance between IRW45 and HFD ( $p = 0.2332$ ), while in IRW15 p-mTOR (Ser2448) was increased ( $p < 0.0138$ ) (Figure 6D). Total mTOR was not affected (Figure 6E); however, p-mTOR was statistically increased by IRW45 ( $p < 0.001$ ) (Figure 6F). The downstream p70 S6K protein phosphorylation trended to elevated IRW45 relative to total p70 S6K (Figure 6G,  $p = 0.2075$ ) and 3-fold relative to GAPDH (Figure 6I,  $p = 0.15$ ); however, total p70 S6K

protein was significantly increased ( $p < 0.045$ ) in IRW45 compared to HFD (Figure 6H). In adipose tissue, no changes were seen in total and phosphorylated mTOR or p70 S6K in both retroperitoneal and epididymal WAT (Supplementary Figures S4 and S5, respectively).

### 3.7. Adipose Tissue UCP-1 Abundance

The investigation of UCP-1 abundance in retroperitoneal and epididymal WAT is shown in Figure 7. UCP-1 was decreased by HFD compared with LFD and this was significant in epididymal WAT ( $p < 0.0188$ ) (Figure 7B). IRW15 and IRW45 exhibited intermediate abundance in epididymal WAT.

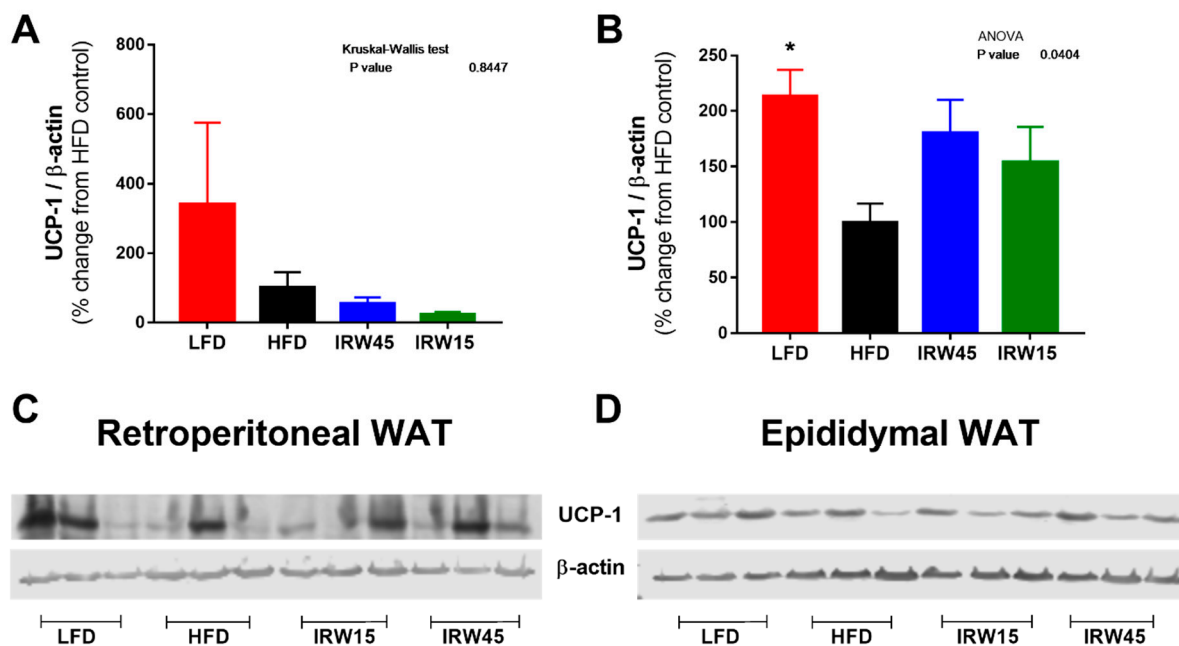


**Figure 7.** White adipose tissue UCP-1 protein abundance. Retroperitoneal WAT UCP-1 (A) and representative blot (C). Epididymal WAT UCP-1 (B) and representative blot (D). UCP-1 was normalized to  $\beta$ -actin. Data expressed as mean  $\pm$  SEM of  $n = 5$ –6 mice. Analysis by one-way ANOVA followed by Bonferroni's post-hoc test or Kruskal–Wallis followed by Dunn's post hoc test when appropriate. \*  $p < 0.05$  versus HFD. UCP, uncoupling protein.

## 4. Discussion

Natural health products [25] are used by a wide range of the population but their efficacy in managing complex metabolic diseases is still debated. Despite that, food-derived bioactive peptides exhibit positive physiological effects related to metabolic diseases and their complications [14,26,27]. IRW is an ovotransferrin-derived bioactive peptide previously shown to exert antihypertensive and anti-inflammatory effects [17,19]. In addition, *in vitro*, IRW presented antioxidant effects and improved insulin signaling [20,21]. In this study, using an obese, IR rodent model we demonstrated that IRW supplementation at a dose of 45 mg/kg BW: (1) prevented BW and fat mass gain during HFD treatment while protecting lean body mass; (2) improved glucose tolerance and fasting blood glucose and insulin concentrations; and (3) enhanced insulin-dependent and -independent signaling governing glucose uptake in skeletal muscle. IRW15 was not as effective as IRW45, illustrating dose dependence. For this reason, the discussion is focused on IRW45 findings. Contrary to our hypothesis, these activities of IRW did not appear to involve the inhibition of local RAS.

As previously demonstrated [18,19], IRW retained biological activity *in vivo* possibly because we mixed IRW into the HFD, which may have protected from degradation by digestive enzymes [28]. However, IRW can be degraded into the dipeptide IR in simu-

lated gastrointestinal digestion, which decreases its ACE inhibitory activity drastically *in vitro* [15]. We did not calculate the concentration or characterize the bioactive form reaching the bloodstream in the current study and we cannot exclude the possibility of the dipeptide IR being bioactive *in vivo*, therefore it is only a speculation. Nevertheless, IRW at a dosage of 45 mg/kg BW promoted enhanced glucose homeostasis. This dosage is comparable to other studies investigating the role of small-molecules, natural products or bioactive peptides in cardio-metabolic conditions using rodent models. For example, AdipoRon, a small-molecule agonist of adiponectin receptor is used at 50 mg/kg BW [29], curcumin at 100 mg/kg BW [30], soy  $\beta$ -Conglycin at 10% of diet (*w/w*) [31] and the di-peptide (Trp-His) at dosages ranging between 10–100 mg/kg BW [32,33]. Moreover, metformin is used at 200 mg/kg BW in rodent models of diabetes [34,35].

In this study, IRW45 improved both fasting and insulin-stimulated glucose indices and decreased fasting insulin in HFD-fed, glucose-intolerant mice, consistent with reduced HOMA-IR. Similarly, an egg white hydrolysate improved glucose tolerance and insulin sensitivity in HFD rats [10]. In Zucker Fatty rats, egg white hydrolysate treatment lowered fasting insulin but not glucose concentrations, resulting in reduced HOMA-IR and HOMA- $\beta$  indices [36]. Although our ITT study shows that IRW45 treatment improved insulin sensitivity compared to the HFD group, the significance was lost after adjustment for baseline blood glucose concentration, suggesting that the effects observed were dependent on differences in fasting blood glucose concentration.

Glucose uptake in skeletal muscle occurs via insulin-dependent and -independent pathways. Insulin activates the PI3K-AKT cascade leading to translocation of GLUT4 to the plasma membrane, and thus increases glucose uptake [37], which was demonstrated in skeletal muscle of IRW45 treated animals compared to the HFD. However, because ITT was not different between groups, insulin-independent pathways may also play a role. AMPK activation, such as in muscle contraction, enhances GLUT4 translocation [38] and increases glucose entry independently of insulin [39]. Indeed, AMPK $\alpha$  phosphorylation in skeletal muscle of IRW45 animals was significantly increased. Both AKT and AMPK pathways could contribute to improved glucose tolerance observed in IRW45 mice. We also acknowledge the possibility of enhanced basal AKT phosphorylation by IRW directly. In this study, only insulin-stimulated animals were included, which did not allow for this latter analysis.

We initially hypothesized that IRW-mediated improvements in insulin signaling would be associated with reduced local RAS activity, based on previous studies [15,18,19,40]. Despite IRW being an ACE inhibitor *in vitro* [15], we found no effect of IRW on systemic ACE activity in this IR model, similar to previous results using IRW in SHR rats [18]. However, IRW reduced ACE protein abundance in skeletal muscle, which might contribute to lower local ACE activity. Moreover, plasma ACE2 activity was increased in our study, consistent with previous studies showing that oral IRW supplementation enhanced circulating ACE2 abundance and activity [18], and ACE2 protein expression in the aorta of SHR rats [40]. ACE2 antagonizes the actions of angiotensin II, thereby reducing blood pressure, and reducing CVD risk through angiotensin (1–7)/Mas receptor axis as reviewed [41]. Interestingly, in this study angiotensin (1–7) was not increased by IRW treatment.

In skeletal muscle, modulation of AT1R and AT2R regulates insulin action locally, with systemic AT2R blockade impairing insulin-stimulated AKT phosphorylation, whole body glucose uptake, and muscular microvascular function, while systemic AT1R blockade restored muscle insulin signaling [4]. AT2R opposes the effects of AT1R activation in blood vessels with their interplay regulating blood flow and glucose utilization in skeletal muscle [42]. In our study, IRW45 increased AT2R abundance in skeletal muscle. Similarly, we previously showed that egg hydrolysate enhanced AT2R abundance in WAT and liver, and improved glucose tolerance [10]. Possibly, increased AT2R abundance in skeletal muscle tissue permits increased binding of angiotensin II to AT2R in the capillary endothelium, thus improving blood flow to facilitate insulin access to muscle cells and enhancing glucose uptake. Moreover, IRW may directly activate AT2R in muscle cells, which we speculate

may improve glucose transport via AMPK and PPAR $\gamma$  activation. Despite no clear direct link between AT2R and AMPK yet being demonstrated, RAS modulation improves glucose tolerance and insulin sensitivity via AMPK activation [43,44].

In some tissues, such as WAT, AT2R is linked to PPAR $\gamma$  as evidenced by PPAR $\gamma$  mRNA and activation being enhanced by AT2R agonists [45] and egg white hydrolysate concomitantly increased AT2R and PPAR $\gamma$  abundance [10]. Thiazolidinediones (TZDs) are PPAR $\gamma$  agonists and cause insulin sensitizing effects by enhancing skeletal muscle glucose uptake, reducing liver glucose output, and affecting WAT physiology [46]. PPAR $\gamma$  agonists potentiate AKT phosphorylation in WAT and skeletal muscle [47] and specific deletion of PPAR $\gamma$  in skeletal muscle of mice induces IR [48]. In IR hamsters, PPAR $\gamma$  RNA expression in skeletal muscle is downregulated, along with other genes regulated by PPAR $\gamma$  such as *Ppargc1a*, *Lpl*, and *Adipoq* (adiponectin) genes [49]. In this study, IRW45 treatment upregulated *Pparg* and *Lpl* in skeletal muscle while increasing PPAR $\gamma$  protein abundance, suggesting that IRW may upregulate a cassette of PPAR $\gamma$ -related genes as part of its metabolic activity.

Despite similar caloric intake, IRW45 improved body composition by reducing BW and fat mass gain, while protecting lean mass. In humans, the reduction of whole-body fat mass after an exercise intervention was associated with increased insulin sensitivity index [50]. Recently, an extract from rice hulls decreased fat mass by suppressing adipogenic genes in epididymal WAT and liver while enhancing AMPK $\alpha$  protein, consistent with increased fatty acid oxidation [51]. However, neither AMPK $\alpha$  nor PPAR $\gamma$  abundance changed in visceral WAT after IRW treatment. We also investigated whether enhanced thermogenesis in WAT induced by IRW might explain reduced fat mass because AT2R activation was previously shown to induce UCP-1 in epididymal WAT [52] and brown adipose tissue [53]. We found that compared with LFD, UCP-1 was reduced in HFD epididymal WAT, similar to other findings [54]. IRW45 treatment tended to increase UCP-1 but not as strongly as expected if thermogenesis was the main route eliciting fat mass loss. The mechanism by which IRW reduced fat mass is still unclear and other pathways deserve investigation.

Skeletal muscle synthesis is a key indicator of metabolic health and is regulated by insulin [55]. Upregulation of genes involved in muscle synthesis was induced by IRW. Primarily, mTOR activation is modulated by nutrients and, once activated, is involved in protein and lipid synthesis [56]. However, despite increased AMPK phosphorylation and expression of muscle synthesis genes in skeletal muscle, phosphorylation of mTOR (Ser2448) by IRW was not dose-dependent nor correlated with phosphorylation of the downstream S6K P70. Nevertheless, the gene upregulation observed after IRW supplementation indicates a possible ability of IRW to trigger myogenesis pathways, which may be related to our observation of protected lean body mass. Alternatively, IRW may be acting independently of mTOR to promote these effects.

In summary, IRW reduced BW and fat mass gain while improving glucose tolerance and insulin sensitivity in HFD mice. We identified several mechanisms of action for IRW in skeletal muscle and, to a lesser extent, WAT that were independent of ACE inhibition. Pathways influenced by IRW include the AKT/GLUT4 and AMPK $\alpha$ /GLUT4, which both enhance glucose uptake in skeletal muscle, while activation of the AT2R/PPAR $\gamma$  pathway could improve insulin sensitivity. Furthermore, IRW may reduce inflammation [18,21], contributing to insulin sensitization. Because the liver regulates fasting glucose homeostasis, IRW may also improve liver insulin sensitivity during fasting, leading to better glucose tolerance. IRW effects in the liver are currently being investigated by our group. Thus, IRW has the potential to exert beneficial effects on glucose homeostasis, making it a strong candidate to be further studied in the context of metabolic diseases.

**Supplementary Materials:** The following supporting information can be downloaded at: <https://www.mdpi.com/article/10.3390/biomedicines10061235/s1>, Figure S1: Food intake measured as kcal intake per day per animal during 8 weeks of IRW treatment. Figure S2: Insulin Tolerance test (ITT) and area under the curve (AUC) for OGTT after 8 weeks of IRW supplementation. Figure S3: White adipose tissue (WAT) insulin signaling and PPAR $\gamma$  protein abundance. Figure S4: Retroperitoneal

white adipose tissue (WAT) AMPK $\alpha$ , mTOR and P70 S6K protein abundance. Figure S5: Epididymal white adipose tissue (WAT) AMPK $\alpha$ , mTOR and P70 S6K protein abundance. Table S1. Body composition of C57BL/6 mice after 6 weeks of LFD or HFD feeding. Table S2. Primers sequences used for RT-PCR assay.

**Author Contributions:** Conceptualization, M.S., C.B.C. and J.W.; Formal analysis, S.C.d.C.Z., M.S. and K.S.B.; Funding acquisition, J.W.; Investigation, S.C.d.C.Z., M.S. and K.S.B.; Methodology, M.S.; Project administration, M.S. and J.W.; Supervision, C.B.C. and J.W.; Visualization, S.C.d.C.Z. and K.S.B.; Writing—original draft, S.C.d.C.Z.; Writing—review & editing, S.C.d.C.Z., K.S.B., C.B.C. and J.W. All authors have read and agreed to the published version of the manuscript.

**Funding:** None of the following sources had other involvement except providing funding for the study presented. This work was supported by Natural Sciences and Engineering Research Council of Canada [grant numbers CRDPJ 532150-18], Egg Farmers of Canada, and Global Egg Corporation.

**Institutional Review Board Statement:** The animal study protocol was approved by the Animal Care and Use Committee of the University of Alberta (Protocol# 1402) in accordance with guidelines issued by the Canadian Council on Animal Care.

**Informed Consent Statement:** Not applicable.

**Data Availability Statement:** Data is contained within the article or supplementary material.

**Acknowledgments:** We sincerely thank Nicole Coursen for the help with the animal trial and Juan Jovel and the genomics core facility for their assistance with the RNA sequencing.

**Conflicts of Interest:** The authors declare no conflict of interest.

## References

1. McCracken, E.; Monaghan, M.; Sreenivasan, S. Pathophysiology of the metabolic syndrome. *Clin. Dermatol.* **2018**, *36*, 14–20. [[CrossRef](#)] [[PubMed](#)]
2. Putnam, K.; Shoemaker, R.; Yiannikouris, F.; Cassis, L.A. The renin-angiotensin system: A target of and contributor to dyslipidemias, altered glucose homeostasis, and hypertension of the metabolic syndrome. *Am. J. Physiol. Heart Circ. Physiol.* **2012**, *302*, H1219–H1230. [[CrossRef](#)] [[PubMed](#)]
3. Agoudemos, M.M.; Greene, A.S. Localization of the renin-angiotensin system components to the skeletal muscle microcirculation. *Microcirculation* **2005**, *12*, 627–636. [[CrossRef](#)] [[PubMed](#)]
4. Chai, W.; Wang, W.; Dong, Z.; Cao, W.; Liu, Z. Angiotensin II receptors modulate muscle microvascular and metabolic responses to insulin in vivo. *Diabetes* **2011**, *60*, 2939–2946. [[CrossRef](#)] [[PubMed](#)]
5. Frantz, E.D.; Crespo-Mascarenhas, C.; Barreto-Vianna, A.R.; Aguila, M.B.; Mandarim-de-Lacerda, C.A. Renin-angiotensin system blockers protect pancreatic islets against diet-induced obesity and insulin resistance in mice. *PLoS ONE* **2013**, *8*, e67192. [[CrossRef](#)]
6. van der Zijl, N.J.; Moors, C.C.; Goossens, G.H.; Hermans, M.M.; Blaak, E.E.; Diamant, M. Valsartan improves  $\beta$ -cell function and insulin sensitivity in subjects with impaired glucose metabolism: A randomized controlled trial. *Diabetes Care* **2011**, *34*, 845–851. [[CrossRef](#)]
7. Wang, Y.; Wei, R.B.; Yang, Y.; Su, T.Y.; Huang, M.J.; Li, P.; Chen, X.M. Valsartan Alleviates Insulin Resistance in Skeletal Muscle of Chronic Renal Failure Rats. *Med. Sci. Monit.* **2018**, *24*, 2413–2419. [[CrossRef](#)]
8. Mitsuishi, M.; Miyashita, K.; Muraki, A.; Itoh, H. Angiotensin II reduces mitochondrial content in skeletal muscle and affects glycemic control. *Diabetes* **2009**, *58*, 710–717. [[CrossRef](#)]
9. Diplock, A.T.; Action, E.C. Scientific concepts of functional foods in Europe-consensus document. *Br. J. Nutr.* **1999**, *81*, S1–S27.
10. Jahandideh, F.; Zani, S.C.C.; Son, M.; Proctor, S.D.; Davidge, S.T.; Chan, C.B.; Wu, J. Egg white hydrolysate enhances insulin sensitivity in high-fat diet-induced insulin-resistant rats via Akt activation. *Br. J. Nutr.* **2019**, *122*, 14–24. [[CrossRef](#)]
11. Jahandideh, F.; Liu, P.; Wu, J. Purification and identification of adipogenic-differentiating peptides from egg white hydrolysate. *Food Chem.* **2018**, *259*, 25–30. [[CrossRef](#)] [[PubMed](#)]
12. Shang, N.; Bhullar, K.S.; Hubbard, B.P.; Wu, J.P. Tripeptide IRW initiates differentiation in osteoblasts differentiation via the RUNX2 pathway. *BBA-Gen. Subj.* **2019**, *1863*, 1138–1146. [[CrossRef](#)]
13. Martin, M.; Deussen, A. Effects of natural peptides from food proteins on angiotensin converting enzyme activity and hypertension. *Crit. Rev. Food Sci. Nutr.* **2019**, *59*, 1264–1283. [[CrossRef](#)] [[PubMed](#)]
14. de Campos Zani, S.C.; Wu, J.; Chan, C.B. Egg and soy-derived peptides and hydrolysates: A review of their physiological actions against diabetes and obesity. *Nutrients* **2018**, *10*, 549. [[CrossRef](#)] [[PubMed](#)]
15. Majumder, K.; Wu, J. Purification and characterisation of angiotensin I converting enzyme (ACE) inhibitory peptides derived from enzymatic hydrolysate of ovotransferrin. *Food Chem.* **2011**, *126*, 1614–1619. [[CrossRef](#)] [[PubMed](#)]
16. Majumder, K.; Chakrabarti, S.; Davidge, S.T.; Wu, J. Structure and activity study of egg protein ovotransferrin derived peptides (IRW and IQW) on endothelial inflammatory response and oxidative stress. *J. Agric. Food Chem.* **2013**, *61*, 2120–2129. [[CrossRef](#)]

17. Huang, W.; Chakrabarti, S.; Majumder, K.; Jiang, Y.; Davidge, S.T.; Wu, J. Egg-derived peptide IRW inhibits TNF-alpha-induced inflammatory response and oxidative stress in endothelial cells. *J. Agric. Food Chem.* **2010**, *58*, 10840–10846. [[CrossRef](#)]
18. Liao, W.; Fan, H.; Davidge, S.T.; Wu, J. Egg White-Derived Antihypertensive Peptide IRW (Ile-Arg-Trp) Reduces Blood Pressure in Spontaneously Hypertensive Rats via the ACE2/Ang (1–7)/Mas Receptor Axis. *Mol. Nutr. Food Res.* **2019**, *63*, e1900063. [[CrossRef](#)]
19. Majumder, K.; Chakrabarti, S.; Morton, J.S.; Panahi, S.; Kaufman, S.; Davidge, S.T.; Wu, J. Egg-derived tri-peptide IRW exerts antihypertensive effects in spontaneously hypertensive rats. *PLoS ONE* **2013**, *8*, e82829. [[CrossRef](#)]
20. Son, M.; Chan, C.B.; Wu, J. Egg white ovotransferrin-derived ACE inhibitory peptide ameliorates angiotensin II-stimulated insulin resistance in skeletal muscle cells. *Mol. Nutr. Food Res.* **2018**, *62*, 1700602. [[CrossRef](#)]
21. Son, M.; Wu, J. Egg white hydrolysate and peptide reverse insulin resistance associated with tumor necrosis factor-alpha (TNF-alpha) stimulated mitogen-activated protein kinase (MAPK) pathway in skeletal muscle cells. *Eur. J. Nutr.* **2019**, *58*, 1961–1969. [[CrossRef](#)]
22. Williams, L.M.; Campbell, F.M.; Drew, J.E.; Koch, C.; Hoggard, N.; Rees, W.D.; Kamolrat, T.; Thi Ngo, H.; Steffensen, I.L.; Gray, S.R.; et al. The development of diet-induced obesity and glucose intolerance in C57BL/6 mice on a high-fat diet consists of distinct phases. *PLoS ONE* **2014**, *9*, e106159. [[CrossRef](#)]
23. Heikkinen, S.; Argmann, C.A.; Champy, M.F.; Auwerx, J. Evaluation of glucose homeostasis. *Curr. Protoc. Mol. Biol.* **2007**, *77*, 29B.3.1–29B.3.22. [[CrossRef](#)]
24. Bustin, S.A.; Benes, V.; Garson, J.A.; Hellemans, J.; Huggett, J.; Kubista, M.; Mueller, R.; Nolan, T.; Pfaffl, M.W.; Shipley, G.L.; et al. The MIQE guidelines: Minimum information for publication of quantitative real-time PCR experiments. *Clin. Chem.* **2009**, *55*, 611–622. [[CrossRef](#)]
25. Non-Prescription Health Products Directorate (NNHPD). *What Are Natural Health Products*; Government of Canada: Ottawa, ON, Canada, 2004.
26. Li, S.; Liu, L.; He, G.; Wu, J. Molecular targets and mechanisms of bioactive peptides against metabolic syndromes. *Food Funct.* **2018**, *9*, 42–52. [[CrossRef](#)]
27. Rivero-Pino, F.; Espejo-Carpio, F.J.; Guadix, E.M. Antidiabetic Food-Derived Peptides for Functional Feeding: Production, Functionality and In Vivo Evidences. *Foods* **2020**, *9*, 983. [[CrossRef](#)]
28. Grootaert, C.; Jacobs, G.; Matthijs, B.; Pitart, J.; Baggerman, G.; Possemiers, S.; Van der Saag, H.; Smagghe, G.; Van Camp, J.; Voorspoels, S. Quantification of egg ovalbumin hydrolysate-derived anti-hypertensive peptides in an in vitro model combining luminal digestion with intestinal Caco-2 cell transport. *Food Res. Int.* **2017**, *99*, 531–541. [[CrossRef](#)]
29. Okada-Iwabuchi, M.; Yamauchi, T.; Iwabuchi, M.; Honma, T.; Hamagami, K.; Matsuda, K.; Yamaguchi, M.; Tanabe, H.; Kimura-Someya, T.; Shirouzu, M.; et al. A small-molecule AdipoR agonist for type 2 diabetes and short life in obesity. *Nature* **2013**, *503*, 493–499. [[CrossRef](#)]
30. Jain, S.K.; Rains, J.; Croad, J.; Larson, B.; Jones, K. Curcumin supplementation lowers TNF-alpha, IL-6, IL-8, and MCP-1 secretion in high glucose-treated cultured monocytes and blood levels of TNF-alpha, IL-6, MCP-1, glucose, and glycosylated hemoglobin in diabetic rats. *Antioxid. Redox Signal.* **2009**, *11*, 241–249. [[CrossRef](#)]
31. Kawabeta, K.; Hase-Tamaru, S.; Yuasa, M.; Suruga, K.; Sugano, M.; Koba, K. Dietary beta-Conglycinin Modulates Insulin Sensitivity, Body Fat Mass, and Lipid Metabolism in Obese Otsuka Long-Evans Tokushima Fatty (OLETF) Rats. *J. Oleo Sci.* **2019**, *68*, 339–350. [[CrossRef](#)]
32. Matsui, T.; Sato, M.; Tanaka, M.; Yamada, Y.; Watanabe, S.; Fujimoto, Y.; Imaizumi, K.; Matsumoto, K. Vasodilating dipeptide Trp-His can prevent atherosclerosis in apo E-deficient mice. *Br. J. Nutr.* **2010**, *103*, 309–313. [[CrossRef](#)]
33. Tanaka, M.; Hong, S.M.; Akiyama, S.; Hu, Q.Q.; Matsui, T. Visualized absorption of anti-atherosclerotic dipeptide, Trp-His, in Sprague-Dawley rats by LC-MS and MALDI-MS imaging analyses. *Mol. Nutr. Food Res.* **2015**, *59*, 1541–1549. [[CrossRef](#)]
34. Al Za'abi, M.; Ali, B.H.; Al Suleimani, Y.; Adham, S.A.; Ali, H.; Manoj, P.; Ashique, M.; Nemmar, A. The Effect of Metformin in Diabetic and Non-Diabetic Rats with Experimentally-Induced Chronic Kidney Disease. *Biomolecules* **2021**, *11*, 814. [[CrossRef](#)] [[PubMed](#)]
35. Zhang, Z.M.; Liu, Z.H.; Nie, Q.; Zhang, X.M.; Yang, L.Q.; Wang, C.; Yang, L.L.; Song, G.Y. Metformin improves high-fat diet-induced insulin resistance in mice by downregulating the expression of long noncoding RNA NONMMUT031874.2. *Exp. Ther. Med.* **2022**, *23*, 332. [[CrossRef](#)]
36. Garcés-Rimon, M.; Gonzalez, C.; Vera, G.; Uranga, J.A.; Lopez-Fandino, R.; Lopez-Miranda, V.; Miguel, M. Pepsin egg white hydrolysate improves glucose metabolism complications related to metabolic syndrome in Zucker fatty rats. *Nutrients* **2018**, *10*, 441. [[CrossRef](#)]
37. Zhou, X.; Shentu, P.; Xu, Y. Spatiotemporal regulators for insulin-stimulated GLUT4 vesicle exocytosis. *J. Diabetes Res.* **2017**, *2017*, 1683678. [[CrossRef](#)]
38. Kurth-Kraczek, E.J.; Hirshman, M.F.; Goodyear, L.J.; Winder, W.W. 5' AMP-activated protein kinase activation causes GLUT4 translocation in skeletal muscle. *Diabetes* **1999**, *48*, 1667–1671. [[CrossRef](#)]
39. Bergeron, R.; Russell, R.R., 3rd; Young, L.H.; Ren, J.M.; Marcucci, M.; Lee, A.; Shulman, G.I. Effect of AMPK activation on muscle glucose metabolism in conscious rats. *Am. J. Physiol.* **1999**, *276*, E938–E944. [[CrossRef](#)]
40. Liao, W.; Bhullar, K.S.; Chakrabarti, S.; Davidge, S.T.; Wu, J. Egg White-Derived Tripeptide IRW (Ile-Arg-Trp) Is an Activator of Angiotensin Converting Enzyme 2. *J. Agric. Food Chem.* **2018**, *66*, 11330–11336. [[CrossRef](#)]

41. Gheblawi, M.; Wang, K.; Viveiros, A.; Nguyen, Q.; Zhong, J.C.; Turner, A.J.; Raizada, M.K.; Grant, M.B.; Oudit, G.Y. Angiotensin-Converting Enzyme 2: SARS-CoV-2 Receptor and Regulator of the Renin-Angiotensin System: Celebrating the 20th Anniversary of the Discovery of ACE2. *Circ. Res.* **2020**, *126*, 1456–1474. [[CrossRef](#)]
42. Chai, W.; Wang, W.; Liu, J.; Barrett, E.J.; Carey, R.M.; Cao, W.; Liu, Z. Angiotensin II type 1 and type 2 receptors regulate basal skeletal muscle microvascular volume and glucose use. *Hypertension* **2010**, *55*, 523–530. [[CrossRef](#)] [[PubMed](#)]
43. Huang, Y.; Li, Y.; Liu, Q.; Zhang, J.; Zhang, Z.; Wu, T.; Tang, Q.; Huang, C.; Li, R.; Zhou, J.; et al. Telmisartan attenuates obesity-induced insulin resistance via suppression of AMPK mediated ER stress. *Biochem. Biophys. Res. Commun.* **2020**, *523*, 787–794. [[CrossRef](#)]
44. Shinshi, Y.; Higashiura, K.; Yoshida, D.; Togashi, N.; Yoshida, H.; Miyazaki, Y.; Ura, N.; Shimamoto, K. Angiotensin II inhibits glucose uptake of skeletal muscle via the adenosine monophosphate-activated protein kinase pathway. *J. Am. Soc. Hypertens.* **2007**, *1*, 251–255. [[CrossRef](#)]
45. Ohshima, K.; Mogi, M.; Jing, F.; Iwanami, J.; Tsukuda, K.; Min, L.J.; Ogimoto, A.; Dahlof, B.; Steckelings, U.M.; Unger, T.; et al. Direct angiotensin II type 2 receptor stimulation ameliorates insulin resistance in type 2 diabetes mice with PPARgamma activation. *PLoS ONE* **2012**, *7*, e48387. [[CrossRef](#)] [[PubMed](#)]
46. Olefsky, J.M. Treatment of insulin resistance with peroxisome proliferator-activated receptor gamma agonists. *J. Clin. Investig.* **2000**, *106*, 467–472. [[CrossRef](#)] [[PubMed](#)]
47. Jiang, G.; Dallas-Yang, Q.; Li, Z.; Szalkowski, D.; Liu, F.; Shen, X.; Wu, M.; Zhou, G.; Doebber, T.; Berger, J.; et al. Potentiation of insulin signaling in tissues of Zucker obese rats after acute and long-term treatment with PPARgamma agonists. *Diabetes* **2002**, *51*, 2412–2419. [[CrossRef](#)]
48. Hevener, A.L.; He, W.; Barak, Y.; Le, J.; Bandyopadhyay, G.; Olson, P.; Wilkes, J.; Evans, R.M.; Olefsky, J. Muscle-specific Pparg deletion causes insulin resistance. *Nat. Med.* **2003**, *9*, 1491–1497. [[CrossRef](#)]
49. Li, G.S.; Liu, X.H.; Zhu, H.; Huang, L.; Liu, Y.L.; Ma, C.M. Skeletal muscle insulin resistance in hamsters with diabetes developed from obesity is involved in abnormal skeletal muscle LXR, PPAR and SREBP expression. *Exp. Ther. Med.* **2016**, *11*, 2259–2269. [[CrossRef](#)]
50. Amankwaah, A.F.; Hudson, J.L.; Kim, J.E.; Campbell, W.W. Reductions in whole-body fat mass but not increases in lean mass predict changes in cardiometabolic health indices with exercise training among weight-stable adults. *Nutr. Res.* **2019**, *63*, 63–69. [[CrossRef](#)]
51. Kim, G.H.; Ju, J.Y.; Chung, K.S.; Cheon, S.Y.; Gil, T.Y.; Cominguez, D.C.; Cha, Y.Y.; Lee, J.H.; Roh, S.S.; An, H.J. Rice Hull Extract (RHE) Suppresses Adiposity in High-Fat Diet-Induced Obese Mice and Inhibits Differentiation of 3T3-L1 Preadipocytes. *Nutrients* **2019**, *11*, 1162. [[CrossRef](#)]
52. Quiroga, D.T.; Munoz, M.C.; Gil, C.; Pfeifer, M.; Toblli, J.E.; Steckelings, U.M.; Giani, J.F.; Dominici, F.P. Chronic administration of the angiotensin type 2 receptor agonist C21 improves insulin sensitivity in C57BL/6 mice. *Physiol. Rep.* **2018**, *6*, e13824. [[CrossRef](#)] [[PubMed](#)]
53. Nag, S.; Patel, S.; Mani, S.; Hussain, T. Role of angiotensin type 2 receptor in improving lipid metabolism and preventing adiposity. *Mol. Cell Biochem.* **2019**, *461*, 195–204. [[CrossRef](#)] [[PubMed](#)]
54. Fromme, T.; Klingenspor, M. Uncoupling protein 1 expression and high-fat diets. *Am. J. Physiol. Regul. Integr. Comp. Physiol.* **2011**, *300*, R1–R8. [[CrossRef](#)]
55. Rubio-Ruiz, M.E.; Guarner-Lans, V.; Perez-Torres, I.; Soto, M.E. Mechanisms Underlying Metabolic Syndrome-Related Sarcopenia and Possible Therapeutic Measures. *Int. J. Mol. Sci.* **2019**, *20*, 647. [[CrossRef](#)]
56. Albert, V.; Hall, M.N. mTOR signaling in cellular and organismal energetics. *Curr. Opin. Cell Biol.* **2015**, *33*, 55–66. [[CrossRef](#)]